POLITECNICO DI MILANO

FACOLTÀ DI INGEGNERIA INDUSTRIALE E DELL'INFORMAZIONE

CORSO DI LAUREA MAGISTRALE IN INGEGNERIA NUCLEARE

A CONTROL-ORIENTED MODEL

FOR PRESSURIZER TRANSIENT DYNAMICS

Relatore: **Prof. Antonio Cammi**

Tesi di Laurea Magistrale di:

Alessandro Pini

Matr. 783319

Anno Accademico 2012 - 2013

POLITECNICO DI MILANO

FACOLTÀ DI INGEGNERIA INDUSTRIALE E DELL'INFORMAZIONE

CORSO DI LAUREA MAGISTRALE IN INGEGNERIA NUCLEARE

A CONTROL-ORIENTED MODEL FOR PRESSURIZER TRANSIENT DYNAMICS

Relatore: **Prof. Antonio Cammi**

Tesi di Laurea Magistrale di:

Alessandro Pini

Matr. 783319

Anno Accademico 2012 - 2013

CONTENTS

LIST OF FIGURES

LIST OF TABLES

ABSTRACT

This study develops a control-oriented model for the pressurizer subsystem of Pressurized Water Reactors (PWRs).
The purpose of this modelling activity is to faithfully reproduce the dynamic behaviour of the pressurizer along its entire range of operations using both block-diagrams and object-oriented approach. For this reason Simulink® and Dymola® pressurizer simulation programs are realized.
Regarding accuracy, the created model leaves behind previous control-oriented approaches: old control-oriented models used to provide rough reproductions of real physic transients occurring inside the pressurizer tank, while the new one is able to closely follow them. The studied model is based on the non-equilibrium multi-region approach: water and steam present in the pressurizer tank are treated as different phases and can be at saturation conditions or, respectively, at subcooled or superheated ones. No a priori assumptions are made concerning the particular thermodynamics process followed during transients. The basic mathematical model is derived from mass and energy conservation equations and includes all the important thermal-hydraulic processes which can occur inside the pressurizer. These processes are: spray condensation, bulk and surface condensation and evaporation, condensate fall and heat transfer from heaters. Furthermore, the model takes into account heat exchange processes between vapour and liquid regions and thermal dissipations between the entire pressurizer and the external ambient. To obtain the best achievable performances, the model is declined into three variants: complete lumped parameter and quasi 1D representations.
Each different version has been developed as a natural evolution of the previous one, therefore, in the following pages, zero-dimensional, two-volumes and three-volumes pressurizer models are presented in order of increasing complexity and accuracy.
Finally, the three models are compared with experimental data coming from Shippingport pressurizer tests and with the RELAP5® simulations.

ESTRATTO

Questa tesi nasce con lo scopo di realizzare un modello, orientato al controllo, per la simulazione del comportamento dinamico di un componente fondamentale per i reattori nucleari ad acqua in pressione (Pressurized Water Reactor PWR): il pressurizzatore.
Tale sistema, che ha il compito di mantenere la pressione dell'impianto entro un certo intervallo di valori, è tipicamente costituito da un recipiente in acciaio al carbonio rivestito internamente in acciaio inossidabile contenente in parte acqua e in parte vapore. Di forma generalmente cilindrica ad orientazione verticale, esso è collegato alla gamba calda del circuito primario e contiene riscaldatori elettrici nella parte inferiore ed un ugello per lo spruzzo di acqua, proveniente dalla gamba fredda, nella parte superiore.
Quando la pressione nell'impianto tende a diminuire, parte dell'acqua contenuta nel pressurizzatore evapora: i riscaldatori sono quindi accesi per ristabilire la pressione nominale. Quando, per contro, la pressione tende ad aumentare, il vapore è condensato mediante l'azionamento di un sistema di spruzzatori.
La modellazione dinamica è di primaria importanza in un reattore nucleare e, nel caso specifico di un PWR, è essenziale simulare e prevedere l'andamento della pressione durante differenti transitori, al fine di operare il reattore in sicurezza o decidere le azioni di controllo e mitigazione necessarie in caso di eventuali incidenti.
Per questa ragione appositi programmi di simulazione del comportamento del pressurizzatore sono stati sviluppati già a partire dagli anni Cinquanta del secolo scorso.
I primi modelli sono stati basati su un approccio a parametri concentrati in cui l'acqua e il vapore contenuti nel pressurizzatore sono trattati come una miscela omogenea in condizione di saturazione.
Successivamente sono stati studiati i cosiddetti modelli di non-equilibrio in cui acqua e vapore, considerati come due fasi separate, possono dare luogo, all'interno del volume del pressurizzatore, ad una qualsiasi combinazione degli stati termodinamici possibili.
Vale a dire saturazione o sottoraffreddamento per la fase liquida, saturazione o surriscaldamento per quella gassosa.
In questo modo, considerando una semplice suddivisione in due regioni del pressurizzatore, si possono verificare quattro differenti stati: liquido saturo e vapore

saturo, liquido sottoraffreddato e vapore surriscaldato, liquido saturo e vapore surriscaldato, liquido sottoraffreddato e vapore saturo. Stati di surriscaldamento per la fase liquida non sono invece ammessi, in quanto in tali condizioni avviene un fenomeno di evaporazione di massa (bulk evaporation); analogamente la regione gassosa non sperimenta stati di sottoraffreddamento per il verificarsi di un processo di condensazione di massa (bulk condensation).
Con l'avvento dei cosiddetti codici di sistema (come ad esempio RELAP5®), attraverso i quali le autorità competenti impongono che l'impianto nucleare da licenziare debba essere simulato al fine di certificarne la sicurezza, può sorgere il dubbio che programmi di simulazione realizzati ad hoc per i singoli componenti di un reattore non abbiano più ragione di esistere.
Tuttavia questa perplessità, che inizialmente può sembrare ragionevole, entra rapidamente in crisi se si osserva che negli ultimi decenni si è assistito ad un sempre più massiccio uso di strumenti di simulazione molto diversi dai già citati codici di sistema.
Questi ultimi, infatti, benché siano certificati, affidabili e certamente fungano da standard di riferimento, sono affetti da un grande problema: possono richiedere ore per ricreare un singolo transitorio.
Questo punto debole, in particolare, non deve essere valutato solo dal punto di vista del tempo macchina, che in molti casi è una risorsa scarsa, ma anche tenendo presente che, durante la progettazione di un componente o di un impianto, devono essere accuratamente studiati anche il sistema e la logica di controllo.
In questo senso i codici di sistema, se da un lato permettono di ottenere simulazioni straordinariamente aderenti alla realtà, dall'altro impediscono un profonda integrabilità fra il modello dinamico del sistema stesso e il modello del sistema di controllo.
È quindi tangibile la necessità di sviluppare opportuni strumenti per la simulazione del comportamento di un impianto, gestito da un controllore dinamico, su intervalli temporali che possano comprendere pochi minuti, così come alcune ore. Per questo scopo si deve ricorrere a modelli non lineari, basati sui principi primi, che non si limitino a descrivere il comportamento del sistema attorno a un punto di equilibrio, ma permettano di abbracciare l'intero campo dei punti di funzionamento valutando anche condizioni di lavoro al di fuori di quelle progettuali.
Ritornando al caso del pressurizzatore, mentre i modelli di pura simulazione, da anni ormai sono orientati al già citato approccio di non-equilibrio termodinamico, quelli specificamente orientati al controllo continuano a fondarsi sull'ipotesi, molto lontana dalla realtà, che l'acqua e il vapore presenti nel suddetto componente possano essere trattati come una miscela omogenea in condizioni di saturazione.
In questo modo, i modelli appositamente sviluppati per lo studio del sistema di controllo, da un lato, essendo caratterizzati da una formulazione particolarmente semplice, permettono di studiare facilmente le caratteristiche dinamiche e la stabilità del sistema, dall'altro, invece, hanno scarse capacità nel riprodurre in modo effettivo i transitori reali.
Di conseguenza si vuole creare un nuovo modello, che pur rimanendo "control-oriented", sia fedele alla fisica dei processi che avvengono all'interno del pressurizzatore. Attraverso tale modello e alla sua aderenza alla realtà sarà possibile studiare l'influenza sulla dinamica del sistema di tutti i fenomeni che realmente entrano in gioco e sviluppare,

di conseguenza, logiche di controllo più avanzate rispetto a quelle tradizionalmente applicate.
Alla creazione di questo nuova tipologia di simulazione è volto il seguente lavoro di tesi, il quale infatti si conclude con la realizzazione di un modello che non solo abbandona l'ipotesi semplificativa di sistema all'equilibrio termodinamico, ma supera anche l'approccio a parametri concentrati.
È importante sottolineare come lo studio compiuto sia il frutto di una progressiva evoluzione che ha come punto di inizio un approccio in parte "lumped parameter" in cui il pressurizzatore è diviso in due regioni a volumi variabili, una per la fase liquida ed una per il vapore, con il vincolo che il volume totale, ossia quello del recipiente, rimanga costante. A tali volumetti sono quindi applicati i bilanci di massa ed energia che comprendono anche fenomeni di scambio termico e processi di dissipazione del calore tra pressurizzatore e ambiente esterno.
Le equazioni di conservazione della massa, dell'energia ed il vincolo sul volume, i quali costituiscono un sistema fortemente non lineare, sono la base fondamentale dell'intero lavoro di tesi.
Bisogna sottolineare che la presenza del vincolo algebrico sul volume rende il sistema di equazioni sopra descritto non un classico sistema di equazioni differenziali ordinarie (Ordinary Differential Equation ODE), bensì un sistema di equazioni algebrico-differenziali (Differential Algebraic Equation DAE), che presenta alcune peculiarità e che per poter essere risolto, generalmente, deve essere ricondotto in forma di ODE. Per potere effettuare ciò, seguendo un approccio consueto, il vincolo sul volume deve essere derivato rispetto al tempo. In questo modo si ricava un'equazione differenziale governante la pressione del sistema. Ovviamente il sistema ODE ottenuto è anch'esso non lineare, inoltre, alcune grandezze che vi compaiono, cambiano a seconda dello stato termodinamico delle regioni cui fanno riferimento.
Sulla carta questo modello potrebbe bastare, tuttavia, grazie al confronto coi dati sperimentali (sono stati utilizzati quelli ricavati alla fine degli anni Sessanta del XIX secolo in seguito agli esperimenti condotti sul pressurizzatore della centrale di Shippingport) ci si può rendere conto che i risultati delle simulazioni sono in verità ben lontani dalla realtà. Questo fatto induce a supporre che la regione liquida non possa essere considerata puntiforme, ma sia necessario tener conto di una certa distribuzione di temperatura al suo interno.
A questo primo modello ne segue pertanto un secondo caratterizzato dal fatto che la ragione liquida è ora suddivisa, in altezza, in due volumi, di cui quello superiore rimane variabile e segue il vincolo sul volume totale del pressurizzatore, mentre quello inferiore è fisso. Confrontando nuovamente i risultati delle simulazioni con i dati sperimentali, si nota un notevole miglioramento delle prestazioni del modello.
Tuttavia, per ottenere risultati veramente soddisfacenti, un terzo modello conclude la serie. Quest'ultima evoluzione si basa sulla suddivisione della regione liquida in tre volumi, due costanti ed un terzo variabile.
È necessario infine sottolineare che solo i volumi variabili possono sperimentare diversi stati termodinamici, mentre quelli fissi, ovvero quelli che occupano le zone inferiori della regione liquida, permangono sempre nello stato di sottoraffreddamento. A priori ciò non

si potrebbe imporre, ma l'analisi del pressurizzatore condotta usando RELAP5® lo mette evidenza. Infatti, con l'impiego di RELAP5®, è possibile ottenere risultati attendibili circa la distribuzione di temperatura presente nella regione liquida del sistema (per la quale mancano dati sperimentali) con cui validare il modello "control-oriented".
Dalle elaborazioni effettuate da RELAP5® si evince che le regioni inferiori del pressurizzatore, durante i transitori di ingresso e uscita dell'acqua dal sistema, permangono sempre in condizioni di sottoraffreddamento. Questo fatto permette di semplificare, senza alcuna perdita di accuratezza, il modello. Se infatti anche tali regioni fossero soggette a cambiamento di stato termodinamico, le equazioni caratteristiche di tutto il sistema sarebbero ancora più complesse.
Questa procedura dimostra come i codici di sistema e codici ad hoc per il controllo non si escludano reciprocamente, ma possano essere usati sinergicamente per ottenere migliori risultati nel modo più semplice.
A questo punto sorge spontanea la domanda circa le modalità con cui i modelli descritti siano stati effettivamente implementati a calcolatore al fine di ottenere i risultati da confrontare coi dati sperimentali.
In particolare, sono stati seguiti due approcci differenti: tutti e tre i modelli sono stati compilati utilizzando sia il linguaggio MATLAB-Simulink®, sia quello Modelica-Dymola®. Questo al fine di creare dei programmi di simulazione che diano circa i medesimi risultati, permettendo tuttavia di implementare i modelli matematici che ne stanno alla base in modalità completamente differenti.
Tradizionalmente i modelli "control-oriented" sono convertiti in codice usando il cosiddetto approccio causale, su cui si basa Simulink®.
In questo modo si realizzano modelli ingresso-uscita in cui il problema è formulato sfruttando i nessi di causalità presenti nel sistema.
Le equazioni che esprimono le grandezze di interesse (variabili di uscita) sono espresse in funzione di quantità note (variabili di ingresso), attraverso una serie rigidamente definita di operazioni impiegate per risolvere il problema considerato.
La forma che assume il modello risulta così più simile all'algoritmo usato per risolvere il problema, piuttosto che alla struttura fisica del sistema stesso, rendendo difficoltoso qualsiasi tentativo di recupero o approfondimento del lavoro svolto.
Le variabili di ingresso rappresentano le azioni compiute sull'oggetto in esame da agenti esterni che ne influenzano il comportamento, mentre le variabili di uscita rappresentano quanto del comportamento del sistema è di interesse: tra queste variabili vi è un rapporto di causa ed effetto, dato che l'evoluzione delle seconde descrive il modo in cui il sistema risponde alle sollecitazioni impresse dalle prime. In generale, però, la conoscenza del valore in un certo istante delle variabili di ingresso non è sufficiente ad individuare il valore, nello stesso istante, delle variabili di uscita: è allora necessario introdurre un terzo tipo di variabili, le variabili di stato, che descrivono la situazione interna del sistema.
La formulazione causale del problema sfrutta una rappresentazione grafica basata sui cosiddetti schemi a blocchi che consente di mettere in luce con chiarezza le interazioni tra i diversi sottosistemi.
I diagrammi a blocchi costituiscono la formulazione naturale con cui descrivere un sistema di controllo, il quale è intrinsecamente procedurale. È per questa ragione che

l'approccio causale è il più diffuso per descrivere modelli orientati al controllo, in quanto permette di focalizzare immediatamente le grandezze sulle quali è possibile esercitare un'azione per gestire l'evoluzione del sistema.
Infine la necessità di dover pesantemente manipolare le equazioni per codificarle ed implementarle nell'ambiente di simulazione, porta ad una maggiore comprensione della dinamica e dei processi caratteristici del sistema.
Tuttavia l'aver imposto a priori, prima ancora di realizzare il modello, quali grandezze siano da considerare note e quali incognite, non permette di operare modifiche: se il modello dovesse essere adottato in nuovi contesti, molto probabilmente tali assunzioni potrebbero risultare violate e il modello di conseguenza essere inutile.
Negli ultimi anni, grazie all'aumento delle capacità di calcolo, si è però diffusa un'altra tipologia di modellazione basata sul cosiddetto approccio a-causale.
Si tratta di un modo strutturato di realizzare modelli direttamente basato sulle equazioni costitutive e sulle leggi di conservazione del sistema in esame, le quali determinano l'insieme di equazioni che deve essere risolto.
Realizzare modelli dinamici secondo questa formulazione del problema non richiede di specificare a priori quali grandezze debbano agire come ingressi e quali come uscite: le equazioni sono scritte in forma dichiarativa indipendentemente dalle condizioni al contorno e i nessi di causalità non sono specificati fino a quando le equazioni non sono risolte, in base alle condizioni al contorno imposte dal contesto applicativo. Per questo motivo, quando si parla di modellazione a-causale, spesso è anche usato il termine "modellazione fisica", in quanto questo tipo di approccio è adatto per rappresentare la struttura fisica del sistema descritto. Il vantaggio principale della modellazione a-causale è che la direzione secondo la quale le equazioni sono risolte si può facilmente adattare di volta in volta in base al flusso di dati caratteristico della situazione cui si fa riferimento. In questo modo, l'attenzione rimane focalizzata sui componenti fisici del sistema, il cui comportamento è descritto da sistemi DAE. Per realizzare dei modelli a-causali è necessario selezionare i componenti e collegarli in uno schema: i modelli di ciascun componente sono formulati indipendentemente dalla conoscenza dei legami o delle equazioni che regolano altre parti del sistema. Partendo dal modello generale, che inquadra solo gli elementi fondamentali, è possibile arricchirlo (aggiungendo sensori, attuatori, ecc.) fino a renderlo completo. Con questo approccio, si riducono notevolmente le tempistiche e le difficoltà di modellazione, producendo modelli più comprensibili e vicini al mondo fisico. Per contro, è necessario che il simulatore sia in grado di effettuare un'analisi simbolica su sistemi DAE di grandi dimensioni.
Tra i vari interpreti, uno dei più affidabili e robusti è Dymola®.
Per quanto detto, i programmi del pressurizzatore realizzati in Simulink® risultano essere più rigidi da un punto di vista di una futura implementazione come singolo componente in un sistema di modellazione più generale, come ad esempio quello di un intero reattore nucleare, mentre risultano certamente più comodi per lo studio e lo sviluppo di un sistema di controllo. Al contrario i programmi realizzati in Dymola® sono di più semplice ri-utilizzo e di più facile interpretazione; lo studio del controllo è, invece, meno immediato.
I risultati delle simulazioni del pressurizzatore, considerato come singola entità, sono comunque molto simili ad indicare che entrambi gli approcci sono validi e performanti.

La scelta dell'uno piuttosto che dell'altro dipende soltanto dal contesto di utilizzo del programma di simulazione.
Per valutare le caratteristiche di stabilità del sistema, si è infine proceduto alla linearizzazione attorno ad un punto di equilibrio del modello non lineare. Da questo studio si è giunti ad una conclusione particolarmente significativa: i processi di scambio termico, che nei modelli di pressurizzatore presenti in letteratura, sono spesso trascurati, divengono fondamentali per le proprietà di controllo dinamico del sistema. Solo se essi sono presi in considerazione, il pressurizzatore è un vero e proprio sistema dinamico, che può presentare tanto una risposta forzata dipendente dagli ingressi esterni, quanto una risposta libera funzione dello stato del sistema.

INTRODUCTION

The continuously increasing demand related to the development of safer and more effective nuclear power plants needs either the improvement or complete re-design of different components.
In this regard, dynamic simulation is an essential tool since the development of detailed dynamic models aids the study of a system in order to build or improve it. Modelling leads to deeper understanding of the behaviour of a system, to the optimization of its technical specifications and to the discovery of its possible weaknesses.
Moreover, a model can be used to answer questions about a system without doing experiments on the real object, especially when these might be too expensive, too dangerous or the system needed for the experiment might not exist yet.
Of course experiments cannot be completely avoided. A model must be always validate with experimental data coming from facilities and prototypes. A model is seldom universal, it gives correct results only inside its range of validity depending on the assumptions on which the model itself is fulfilled.
There are different kinds of models depending on how the model is represented:

- Physical model: this is a physical object that mimics some properties of a real system, to help answer questions about that system.
- Mathematical model: a description of a system where the relationships between variables of the system are expressed in mathematical form. Variables can be measurable. Most laws of nature are mathematical models in this sense.

The kind of model developed in this study is the mathematical one. It will be represented in various ways, as equations and computer programs. In this regards, artefacts represented by mathematical models in a computer are often called virtual prototypes and the process of constructing and investigating such models is virtual prototyping.
Sometimes the term physical modelling is used also for the process of building mathematical models of physical systems in the computer if the structuring and synthesis process is the same as when building real physical models.

Within virtual prototyping there are two different ways:

- the causal approach
- the a-causal approach

Using tools, as MATLAB-Simulink® it is possible to realize ad hoc models of a system, based on the widespread causal approach: this modelling language makes use of block diagram to described the system. It is a refined representation of the behaviour of dynamical systems allowing a natural formulation of control problem. In fact they focalize directly on quantities on which it is possible to exercise an action to operate the evolution of the system.
In the causal approach, variables of the environment that influence the behaviour of the system (inputs) and variables that are determined by the system and may influence the surrounding environment (outputs) are a priori fixed and depend strictly on the boundary conditions. In these models, relationships between quantities are expressed using assignments. An assignment statement sets and/or re-sets the value stored in the storage location(s) denoted by a variable name; in other words, it copies the value into the variable. In most imperative programming languages, the assignment statement (or expression) is a fundamental construct.
A very simple example of assignment is:

$$A=B \tag{I.1}$$

Then the value of B is assigned to A.
However in a lot of systems the same variables act as both inputs and outputs. Precisely, you talk about a-causal behaviour if the relationships or influences between variables do not have a causal direction, which is the case for relationships described by equations. The equivalent equation formulation of the previous assignment example is:

$$f(A,B)=0 \tag{I.2}$$

Which must be solved numerically.
Regarding the a-causal approach, one of the most promising programming languages is Modelica®.
Generally speaking, a system can be almost everything: in nuclear engineering it can be an entire power plant or one of its components whose properties must be studied.
Dynamic modelling has primary importance for a nuclear reactor, which can be licensed if and only if its safety systems and its capability to effectively respond to abnormal transient are verified by a special nuclear regulatory commission. For this purpose certified programs, as RELAP5®, exist but they can take a long time to reproduce just a single transient, with the result that dynamic model of the system and control model can be coupled poorly.

Therefore the development of appropriate tools for the simulation of a nuclear power plant and its subsystems operated with dynamic control for any time interval is very attractive.
Historically models can be distinguished into two main families:

- Linear models, which have the advantage of being able to use simple and systematic linear control design techniques, but also the disadvantage of being valid only when the system operates in a sufficiently small range around an equilibrium point. In fact, as almost every physical system contains nonlinearities, linear models usually derive from the linearization procedure, which is an approximation one, of the non-linear equation of the physical system.
- Non-linear model, which are based directly on fundamental principles without linearization process, can describe the system not only around an equilibrium point, but also along the whole operating range. However they cannot use directly helpful tools which are available for their linear counterparts.

As far as a pressurized water reactor (PWR) is concerned, a very interesting subsystem to study is the so-called pressurizer.
As matter of fact, an accurate modelling of the pressurizer is needed to determine the pressure response of the primary coolant system, and thus to successfully simulate overall PWR nuclear power plant behaviour during normal operations and transients.
So the following study arises with the object to develop a simple but accurate model for the pressurizer component of PWR .
To be able to simulate all possible transients which can occur in a nuclear reactor, the model will be a non-linear one, but it will be subsequently subjected to the linearization procedure in order to do a preliminary study of the stability properties of the pressurizer system. The model will be based on a rigorous application of the first law of the thermodynamics:

$$\Delta U = Q + L \qquad \text{I.3}$$

together with heat and mass transfer laws without making a priori assumptions concerning the thermodynamics path of the processes which take place. Moreover the model would like to put rigorous mathematical bases for a more accurate dynamical control scheme based on the principle of optimum control to be developed in future.
In this regard, the developed model is basically control-oriented, but, unlike previous studies which can be found in literature, it has also the claim to follow in a quantitative way the real physical phenomena occurring inside the pressurizer. Classical pressurizer control models give just a qualitative response.
Therefore model equations will be later implemented using both Simulink®, Modelica® languages.
Simulink® codes, based on causal approach, will show an intrinsically control-oriented method to create a simulation program, in which the problem of control can be treated in a natural, way being itself causal.

However, although Simulink® allows to implement in a simply way any control logic, it requires a long algebraic manipulation of the constitutive equations, which have to be put in assignments form.
On the contrary, Modelica® codes, based on the acausal approach, will demonstrate the potentialities of object-oriented programming: model equations can be directly written down in the simulation program.
Then simulation results, obtained both with Simulink® and Modelica®, will be validated by the comparison with experimental data coming from Shippingport pressurizer experiments.
It must be underlined that the possibility to compare simulations results to real data is a great opportunity and you must not neglect this very important point.
Not always experimental data are available and so a modeller can only hope that his model is close to the reality and unfortunately not always this happens, as you can see later in this work. When any experimental data is not available, the modeller can just compare his model results to those coming from other simulation codes.
Concerning this, another pressurizer model will be created using directly Relap5®, this passage will be fundamental in order to support some hypothesis that will be made in the derivation of the model and to make a validation process possible for those results of Simulink® and Modelica® codes for which any experimental counterparts are not available. To summarize, this is a typical occurrence of the so-called model validation process: a model, to be believable, must be compared with experimental data when these are available, otherwise with the results of other codes.
Therefore the structure of this thesis is the following one:

- CHAPTER 1: where the pressurizer PWR subsystem and the Shippingport experiments results are exposed
- CHAPTER 2: where the pressurizer models are derived
- CHAPTER 3: where simulation codes are developed
- CHAPTER 4: where simulation results are compared together and with the experimental ones
- CHAPTER 5: where a linearized model for the pressurizer is created in order to study its stability properties.

Chapter 1 – THE PRESSURIZER SUBSYSTEM OF PWRs

1.1 INTRODUCTION

In this first chapter the pressurizer subsystem of PWRs (Pressurized Water Reactor) is introduced together with its main components. Then an accurate description of the Shippingport pressurizer follows: in this regard all the geometrical and control logic characteristics are reported in specific tables. The detailed description of the test performed on Shippingport pressurizer closes the chapter.This test was the first study about the transient behaviour of the pressurizer subsystem and nowadays it still represents one of the most important experimental references with which a pressurizer model (having the purpose to simulate real physical phenomena) must be confronted. Such test, carried out in 1960s, includes three different transients induced by loss-of-load starting from three different power levels:

- 51 MW
- 74 MW
- 105 MW

Loss-of-load transients were caused by abrupt reduction of secondary steam flow.

1.2 GENERAL COMPONENT DESCRIPTION

In nuclear Power plants using pressurized water as main coolant, it is necessary to maintain system pressure within prescribed limits. An increase in electricity demand causes the turbine throttle valve to open, thus increasing the steam flow. This causes more heat to flow out of the main coolant causing initial drop in average main coolant temperature. The main coolant average system temperature settles at somewhat higher steady state value after the throttle action ceases. As the turbine throttle valve is closed the reverse action takes place with the main coolant average temperature increasing initially and then settling at a lower value. The volume of the main coolant expands and contracts with these average temperature variations. So a proper component to accommodate these volume changes is required, the pressurizer [1] [2] [3]. Any volume change of main coolant induces water insurges and outsurges in the pressurizer volume. Therefore PWR pressurizer maintains the main coolant pressure within certain boundaries during normal operations and limits pressure excursions during transients and hypothetical accidents.

The pressurizer is made up of a steel tank which contains, at normal operation, saturated water in the lower section and saturated steam in the upper section at a desired saturation temperature and pressure. It is connected to the hot leg of the loop through a surge line.

Important components in the pressurizer include sprayers, electric heaters, power-operated relief valves (PORVs), safety valves (SVs), surge line, and relief tank.

The sprayers, the PORVs and the SVs are equipped at the top of the tank, while electric heaters are immersed in the water. The sprayer and the electric heaters are used to control the system pressure during load transients.

The function of the spray system is to prevent pressure increase by injecting subcooled water into the pressurizer vessel atmosphere to condense steam during water insurges causing pressure increases.

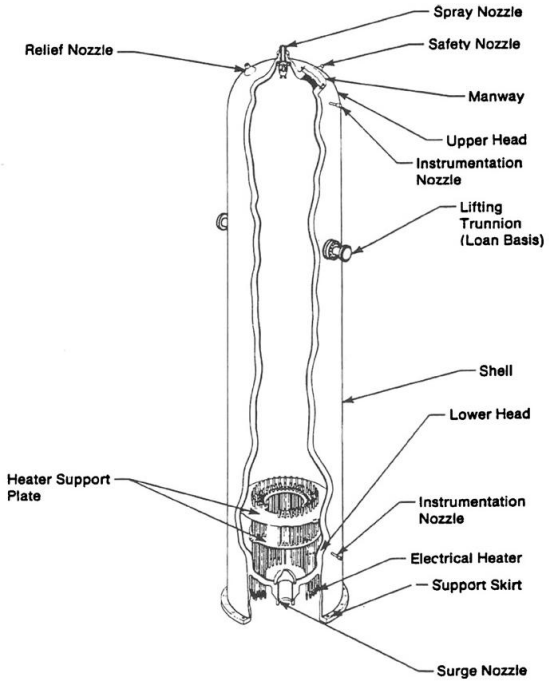

FIG. 1.1 Pressurizer Scheme

The spray water is extracted from the reactor coolant cold piping at the discharge side of the main coolant pump. The pressurizer spray droplets are projected at an angle from the spray nozzle with a high initial velocity and travel to either the pressurizer vessel interior wall or the surface of the saturated water, absorbing heat and mass from the mixture. Contrariwise electrical heaters are activated to heat up the water in the tank during water outsurges causing pressure decrease. The heat flux induces specific water specific volume to rise counteracting pressure negative variations. Generally electric heaters can be classified into proportional heaters and backup heaters. The control of the proportional heater and backup heater is based on the pressure-difference set-points and water-level set-points. The proportional heater adds one half of the rated heating rate to the liquid at normal operation, for a typical PWR they generates power of 350kW at a full rate if the pressure error signal is less than -100 kPa, and is fully turned off if the pressure error signal is greater than +100 kPa. The backup heater can only be fully turned on or off, and is controlled by the pressure error signal together.

So pressurizer is a very important component in the nuclear reactor system not only when the power plant is under steady state operation, but also in case of accident, when pressurizer prevents the main loop system overpressure and keeps the integrity of the main loop system thanks to the safety valve.

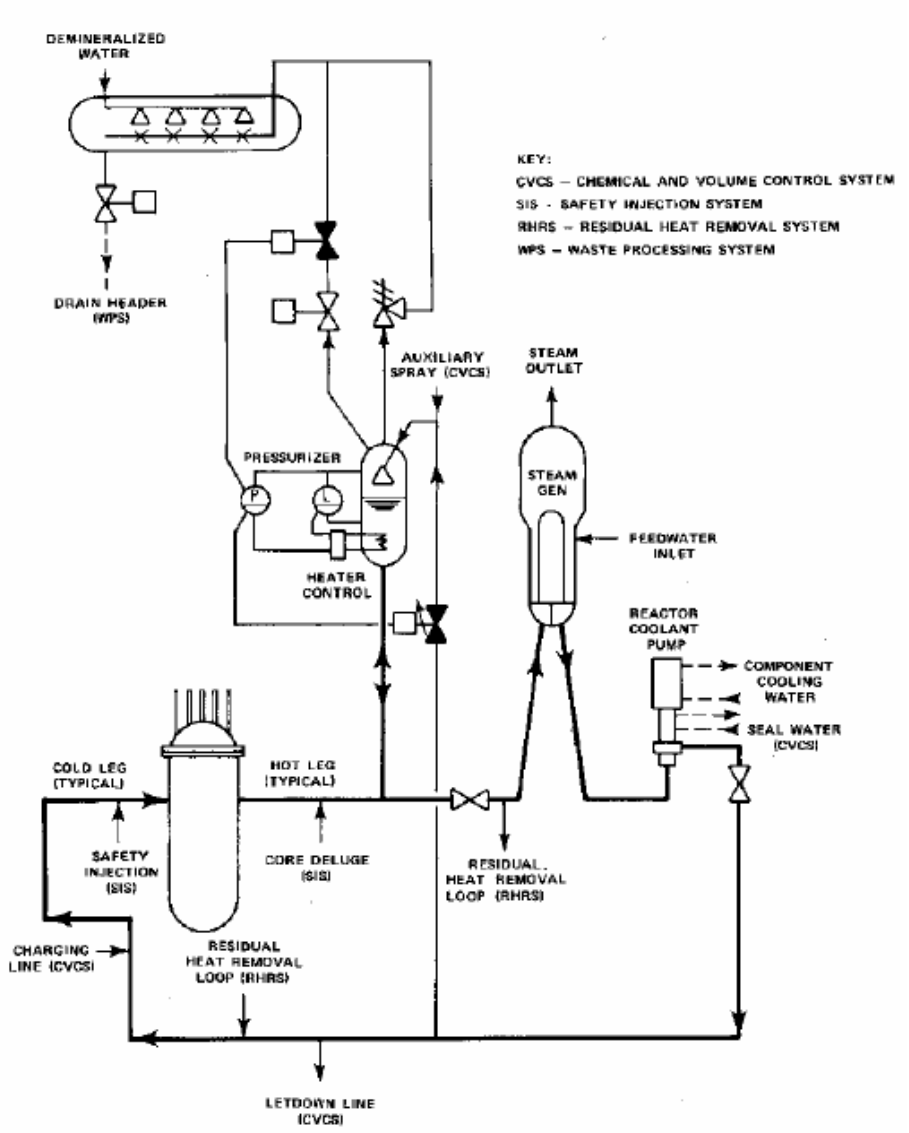

FIG. 1.2 Pressurizer Control Scheme

1.3 SHIPPINGPORT POWER PLANT

LOCATION:	Shippingport, Pennsylvania, 25 miles northwest of Pittsburgh, Beaver County, Pennsylvania, on the Ohio River. UTM Coordinates: Zone 17, Northern Half, 477966 meters (to nearest 100 *m)*
SIGNIFICANCE:	Operational in December, 1957, Shippingport Atomic Power Station was the first large-scale central station nuclear power plant in the United States and the first plant of such size in the world operated solely to produce electric power; it was the first to have training classes for operators and supervisors; it was the first to use a water-cooled breeder core for a power plant.
PROJECT INFORMATION:	The plant which had been run for 25 years by the DOE Naval Reactors program has been shut down and responsibility transferred to DOE's Office of Terminal Waste Disposal and Remedial Action. The objective of this Office is to decontaminate and decommission the site, making it safe from a radiation standpoint for unrestricted return to the owner. An auxiliary objective of the project is to serve as a decommissioning demonstration to the nuclear industry by providing useful information and data for future decommissioning projects.

TABLE 1.1 Shippingport History

At 4:30 a.m. on December 2, 1957, the Shippingport Atomic Power Station reached criticality, becoming the first large-scale central station nuclear power plant to attain a chain reaction. It reached full power at sixty-eight megawatts five days later.
In 1964 the plant was temporarily shut down to install a new reactor core that increased the electrical generating capacity to one hundred megawatts.
The Shippingport Atomic Power Station reactor was of the pressurised water type. In this approach uranium is the fuel and water, kept under pressure to prevent boiling, removed heat from the core and moderated the neutrons to the energies at which the fission process could continue.
Movable hafnium control rods absorbed excess neutrons. Two separate systems converted the reactor's heat to steam to produce electricity.
In the first or primary system, water flowed from the core through a heat exchanger called a steam generator and back again. In the steam generator, heat from the primary system passed through tubes to water in a secondary system.

In the secondary system water flashed to steam to drive the turbine and electric generator, condensed, and returned to the steam generator. Shippingport proved that an atomic power station could function on a utility network as a base load plant or as a swing load plant meeting the demand for power which increases and decreases during a given period. The success of Shippingport was of particular concern to the Eisenhower administration. At the United Nations Second International Conference on the Peaceful Uses of Atomic Energy, held in Geneva, Switzerland from September 1-13, 1958, a cutaway model of the Shippingport pressure vessel and core easily dominated the American exhibit.
A collection of technical papers on the atomic power station made up one of the thirteen presentation volumes describing the American atomic energy program.
The station even became a piece in the game of international politics, for it was a prominent feature on the itineraries of many foreign dignitaries as evidence of American leadership in peaceful application of the atom.
Most of Shippingport contributions were highly technical. Some of the reactor components (main coolant pumps, valves, piping, and steam generators) were the first to be designed, developed, and fabricated for civilian nuclear power application. Shippingport was the first reactor to have a containment, a structure which housed in a series of large, interconnected, steam-tight vessels all parts of the plant containing the reactor and primary system. The development of uranium dioxide fuel contained in Zircaloy tubing proved outstandingly successful and has been widely adopted in the industry. In 1977 Shippingport began operating on a thorium-uranium 233 core to demonstrate the feasibility of breeding in a water-cooled reactor; that is, producing more reactor fuel than was consumed.

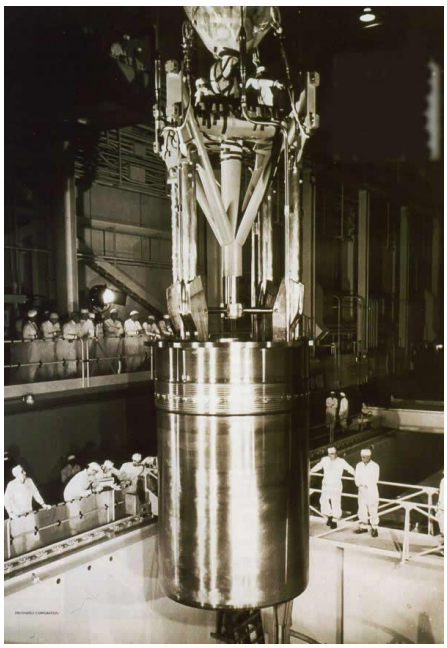

FIG. 1.3 Shippingport Pressure-Vessel

The project was called the "LWBR" or the "Light Water Breeder Reactor". The light water breeder core was designed so that the concept could be widely adopted by other pressurized water reactor power plants. Because it was a government-owned reactor, Shippingport was not subject to many regulatory requirements. However, so that commercial application could be fully demonstrated, Admiral Rickover determined from the beginning that Shippingport was to adhere to the regulations which would govern commercial ventures to the fullest extent possible for design, construction, and operation. Thus the Reactor Safeguard Committee (predecessor of the Advisory Committee on Reactor Safeguards) reviewed the original site selection. For the same reason, Admiral Rickover applied industry standards, such as the ASME (American Society of Mechanical Engineers) Boiler and pressure Vessel Code, which included a special state permit, as the basis to develop nuclear standards; and environmental standards, which included obtaining a special state permit for release of processed, purified, radioactive waste water. The design, technology and standards were to be unclassified. An independent regulatory group within the Atomic Energy Commission responsible for licensing commercial reactors reviewed a safety analysis reports at each partial and complete re-fuelling of the reactor. Modifications to the reactor plant were made periodically to upgrade the reactor and reactor operations to reflect lessons learned at Shippingport and at other licensed commercial reactors.

1.4 SHIPPINGPORT PRESSURIZER TEST

Shippingport pressurizer tests were conducted in 1967 [4].
Descriptions of these experimental studies are reported in the subsequent pages.
Abrupt reduction of the secondary steam flow in a pressurized water reactor results first in a reduction of the rate of heat removal from the primary coolant.
At first, the rate of heat addiction within the reactor remains constant, so heat addiction exceeds heat removal, and the primary coolant becomes hotter and expands. The result is a pressurizer insurge, a flow of water from the primary loop thought the surge line into the pressurizer.
The first increase in primary coolant temperature occurs within the steam generator. This temperature increase reaches the core inlet after a delay equal to the time required for the coolant to flow through the steam generator outlet plenum, the cold leg piping and the reactor inlet plenum and when it does reach the core, its immediate effect is to introduce negative reactivity and hence to start reduce in reactor power.
In typical transients, the reduction in reactor power continues until the power delivered by the reactor actually drops below the power being removed by the secondary system. Thus the net rate of heat addition goes from a positive value just after the reduction in secondary steam flow, passes through zero, becomes negative, and finally approaches zero as the reactor power recovers from its undershoot and approaches the power being removed by the secondary steam flow. Correspondingly, the pressurizer sees an insurge which slows, drops to zero, reverses, and becomes outsurge. Pressure normally increase during an insurge and decrease during an outsurge. Heaters and a spray system are used to maintain the pressure within a control band. While an insurge normally causes an increase in pressure and an outsurge a decrease in pressure, the activation of the pressurizer spray and pressurizer heaters may override the surge effects. Thus with a spray on, it is possible to have decreasing pressure during an insurge.
Loss-of-load transients form high power levels induce the most rapid insurges that a pressurizer will ever experience and are much more severe than normal load demand transients. To reduce the severity of these transients, Shippingport plant has a controlled steam relief system in the secondary side to prevent excessive primary-plant pressure surges following greater-than-normal system steam-plant load reductions. The controlled steam relief system permits the transfer of large steam-generator load reductions to the reactor in a series of smaller steps. The system operates by dumping secondary steam through relief valves while feed water is simultaneously supplied from special makeup tanks. When the initial power level is between 75 and 108 MWe and complete loss of load occurs, the system releases a steam flow equivalent to approximately 35 MWe through the steam relief valves. After several minutes, one of the two valves allowing steam flow is closed, reducing the equivalent power to 10MWe. The second valve is closed several minutes later, terminating all secondary steam flow. Similarly, when the initial power level is between 52 and 74 MWe a complete loss of load results in a steam flow equivalent to a power level of 10MWe before steam flow finally terminates. Loss of load transient form 51MWe or below does not cause a pressure transient severe enough to

warrant operation of the controlled steam relief system. As the load is thus reduced to zero in a series of steps, the flow through the surge line executes a series of insurges-outsurges cycles. This surge behaviour will be described in more detail below.
The Shippingport pressurizer was cylindrical, with a diameter of 1.371 m and a total volume of 7.419 m^3(total primary volume was ≈ 84.951 m^3). Pressure is maintained within control by three banks of electrical heaters, a spray system, and both steam and water relief valves. These systems have on-off control, and typical capacities and set pints are indicate in table 1.2, the pressurizer and its instrumentation sensors are shown in figure 1.4.

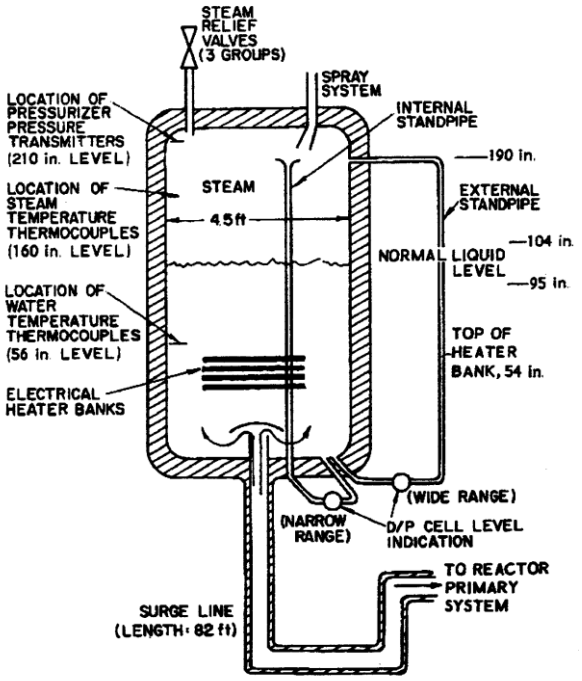

FIG. 1.4 Functional drawing of Shippingport pressurizer

SPRAY FLOW [kg/s]	1.9089	TURN-ON PRESSURE [bar]	142.721	SHUT-OFF PRESSURE [bar]	139.619
SPRAY TEMPERATURE [°C]	260				
HEATING RATING bank 1 [kW]	40	TURN-ON TEMPERATURE [°C]	332.222	TURN-OFF TEMPERATURE [°C]	335.556
HEATING RATING bank 2 [kW]	80	TURN-ON PRESSURE [bar]	133.516	SHUT-OFF PRESSURE [bar]	137.895
HEATIN RATING bank 3 [kW]	250	TURN-ON PRESSURE [bar]	131.414	SHUT-OFF PRESSURE [bar]	138.929

TABLE 1.2 Pressure Control Parameters

The following instruments were used to measure pressurizer data during the loss-of-load transient test: wide- and narrow-range pressurizer pressure, wide and narrow-range pressurizer level, wide- and narrow-range pressurizer water temperature and wide- and

narrow-range pressurizer steam temperature. Range, accuracy and response time are summarize in table 1.3.

CHANNEL	SENSOR	RANGE	ACCURACY		RESPOND TIME
			ABSOLUTE	DIFFERENTIAL	
Wide-range pressure	Bourdon tube	0-206 [bar]	± 2 [bar]	± 0.35 [bar]	1 [s]
Narrow-range pressure	Bourdon tube	120-155 [bar]	± 0.35 [bar]	± 0.35 [bar]	1 [s]
Wide-range level	External standpipe; differential pressure transducer	0-5 [m]	± 0.05 [m]	± 0.05 [m]	3 [s]
Narrow-range level	Internal standpipe; differential pressure transducer	0.6-3.2 [m]	± 0.025 [m]	± 0.025 [m]	3 [s]
Wide-range water temperature	Resistance thermometer	38-370 [°C]	± 5 [°C]	± 0.5 [°C]	5 [s]
Wide-range steam temperature	Thermocouple	38-370 [°C]	± 3 [°C]	± 0.5 [°C]	5 [s]

TABLE 1.3 Instrumentation for loss of load transient test

Pressure was measured by two instruments mounted ≈ 5.334 m from the bottom of the pressurizer. The narrow-range and wide-range pressurizer pressure instruments are both bourdon tube. Both instrument chains are identical, except that the narrow-range dial indicator reads from 120.658 bar to 155.132 bar, while the wide-range indicator reads from 0 to 206.843 bar. The uncertainty in absolute pressure of the indicated wide-range pressurizer pressure is approximately ± 2.068 bar, based on 1% full scale. However, the accuracy for pressure swings, using differential pressure measurements, is ± 0.345 bar. This accuracy has been arrived at by inter-comparison of the narrow-range and wide-range pressurizer pressure data with pressurizer steam and water temperature data during large pressurizer outsurges when saturation conditions exist.

Two pressurizer level instrumentations are installed in the Shippingport pressurizer. As shown in figure 1.4, each operates by using a transducer to measure the differential pressure between a reference standpipe and a tap in the lower shell of the pressurizer. The wide-range level instrument uses an external standpipe at ambient temperature to provide reference leg, while the narrow-range pressurizer level instrument uses an internal standpipe at pressurizer temperature and pressure. Otherwise, the wide-range and the narrow-range instruments are similar. The narrow-range pressurizer level indicator has a full-scale reading from 0.635 to 3.175 m, which covers the normal liquid range of 2.388 to 2.642 m. The wide-range indicator has a full-scale reading from 0 to 5.080 m. The absolute static accuracy of the pressurizer level instrument is ±1% of the full-scale dial face, or ± 0.051 m for the wide-range instrument and ±0.025 m for the narrow-range instrument. In pressurizer level systems using an external standpipe, the liquid in the external standpipe is, in general, not at the same temperature as the liquid in the

pressurizer. For this reason, the level indications must be corrected for the density variation with temperature. These density variations are negligible for an internal standpipe where the standpipe liquid has the same temperature and density as pressurizer liquid. Because any density corrections are needed, the internal-standpipe system has better static accuracy than the external-standpipe system. On the other hand, the internal standpipe is filled with water at pressurizer temperature and pressure and hence is subject to flashing during rapid outsurges. For this reason, more reliable transients indications are obtained from the wide-range instrument which has an ambient temperature standpipe and hence is not subject to flashing. During insurges and slow outsurges, when flashing did not occur, visual observation of the narrow –range pressurizer level instrument were found to confirm the corrected wide-range pressurizer level data as expected. The pressurizer water temperature, wide range, is measured by a thermal resistance detector mounted in a well in the pressurizer wall at a height of 1.422 m from the bottom of the pressurizer. A narrow-range water temperature instrument is installed, and, although not used to supply data during the loss-of-load transient testing, it did provide an initial steady-state comparison to the wide-range pressurizer water temperature. During steady state and also during outsurges, the bulk temperature of water in expected to be relatively uniform, so that the water temperature as measured at 1.422 m would be indicative of the average, or bulk, temperature (The normal pressurizer water level is 2.540 m). However, even in steady state, this regarding may be influenced by local effects when the heaters are on since the top row of heaters is at 1.372 m. The absolute value of water temperature is stated to be accurate to 5 °C, although the differential accuracy is believed to be accurate over short ranges (15°C) to ±0.5 °C.

The first load-drop test was initiated form 51MWe to indicate the maximum pressure variation when the controlled steam relief system was inoperative. The experimental results for this transient are presented in figure 1.5. The forcing function is the steam load which is seen to fall rapidly to zero. The swell of the primary coolant causes the resulting rise in the pressurizer level. The water level rises rapidly for the first two minutes, then reaches a peak at about three minutes, and finally recedes very slightly. The maximum water-level change was 0.777 m which correspond to a 1.147 m^3 volume change. The water level remains high due to the increase in stored heat in the primary loop, and the reactor core is essentially shut down by the negative temperature coefficient of reactivity. The rapid insurge of water causes a compression of the pressurizer steam and a pressure rise. The pressurizer spray is actuated within the first 0.25 minutes and has a significant effect in limiting the pressure peak. This is indicated at about 1 minute, while the insurge continues until 3 minutes. The primary steam and water relief valve were not actuated in this transient or in any other loss off transient in the series (the steam relief valve shown figure 1.4 are in the primary system and should not be confused with the secondary steam relief system described above. The primary steam relief valves were not operated during test described). The surge flow were deduced from measured water-level data. Note that a level change cannot be interpreted directly in terms of surge flow since the level change includes stream condensation or evaporation.

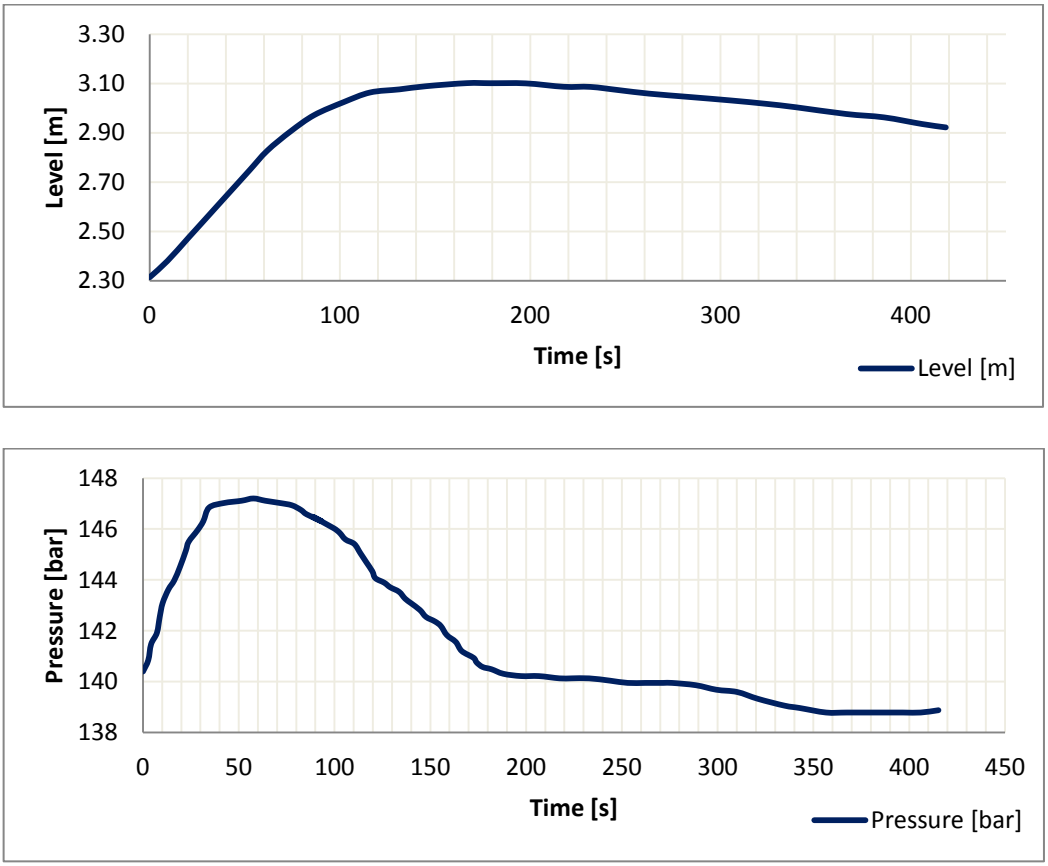

FIG. 1.5 Pressurizer transient loss of load from 51 MWe. Experimental results [level: m vs. s] [pressure: bar vs. s]

The second load-drop test was initiated form 74 MWe to indicate the maximum pressure variation when the controlled steam relief system had only on intermediate secondary steam load. The result for this transient are presented in figure 1.6. the steam load forcing function falls immediately to 10 MWe and remains there until slightly after six minutes when the load is reduced to zero. These power imbalances induce two cyclic pressurizer level changes. The first insurge raises the pressurizer level 0.635 m (0.934 m^3) at two minutes and is followed by a level drop of about equal magnitude which reaches a minimum slightly after six minutes. The load decreases at six and one-half minutes induces a second pressurizer level change of 0.457 m (0.680 m^3). Which is followed by an outsurge of about the same magnitude.

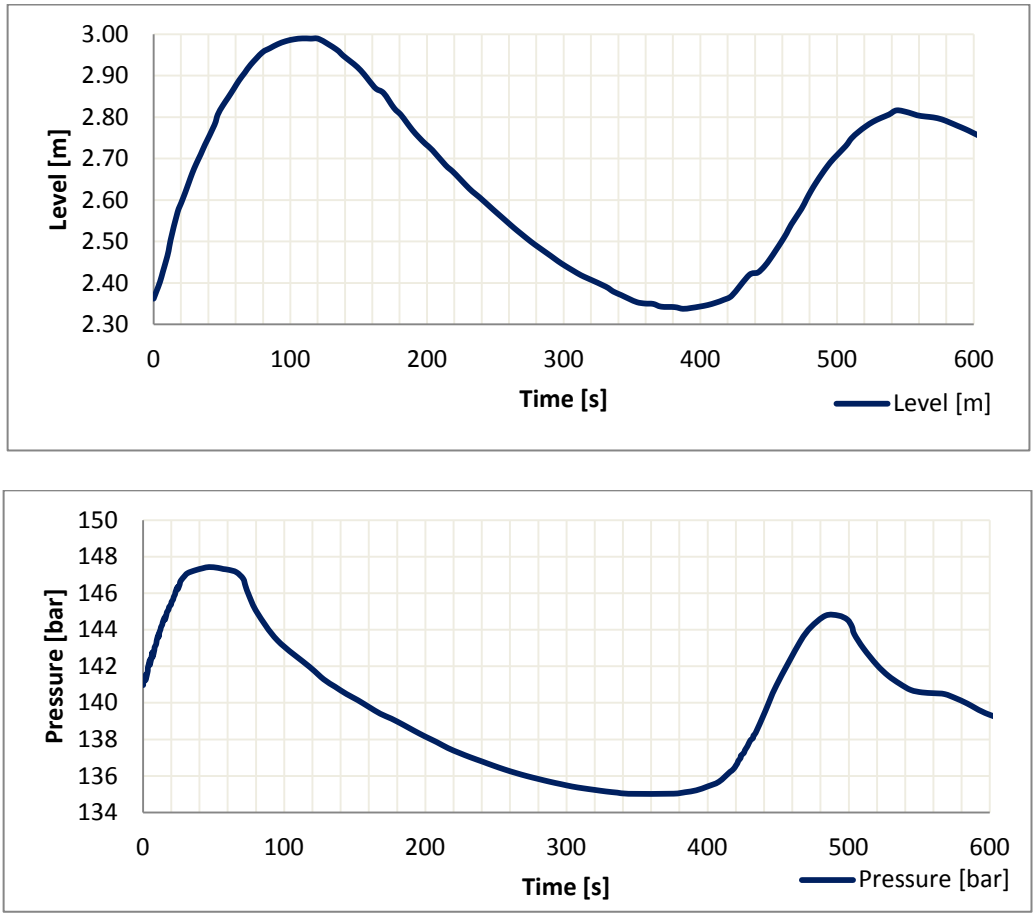

FIG. 1.6 Pressurizer transient loss of load from 74 MWe. Experimental results [level: m vs. s] [pressure: bar vs. s]

The third load-drop test was initiated form 105 MWe and indicates the plant response as the controlled steam relief system reduced load sequentially to 35 MWe, 10 MWe and then to zero. Figure 1.7. represent the steam load forcing function, the pressurizer level change and the resulting pressure variation for this transient. The pressurizer level shows three cyclic variations: an insurge of 0.483 m (0.708 m^3), an outsurge of 0.406 m (0.595 m^3), an insurge of 0.292 m (0.425 m^3), an outsurge of 0.254 m (0.368 m^3), an insurge of 0.051 m (0.074 m^3), and finally an outsurge of 0.254 m (0.368 m^3).

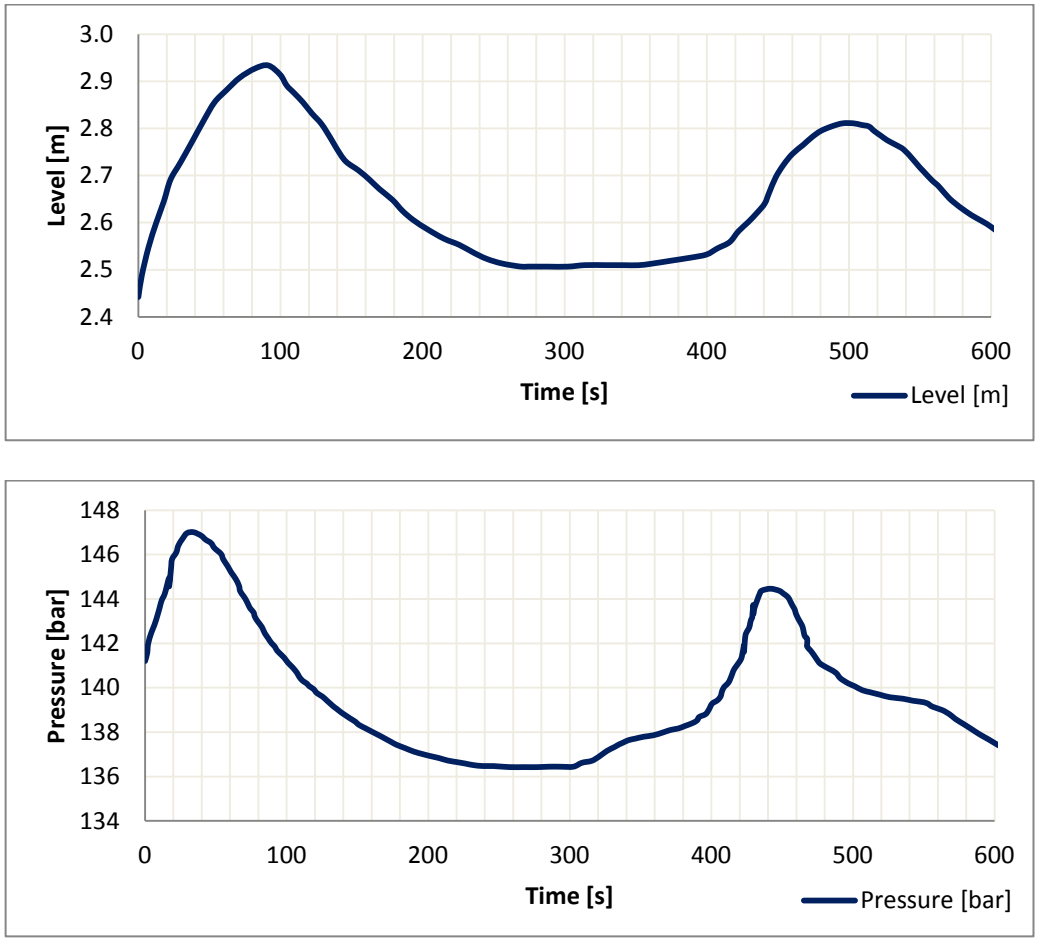

FIG. 1.7 Pressurizer transient loss of load from 105 MWe. Experimental results [level: m vs. s] [pressure: bar vs. s]

1.5 CONCLUDING REMARKS

In this chapter the entire description about the pressurizer subsystem and its characteristic have been reported and Shippingport experimental campaign has been described.
Now it is possible to imagine the numerous thermodynamic processes which can happen inside the water-steam tank of the pressurizer: evaporation, condensation mass, and heat exchanges.
Moreover it can be understood that transients which will be simulated are very far from simply step inputs: rapid changes of mass flow rate, and therefore of pressure, occur.
So the computer simulation will deal with a very stiff problem.

1.6 REFERENCES

[1] IMPIANTI NUCLEARI
Carlo Lombardi
Polipress
3rd edition 2009

[2] IMPIANTI NUCLEARI
Maurizio Cumo
Università la Sapienza
3rd edition 2009

[3] NUCLEAR SYSTEMS VOLUME 0NE-THERMAL-HYDRAULICS FUNDAMENTALS
Neil E. Todreas and Mujid J. Kazimi
CRC PRESS –Second Ediction 2012

[4] REDFIELD, J.A.; PRESCOP, V.; MARGOLIS, S.G.
Pressurizer performance during-load drop. Tests at Shippingport: analysis and test.
Trans. Am. Nucl. Soc: 323, June1967.

Chapter 2 – THE PRESSURIZER MATHEMATICAL MODEL

2.1 INTRODUCTION

In this chapter the fundamental formulation of the so-called two-regions pressurizer model is presented. The developed model is a non-equilibrium thermodynamic one, in which water and steam phase present in the pressurizer tank can be either at saturation condition or, respectively, either at subcooled or superheated one.
Any thermodynamics path is assumed a priori.
In the first section, the state of the art of pressurizer modelling is depicted starting from the first simple equilibrium models to the more complex non-equilibrium ones.
Then a very simple homogeneous mixture model, usually used for control application, is presented in order to demonstrate the poor agreement of this kind of model with the experimental data and, therefore, the need to develop a more detailed control-oriented approach. So the so-called two-regions-one-volume model is explained [3], based on the application of the mass and energy conservation equations to the steam and liquid regions; exchanges between the two regions, due to evaporation of liquid and condensation of steam, are taken into account. Subsequently, to consider temperature distribution across the liquid region, which is necessary to create an accurate model, the so-called two-regions-two-volumes and two-regions-three-volumes models are shown. In the first, just a single liquid control volume is added to the original two-phase one, in the second, the added only liquid volumes are two in order to obtain a better estimation of temperature distribution. At the boundary layers of new control volumes, heat and mass exchanges with the original two-phase volume can occur. In this way both climbing and descendant water mass flow across the different liquid volumes, respectively during insurge and outsurge transient, are also considered. At the end of every model computation, the non linear system of equation describing it, is put into matrix form.

2.2 STATE OF THE ART

In a pressurized water reactor system, the prediction of the pressure during various transients is essential to operate the reactor safely or to decide what actions should be taken to control or mitigate the consequence of an accident. After the TMI-2[1] accident a lot of people realized the importance of small break LOCA's and the necessity to have reliable physical models for all of the components in the loop so that computer experiments could be run and the best strategies adopted for handling accidents.
For this purpose, the pressure predictions made by the computer codes based on the equilibrium pressurizer models developed in the early 1960's are not always satisfactory.
In fact among analytical approaches to the dynamic analysis of a pressurizer, the two following methods are worthy of particular consideration:

- Equilibrium thermodynamic model
- Non-equilibrium thermodynamic model.

The equilibrium model applies the conservation equations of mass and energy to the liquid and steam as a whole, while treating the pressurizer steam and liquid content as saturated masses at the same temperature. The non-equilibrium model applies the conservation equations of mass and energy to the liquid and steam in the pressurizer separately, considering a distinct temperature for each phase. Each model is further equipped with provisions to consider the effect of the operation of sprayer, heaters, relief valve, as well as the reactor coolant system surge.
A comparison of the equilibrium and the non-equilibrium thermo-dynamic models has been undertaken and the relative merits of these two concepts in predicting the pressurizer transient behaviour have been assessed. The comparison revealed that for the case of insurge where single-phase liquid prevails, the non-equilibrium model can be made to approximate experimental data quite well, while the performance of the equilibrium model is very poor. However, for outsurge when the two phase liquid prevails, the equilibrium model, automatically accounting for bulk boiling and condensation, reduces the distances between non-equilibrium one.

[1] The Three Mile Island accident was a partial nuclear meltdown which occurred in one of the two Three Mile Island nuclear reactors in Dauphin County, Pennsylvania, United States, on March 28, 1979. It was the worst accident in U.S. commercial nuclear power plant history. The power plant was named after the island on which it was situated, and was owned and operated by General Public Utilities and Metropolitan Edison (Met Ed). The reactor involved in the accident, Unit 2, was a pressurized water reactor manufactured by Babcock & Wilcox. The accident began at 4 a.m. on Wednesday, March 28, 1979, with failures in the non-nuclear secondary system, followed by a stuck-open pilot-operated relief valve (PORV) in the primary system, which allowed large amounts of nuclear reactor coolant to escape

Moreover a lot of pressurizer analysis methods developed employ combinations of various a priory assumptions on the thermodynamic state of water and steam, but realistic pressurizer calculations require not a priori assumed thermodynamic path of the process to be simulated.
Numerous theoretical and experimental studies have been undertaken to evaluate the behaviour of the pressurizer in a nuclear power plant following insurge or outsurge transients.
In 1955, W.J. GAJEWSKI [5] presents an equilibrium model for the pressurizer behaviour. Two basic assumptions are used:

- The steam and water always remain saturated and form an homogenous mixture
- Due to poor water conductivity and insulation of walls, isentropic compression occurs

Subsequently, in 1960, C.W. SORENSON [6] obtains simple equations relating pressure variations to insurge or outsurge mass flow. The method permits fast calculations of the behaviour of the pressurizer without the need of a computer. Sorenson finds that there are three regions in the pressurizer: an upper region of saturated steam, a region intermediate liquid saturated and a lower region of compressed fluid from the hot leg from the reactor. The thermodynamics states of three the regions are fixed.
In 1965, K. D. COUGHREN [7] establishes using the same three regions Sorenson, certain equations for the pressurizer, having as main hypothesis always saturated steam. However, he does not show any calculation or comparison with experiments.
DRUCKER TONG [8] and later DRUCKER and GORMAN [9] in 1965 develop a model in which the steam is a thermodynamic system that loses latent and sensible heat to the walls and the liquid, considered as sinks heat. Their model takes into account also the condensation of steam on the drops of spray.
BOSLEY, LEDDICK and DRUCKER [10] shows that the assumption of isentropic compression was unrealistic, precisely because of heat losses. Furthermore, G.BROWN [11] demonstrates that the spray droplets reach saturation temperature before arriving into water.
In 1965, REDFIELD and MARGOLIS [4] use the results of Drucker and Gorman, that not only the steam cannot be always assumed saturated, but, on the contrary, their status cannot be determined a priori, and must be determined at each instant of the transient. Thus, they create the “TOPS” program, based on a rigorous application of the first law of thermodynamics coupled with heat and mass transfer coefficients empirically determined. In the "TOPS" code the evaporation (the so-called flashing) process is assumed to be a water surface phenomenon and consequently the flashing rate is independent of the water phase mass. This latter model seems to be unrealistic because the bulk of water phase (with steady state spray) actually flashes as the pressure drops below the saturation pressure.

In 1967, NAHAVANDI [12] shows that non-equilibrium models (thermodynamic state and the temperature of the steam may be distinct from those for the liquid) are much more realistic than the saturated ones. Moreover, their work shows that the theoretical curve of pressure in non-equilibrium model can be extremely sensitive to a certain coefficient.
In 1970 NAHAVANDI and MAKKENCHERY [13] publish a work about a non-equilibrium model applying conservation equations of mass and energy separately to vapor and liquid under conditions of transient complex load. Their merit is to have realized that the extreme sensitivity of the theoretical curves to a coefficient of condensation or evaporation in the vapor-liquid interface could be resolved if both the mechanisms of condensation on the spray droplets and bulk evaporation and condensation are taken into account. For the definition of the flashing and condensing process, Nahavandi and Makkenchery use a thermodynamic criteria which is very robust : it is assumed that neither phase can exist in meta-stable form; i.e, the steam can be either satured or superheated but not subcooled, whereas the liquid can be either satured or subcooled but not superheated.
In 1973, BARON [14], using a similar model to that of Nahavandi, develops a digital program and applies it to transient load pressurizer Shippingport, obtaining good results. In the model proposed by Baron, the flashing and condensing rate are dependent respectively on the steam bubble rise and condensate drop velocities. These velocities are extracted from the experimental data obtained by Patterson [15] et al., however, these measurements are conducted at-specific thermodynamic and geometrical conditions (20.684-41.369 bar pressure and 0.483 m in vessel diameter), which are much different from the real pressurizer conditions (151.685 bar pressure and 2.540 m diameter).
In 1986 a very simple homogenous model is developed by HACK YEONG CHUNG, TAE WOON KIM, SOON HEUNG CHANG and BYUNG HO LEE [16].
This model, unlike the previous ones, is a control-oriented one. Its main task is the development of an adaptive Kalman gain approach to on-line instrument failure detection and not the exact simulation of pressure transients. Water and steam inside the pressurizer tank are considered, as in the model of W.J. Gajewski, as a homogeneous mixture. Moreover, the authors, by expanding model equations in Taylor series about a nominal operation point (ignoring terms higher than the first order), obtain a linearized model to which typical tools of control are applied.
In 1998 a very interesting model is developed by BEYNON and KURIDAN [17]. It is a non-equilibrium model, to which a linearization process is applied. Therefore it could act as starting point to implement the typical tools of automatic control to a more efficient model for the pressurizer.
Finally in 2008 DAVID A. BOTELHO, PAULO A.B. DE SAMPAIO, CELSO M.F. LAPA, CLAUDIO M.N.A. PEREIRA , MARIA DE LOURDES MOREIRA AND ANTONIO CARLOS DE O. BARROSO [18] developed a pressurizer model for the IRIS reactor characterized by the absence of the sprayers system, which is not present in IRIS project. In this model two liquid control volumes have been introduced, one with a fixed boundary and the other with a moving one. Moreover, they calculated the mass

flow rate due to steam condensation on the wall in the steam volume using the Nusselt's [19] [20] theory to compute the heat transfer coefficient.
Finally the most important studies present in literature are based on these assumptions:

- The space inside the pressurizer is divided into two independent control volumes, steam and water, separated with a liquid interface. During steady state the steam and water phases are in thermal equilibrium.
- Conservation equations of energy and mass are applied to each phase
- The processes of mass transfer taking place between steam and liquid phases inside a pressurizer are due to the rate of steam condensation and the rate of bubbles rise. Variation in the average primary coolant temperature in a pressurized water reactor systems leads to a direct variation in the water volume and hence the pressure inside the pressurizer.
- Spray plus condensate mixture enters the water phase as saturated liquid
- The enthalpy of the sprayed water inside the pressurizer is the same as that of the reactor coolant cold leg
- Pressurizer is adiabatic
- The processes of steam condensation on vessel wall and water surface are neglected compared to other mass transfer terms
- Delay times of bubbles rise and condensate fall are neglected
- Insurge water mixes completely with water already present in the pressurizer.
- Steam discharged through the relief valve is taken zero.

As shown in the new model presented in the next pages, not all of these assumptions are really verified, in particular the splitting up of pressurizer volume in only two regions lead to an elegant model, but too simple to take into account temperature distributions occurring inside liquid volume. Moreover both thermal dissipations and wall steam condensing are important for the control of pressure in pressurizer volume.

2.3 EQUILIBRIUM PRESSURIZER MODEL

A lot of control-oriented models are based on thermodynamic equilibrium approach for the pressurizer two phase system.
In this case, characteristic equations are much simpler than those arising from the non-equilibrium study: water and steam homogeneous mixture remains always at saturation condition, so that the system description does not chance during transients.
Therefore the non-linear system describing the equilibrium pressurizer can be manipulated easily to make it suitable for the development of a control analysis.
However, the price to pay for this simpler study of control properties of the system, is a poor reproduction of the real behaviour of the physical system, as it will be shown in the next chapter.
In the model introduced here, water and steam are assumed to be a homogeneous satured mixture. Appling mass and energy balance to the whole volume of the pressurizer:

$$\frac{dM_P}{dt} = \dot{m}_P = \dot{m}_{IN} - \dot{m}_{OUT} + \dot{m}_{SP} - \dot{m}_{VLV} \tag{2.1}$$

$$\frac{dU_P}{dt} = \dot{m}_{IN} \cdot h_f - \dot{m}_{OUT} \cdot h_P + \dot{m}_{SP} \cdot h_{SP} - \dot{m}_{VLV} \cdot h_g + Q \tag{2.2}$$

Q is the power of the heaters. Generally in this kind of models the pressurizer is considered adiabatic. Remembering that:

$$h = u - pv \tag{2.3}$$

Then the energy conservation principle for the mixture can be written:

$$m_P \cdot \dot{h}_P - V_P \cdot \dot{p} = \dot{m}_{IN} \cdot \left(h_f - h_P\right) + \dot{m}_{SP} \cdot (h_{SP} - h_P) - \dot{m}_{VLV} \cdot \left(h_g - h_P\right) + Q \tag{2.4}$$

It must be underlined that, from a physical point of view the enthalpy of water entering in the pressurizer volume during insurges is not the satured liquid enthalpy at the pressurizer pressure, but it is the enthalpy at pressure and temperature of the hot leg of the reactor. However, this unphysical simplification (which points the roughness of the model up) is necessary in order to maintain saturation conditions inside the pressurizer tank. If water came with its real enthalpy, the model would fail because of the steam quality would become negative. h_P and v_P are respectively the mean mixture enthalpy and the mean mixture specific volume, which can be obtained in the subsequent way:

$$v_P = \frac{V_P}{M_P} = v_f + X_P \cdot \left(v_g - v_f\right) \tag{2.5}$$

$$h_P = h_f + X_P \cdot \left(h_g - h\right) \tag{2.6}$$

Where h_f, h_g , ν_f and ν_g are respectively satured liquid and satured steam enthalpy and satured liquid and satured steam specific volume. X_P is the quality of fluid mixture in the pressurizer.
Taking into account the constraint on fixed pressurizer volume:

$$\dot{V}_P = \frac{d\left(\frac{M_P}{V_P}\right)}{dt} = \frac{\dot{m}_P \cdot \rho_P - \dot{\rho}_P \cdot m_p}{\rho_P^2} = 0 \rightarrow V_P \cdot \dot{\rho}_P = \dot{m}_P \tag{2.7}$$

Now, all the equations can be summarized in form of matrix:

$$\Psi \cdot \dot{z} = \eta \tag{2.8}$$

To obtain the ODE system it is sufficient to resolve this set of equation respect to $\dot{z}$ reverting matrix Ψ:

$$\dot{z} = \Psi^{-1}\eta \tag{2.9}$$

So the system is finally put in this form:

$$\dot{z} = f(z, u) \tag{2.10}$$

Where, in the language of control, z is the state variables vector and u the input variable vector. The desired state variables for the pressurizer model are P, pressure, and Xp, mixture quality.

$$z = \{p, X_P\}^T$$

Using enthalpy and quality as natural thermodynamic variables:

$$h = h(p, x) \rightarrow \frac{dh}{dt} = \frac{\partial h}{\partial p}\frac{dp}{dt} + \frac{\partial h}{\partial x}\frac{dx}{dt} = \frac{\partial h}{\partial p}\dot{p} + \frac{\partial h}{\partial x}\dot{x} \tag{2.11}$$

$$\rho = \rho(p, x) \rightarrow \frac{d\rho}{dt} = \frac{\partial \rho}{\partial p}\frac{dp}{dt} + \frac{\partial \rho}{\partial x}\frac{dx}{dt} = \frac{\partial \rho}{\partial p}\dot{p} + \frac{\partial \rho}{\partial x}\dot{x} \tag{2.12}$$

Finally:

$$\begin{aligned}\rho_P V_p \left(\frac{\partial h_P}{\partial p}\dot{p} + \frac{\partial h_P}{\partial X_P}\dot{X}_P\right) - V_P \cdot \dot{p} \\ = \dot{m}_{IN} \cdot \left(h_f - h_P\right) + \dot{m}_{SP} \cdot (h_{SP} - h_P) - \dot{m}_{VLV} \cdot \left(h_g - h_P\right) + Q\end{aligned} \tag{2.13}$$

$$V_P \cdot \left(\frac{\partial \rho_P}{\partial p}\dot{p} + \frac{\partial \rho_P}{\partial X_P}\dot{X}_P\right) = \dot{m}_{IN} - \dot{m}_{OUT} + \dot{m}_{SP} - \dot{m}_{VLV} \tag{2.14}$$

In matrix form:

$$\Psi = \begin{vmatrix} V_P \dfrac{\partial \rho_P}{\partial p} & V_P \dfrac{\partial \rho_P}{\partial X_P} \\ V_P \left(\rho_P \dfrac{\partial h_P}{\partial p} - 1\right) & V_P \rho_P \dfrac{\partial h_P}{\partial X_P} \end{vmatrix}$$

$$\dot{z} = \left\{\dot{p}, \dot{X}_P\right\}^T$$

$$\eta = \begin{vmatrix} \dot{m}_{IN} - \dot{m}_{OUT} + \dot{m}_{SP} - \dot{m}_{VLV} \\ \dot{m}_{IN} \cdot \left(h_f - h_P\right) + \dot{m}_{SP} \cdot \left(h_{SP} - h_P\right) - \dot{m}_{VLV} \cdot \left(h_g - h_P\right) + Q \end{vmatrix}$$

2.4 TWO-REGIONS-SINGLE VOLUME PRESSURIZER

Now the mathematical formulation for the pressurizer is based on the selection of one control volume: the entire pressurizer.
This volume is fixed, but it is divided into two regions with a moving boundary. The upper one contains only steam and the lower one only liquid. These two regions can change their proper volume under the constraint that the total pressurizer volume remains constant. The pressure is the same for every volume. The model is based on the rigours application of the first law of thermodynamics together with heat and mass transfer laws. No a priori assumptions concerning the thermodynamic path of processes occurring are made. The results will be presented in chapter four.

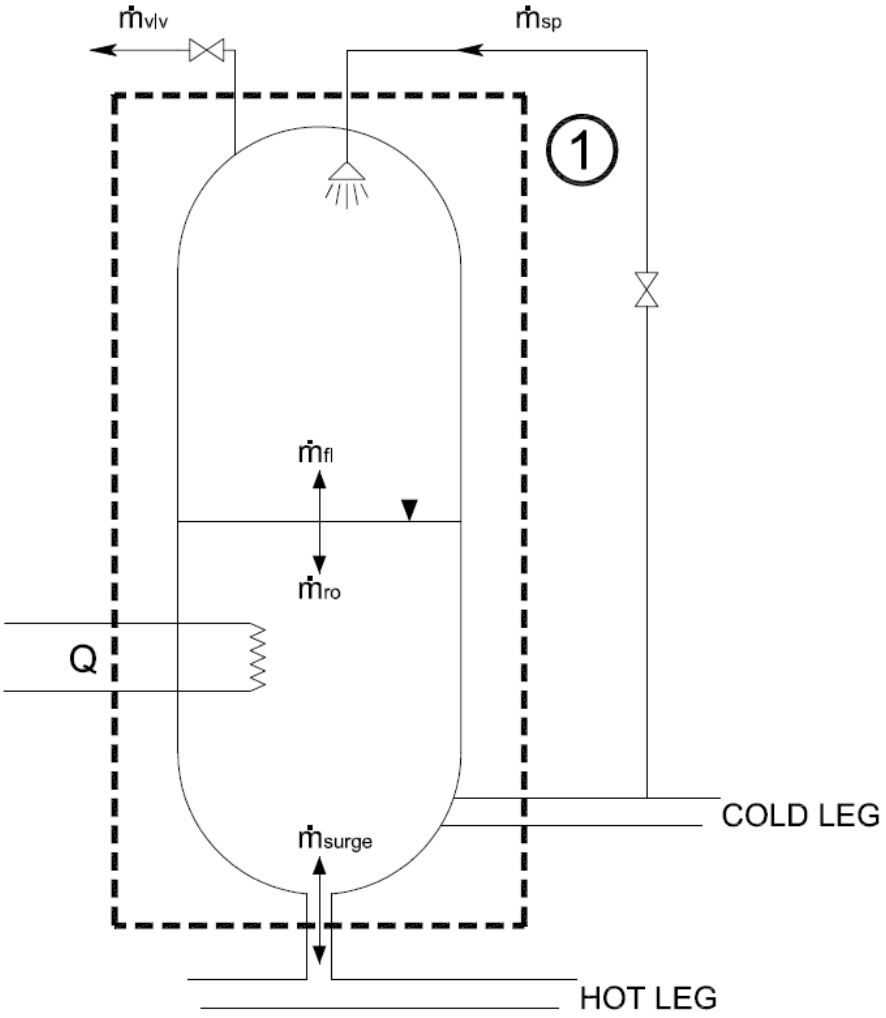

FIG. 2.1 Two-regions-single-volume pressurizer

Also in this simple version, the model is a non-equilibrium one, in fact the lower liquid-only control volume could contain subcooled liquid or boiling water, while the upper control volume could contain superheated or condensing steam. Consequently the pressurizer could be defined by the information in table 2.1.

STATE DESIGNATION	DESCRIPTION OF STATE WITHIN ELEMENT
1	Top Super-Heated, Bottom Subcooled
2	Top Super-Heated, Bottom Boiling
3	Top Condensing, Bottom Subcooled
4	Top Condensing, Bottom Boiling

TABLE 2.1 Pressurizer regions description

Water coming form sprayers $\dot{m}_{SP}$ is thus assumed to instantaneously reach the lower liquid region together with the condensate from the upper region. The condensate comprises the condensed steam on both the spray during its descent $\dot{m}_{SC}$ and on the pressurizer wall $\dot{m}_{WC}$. Additional steam and liquid phase transformations are allowed owing to pressure change. Specifically, flashing of liquid into steam $\dot{m}_{FL}$ and condensation $\dot{m}_{RO}$ (also called rainout) of steam into new liquid drops are allowed. The rainout liquid drops and flashed steam bubbles are assumed to be added instantaneously to the liquid-only and steam-only regions, respectively. So, at steam-liquid interfaces heat, mass and work exchanges are allowed. The corresponding steam and liquid mass transfer rates across this interface are:

$$\dot{m}_v = \dot{m}_{FL} - \dot{m}_{RO} - \dot{m}_{SC} - \dot{m}_{WC} \tag{2.15}$$

$$\dot{m}_l = -\dot{m}_{FL} + \dot{m}_{RO} + \dot{m}_{SC} + \dot{m}_{WC} \tag{2.16}$$

Within the liquid region, mass and energy transfers occur owing to bulk flashing, while, within the steam region, they occur at three condensation locations, i.e. bulk condensation, on the pressurizer wall and on the spray droplets. Moreover, heat fluxes between regions occur due to temperature differences between liquid and steam at interface.

Assuming that the flashing occurs only at saturation conditions and that the latent heat of evaporation is supplied only by the liquid region:

$$\dot{m}_v h_v = \dot{m}_{FL} h_g \tag{2.17}$$

$$\dot{m}_l h_l = -\dot{m}_{FL} h_f \tag{2.18}$$

Similarly, under the assumption that rainout occurs only at saturation conditions and the latent heat of condensation is released only to the steam region:

$$\dot{m}_v h_v = -\dot{m}_{RO} h_f \tag{2.19}$$

$$\dot{m}_l h_l = \dot{m}_{RO} h_g \tag{2.20}$$

Next, considering condensation on spray drops, if the condensation occurs only to at saturation conditions and that the latent heat of condensation is released totally to the spray by conduction through the condensate shell:

$$\dot{m}_v h_v = -\dot{m}_{SC} h_g \tag{2.21}$$

$$\dot{m}_l h_l = \dot{m}_{SC} h_f \tag{2.22}$$

If it is assumed that the rate of condensation is just sufficient to raise the enthalpy of the spray to saturation :

$$\dot{m}_{SC} = \dot{m}_{SP} \left(\frac{h_f - h_{SP}}{h_g - h_f} \right) \tag{2.23}$$

Considering now the condensation on pressurizer wall, assuming it occurs only at saturation :

$$\dot{m}_v h_v = -\dot{m}_{WC} h_g \tag{2.24}$$

Supposing that the latent heat of condensation released to condensate is transferred by conduction completely to the pressurizer wall:

$$\dot{m}_{WC} = \frac{\dot{Q}_{Wv}}{(h_g - h_f)} \tag{2.25}$$

The heat transfer coefficient for condensation is calculated using the model derived by Nusselt [21]:

$$h_v = 0.943 \left[\frac{\rho_l (\rho_l - \rho_g) g h_{fg} k_l^3}{L_v \mu_l (T_{sat} - T_W)} \right]^{\frac{1}{4}} \tag{2.26}$$

All liquid properties appearing in equation 2.30 should be evaluated at the film temperature:

$$T_{film} = \frac{T_{sat} + T_W}{2} \tag{2.27}$$

The total heat transfer to the surface may be obtained by using equation 2.30 with the following form of Newton's law of cooling:

$$\dot{Q}_{vW} = h_v S_v (T_{sat} - T_W) \tag{2.28}$$

In a similar way equations for heat flow from liquid region to the pressurizer wall and the heat flow from the pressurizer wall to outside can derived:

$$\dot{Q}_{lW} = h_l S_l (T_l - T_W) \tag{2.29}$$

$$\dot{Q}_{Wext} = h_e S_{Press} (T_W - T_{ext}) \tag{2.30}$$

where the heat transfer coefficient must be considered constant. S_v, S_l, and S_{TOT} are respectively the internal pressurizer surface inside the steam region, the internal pressurizer surface inside the liquid region and the total external pressurizer surface:

$$s_v = 2\frac{V_V}{R_{Pres\_in}} \tag{2.31}$$

$$s_l = 2\frac{(V - V_V)}{R_{Pres\_in}} \tag{2.32}$$

$$s_{TOT} = 2\pi R_{Pres\_out} \cdot L_{Press} \tag{2.33}$$

L_{Press} is the entire pressurizer height. The wall temperature can be derived solving the subsequent equation, where C_W is the wall thermal capacity:

$$C_W \frac{dT_W}{dt} = Q_{lW} + Q_{vW} - Q_{Wext} \tag{2.34}$$

Finally the heat exchange between liquid and steam region can be obtained from:

$$\dot{Q}_{vl} = hS(T_v - T_l) \tag{2.35}$$

Where S is the area of the cross section of the pressurizer tank.
At this point the governing differential equations for each state are derived by first applying the continuity and energy equations. The resulting equations are then manipulated algebraically until obtaining a system in this form: $\Psi \cdot \dot{z} = \eta$ where Ψ is the coefficients matrix, η the inputs vector and z is the state variables vector [22].

$$\dot{m}_V = \dot{m}_{FL} - \dot{m}_{RO} - \dot{m}_{SC} - \dot{m}_{SP} - \dot{m}_{VLV} - \dot{m}_{WC} \tag{2.36}$$

MASS CONSERVATION

$$\dot{m}_L = -\dot{m}_{FL} + \dot{m}_{RO} + \dot{m}_{SC} + \dot{m}_{SP} + \dot{m}_{WC} + \dot{m}_{INSURGE} - \dot{m}_{OUTSURGE} \tag{2.37}$$

ENERGY CONSERVATION

$$\dot{U}_V = \dot{m}_{FL} \cdot h_G - \dot{m}_{RO} \cdot h_F - \dot{m}_{SC} \cdot h_G - \dot{m}_{WC} \cdot h_G - \dot{m}_{VLV} \cdot h_V - p \cdot \dot{V}_V - \dot{Q}_{Wv} - \dot{Q}_{vl} \tag{2.38}$$

$$\dot{U}_L = -\dot{m}_{FL} \cdot h_G + \dot{m}_{RO} \cdot h_F + \dot{m}_{SC} \cdot h_G + \dot{m}_{SP} \cdot h_{SP} + \dot{m}_{WC} \cdot h_G + \dot{m}_{INSURGE} \cdot h_{INSURGE} - \dot{m}_{OUTSURGE} \cdot h_L - p \cdot \dot{V}_{3L} + \dot{Q}_H - \dot{Q}_{Wl} + \dot{Q}_{vl} \tag{2.39}$$

VOLUME CONSTRAINT

$$\dot{V} = 0 \tag{2.40}$$

$$\dot{V} = \dot{V}_V + \dot{V}_L = 0 \tag{2.41}$$

It must be underlined that the original ensemble of equations is not a traditional ODE (Ordinary Differential Equation) system, but it is a DAE (Differential-Algebraic Equation) system [23]. In particular it belongs to a particular subclass of DAE, called ODE with constraints. Here there is only one constraint: the volume one. To turn the DAE system into an equivalent ODE one it is necessary to derive volume constraint equation, doing that an ODE for pressure can be obtained. For this reason, regarding DAE system formalism, volume is not a real state variable, but a dynamic variable.
The mathematics passages are the following.
Writing steam volume as:

$$V_V = \frac{m_V}{\rho_V} \tag{2.42}$$

Differentiating it with respect to time, and applying the mass conservation principle:

$$\dot{V}_V \cdot \rho_V + V_V \cdot \dot{\rho}_V = \dot{m}_{FL} - \dot{m}_{RO} - \dot{m}_{SC} - \dot{m}_{WC} - \dot{m}_{VLV} \tag{2.43}$$

Similarly, for liquid region:

$$\dot{V}_L \cdot \rho_L + V_L \cdot \dot{\rho}_L + \dot{m}_{FL} - \dot{m}_{RO} = +\dot{m}_{SC} + \dot{m}_{WC} + \dot{m}_{SP} + \dot{m}_{INSURGE} - \dot{m}_{OUTSURGE} \tag{2.44}$$

Remembering that:

$$h = u - pv \tag{2.45}$$

the energy conservation principle for steam fraction can be written in this form:

$$m_V \cdot \dot{h}_V - \dot{p} \cdot V_V - \dot{m}_{FL} \cdot (h_G - h_{3V}) - \dot{m}_{RO} \cdot (h_G - h_{3V}) = -\dot{m}_{SC} \cdot (h_G - h_V) - \dot{m}_{WC} \cdot (h_G - h_V) - \dot{Q}_{vW} - \dot{Q}_{vl} \tag{2.46}$$

The same for the liquid:

$$\begin{aligned} m_L \cdot \dot{h}_L - \dot{p} \cdot V_L - \dot{m}_{FL} \cdot (h_L - h_G) - \dot{m}_{RO} \cdot (h_F - h_L) \\ = \dot{m}_{SC} \cdot (h_G - h_L) + \dot{m}_{WC} \cdot (h_G - h_L) + \dot{m}_{SP} \cdot (h_{SP} - h_L) \\ + \dot{m}_{INSURGE} \cdot (h_{INSURGE} - h_L) + \dot{Q}_H - \dot{Q}_{lW} + \dot{Q}_{vl} \end{aligned} \tag{2.47}$$

Now, as in the equilibrium model, all the equations can be summarized in form of matrix:

$$\Psi \cdot \dot{z} = \eta \tag{2.48}$$

For the ODE system:

$$\dot{z} = \Psi^{-1}\eta \tag{2.49}$$

So also this system can be finally put in this form:

$$\dot{z} = f(z, u) \tag{2.50}$$

Where, in the language of control, z is the state variables vector and u the input variable vector. Due to the possible thermodynamic states which can exist within the pressurizer, the state variables can change during transient:

STATE 1	$z = \{p, V_v, h_v, h_l\}^T$
STATE 2	$z = \{p, V_v, h_v, m_{FL}\}^T$
STATE 3	$z = \{p, V_v, m_{RO}, h_l\}^T$
STATE 4	$z = \{p, V_v, m_{RO}, m_{FL}\}^T$

TABLE 2.2 Pressurizer state variables

In fact enthalpy cannot be a state variable at saturation condition, when it depends on pressure. Using enthalpy and pressure as natural thermodynamic variables and considering all the possible thermodynamic states, time derivatives appearing in the equations can be made explicit:

$if\ h_L < h_f\ or\ h_V > h_G$	$\rho = \rho(p,h) \rightarrow \frac{d\rho}{dt} = \frac{\partial\rho}{\partial p}\frac{dp}{dt} + \frac{\partial\rho}{\partial h}\frac{dh}{dt} = \frac{\partial\rho}{\partial p}\dot{p} + \frac{\partial\rho}{\partial h}\dot{h}$
$if\ h_L = h_f\ or\ h_V = h_G$	$\rho = \rho(p) \rightarrow \frac{d\rho}{dt} = \frac{d\rho}{dp}\frac{dp}{dt} = \frac{d\rho}{dp}\dot{p}$ $h = h(p) \rightarrow \frac{dh}{dt} = \frac{dh}{dp}\frac{dp}{dt} = \frac{dh}{dp}\dot{p}$

TABLE 2.3 Thermodynamic partial derivatives

Although ODE formulation is more formal, matrix formulation is much more compact and elegant. In the following pages, there are all the matrices for all possible thermodynamic states which can occur:

STATE 1 $h_L < h_f \cap h_V > h_g$

$$\Psi = \begin{vmatrix} V_V * \frac{\partial\rho_V}{\partial p} & \rho_V & V_V * \frac{\partial\rho_V}{\partial h_V} & 0 \\ (V - V_V) * \frac{\partial\rho_L}{\partial p} & -\rho_L & 0 & (V - V_V) * \frac{\partial\rho_L}{\partial h_L} \\ -V_V & 0 & \rho_V * V_V & 0 \\ -(V - V_V) & 0 & 0 & \rho_L * (V - V_V) \end{vmatrix}$$

$$\dot{z} = \{\dot{p}, \dot{V}_v, \dot{h}_v, \dot{h}_l\}^T$$

$$\eta = \begin{vmatrix} -\dot{m}_{SC} - \dot{m}_{WC} - \dot{m}_{VLV} \\ \dot{m}_{SC} + \dot{m}_{WC} + \dot{m}_{SP} + \dot{m}_{INSURGE} - \dot{m}_{OUTSURGE} \\ -\dot{m}_{SC} \cdot (h_G - h_V) - \dot{m}_{WC} \cdot (h_G - h_V) - \dot{Q}_{Wv} - \dot{Q}_{Sv} \\ \dot{m}_{SC} \cdot (h_G - h_L) + \dot{m}_{WC} \cdot (h_G - h_L) + \dot{m}_{SP} \cdot (h_{SP} - h_L) + \dot{m}_{INSURGE} \cdot (h_{INSURGE} - h_L) + \dot{Q}_H - \dot{Q}_{Wl} + \dot{Q}_{vl} \end{vmatrix}$$

STATE 2 $h_L = h_f \cap h_V > h_g$

$$\Psi = \begin{vmatrix} V_V * \frac{\partial \rho_V}{\partial p} & \rho_V & V_V * \frac{\partial \rho_V}{\partial h_V} & \textit{-1} \\ (V - V_V) * \frac{d\rho_F}{dp} & -\rho_F & \textit{0} & 1 \\ -V_V & \textit{0} & \rho_V * V_V & (h_V - h_G) \\ (V - V_V) * \left(\rho_F * \frac{dh_F}{dp} - 1\right) & \textit{0} & \textit{0} & (h_G - h_F) \end{vmatrix}$$

$$\dot{z} = \left\{\dot{p}, \dot{V}_v, \dot{h}_v, \dot{m}_{FL}\right\}^T$$

$$\eta = \begin{vmatrix} -\dot{m}_{SC} - \dot{m}_{WC} - \dot{m}_{VLV} \\ \dot{m}_{SC} + \dot{m}_{WC} + \dot{m}_{SP} + \dot{m}_{INSURGE} - \dot{m}_{OUTSURGE} \\ -\dot{m}_{SC} \cdot (h_G - h_V) - \dot{m}_{WC} \cdot (h_G - h_V) - \dot{Q}_{Wv} - \dot{Q}_{Sv} \\ \dot{m}_{SC} \cdot (h_G - h_F) + \dot{m}_{WC} \cdot (h_G - h_F) + \dot{m}_{SP} \cdot (h_{SP} - h_F) + \dot{m}_{INSURGE} \cdot (h_{INSURGE} - h_F) + \dot{Q}_H - \dot{Q}_{Wl} + \dot{Q}_{vl} \end{vmatrix}$$

STATE 3 $h_L < h_f \cap h_V = h_g$

$$\Psi = \begin{vmatrix} V_V * \frac{d\rho_G}{dp} & \rho_G & 1 & \textit{0} \\ (V - V_V) * \frac{\partial \rho_L}{\partial p} & -\rho_L & \textit{-1} & (V - V_V) * \frac{\partial \rho_L}{\partial h_L} \\ V_V * \left(\rho_G * \frac{dh_G}{dp} - 1\right) & \textit{0} & (h_F - h_G) & \textit{0} \\ -(V - V_V) & \textit{0} & (h_L - h_F) & \rho_L * (V - V_V) \end{vmatrix}$$

$$\dot{z} = \left\{\dot{p}, \dot{V}_v, \dot{m}_{RO}, \dot{h}_l\right\}^T$$

$$\eta = \begin{vmatrix} -\dot{m}_{SC} - \dot{m}_{WC} - \dot{m}_{VLV} \\ \dot{m}_{SC} + \dot{m}_{WC} + \dot{m}_{SP} + \dot{m}_{INSURGE} - \dot{m}_{OUTSURGE} \\ -\dot{Q}_{Wv} - \dot{Q}_{vl} \\ \dot{m}_{SC} \cdot (h_G - h_L) + \dot{m}_{WC} \cdot (h_G - h_L) + \dot{m}_{SP} \cdot (h_{SP} - h_L) + \dot{m}_{INSURGE} \cdot (h_{INSURGE} - h_L) + \dot{Q}_H - \dot{Q}_{Wl} + \dot{Q}_{vl} \end{vmatrix}$$

STATE 4 $h_L = h_f \cap h_V = h_g$

$$\Psi = \begin{vmatrix} V_V * \frac{d\rho_G}{dp} & \rho_G & 1 & -1 \\ (V - V_V) * \frac{d\rho_F}{dp} & -\rho_F & -1 & 1 \\ V_V * \left(\rho_G * \frac{dh_G}{dp} - 1\right) & 0 & (h_F - h_G) & 0 \\ (V - V_V) * \left(\rho_F * \frac{dh_F}{dp} - 1\right) & 0 & 0 & (h_G - h_F) \end{vmatrix}$$

$$\dot{z} = \left\{\dot{p}, \dot{V}_v, \dot{m}_{RO}, \dot{m}_{FL}\right\}^T$$

$$\eta = \begin{vmatrix} -\dot{m}_{SC} - \dot{m}_{WC} - \dot{m}_{VLV} \\ \dot{m}_{SC} + \dot{m}_{WC} + \dot{m}_{SP} + \dot{m}_{INSURGE} - \dot{m}_{OUTSURGE} \\ -\dot{Q}_{Wv} \\ \dot{m}_{SC} \cdot (h_G - h_F) + \dot{m}_{WC} \cdot (h_G - h_F) + \dot{m}_{SP} \cdot (h_{SP} - h_F) + \dot{m}_{INSURGE} \cdot (h_{INSURGE} - h_F) + \dot{Q}_H - \dot{Q}_{Wl} \end{vmatrix}$$

2.5 TWO-REGIONS-TWO-VOLUMES MODEL

Although it is simple and elegant, the model previously shown has a big weakness: it cannot take into account the temperature distribution which occurs across the liquid region, as it will be demonstrated in the next chapter.
Before the transient start, it is supposed that the temperature of water is uniform throughout the entire liquid volume.
However, during insurges, cold water from hot leg goes up through the pressurizer liquid region and it is progressively warmed. On the other hand, due to the insurge, the temperature of liquid region drops, but this fact does not happen in a uniform way: the lower regions, where the colder water directly arrives, experiment a bigger decrease.
During outsurges, instead, water goes down from the upper liquid regions, where is hotter, to the hot leg of reactor and so it is progressively cooled. Therefore, due to outsurge, the temperature of lower liquid regions increases, this fact is more pronounced for lower zones, which experiment the arrival of water much hotter than them.

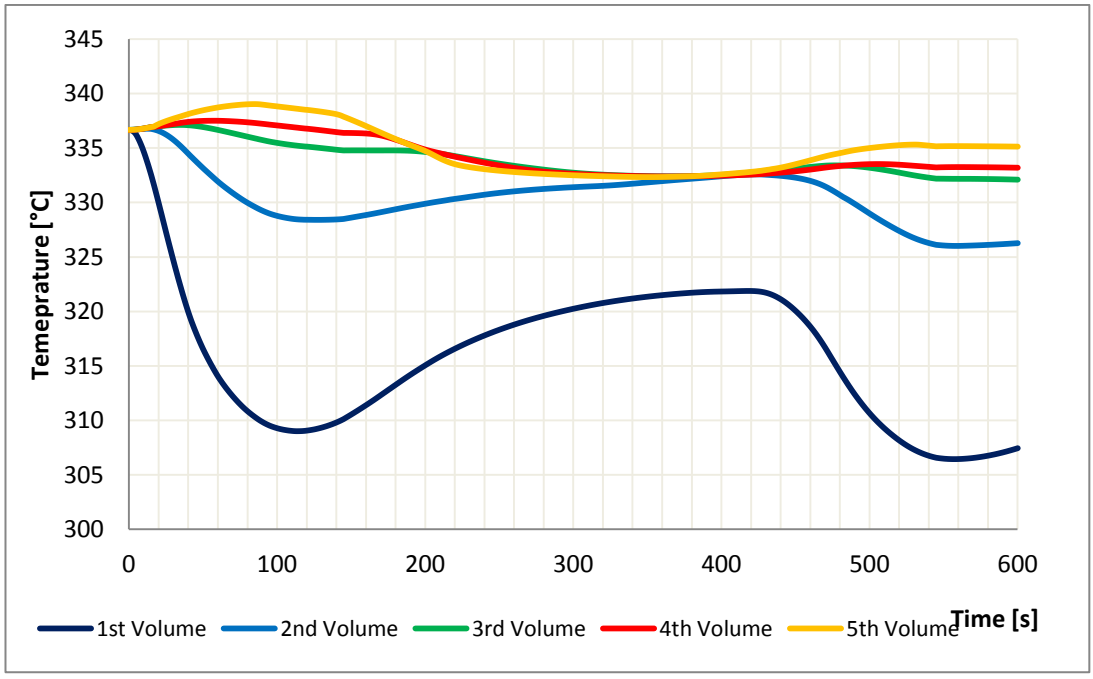

FIG. 2.2 Temperature distribution inside the pressurizer

Originally, the occurrence of temperature distribution was only an assumption introduced to explain the poor performances of one volume model. Subsequently it has been highlighted by a RELAP5® code for pressurizer which will be presented later in this study. The mathematical formulation of this improved model is based on the selection of

two control volumes within the pressurizer. These volumes are fixed. Starting from the bottom, the first control volume is an only liquid region, which remains always subcooled. This volume is the solution adopted to take into account temperature non-uniformities occurring during transients. The second control volume, at the upper portion of the pressurizer is then sub-divided into two regions, one for steam and one for liquid, which can change their proper volume, under the constraint of conservation of the total volume of the second portion. These two sub-control volumes are separated by an interface across which mass exchanges could occur. The lower sub-control volume could contain subcooled liquid or boiling water, while the upper control volume could contain superheated or condensing steam as in the previous model.
Between all volumes and sub volumes heat exchanges can occur:

- Heat exchange between lower liquid region and upper liquid region

$$Q_{ll} = h_{ll} S (T_{Ll} - T_{Lu}) \tag{2.50}$$

- Heat exchange between upper liquid region and steam region

$$Q_{lv} = h_{lv} S (T_{Ll} - T_{Lu}) \tag{2.51}$$

- Heat exchange between lower liquid region and pressurizer wall

$$Q_{Ll-W} = h_{Ll-ext} S_{Ll} (T_{Ll} - T_W) \tag{2.52}$$

- Heat exchange between upper liquid region and pressurizer wall

$$Q_{Lu-W} = h_{Lu-ext} S_{Lu} (T_{Lu} - T_W) \tag{2.53}$$

- Heat exchange between steam region and pressurizer wall

$$Q_{V-W} = h_v S_v (T_{sat} - T_W) \tag{2.54}$$

- Heat exchange between wall and the outside

$$\dot{Q}_{Wext} = h_e S_{Press} (T_W - T_{ext}) \tag{2.55}$$

Inside the upper volume, between steam and liquid regions the same exchange of mass, heat and work presented in two-regions-one-volume model can occur. Of course insurge and outsurge mass rates pass through all liquid volumes.

Although this model is much more accurate than the previous one, it loses the possibility to explain with the same equations insurges and outsurges transient. Now, the two cases must be treated separately.
However no a priori assumption about the thermodynamic path of processes simulated is done. So, to take into account inversions of surge flow rate, equations are split into two groups, the first for insurge transients and the second for outsurge ones.

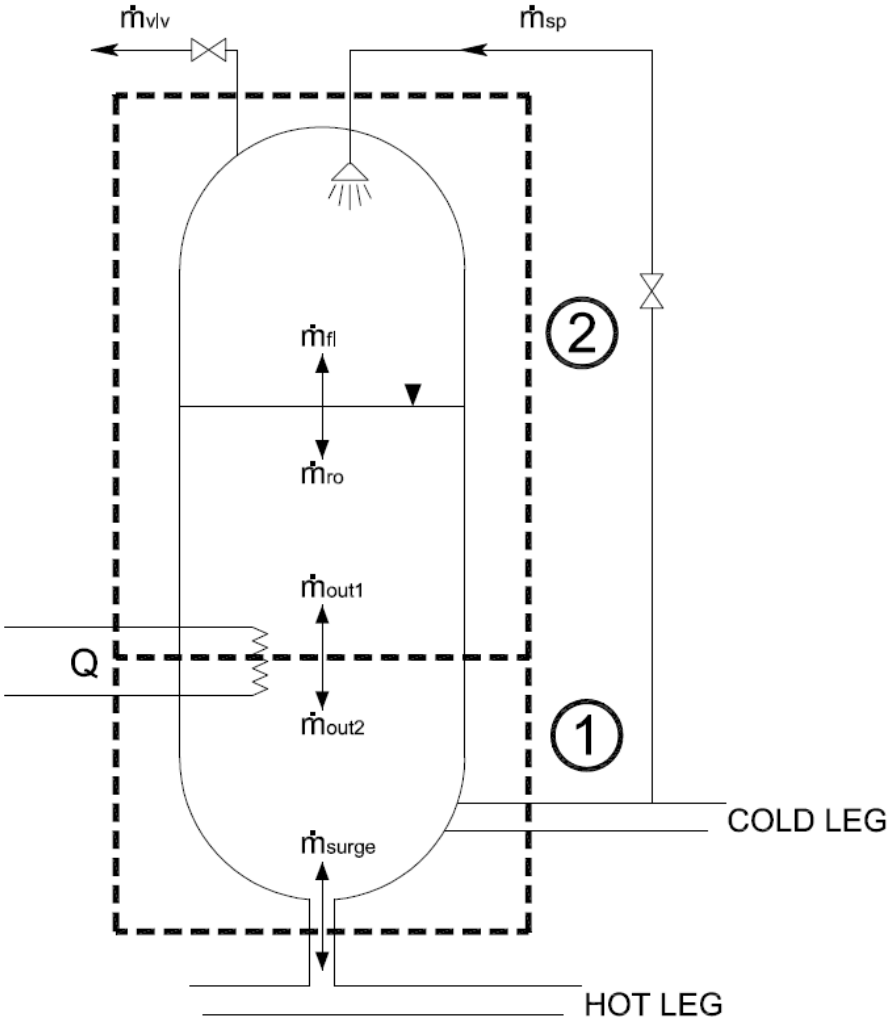

FIG. 2.3 Two-regions-two- volume pressurizer

In case of insurge transient, applying mass and energy conservation and volume constraint to the lower only liquid region, here called simply “Volume 1” the sequent equations are obtained.

MASS CONSERVATION

$$\dot{m}_1 = \dot{m}_{INsurge} - \dot{m}_{OUT\_1} \tag{2.56}$$

ENERGY CONSERVATION

$$\dot{U}_1 = \dot{m}_{INsurge} \cdot h_{INsurge} - \dot{m}_{OUT\_1} \cdot h_1 + Q_{l-l} - Q_{Ll-W} \tag{2.57}$$

VOLUME CONSTRAINT

$$\dot{V}_1 = 0 \tag{2.58}$$

Then, differentiating the volume with respect to time:

$$V_1 \cdot \dot{\rho}_1 + \dot{m}_{OUT\_1} = \dot{m}_{INsurge} \tag{2.59}$$

Where $\dot{m}_{OUT\_1}$ is mass flow rate from volume 1 to liquid region of volume 2. Putting into evidence the enthalpy:

$$m_1 \cdot \dot{h}_1 - \dot{p} \cdot V_1 = \dot{m}_{INsurge} \cdot \left(h_{INsurge} - h_1\right) + Q_{l-l} - Q_{Ll-W} \tag{2.60}$$

For the second volume, here called "volume 2", because it is divided into two regions, mass and energy conservation and the volume constraint have to be applied separately to steam and liquid regions as done for two-regions-one-volume model.

MASS CONSERVATION

$$\dot{m}_{2V} = \dot{m}_{FL} - \dot{m}_{RO} - \dot{m}_{SC} - \dot{m}_{SP} - \dot{m}_{VLV} - \dot{m}_{WC}$$
$$\dot{m}_{2L} = -\dot{m}_{FL} + \dot{m}_{RO} + \dot{m}_{SC} + \dot{m}_{SP} + \dot{m}_{WC} + \dot{m}_{OUT\_1} \tag{2.61}$$

ENERGY CONSERVATION

$$\dot{U}_{2V} = \dot{m}_{FL} \cdot h_G - \dot{m}_{RO} \cdot h_F - \dot{m}_{SC} \cdot h_G - \dot{m}_{VLV} \cdot h_{2V} - \dot{m}_{WC} \cdot h_G - p \cdot \dot{V}_{2V} - Q_{l-v} - Q_{V-W}$$
$$\dot{U}_{2L} = -\dot{m}_{FL} \cdot h_G + \dot{m}_{WC} \cdot h_G + \dot{m}_{RO} \cdot h_F + \dot{m}_{SC} \cdot h_G + \dot{m}_{SP} \cdot h_{SP} + \dot{m}_{OUT\_1} \cdot h_2 - p \cdot \dot{V}_{2L} + \dot{Q}_H + Q_{l-v} - Q_{l-l} - Q_{Lu-W} \tag{2.62}$$

VOLUME CONSTRAINT

$$\dot{V}_2 = 0$$
$$\dot{V}_2 = \dot{V}_{2V} + \dot{V}_{2L} = 0 \tag{2.63}$$

Differentiating steam and liquid volume with respect to time

$$\dot{V}_{2V} \cdot \rho_{2V} + V_{2V} \cdot \dot{\rho}_{2V} - \dot{m}_{FL} + \dot{m}_{RO} = -\dot{m}_{SC} - \dot{m}_{SP} - \dot{m}_{VLV} - \dot{m}_{WC} \tag{2.64}$$

$$\dot{V}_{2L} \cdot \rho_{2L} + V_{2L} \cdot \dot{\rho}_{2L} + \dot{m}_{FL} - \dot{m}_{RO} - \dot{m}_{OUT\_1} = \dot{m}_{SC} + \dot{m}_{SP} + \dot{m}_{WC} \tag{2.65}$$

Extracting from energy equations enthalpies of steam and liquid:

$$\begin{aligned} m_{2V} \cdot \dot{h}_{2V} - \dot{p} \cdot V_{2V} - \dot{m}_{FL} \cdot (h_G - h_{2V}) - \dot{m}_{RO} \cdot (h_G - h_{2V}) \\ = -\dot{m}_{SC} \cdot (h_G - h_{2V}) - \dot{m}_{WC} \cdot (h_G - h_{2V}) - Q_{l-v} - Q_{V-ext} \end{aligned} \tag{2.66}$$

$$\begin{aligned} m_{2L} \cdot \dot{h}_{2L} - \dot{p} \cdot V_{2L} - \dot{m}_{FL} \cdot (h_{2L} - h_G) - \dot{m}_{RO} \cdot (h_F - h_{2L}) - \dot{m}_{OUT\_2} \\ \cdot (h_1 - h_{2L}) \\ = \dot{m}_{SC} \cdot (h_G - h_{2L}) + \dot{m}_{WC} \cdot (h_G - h_{2L}) + \dot{m}_{SP} \cdot (h_{SP} - h_{2L}) \\ + \dot{Q}_H + Q_{l-v} - Q_{l-l} - Q_{Lu-W} \end{aligned} \tag{2.67}$$

Following the same way, equations for outsurge transients can be obtained. For volume 1:

MASS CONSERVATION

$$\dot{m}_1 = \dot{m}_{OUT\_2} - \dot{m}_{OUTsurge} \tag{2.68}$$

ENERGY CONSERVATION

$$\dot{U}_1 = \dot{m}_{OUT\_2} \cdot h_{OUT\_2} - \dot{m}_{OUT\_surge} \cdot h_1 + Q_{l-l} - Q_{Ll-W} \tag{2.69}$$

VOLUME CONSTRAINT

$$\dot{V}_1 = 0 \tag{2.70}$$

So it is obtained:

$$V_1 \cdot \dot{\rho}_1 - \dot{m}_{OUT\_2} = -\dot{m}_{OUTsurge} \tag{2.71}$$

$$m_1 \cdot \dot{h}_1 - \dot{p} \cdot V_1 - \dot{m}_{OUT\_2} \cdot (h_2 - h_1) = Q_{l-l} - Q_{Ll-W} \tag{2.72}$$

For volume 2:

$$\dot{m}_{2V} = \dot{m}_{FL} - \dot{m}_{RO} - \dot{m}_{SC} - \dot{m}_{WC} - \dot{m}_{SP} - \dot{m}_{VLV} \tag{2.73}$$

MASS CONSERVATION

$$\dot{m}_{2L} = -\dot{m}_{FL} + \dot{m}_{RO} + \dot{m}_{SC} + \dot{m}_{WC} + \dot{m}_{SP} - \dot{m}_{OUT\_2} \tag{2.74}$$

ENERGY CONSERVATION

$$\dot{U}_{2V} = \dot{m}_{FL} \cdot h_G - \dot{m}_{RO} \cdot h_F - \dot{m}_{SC} \cdot h_G - \dot{m}_{WC} \cdot h_G - \dot{m}_{VLV} \cdot h_{2V} - p \cdot \dot{V}_{2V} - Q_{l-v} - Q_{V-W} \tag{2.75}$$

$$\dot{U}_{2L} = -\dot{m}_{FL} \cdot h_G + \dot{m}_{RO} \cdot h_F + \dot{m}_{SC} \cdot h_G + \dot{m}_{WC} \cdot h_G + \dot{m}_{SP} \cdot h_{SP} - \dot{m}_{OUT\_2} \cdot h_2 - p \cdot \dot{V}_{2L} + \dot{Q}_H + Q_{l-v} - Q_{l-l} - Q_{Lu-W} \quad (2.76)$$

VOLUME CONSTRAINT

$$\dot{V}_2 = 0$$
$$\dot{V}_2 = \dot{V}_{2V} + \dot{V}_{2L} = 0 \quad (2.77)$$

The mass flow rate going out from volume 2 during outsurges is called $\dot{m}_{OUT\_2}$.The final equations are:

$$\dot{V}_{2V} \cdot \rho_{2V} + V_{2V} \cdot \dot{\rho}_{2V} - \dot{m}_{FL} + \dot{m}_{RO} = -\dot{m}_{SC} - \dot{m}_{WC} - \dot{m}_{SP} - \dot{m}_{VLV} \quad (2.78)$$

$$\dot{V}_{2L} \cdot \rho_{3L} + V_{2L} \cdot \dot{\rho}_{3L} + \dot{m}_{FL} - \dot{m}_{RO} + \dot{m}_{OUT\_2} = \dot{m}_{SC} + \dot{m}_{WC} + \dot{m}_{SP} \quad (2.79)$$

$$m_{2V} \cdot \dot{h}_{2V} - \dot{p} \cdot V_{2V} - \dot{m}_{FL} \cdot (h_G - h_{2V}) - \dot{m}_{RO} \cdot (h_G - h_{3V}) = -\dot{m}_{SC} \cdot (h_G - h_{2V}) - \dot{m}_{WC} \cdot (h_G - h_{2V}) - Q_{l-v} - Q_{V-W} \quad (2.80)$$

$$m_{2L} \cdot \dot{h}_{2L} - \dot{p} \cdot V_{2L} - \dot{m}_{FL} \cdot (h_{2L} - h_G) - \dot{m}_{RO} \cdot (h_F - h_{2L}) = \dot{m}_{SC} \cdot (h_{2L} - h_G) + \dot{m}_{WC} \cdot (h_{2L} - h_G) + \dot{m}_{SP} \cdot (h_{SP} - h_{2L}) + \dot{Q}_H + Q_{l-v} - Q_{l-l} - Q_{Lu-W} \quad (2.81)$$

Partial derivative can be expressed in the same way shown for one volume two regions model. Also in this model all the equations can be put into $\Psi \cdot \dot{z} = \eta$ form and into $\dot{z} = f(z, u)$ form. The state variables are:

STATE 1in	$z = \{p, V_{2v}, h_{2v}, h_{2l}, h_1, m_{OUT\_1}\}^T$	STATE 1 out	$z = \{p, V_{2v}, h_{2v}, h_{2l}, h_1, m_{OUT\_2}\}^T$
STATE 2 in	$z = \{p, V_{2v}, h_{2v}, m_{FL}, h_1, m_{OUT\_1}\}^T$	STATE 2 out	$z = \{p, V_{2v}, h_{2v}, m_{FL}, h_1, m_{OUT\_2}\}^T$
STATE 3 in	$z = \{p, V_{2v}, m_{RO}, h_{2l}, h_1, m_{OUT\_1}\}^T$	STATE 3 out	$z = \{p, V_{2v}, m_{RO}, h_{2l}, h_1, m_{OUT\_2}\}^T$
STATE 4 in	$z = \{p, V_v, m_{RO}, m_{FL}, h_1, m_{OUT\_1}\}^T$	STATE 4 out	$z = \{p, V_v, m_{RO}, m_{FL}, h_1, m_{OUT\_2}\}^T$

TABLE 2.4 Pressurizer state variables

In the following pages, there are all the matrices for all possible thermodynamic states which can occur.

INSURGE-STATE 1 $h_1 < h_f \cap h_{2L} < h_f \cap h_{2V} > h_g$

$$\Psi = \begin{vmatrix} V_{2V} * \frac{\partial \rho_{3V}}{\partial p} & \rho_{2V} & V_{2V} * \frac{\partial \rho_{2V}}{\partial h_{2V}} & 0 & 0 & 0 \\ (V_2 - V_{2V}) * \frac{\partial \rho_{2L}}{\partial p} & -\rho_{2L} & 0 & (V_2 - V_{2V}) * \frac{\partial \rho_{2L}}{\partial h_{2L}} & 0 & -1 \\ V_1 * \frac{\partial \rho_1}{\partial p} & 0 & 0 & 0 & V_1 * \frac{\partial \rho_1}{\partial h_1} & 1 \\ -V_{2V} & 0 & \rho_{2V} * V_{2V} & 0 & 0 & 0 \\ -(V_2 - V_{2V}) & 0 & 0 & \rho_{2L} * (V_2 - V_{2V}) & 0 & -(h_1 - h_{2L}) \\ -V_1 & 0 & 0 & 0 & \rho_1 * V_1 & 0 \end{vmatrix}$$

$$\dot{z} = \left\{\dot{p}, \dot{V}_{2v}, \dot{h}_{2v}, \dot{h}_{2l}, \dot{h}_1, \dot{m}_{OUT\_1}\right\}^T$$

$$\eta = \begin{vmatrix} -\dot{m}_{SC} - \dot{m}_{SP} - \dot{m}_{VLV} - \dot{m}_{WC} \\ \dot{m}_{SC} + \dot{m}_{SP} + \dot{m}_{WC} \\ \dot{m}_{INsurge} \\ -\dot{m}_{SC} \cdot (h_G - h_{2V}) - \dot{m}_{WC} \cdot (h_G - h_{2V}) - Q_{l-v} - Q_{V-W} \\ \dot{m}_{SC} \cdot (h_G - h_F) + \dot{m}_{WC} \cdot (h_G - h_F) + \dot{m}_{SP} \cdot (h_{SP} - h_F) + \dot{Q}_H + Q_{l-v} - Q_{l-l} - Q_{Lu-W} \\ \dot{m}_{INsurge} \cdot \left(h_{INsurge} - h_1\right) + Q_{l-l} - Q_{Ll-W} \end{vmatrix}$$

INSURGE-STATE 2 $h_1 < h_f \cap h_{2L} = h_f \cap h_{2V} > h_g$

$$\Psi = \begin{vmatrix} V_{2V} * \frac{\partial \rho_{2V}}{\partial p} & \rho_{2V} & V_{2V} * \frac{\partial \rho_{2V}}{\partial h_{2V}} & -1 & 0 & 0 \\ (V_2 - V_{2V}) * \frac{d\rho_F}{dp} & -\rho_F & 0 & 1 & 0 & -1 \\ V_1 * \frac{\partial \rho_1}{\partial p} & 0 & 0 & 0 & V_1 * \frac{\partial \rho_1}{\partial h_1} & 1 \\ -V_{2V} & 0 & \rho_{2V} * V_{2V} & (h_{2V} - h_G) & 0 & 0 \\ (V_2 - V_{2V}) * \left(\rho_F * \frac{dh_F}{dp} - 1\right) & 0 & 0 & (h_G - h_F) & 0 & -(h_1 - h_F) \\ -V_1 & 0 & 0 & 0 & \rho_1 * V_1 & 0 \end{vmatrix}$$

$$\dot{z} = \left\{\dot{p}, \dot{V}_{2v}, \dot{h}_{2v}, \dot{m}_{FL}, \dot{h}_1, \dot{m}_{OUT\_1}\right\}^T$$

$$\eta = \begin{vmatrix} \dot{m}_{FL} - \dot{m}_{RO} - \dot{m}_{SC} - \dot{m}_{SP} - \dot{m}_{VLV} - \dot{m}_{WC} \\ \dot{m}_{SC} + \dot{m}_{SP} + \dot{m}_{WC} \\ \dot{m}_{INsurge} \\ -\dot{m}_{SC} \cdot (h_G - h_{2V}) - \dot{m}_{WC} \cdot (h_G - h_{2V}) - Q_{l-v} - Q_{V-W} \\ \dot{m}_{SC} \cdot (h_G - h_{2V}) + \dot{m}_{WC} \cdot (h_G - h_{2V}) + \dot{m}_{SP} \cdot (h_{SP} - h_{3L}) + \dot{Q}_H + Q_{l-v} - Q_{l-l} - Q_{Lu-W} \\ \dot{m}_{INsurge} \cdot \left(h_{INsurge} - h_1\right) + Q_{l-l} - Q_{Ll-W} \end{vmatrix}$$

INSURGE-STATE 3 $h_1 < h_f \cap h_{2L} < h_f \cap h_{2V} = h_g$

$$\Psi = \begin{vmatrix} V_{2V} * \frac{d\rho_G}{dp} & \rho_G & 1 & 0 & 0 & 0 \\ (V_2 - V_{2V}) * \frac{\partial \rho_{2L}}{\partial p} & -\rho_{2L} & -1 & (V_2 - V_{2V}) * \frac{\partial \rho_{2L}}{\partial h_{2L}} & 0 & -1 \\ V_2 * \frac{\partial \rho_2}{\partial p} & 0 & 0 & 0 & V_2 * \frac{\partial \rho_2}{\partial h_2} & 1 \\ V_{2V} * \left(\rho_G * \frac{dh_G}{dp} - 1\right) & 0 & (h_F - h_G) & 0 & 0 & 0 \\ -(V_2 - V_{2V}) & 0 & (h_{2L} - h_F) & \rho_{2L} * (V_2 - V_{2V}) & 0 & -(h_1 - h_{2L}) \\ -V_1 & 0 & 0 & 0 & \rho_1 * V_1 & 0 \end{vmatrix}$$

$$\dot{z} = \{\dot{p}, \dot{V}_{2v}, \dot{m}_{RO}, \dot{h}_{2l}, \dot{h}_1, \dot{m}_{OUT\_1}\}^T$$

$$\eta = \begin{vmatrix} -\dot{m}_{SC} - \dot{m}_{SP} - \dot{m}_{VLV} - \dot{m}_{WC} \\ \dot{m}_{SC} + \dot{m}_{SP} + \dot{m}_{WC} \\ \dot{m}_{INsurge} \\ -Q_{l-v} - Q_{V-ext} \\ \dot{m}_{SC} \cdot (h_G - h_{2L}) + \dot{m}_{WC} \cdot (h_G - h_{2L}) + \dot{m}_{SP} \cdot (h_{SP} - h_{2L}) + \dot{Q}_H + Q_{l-v} - Q_{l-l} - Q_{Lu-ext} \\ \dot{m}_{INsurge} \cdot (h_{INsurge} - h_1) + Q_{l-l} - Q_{Ll-ext} \end{vmatrix}$$

INSURGE-STATE 4 $h_1 < h_f \cap h_{2L} = h_f \cap h_{2V} = h_g$

$$\Psi = \begin{vmatrix} V_{2V} * \frac{d\rho_G}{dp} & \rho_G & 1 & -1 & 0 & 0 \\ (V_2 - V_{2V}) * \frac{d\rho_F}{dp} & -\rho_F & -1 & 1 & 0 & -1 \\ V_1 * \frac{\partial \rho_1}{\partial p} & 0 & 0 & 0 & V_1 * \frac{\partial \rho_1}{\partial h_1} & 1 \\ V_{2V} * \left(\rho_G * \frac{dh_G}{dp} - 1\right) & 0 & (h_F - h_G) & 0 & 0 & 0 \\ (V_2 - V_{2V}) * \left(\rho_F * \frac{dh_F}{dp} - 1\right) & 0 & 0 & (h_G - h_F) & 0 & -(h_1 - h_F) \\ -V_1 & 0 & 0 & 0 & \rho_1 * V_1 & 0 \end{vmatrix}$$

$$\dot{z} = \{\dot{p}, \dot{V}_{2v}, \dot{m}_{RO}, \dot{h}_{2l}, \dot{h}_1, \dot{m}_{OUT\_1}\}^T$$

$$\eta = \begin{vmatrix} -\dot{m}_{SC} - \dot{m}_{SP} - \dot{m}_{VLV} - \dot{m}_{WC} \\ \dot{m}_{SC} + \dot{m}_{SP} + \dot{m}_{WC} \\ \dot{m}_{INsurge} \\ -Q_{V-ext} \\ \dot{m}_{SC} \cdot (h_G - h_F) + \dot{m}_{WC} \cdot (h_G - h_F) + \dot{m}_{SP} \cdot (h_{SP} - h_F) + \dot{Q}_H - Q_{l-l} - Q_{Lu-ext} \\ \dot{m}_{INsurge} \cdot (h_{INsurge} - h_1) + Q_{l-l} - Q_{Ll-ext} \end{vmatrix}$$

OUTSURGE-STATE 1 $h_1 < h_f \cap h_{2L} < h_f \cap h_{2V} > h_g$

$$\Psi = \begin{vmatrix} V_{2V} * \frac{\partial \rho_{2V}}{\partial p} & \rho_{2V} & V_{2V} * \frac{\partial \rho_{2V}}{\partial h_{2V}} & 0 & 0 & 0 \\ (V_2 - V_{2V}) * \frac{\partial \rho_{2L}}{\partial p} & -\rho_{2L} & 0 & (V_2 - V_{2V}) * \frac{\partial \rho_{2L}}{\partial h_{2L}} & 0 & 0 \\ V_1 * \frac{\partial \rho_1}{\partial p} & 0 & 0 & 0 & V_1 * \frac{\partial \rho_1}{\partial h_1} & 1 \\ -V_{2V} & 0 & \rho_{2V} * V_{2V} & 0 & 0 & 0 \\ -(V_2 - V_{2V}) & 0 & 0 & \rho_{2L} * (V_2 - V_{2V}) & 0 & 0 \\ -V_1 & 0 & 0 & 0 & \rho_1 * V_1 & 0 \end{vmatrix}$$

$$\dot{z} = \left\{\dot{p}, \dot{V}_{2v}, \dot{h}_{2v}, \dot{h}_{2l}, \dot{h_1}, \dot{m}_{OUT\_2}\right\}^T$$

$$\eta = \begin{vmatrix} -\dot{m}_{SC} - \dot{m}_{WC} - \dot{m}_{SP} - \dot{m}_{VLV} \\ \dot{m}_{SC} + \dot{m}_{WC} + \dot{m}_{SP} \\ -\dot{m}_{OUTsurge} \\ -\dot{m}_{SC} \cdot (h_G - h_{2V}) - \dot{m}_{WC} \cdot (h_G - h_{2V}) - Q_{l-v} - Q_{V-ext} \\ \dot{m}_{SC} \cdot (h_{2L} - h_G) + \dot{m}_{WC} \cdot (h_{2L} - h_G) + \dot{m}_{SP} \cdot (h_{SP} - h_{2L}) + \dot{Q}_H + Q_{l-v} - Q_{l-l} - Q_{Lu-ext} \\ Q_{l-l} - Q_{Ll-ext} \end{vmatrix}$$

OUTSURGE-STATE 2 $h_1 < h_f \cap h_{2L} = h_f \cap h_{2V} > h_g$

$$\Psi = \begin{vmatrix} V_{2V} * \frac{\partial \rho_{2V}}{\partial p} & \rho_{2V} & V_{2V} * \frac{\partial \rho_{2V}}{\partial h_{2V}} & -1 & 0 & 0 \\ (V_2 - V_{2V}) * \frac{d\rho_F}{dp} & -\rho_F & 0 & 1 & 0 & 0 \\ V_1 * \frac{\partial \rho_1}{\partial p} & 0 & 0 & 0 & V_1 * \frac{\partial \rho_1}{\partial h_1} & 1 \\ -V_{2V} & 0 & \rho_{2V} * V_{2V} & (h_{2V} - h_G) & 0 & 0 \\ (V_2 - V_{2V}) * \left(\rho_F * \frac{dh_F}{dp} - 1\right) & 0 & 0 & (h_G - h_F) & 0 & 0 \\ -V_1 & 0 & 0 & 0 & \rho_1 * V_1 & 0 \end{vmatrix}$$

$$\dot{z} = \left\{\dot{p}, \dot{V}_{2v}, \dot{h}_{2v}, \dot{m}_{FL}, \dot{h_1}, \dot{m}_{OUT\_2}\right\}^T$$

$$\eta = \begin{vmatrix} -\dot{m}_{SC} - \dot{m}_{WC} - \dot{m}_{SP} - \dot{m}_{VLV} \\ \dot{m}_{SC} + \dot{m}_{WC} + \dot{m}_{SP} \\ -\dot{m}_{OUTsurge} \\ -\dot{m}_{SC} \cdot (h_G - h_{2V}) - \dot{m}_{WC} \cdot (h_G - h_{2V}) - Q_{l-v} - Q_{V-ext} \\ \dot{m}_{SC} \cdot (h_F - h_G) + \dot{m}_{WC} \cdot (h_F - h_G) + \dot{m}_{SP} \cdot (h_{SP} - h_F) + \dot{Q}_H + Q_{l-v} - Q_{l-l} - Q_{Lu-ext} \\ Q_{l-l} - Q_{Ll-ext} \end{vmatrix}$$

OUTSURGE-STATE 3 $h_1 < h_f \cap h_{2L} < h_f \cap h_{2V} = h_g$

$$\Psi = \begin{vmatrix} V_{2V} * \frac{d\rho_G}{dp} & \rho_G & 1 & 0 & 0 & 0 \\ (V_2 - V_{2V}) * \frac{\partial \rho_{2L}}{\partial p} & -\rho_{2L} & -1 & (V_2 - V_{2V}) * \frac{\partial \rho_{2L}}{\partial h_{2L}} & 0 & 0 \\ V_1 * \frac{\partial \rho_1}{\partial p} & 0 & 0 & 0 & V_1 * \frac{\partial \rho_1}{\partial h_1} & 1 \\ V_{2V} * \left(\rho_G * \frac{dh_G}{dp} - 1\right) & 0 & (h_F - h_G) & 0 & 0 & 0 \\ -(V_2 - V_{2V}) & 0 & (h_{2L} - h_F) & \rho_{2L} * (V_2 - V_{2V}) & 0 & 0 \\ -V_1 & 0 & 0 & 0 & \rho_1 * V_1 & 0 \end{vmatrix}$$

$$\dot{z} = \left\{\dot{p}, \dot{V}_{2v}, \dot{m}_{RO}, \dot{h}_{2l}, \dot{h_1}, \dot{m}_{OUT\_2}\right\}^T$$

$$\eta = \begin{vmatrix} -\dot{m}_{SC} - \dot{m}_{WC} - \dot{m}_{SP} - \dot{m}_{VLV} \\ \dot{m}_{SC} + \dot{m}_{WC} + \dot{m}_{SP} \\ -\dot{m}_{OUTsurge} \\ -Q_{l-v} - Q_{V-ext} \\ \dot{m}_{SC} \cdot (h_{2L} - h_G) + \dot{m}_{WC} \cdot (h_{2L} - h_G) + \dot{m}_{SP} \cdot (h_{SP} - h_{2L}) + \dot{Q}_H + Q_{l-v} - Q_{l-l} - Q_{Lu-ext} \\ Q_{l-l} - Q_{Ll-ext} \end{vmatrix}$$

OUTSURGE-STATE 4 $h_1 < h_f \cap h_{2L} = h_f \cap h_{2V} = h_g$

$$\Psi = \begin{vmatrix} V_{2V} * \frac{d\rho_G}{dp} & \rho_G & 1 & -1 & 0 & 0 \\ (V_2 - V_{2V}) * \frac{d\rho_F}{dp} & -\rho_F & -1 & 1 & 0 & 0 \\ V_1 * \frac{\partial \rho_1}{\partial p} & 0 & 0 & 0 & V_1 * \frac{\partial \rho_1}{\partial h_1} & 1 \\ V_{2V} * \left(\rho_G * \frac{dh_G}{dp} - 1\right) & 0 & (h_F - h_G) & 0 & 0 & 0 \\ (V_2 - V_{2V}) * \left(\rho_F * \frac{dh_F}{dp} - 1\right) & 0 & 0 & (h_G - h_F) & 0 & 0 \\ -V_1 & 0 & 0 & 0 & \rho_1 * V_1 & 0 \end{vmatrix}$$

$$\dot{z} = \left\{\dot{p}, \dot{V}_{2v}, \dot{m}_{RO}, \dot{m}_{FL}, \dot{h_1}, \dot{m}_{OUT\_2}\right\}^T$$

$$\eta = \begin{vmatrix} -\dot{m}_{SC} - \dot{m}_{WC} - \dot{m}_{SP} - \dot{m}_{VLV} \\ \dot{m}_{SC} + \dot{m}_{WC} + \dot{m}_{SP} \\ -\dot{m}_{OUTsurge} \\ -Q_{V-ext} \\ \dot{m}_{SP} \cdot (h_{SP} - h_{2L}) + \dot{Q}_H - Q_{l-l} - Q_{Lu-ext} \\ Q_{l-l} - Q_{Ll-ext} \end{vmatrix}$$

2.6 TWO-REGIONS-THREE-VOLUMES MODEL

This last model is substantially a further improvement of the two-regions-two-volumes one. Another only liquid volume is considered in the lower region of pressurizer to get better the simulation of temperature distribution phenomenon.
As it will be shown in the next chapter, this last model gives results very similar to RELAP5® ones and above all very closed to experimental data. This fact indicates that a zero-dimensional representation of the pressurizer cannot be implemented for a good simulation program, it gives only the qualitative dynamics. The mathematical formulation for the pressurizer is now based on the selection of three control volumes within the pressurizer.

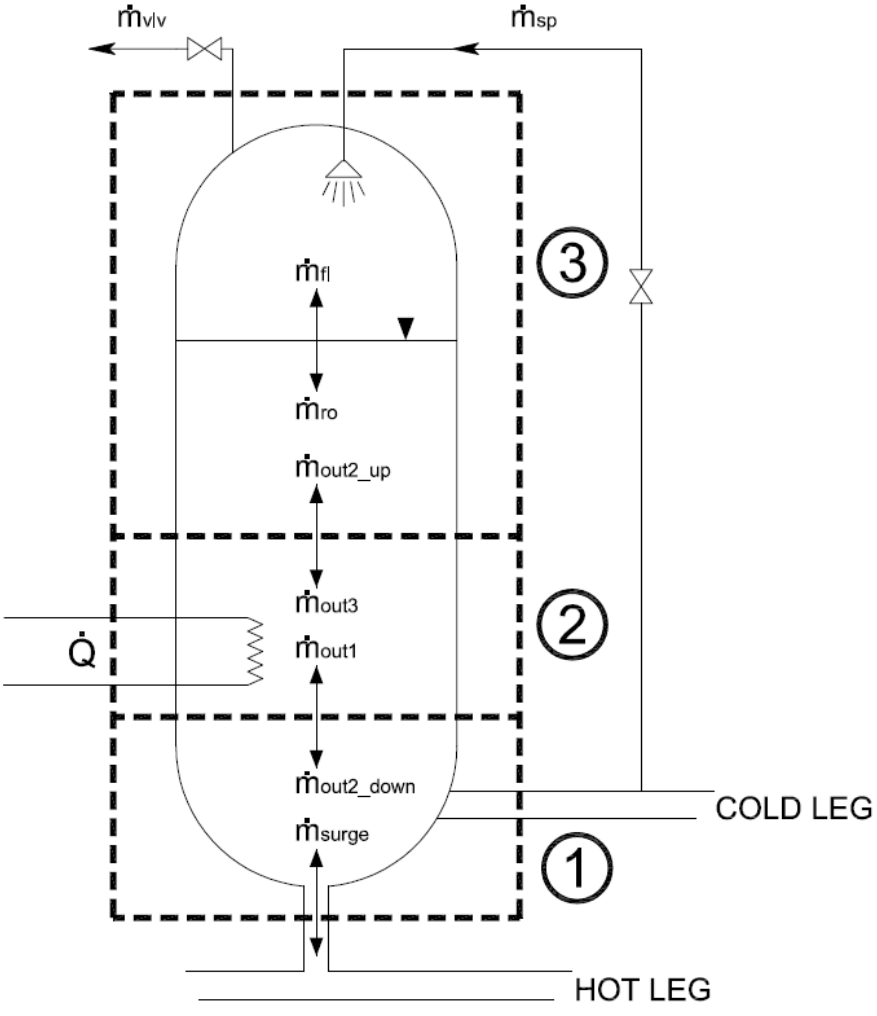

FIG. 2.4 Two-regions-three- volume pressurizer

These volumes are fixed. Starting from the bottom, the first two control volumes are only liquid regions, always at subcooled conditions. These volumes are needed to take into account temperature non-uniformities occurring during transients. The third control volume, at the upper portion of the pressurizer, is then divided into two regions, one for steam and one for liquid, which can change their proper volume, under the constraint of conservation of the total volume of the third portion. These two sub-control volumes are separated by an interface across which mass, heat and work exchanges could occur. The lower sub-control volume could contain subcooled liquid or boiling water, while the upper control volume could contain superheated or condensing steam. The governing differential equations for each state are derived by first applying the continuity and energy equations. The resulting equations are then manipulated algebraically until obtaining a system in matrix form. To take into account inversions of surge flow rate, equations are split into two groups, the first for insurge transients and the second for outsurge ones. In the subsequent pages, all the matrices for all possible thermodynamics states are reported, in particular the notation $\dot{m}_{OUT\_1}$ refers to the mass flow rate during insurge transients from volume one to volume two, $\dot{m}^{UP}_{OUT\_2}$ to the mass flow rate during outsurge transients from volume two to volume three, $\dot{m}_{OUT\_3}$ to mass flow rate during outsurge transients from volume three to volume two. With Q all possible heat exchanges are named.

INSURGE-STATE 1 $\quad h_1 < h_f \cap h_2 < h_f \cap h_{3L} < h_f \cap h_{3V} > h_g$

$$\Psi = \begin{vmatrix} V_{3V} * \frac{\partial \rho_{3V}}{\partial p} & \rho_{3V} & V_{3V} * \frac{\partial \rho_{3V}}{\partial h_{3V}} & 0 & 0 & 0 & 0 & 0 \\ (V_3 - V_{3V}) * \frac{\partial \rho_{3L}}{\partial p} & -\rho_{3L} & 0 & (V_3 - V_{3V}) * \frac{\partial \rho_{3L}}{\partial h_{3L}} & 0 & 0 & -1 & 0 \\ V_2 * \frac{\partial \rho_2}{\partial p} & 0 & 0 & 0 & V_2 * \frac{\partial \rho_2}{\partial h_2} & 0 & 1 & -1 \\ V_1 * \frac{\partial \rho_1}{\partial p} & 0 & 0 & 0 & 0 & V_1 * \frac{\partial \rho_1}{\partial h_1} & 0 & 1 \\ -V_{3V} & 0 & \rho_{3V} * V_{3V} & 0 & 0 & 0 & 0 & 0 \\ -(V_3 - V_{3V}) & 0 & 0 & \rho_{3L} * (V_3 - V_{3V}) & 0 & 0 & -(h_2 - h_{3L}) & 0 \\ -V_2 & 0 & 0 & 0 & \rho_2 * V_2 & 0 & 0 & -(h_1 - h_2) \\ -V_1 & 0 & 0 & 0 & 0 & \rho_1 * V_1 & 0 & 0 \end{vmatrix}$$

$$\dot{z} = \left\{\dot{p}, \dot{V}_{3V}, \dot{h}_{3V}, \dot{h}_{3L}, \dot{h}_2, \dot{h}_1, \dot{m}^{UP}_{OUT\_2}, \dot{m}_{OUT\_1}\right\}^T$$

$$\eta = \begin{vmatrix} -\dot{m}_{SC} - \dot{m}_{VLV} \\ \dot{m}_{SC} + \dot{m}_{SP} \\ 0 \\ \dot{m}_{INsurge} \\ \dot{m}_{SC} * (h_{3V} - h_G) + Q \\ \dot{m}_{SC} * (h_G - h_{3L}) + \dot{m}_{SP} * (h_{SP} - h_{3L}) + Q \\ Q \\ \dot{m}_{INsurge} * (h_{INsurge} - h_1) + Q \end{vmatrix}$$

INSURGE-STATE 2 $h_1 < h_f \cap h_2 < h_f \cap h_{3L} = h_f \cap h_{3V} > h_g$

$$\Psi = \begin{vmatrix} V_{3V} * \frac{\partial \rho_{3V}}{\partial p} & \rho_{3V} & V_{3V} * \frac{\partial \rho_{3V}}{\partial h_{3V}} & -1 & 0 & 0 & 0 & 0 \\ (V_3 - V_{3V}) * \frac{d\rho_F}{dp} & -\rho_F & 0 & 1 & 0 & 0 & -1 & 0 \\ V_2 * \frac{\partial \rho_2}{\partial p} & 0 & 0 & 0 & V_2 * \frac{\partial \rho_2}{\partial h_2} & 0 & 1 & -1 \\ V_1 * \frac{\partial \rho_1}{\partial p} & 0 & 0 & 0 & 0 & V_1 * \frac{\partial \rho_1}{\partial h_1} & 0 & 1 \\ -V_{3V} & 0 & \rho_{3V} * V_{3V} & (h_{3V} - h_G) & 0 & 0 & 0 & 0 \\ (V_3 - V_{3V}) * \left(\rho_F * \frac{dh_F}{dp} - 1\right) & 0 & 0 & (h_G - h_F) & 0 & 0 & -(h_2 - h_F) & 0 \\ -V_2 & 0 & 0 & 0 & \rho_2 * V_2 & 0 & 0 & -(h_1 - h_2) \\ -V_1 & 0 & 0 & 0 & 0 & \rho_1 * V_1 & 0 & 0 \end{vmatrix}$$

$$\dot{z} = \left\{\dot{p}, \dot{V}_{3V}, \dot{h}_{3V}, \dot{m}_{FL}, \dot{h}_2, \dot{h}_1, \dot{m}_{OUT\_2}^{UP}, \dot{m}_{OUT\_1}\right\}^T$$

$$\eta = \begin{vmatrix} -\dot{m}_{SC} - \dot{m}_{VLV} \\ \dot{m}_{SC} + \dot{m}_{SP} \\ 0 \\ \dot{m}_{INsurge} \\ \dot{m}_{SC} * (h_{3V} - h_G) \\ \dot{m}_{SC} * (h_G - h_F) + \dot{m}_{SP} * (h_{SP} - h_F) + Q \\ Q \\ \dot{m}_{INsurge} * \left(h_{INsurge} - h_1\right) + Q \end{vmatrix}$$

INSURGE-STATE 3 $h_1 < h_f \cap h_2 < h_f \cap h_{3L} < h_f \cap h_{3V} = h_g$

$$\Psi = \begin{vmatrix} V_{3V} * \frac{d\rho_G}{dp} & \rho_G & 1 & 0 & 0 & 0 & 0 & 0 \\ (V_3 - V_{3V}) * \frac{\partial \rho_{3L}}{\partial p} & -\rho_{3L} & -1 & (V_3 - V_{3V}) * \frac{\partial \rho_{3L}}{\partial h_{3L}} & 0 & 0 & -1 & 0 \\ V_2 * \frac{\partial \rho_2}{\partial p} & 0 & 0 & 0 & V_2 * \frac{\partial \rho_2}{\partial h_2} & 0 & 1 & -1 \\ V_1 * \frac{\partial \rho_1}{\partial p} & 0 & 0 & 0 & 0 & V_1 * \frac{\partial \rho_1}{\partial h_1} & 0 & 1 \\ V_{3V} * \left(\rho_G * \frac{dh_G}{dp} - 1\right) & 0 & (h_F - h_G) & 0 & 0 & 0 & 0 & 0 \\ -(V_3 - V_{3V}) & 0 & (h_{3L} - h_F) & \rho_{3L} * (V_3 - V_{3V}) & 0 & 0 & -(h_2 - h_{3L}) & 0 \\ -V_2 & 0 & 0 & 0 & \rho_2 * V_2 & 0 & 0 & -(h_1 - h_2) \\ -V_1 & 0 & 0 & 0 & 0 & \rho_1 * V_1 & 0 & 0 \end{vmatrix}$$

$$\dot{z} = \left\{\dot{p}, \dot{V}_{3V}, \dot{m}_{RO}, \dot{h}_{3L}, \dot{h}_2, \dot{h}_1, \dot{m}_{OUT\_2}^{UP}, \dot{m}_{OUT\_1}\right\}^T$$

$$\eta = \begin{vmatrix} -\dot{m}_{SC} - \dot{m}_{VLV} \\ \dot{m}_{SC} + \dot{m}_{SP} \\ 0 \\ \dot{m}_{INsurge} \\ 0 \\ \dot{m}_{SC} * (h_G - h_{3L}) + \dot{m}_{SP} * (h_{SP} - h_{3L}) + Q \\ Q \\ \dot{m}_{INsurge} * (h_{INsurge} - h_1) + Q \end{vmatrix}$$

INSURGE-STATE 4 $\quad h_1 < h_f \cap h_2 < h_f \cap h_{3L} = h_f \cap h_{3V} = h_g$

$$\Psi = \begin{vmatrix} V_{3V} * \frac{d\rho_G}{dp} & \rho_G & 1 & -1 & 0 & 0 & 0 & 0 \\ (V_3 - V_{3V}) * \frac{d\rho_F}{dp} & -\rho_F & -1 & 1 & 0 & 0 & -1 & 0 \\ V_2 * \frac{\partial\rho_2}{\partial p} & 0 & 0 & 0 & V_2 * \frac{\partial\rho_2}{\partial h_2} & 0 & 1 & -1 \\ V_1 * \frac{\partial\rho_1}{\partial p} & 0 & 0 & 0 & 0 & V_1 * \frac{\partial\rho_1}{\partial h_1} & 0 & 1 \\ V_{3V} * \left(\rho_G * \frac{dh_G}{dp} - 1\right) & 0 & (h_F - h_G) & 0 & 0 & 0 & 0 & 0 \\ (V_3 - V_{3V}) * \left(\rho_F * \frac{dh_F}{dp} - 1\right) & 0 & 0 & (h_G - h_F) & 0 & 0 & -(h_2 - h_F) & 0 \\ -V_2 & 0 & 0 & 0 & \rho_2 * V_2 & 0 & 0 & -(h_1 - h_2) \\ -V_1 & 0 & 0 & 0 & 0 & \rho_1 * V_1 & 0 & 0 \end{vmatrix}$$

$$\dot{z} = \left\{\dot{p}, \dot{V}_{3V}, \dot{m}_{RO}, \dot{m}_{FL}, \dot{h}_2, \dot{h}_1, \dot{m}_{OUT\_2}^{UP}, \dot{m}_{OUT\_1}\right\}^T$$

$$\eta = \begin{vmatrix} -\dot{m}_{SC} - \dot{m}_{VLV} \\ \dot{m}_{SC} + \dot{m}_{SP} \\ 0 \\ \dot{m}_{INsurge} \\ 0 \\ \dot{m}_{SC} * (h_G - h_F) + \dot{m}_{SP} * (h_{SP} - h_F) + Q \\ Q \\ \dot{m}_{INsurge} * (h_{INsurge} - h_1) \end{vmatrix}$$

OUTSURGE-STATE 1 $\quad h_1 < h_f \cap h_2 < h_f \cap h_{3L} < h_f \cap h_{3V} > h_g$

$$\Psi = \begin{vmatrix} V_{3V} * \frac{\partial \rho_{3V}}{\partial p} & \rho_{3V} & V_{3V} * \frac{\partial \rho_{3V}}{\partial h_{3V}} & 0 & 0 & 0 & 0 & 0 \\ (V_3 - V_{3V}) * \frac{\partial \rho_{3L}}{\partial p} & -\rho_{3L} & 0 & (V_3 - V_{3V}) * \frac{\partial \rho_{3L}}{\partial h_{3L}} & 0 & 0 & 0 & 1 \\ V_2 * \frac{\partial \rho_2}{\partial p} & 0 & 0 & 0 & V_2 * \frac{\partial \rho_2}{\partial h_2} & 0 & 1 & -1 \\ V_1 * \frac{\partial \rho_1}{\partial p} & 0 & 0 & 0 & 0 & V_1 * \frac{\partial \rho_1}{\partial h_1} & -1 & 0 \\ -V_{3V} & 0 & \rho_{3V} * V_{3V} & 0 & 0 & 0 & 0 & 0 \\ -(V_3 - V_{3V}) & 0 & 0 & \rho_{3L} * (V_3 - V_{3V}) & 0 & 0 & 0 & 0 \\ -V_2 & 0 & 0 & 0 & \rho_2 * V_2 & 0 & 0 & -(h_{3L} - h_2) \\ -V_1 & 0 & 0 & 0 & 0 & \rho_1 * V_1 & -(h_2 - h_1) & 0 \end{vmatrix}$$

$$\dot{z} = \left\{\dot{p}, \dot{V}_{3V}, \dot{h}_{3V}, \dot{h}_{3L}, \dot{h}_2, \dot{h}_1, \dot{m}_{OUT\_2}^{DOWN}, \dot{m}_{OUT\_3}\right\}^T$$

$$\eta = \begin{vmatrix} -\dot{m}_{SC} - \dot{m}_{VLV} \\ \dot{m}_{SC} + \dot{m}_{SP} \\ 0 \\ -\dot{m}_{OUTsurge} \\ \dot{m}_{SC} * (h_{3V} - h_G) \\ \dot{m}_{SC} * (h_G - h_{3L}) + \dot{m}_{SP} * (h_{SP} - h_{3L}) + Q \\ Q \\ 0 \end{vmatrix}$$

OUTSURGE-STATE 2 $\quad h_1 < h_f \cap h_2 < h_f \cap h_{3L} = h_f \cap h_{3V} > h_g$

$$\Psi = \begin{vmatrix} V_{3V} * \frac{\partial \rho_{3V}}{\partial p} & \rho_{3V} & V_{3V} * \frac{\partial \rho_{3V}}{\partial h_{3V}} & -1 & 0 & 0 & 0 & 0 \\ (V_3 - V_{3V}) * \frac{d\rho_F}{dp} & -\rho_F & 0 & 1 & 0 & 0 & 0 & 1 \\ V_2 * \frac{\partial \rho_2}{\partial p} & 0 & 0 & 0 & V_2 * \frac{\partial \rho_2}{\partial h_2} & 0 & 1 & -1 \\ V_1 * \frac{\partial \rho_1}{\partial p} & 0 & 0 & 0 & 0 & V_1 * \frac{\partial \rho_1}{\partial h_1} & -1 & 0 \\ -V_{3V} & 0 & \rho_{3V} * V_{3V} & (h_{3V} - h_G) & 0 & 0 & 0 & 0 \\ (V_3 - V_{3V}) * \left(\rho_F * \frac{dh_F}{dp} - 1\right) & 0 & 0 & (h_G - h_F) & 0 & 0 & 0 & 0 \\ -V_2 & 0 & 0 & 0 & \rho_2 * V_2 & 0 & 0 & -(h_{3L} - h_2) \\ -V_1 & 0 & 0 & 0 & 0 & \rho_1 * V_1 & -(h_2 - h_1) & 0 \end{vmatrix}$$

$$\dot{z} = \left\{\dot{p}, \dot{V}_{3V}, \dot{h}_{3V}, \dot{m}_{FL}, \dot{h}_2, \dot{h}_1, \dot{m}_{OUT\_2}^{DOWN}, \dot{m}_{OUT\_3}\right\}^T$$

$$\eta = \begin{vmatrix} -\dot{m}_{SC} - \dot{m}_{VLV} \\ \dot{m}_{SC} + \dot{m}_{SP} \\ 0 \\ -\dot{m}_{OUTsurge} \\ \dot{m}_{SC} * (h_{3V} - h_G) \\ \dot{m}_{SC} * (h_G - h_F) + \dot{m}_{SP} * (h_{SP} - h_F) + Q \\ Q \\ 0 \end{vmatrix}$$

OUTSURGE-STATE 3 $\quad h_1 < h_f \cap h_2 < h_f \cap h_{3L} < h_f \cap h_{3V} = h_g$

$$\Psi = \begin{vmatrix} V_{3V} * \frac{d\rho_G}{dp} & \rho_G & 1 & 0 & 0 & 0 & 0 & 0 \\ (V_3 - V_{3V}) * \frac{\partial \rho_{3L}}{\partial p} & -\rho_{3L} & -1 & (V_3 - V_{3V}) * \frac{\partial \rho_{3L}}{\partial h_{3L}} & 0 & 0 & 0 & 1 \\ V_2 * \frac{\partial \rho_2}{\partial p} & 0 & 0 & 0 & V_2 * \frac{\partial \rho_2}{\partial h_2} & 0 & 1 & -1 \\ V_1 * \frac{\partial \rho_1}{\partial p} & 0 & 0 & 0 & 0 & V_1 * \frac{\partial \rho_1}{\partial h_1} & -1 & 0 \\ V_{3V} * \left(\rho_G * \frac{dh_G}{dp} - 1\right) & 0 & (h_F - h_G) & 0 & 0 & 0 & 0 & 0 \\ -(V_3 - V_{3V}) & 0 & (h_{3L} - h_F) & \rho_{3L} * (V_3 - V_{3V}) & 0 & 0 & 0 & 0 \\ -V_2 & 0 & 0 & 0 & \rho_2 * V_2 & 0 & 0 & -(h_{3L} - h_2) \\ -V_1 & 0 & 0 & 0 & 0 & \rho_1 * V_1 & -(h_2 - h_1) & 0 \end{vmatrix}$$

$$\dot{z} = \left\{\dot{p}, \dot{V}_{3V}, \dot{m}_{RO}, \dot{h}_{3L}, \dot{h}_2, \dot{h}_1, \dot{m}_{OUT\_2}^{DOWN}, \dot{m}_{OUT\_3}\right\}^T$$

$$\eta = \begin{vmatrix} -\dot{m}_{SC} - \dot{m}_{VLV} \\ \dot{m}_{SC} + \dot{m}_{SP} \\ 0 \\ -\dot{m}_{OUTsurge} \\ Q \\ \dot{m}_{SC} * (h_G - h_{3L}) + \dot{m}_{SP} * (h_{SP} - h_{3L}) + Q \\ Q \\ Q \end{vmatrix}$$

OUTSURGE-STATE 4 $h_1 < h_f \cap h_2 < h_f \cap h_{3L} = h_f \cap h_{3V} = h_g$

$$\Psi = \begin{vmatrix} V_{3V} * \frac{d\rho_G}{dp} & \rho_G & 1 & -1 & 0 & 0 & 0 & 0 \\ (V_3 - V_{3V}) * \frac{d\rho_F}{dp} & -\rho_F & -1 & 1 & 0 & 0 & 0 & 1 \\ V_2 * \frac{\partial \rho_2}{\partial p} & 0 & 0 & 0 & V_2 * \frac{\partial \rho_2}{\partial h_2} & 0 & 1 & -1 \\ V_1 * \frac{\partial \rho_1}{\partial p} & 0 & 0 & 0 & 0 & V_1 * \frac{\partial \rho_1}{\partial h_1} & -1 & 0 \\ V_{3V} * \left(\rho_G * \frac{dh_G}{dp} - 1\right) & 0 & (h_F - h_G) & 0 & 0 & 0 & 0 & 0 \\ (V_3 - V_{3V}) * \left(\rho_F * \frac{dh_F}{dp} - 1\right) & 0 & 0 & (h_G - h_F) & 0 & 0 & 0 & 0 \\ -V_2 & 0 & 0 & 0 & \rho_2 * V_2 & 0 & 0 & -(h_F - h_2) \\ -V_1 & 0 & 0 & 0 & 0 & \rho_1 * V_1 & -(h_2 - h_1) & 0 \end{vmatrix}$$

$$\dot{z} = \left\{\dot{p}, \dot{V}_{3V}, \dot{m}_{RO}, \dot{m}_{FL}, \dot{h}_2, \dot{h}_1, \dot{m}_{OUT\_2}^{DOWN}, \dot{m}_{OUT\_3}\right\}^T$$

$$\eta = \begin{vmatrix} -\dot{m}_{SC} - \dot{m}_{VLV} \\ \dot{m}_{SC} + \dot{m}_{SP} \\ 0 \\ \dot{m}_{OUTsurge} \\ Q \\ \dot{m}_{SC} * (h_G - h_F) + \dot{m}_{SP} * (h_{SP} - h_F) + Q \\ Q \\ Q \end{vmatrix}$$

2.7 CONCLUDING REMARKS

In this chapter the pressurizer models that will be implemented in Simulink® and Dymola® code have been developed.
The models have been derived in order of increasing accuracy and therefore complexity. In particular it is possible to see the great jump between the equilibrium model and the non-equilibrium ones, also in the single volume case, which is, among the non-equilibrium models, the simplest.
In case of equilibrium model, the water and steam mixture is always at saturation condition and so the only temperature which can be computed by the model is the saturation one. The entire pressurizer volume is substantially reduced to a point in a completely lumped parameter approach.
Non-equilibrium two-regions-single-volume model considers two different temperature for liquid and steam region, which are now separated, but it cannot take into account temperature distribution which occurs along the liquid region.
In order to consider this phenomenon, more complex non-equilibrium models have been developed.
The matrix formulation will be used for the Simulink® programs, whose core will be a MATLAB® static function computing Ψ matrix inversion and all the thermodynamic partial derivatives appearing in the mathematical formulation of the models.
Simulink® programs will constitute the best implementation for a control-oriented simulation code.
In Dymola® programs, instead, mass and energy equations and the volume constraint will be used directly, without the necessity to split insurge from outsurge cases for all models and not only for the simple equilibrium and two-regions-one volume ones. Also the partial thermodynamic derivative are compute automatically by Dymola® interpreter. Dymola® programs will demonstrate the great potentialities of acausal and object-oriented modelling.

2.8 REFERENCES

[3] NUCLEAR SYSTEMS VOLUME 0NE-THERMAL-HYDRAULICS FUNDAMENTALS
Neil E. Todreas and Mujid J. Kazimi
CRC PRESS –Second Ediction 2012

[4] REDFIELD, J.A.; PRESCOP, V.; MARGOLIS, S.G.
Pressurizer performance during-load drop. Tests at Shippingport: analysis and test.
Trans. Am. Nucl. Soc: 323, June1967.

[5] GAJEWSKI, W.M.
Study by simulator techniques of transient pressures in high pressure water systems utilizing a surge tank. Westinghouse Eletric Co.1955.

[6] SORENSON, C.W.
Procedure for sizing pressurizers for pressurized water reactor;
3.10-32, 1960 (KAPL--2000-10),

[7] COUGHREN, K.D.
Pressurizing vessel performance equations.
Pacific Northwest Lab., 1965. {BNWL-116).

[8] DRUCKER, E.E.; TONG, K.N.
Behaviour of a steam - -pressurizer surge tank. Trans. Am. Nucl. Society

[5] GAJEWSKI, W.M.
Study by simulator techniques of transient pressures in high pressure water systems utilizing a surge tank. Westinghouse Eletric Co.1955.

[6] SORENSON, C.W.
Procedure for sizing pressurizers for pressurized water reactor;
3.10-32, 1960 (KAPL--2000-10),

[7] COUGHREN, K.D.
Pressurizing vessel performance equations.
Pacific Northwest Lab., 1965. {BNWL-116).

[8] DRUCKER, E.E.; TONG, K.N.
Behaviour of a steam - -pressurizer surge tank. Trans. Am. Nucl. Society

[9] DRUCKER, E.E.; GORMAN, D.J.
A method predicting steam-surge tank transients based on one-dimensional heat sink transients based on one-dimensional heat sink.
NUC. Sci. Eng., 21: 473-80, 1965.

[10] G.BROWN
Insurge transient from a surge tank using CSMP. 109-14, Oct. 1974.

[11] DONALD BRITTON BOSLEY , Lieutenant, United States Navy
ROTH SUMNER LEDDICK, Lieutenant, United States Navy-
Simulation of steam pressurizing tank transients by analog computer

[12] NAHAVANDI, A.N. The loss-of-coolant accident analysis in pressurized water reactors.
Nuc. Sci. Eng., 36;159-88, 1969.

[13] NAHAVANDI, A.N.; MAKKENCHERY, S, An improved pressurizer model with bubble rise and condensate drop dynamics. Nuc. Eng. & Design, 12: 135-47, 1970.

[14] BARON, R.C. Digital simulation of a nuclear pressurizer.
Nuc. Sei. Eng., 52: 283-91, 1973.

[15] J.F.WILSON, R.J GRENDA and J.F.PATTERSON,
Steam volume fraction in a bubbling two-phase mixture, Transactions American Nuclear Society, Session 25 (1961).

[16] HACK YEONG CHUNG, TAE WOON KIM,SOON HEUNG CHANG, BYUNG HO LEE
Dept. of Nuclear Engineering
Korea Advanced Institute of Science and Technology,
Adaptive kalman gain approach to on-line instrument failure detection with improved glr method and suboptimal control on loft pressurizer

[17] R. M. KURIDAN and T. D. BEYNON
A LINEARIZED NON STEADY STATE MODEL FOR THE PRESSURIZER OF THE SAFE INTEGRAL REACTOR CONCEPT
Nuclear Engineering Department, Alfateh University, P.O. Box 13292, Tripoli, Libya
School of Physics and Space Research, University of Birmingham, Edgbaston,
Birmingham, B15 2TT, U.K

[18] DAVID A. BOTELHO, PAULO A.B. DE SAMPAIO, CELSO M.F. LAPA, CLAUDIO M.N.A. PEREIRA,MARIA DE LOURDES MOREIRA, ANTONIO CARLOS DE O. BARROSO
The iris pressurizer: simulation of out-surge transients and optimization procedure to design scaled experiments
Progress in Nuclear Energy 50 (2008) 730e739

[19] I.G. SHEKRILADZE,
V.I. GOMELAURI
Theoretical study of laminar film condensation of flowing steam
Georgian Research Power Institute, Tbilisi, U.S.S.R.

[20] FUNDAMENTALS OF HEAT AND MASS TRANSFER
Theodore l. Bergman
Department of mechanical engineering
University of connecticut
Adrienne s. Lavine
Mechanical and aerospace engineering
Department
University of california, los angeles
Frank p. Incropera
College of engineering
University of notre dame
David p. Dewitt
School of mechanical engineering
Purdue university
JOHN Wiley Seventh Edition 2011

[21] FONDAMENTI DI CONTROLLI AUTOMATICI
Paolo Bolzern, Riccardo Scattolini, Nicola Schiavoni
McGraw-Hill Companies
3rd edition 2008

[22] LINDA PETZOLD
Differential/algebraic equations are not ode's
Siam j. Sci. Stat. Comput.
Vol. 3, no. 3, september 1982
1982 society for industrial and applied mathematics
0196-5204/82/0303-0007 $01.00/0

[23] J. R. COOPER, DR. R. B. DOOLEY
Revised Release on the IAPWS Industrial Formulation 1997
for the Thermodynamic Properties of Water and Steam
School of Engineering and Materials Science
Queen Mary, University of London
Mile End Road
London E1 4NS, England
Executive Secretary:
Structural Integrity Associates, Inc.
2616 Chelsea Drive
Charlotte, NC 28209, USA

Chapter 3 – PRESSURIZER SIMULATION CODES

3.1 INTRODUCTION

This chapter is dedicated to the description of the computer codes programmed to actually run simulations and therefore verify the previously presented models.
Firstly Simulink® programs, where the control-oriented structure is clear, are described for both equilibrium and non-equilibrium case. Of course the attention is particularly focused on non-equilibrium codes, which are the core of this study, while the equilibrium one it is presented only to demonstrate the poor performances of this kind of approach.
Then the Dymola® acausal and object-oriented approach follows. In order not to overload the treatment, just the non-equilibrium model implementations are discussed. In this section the physical structure of the pressurizer virtual model and all the advantages coming from the object-oriented programming are pointed out. On the contrary the control-oriented nature of the model is partially hidden.
Finally, the end of the chapter is occupied by the pressurizer code developed using RELAP5®. In this case the approach is completely different, the pressurizer is simulated using thermo-hydraulics components present in RELAP5® library. No equation must be written: just the structure of the pressurizer tank must be realized and properly initialized. Then RELAP5® automatically applies and integrates mass, energy and also momentum equation for the two phase system. Of course RELAP5® is not a control-oriented code, it will be used as standard reference for a code to code comparison.

3.2 CAUSAL APPROACH

Generally speaking, modelling is based on mathematical representation of physical phenomena occurring in the system of interest. Introducing some simplifications and manipulations of characteristics equations and taking into account boundary conditions, it is possible to create a simplified model of the real system, which is represented in terms of interactions between characteristics variables.
To study dynamic non-linear systems made of different sub-systems connected together, it is possible to realize input-output models using the so-called causal or procedural approach. In this way the problem is formulated using the causality links appearing in the system, in order that equations representing interesting quantities, the outputs, depend on known variables, the inputs. Inputs are actions done on the object analyzed by external agents, outputs are all those which it is of interest about the behaviour of the system.
Between input and output variables there is a cause-effect relationship: the evolutions of the seconds describe how the system responds to the firsts.
However, the knowledge of input variables could be not sufficient to determine the values of output ones, in these cases you must introduce a new vector of variables: the state variables vector. A state variable is one of the set of variables that are used to describe the mathematical "state" of a dynamical system. Intuitively, the state of a system describes enough about the system to determine its future behavior. Models that consist of coupled first-order differential equations are said to be in state-variable form.
Causal formulation provide a clear graphic visualization of individual mathematical relationships based on block schemes. Signals flow in connections between blocks, transmitting the values of every variables from the output of one block to the inputs of other blocks. The processing of input information to output information takes place in the blocks. Interconnection of the blocks thus reflects rather the calculation procedure than the actual structure of the modelled reality. These blocks uses known quantities to compute unknown variables and they can be put in the sequent mathematical form:

$$\dot{x} = f(x(t), y(t), t) \tag{3.1}$$
$$y(t) = g(x(t), y(t), t) \tag{3.2}$$

Where $u \in R^m, x \in R^n \; and \; y \in R^p$ respectively are the vector of inputs, of state variables and of outputs; f and g are two vector functions. Equation 3.1 is the state equation, i.e. an ODE expressing the relationship between inputs and state variables. Equation 3.2, instead, is the transformation output, i.e. an algebraic equation connecting inputs, output and state variables. Generally modelling has as its object time invariant system. For this kind of system f and g functions does not depends explicitly on time:

$$\dot{x} = f\big(x(t), y(t)\big) \tag{3.3}$$
$$y(t) = g(x(t), y(t)) \tag{3.4}$$

When blocks are connected together, they can describe and simulate big systems of differential equations. So the causal approach is a very effective instrument to represent the behaviour of physical system. Causal modelling has a big weakness, because input and outputs are stated a priori, it is essentially impossible to modify the system when the boundary conditions change. You must do it all again. So the critical points of this approach are:

- Equation must be obtained manually from the constitutive equations and conservation principle, as done in the previous chapter.
- Causality assumption must be made at components level and not at system one, so the model is rigid.

3.3 SIMULINK® MODEL

Simulink® is a block diagram environment for multidomain simulation and Model-Based Design. It supports system-level design, simulation, automatic code generation, and continuous test and verification of embedded systems. Simulink® provides a graphical editor, customizable block libraries, and solvers for modelling and simulating dynamic systems. It is integrated with MATLAB®, enabling you to incorporate MATLAB® algorithms into models and export simulation results to MATLAB® for further analysis.
The pressurizer equilibrium and non-equilibrium model realized in Simulink® environment can be seen in figure 3.1, where there are four main blocks: the inputs, the pressurizer dynamic , the controller and finally the outputs (monitor) one.

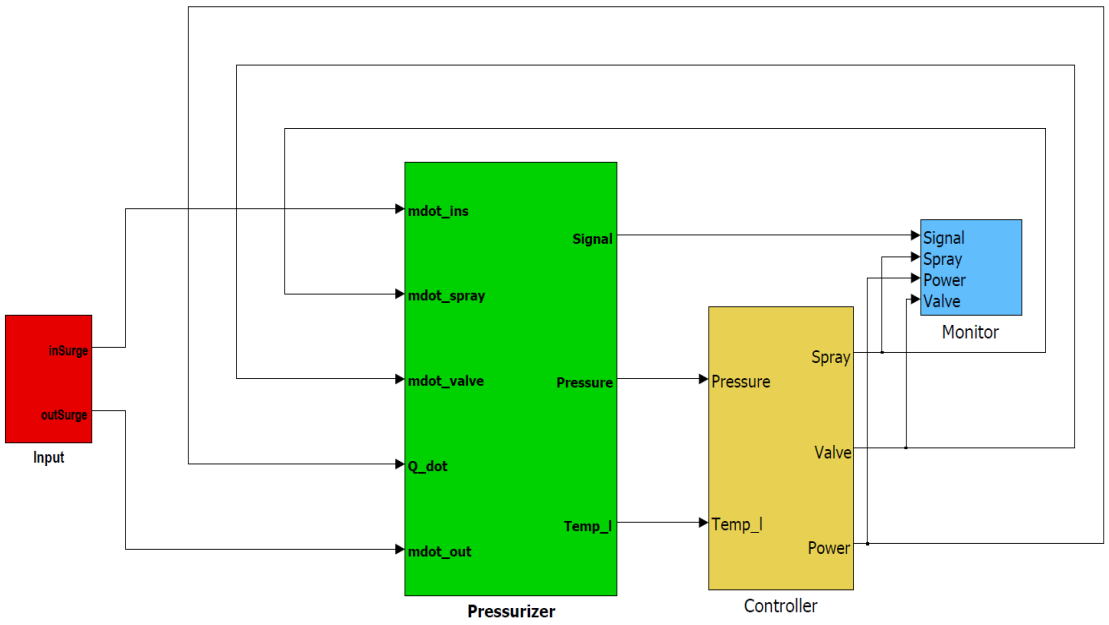

FIG. 3.1 The pressurizer Simulink® model

The input block contains the mass flow rates inputs needed for the simulation. Insurges and outsurges inputs are separated.
To take into account mass flows inversions due to insurges and outsurge two different input ports have been implemented: the first one for insurge transients and the second one for insurges. Of course, during insurges the outsurge input is set to zero and vice versa.
This is a clear example of causal modelling consequence: the physical input is really only one, the pipe connecting the pressurizer to the hot leg of reactor coolant system through which water can enter to or exit from the pressurizer tank, instead the mathematical procedural model requires two different inputs.

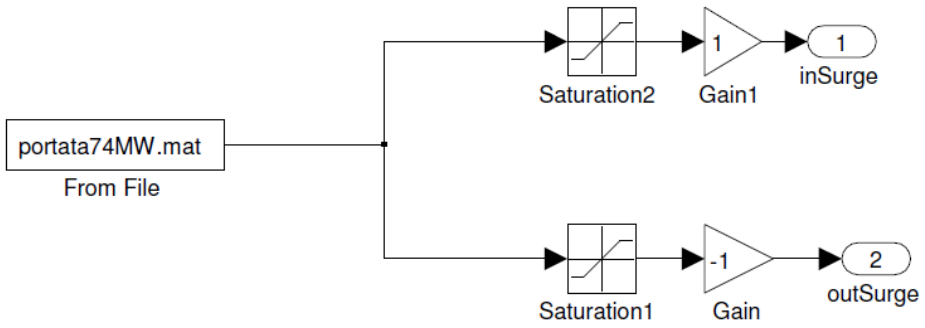

FIG. 3.2 Input block

Apart from the simple equilibrium and two-region-one-volume models, insurges and outsurges are regulated by if statements to choose the correct Ψ_{INSURGE} or $\Psi_{OUTSURGE}$ matrices to be inverted.
The Pressurizer block is composed by three sub-blocks, the "State-dot", the "State" and the "Wall".
State-dot block is then based on a MATLAB® static function which computes the inversion of matrix Ψ to determine the ODE system for all state variables:

$$\dot{z} = \Psi^{-1}\eta \tag{3.5}$$

Inside this functions all thermodynamic quantities for water and steam (enthalpies, specific volume, density...etc) are established using a special freeware utility called XSteam which is based on IAPWS-IF97 tables.
Moreover XSteam program has been modified to directly compute also all the particular thermodynamics partial derivative comparing in the matrix Ψ of non-equilibrium models. In fact all these quantities:

$$\left(\frac{\partial\rho}{\partial h}\right)_p \qquad \left(\frac{\partial\rho}{\partial p}\right)_h \qquad \frac{dh}{dp} \qquad \frac{d\rho}{dp}$$

are not computed using finite difference approximation, but, using Maxwell Relations, Clausius-Clapeyron equation and Dini's theorem, they are taken back to a combination of fundamental thermodynamics quantities, as isobaric compressibility factor β, isothermal compressibility coefficient K_T, specific isobaric heat capacity C_p, specific isochoric heat capacity C_v, temperature and specific volume ν.
In thermodynamics, Maxwell's relations are a set of equations which can be derived from the definitions of the thermodynamic potentials. The four most common Maxwell relations are the equalities of the second derivatives of each of the four thermodynamic potentials, with respect to their thermal natural variable (temperature *T*; or entropy *S*) and their mechanical natural variable (pressure *p*; or volume *V*):

$$\left(\frac{\partial T}{\partial V}\right)_S = -\left(\frac{\partial p}{\partial S}\right)_V = \frac{\partial^2 U}{\partial S \partial V} \tag{3.6}$$

$$\left(\frac{\partial T}{\partial p}\right)_S = \left(\frac{\partial V}{\partial S}\right)_p = \frac{\partial^2 H}{\partial S \partial p} \tag{3.7}$$

$$\left(\frac{\partial S}{\partial V}\right)_T = \left(\frac{\partial p}{\partial T}\right)_V = -\frac{\partial^2 F}{\partial T \partial V} \tag{3.8}$$

$$-\left(\frac{\partial S}{\partial p}\right)_T = \left(\frac{\partial V}{\partial T}\right)_p = \frac{\partial^2 G}{\partial T \partial p} \tag{3.9}$$

where the potentials, as functions of their natural thermal and mechanical variables, are: Internal Energy $U(S, V)$, Enthalpy $H(S, p)$, Helmholtz Free Energy $F(T, V)$ and Gibbs Free Energy $G(T, P)$.
The Clausius–Clapeyron relation, named after Rudolf Clausius and Benoît Paul Émile Clapeyron, is a way of characterizing a discontinuous phase transition between two phases of matter of a single constituent. On a pressure-temperature (p-T) diagram, the line separating the two phases is known as the coexistence curve. The Clausius-Clapeyron relation gives the slope of the tangents to this curve. Mathematically:

$$\frac{dp}{dT} = \frac{(h_g - h_f)}{T \cdot (v_g - v_f)} \tag{3.10}$$

Using Dini's theorem, also known as implicit function theorem, it is possible to change physically unknown thermodynamics partial derivatives in order to transform them in something having physical meaning:

$$\left(\frac{\chi}{\xi}\right)_\varsigma = -\frac{\left(\frac{\varsigma}{\xi}\right)_\chi}{\left(\frac{\varsigma}{\chi}\right)_\xi} \tag{3.11}$$

Finally, after some algebraic passages, the final results are:

$$\left(\frac{\partial \rho}{\partial h}\right)_p = -\frac{\beta}{C_p \upsilon} \tag{3.11}$$

$$\left(\frac{\partial \rho}{\partial p}\right)_h = \frac{\beta + {C_v K_T}/{\upsilon}}{C_p} \tag{3.12}$$

$$\frac{dh}{dp} = v(1 - \beta T) + C_P T \frac{(v_G - v_F)}{(h_G - h_F)} \tag{3.13}$$

$$\frac{d\rho}{dp} = \frac{1}{v}\left(K_T - \beta T \frac{(v_G - v_F)}{(h_G - h_F)}\right) \tag{3.14}$$

After obtaining these expressions, as XSteam does not compute directly isobaric compressibility factor β and isothermal compressibility coefficient K_T, they have been implemented using IAPWS-IF97 rules.

The IAPWS Industrial Formulation 1997 [24] consists of a set of equations for different regions which cover the following range of validity:

$$273.15\ \text{K} \le T \le 1073.15\ \text{K}\ p \le 100\ \text{MPa}$$
$$1073.15\ \text{K} < T \le 2273.15\ \text{K}\ p \le 50\ \text{MPa}$$

Figure 3.2 shows the five regions into which the entire range of validity of IAPWS-IF97 is divided. The boundaries of the regions can be directly taken from figure 3.1. Both regions 1 and 2 are individually covered by a fundamental equation for the specific Gibbs free energy $g(p,T)$, region 3 by a fundamental equation for the specific Helmholtz free energy $f(\rho,T)$, where ρ is the density, and the saturation curve by a saturation-pressure equation $p_s(T)$. The high-temperature region 5 is also covered by a $g(p,T)$ equation. These five equations, shown in rectangular boxes in figure 3.2, form the so-called basic equations.

The specific gas constant of ordinary water used for this formulation is $R = 0.461\ 526$ kJ kg^{-1} K^{-1}. This value results from the recommended values of the molar gas constant and the molar mass of ordinary water. The values of the critical parameters $T_c = 647.096$ K, $p_c = 22.064$ MPa, $\rho_c = 322$ kg m^{-3} are from the corresponding IAPWS release.

The basic equation for region 1 is a fundamental equation for the specific Gibbs free energy g. This equation is expressed in dimensionless form, $\gamma = g/(RT)$, and reads

$$\frac{g(p,T)}{RT} = \gamma(\pi,\tau) = \sum_{i=1}^{34} n_i \cdot (7.1 - \pi)^{I_i} \cdot (\tau - 1.222)^{J_i} \tag{3.15}$$

where $\pi = p/p^*$ and $\tau = T^*/T$ with $p^* = 16.53$ MPa and $T^* = 1386$ K. The coefficients n_i and exponents I_i and J_i of equation 3.15 are listed in Table 3.1.

All thermodynamic properties can be derived from equation 3.15 by using the appropriate combinations of the dimensionless Gibbs free energy and its derivatives. Equation 3.15 covers region 1 of IAPWS-IF97 defined by the following range of temperature and pressure:

$$273.15\ \text{K} \le T \le 623.15\ \text{K}\ p_s(T) \le p \le 100\ \text{MPa}\ .$$

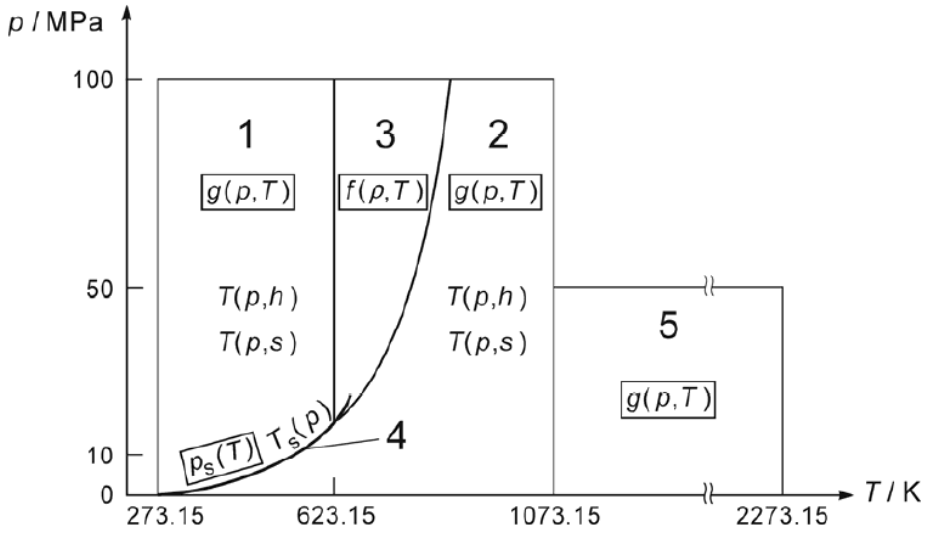

FIG. 3.3 Regions and Equations of IAPWS-IF97

i	I_i	J_i	n_i	i	I_i	J_i	n_i
1	0	−2	0.146 329 712 131 67	18	2	3	$-0.441\,418\,453\,308\,46 \times 10^{-5}$
2	0	−1	−0.845 481 871 691 14	19	2	17	$-0.726\,949\,962\,975\,94 \times 10^{-15}$
3	0	0	$-0.375\,636\,036\,720\,40 \times 10^{1}$	20	3	−4	$-0.316\,796\,448\,450\,54 \times 10^{-4}$
4	0	1	$0.338\,551\,691\,683\,85 \times 10^{1}$	21	3	0	$-0.282\,707\,979\,853\,12 \times 10^{-5}$
5	0	2	−0.957 919 633 878 72	22	3	6	$-0.852\,051\,281\,201\,03 \times 10^{-9}$
6	0	3	0.157 720 385 132 28	23	4	−5	$-0.224\,252\,819\,080\,00 \times 10^{-5}$
7	0	4	$-0.166\,164\,171\,995\,01 \times 10^{-1}$	24	4	−2	$-0.651\,712\,228\,956\,01 \times 10^{-6}$
8	0	5	$0.812\,146\,299\,835\,68 \times 10^{-3}$	25	4	10	$-0.143\,417\,299\,379\,24 \times 10^{-12}$
9	1	−9	$0.283\,190\,801\,238\,04 \times 10^{-3}$	26	5	−8	$-0.405\,169\,968\,601\,17 \times 10^{-6}$
10	1	−7	$-0.607\,063\,015\,658\,74 \times 10^{-3}$	27	8	−11	$-0.127\,343\,017\,416\,41 \times 10^{-8}$
11	1	−1	$-0.189\,900\,682\,184\,19 \times 10^{-1}$	28	8	−6	$-0.174\,248\,712\,306\,34 \times 10^{-9}$
12	1	0	$-0.325\,297\,487\,705\,05 \times 10^{-1}$	29	21	−29	$-0.687\,621\,312\,955\,31 \times 10^{-18}$
13	1	1	$-0.218\,417\,171\,754\,14 \times 10^{-1}$	30	23	−31	$0.144\,783\,078\,285\,21 \times 10^{-19}$
14	1	3	$-0.528\,383\,579\,699\,30 \times 10^{-4}$	31	29	−38	$0.263\,357\,816\,627\,95 \times 10^{-22}$
15	2	−3	$-0.471\,843\,210\,732\,67 \times 10^{-3}$	32	30	−39	$-0.119\,476\,226\,400\,71 \times 10^{-22}$
16	2	0	$-0.300\,017\,807\,930\,26 \times 10^{-3}$	33	31	−40	$0.182\,280\,945\,814\,04 \times 10^{-23}$
17	2	1	$0.476\,613\,939\,069\,87 \times 10^{-4}$	34	32	−41	$-0.935\,370\,872\,924\,58 \times 10^{-25}$

TABLE 3.1 Numerical values of the coefficients and exponents of the dimensionless Gibbs free energy for region 1

In particular K_T coefficient can be expressed as:

$$K_T = -\frac{1}{v}\left(\frac{\partial V}{\partial p}\right)_T = \frac{1}{v}\left(\frac{\partial^2 g}{\partial p^2}\right)_T \tag{3.16}$$

Where:

$$v = \left(\frac{\partial g}{\partial p}\right)_T = \frac{RT}{p}\pi\frac{\partial \gamma}{\partial \pi} \tag{3.17}$$

$$\left(\frac{\partial^2 g}{\partial p^2}\right)_T = \frac{R}{p^2}\pi^2\frac{\partial^2 \gamma}{\partial \pi^2}T \tag{3.18}$$

For β is:

$$\beta = \frac{1}{v}\left(\frac{\partial V}{\partial T}\right)_p = \frac{1}{v}\left(\frac{\partial}{\partial T}\left(\frac{\partial g}{\partial p}\right)_T\right)_p \tag{3.16}$$

Where:

$$v = \left(\frac{\partial g}{\partial p}\right)_T = \frac{RT}{p}\pi\frac{\partial \gamma}{\partial \pi} \tag{3.17}$$

$$\left(\frac{\partial}{\partial T}\left(\frac{\partial g}{\partial p}\right)_T\right)_p = \frac{RT}{p}\left(\frac{\partial \gamma}{\partial \pi}\right) - \tau\left(\frac{\partial^2 \gamma}{\partial \pi \partial \tau}\right) \tag{3.18}$$

The basic equation for region 2 is a fundamental equation for the specific Gibbs free energy g. This equation is expressed in dimensionless form, $\gamma = g/(RT)$, and is separated into two parts, an ideal-gas part γ^0 and a residual part γ^r, so that

$$\frac{g(p,T)}{RT} = \gamma^0(\pi,\tau) + \gamma^r(\pi,\tau) \tag{3.19}$$

where $\pi = p/p^*$ and $\tau = T^*/T$. The equation for the ideal-gas part γ^0 of the dimensionless Gibbs free energy reads:

$$\gamma^0 = \ln\pi + \sum_{i=1}^{9} n_i^0 \cdot \tau^{J_i^0} \tag{3.20}$$

where $\pi = p/p^*$ and $\tau = T^*/T$ with $p^* = 1$ MPa and $T^* = 540$ K. Table 3.2 contains the coefficients and exponents of equation 3.20.

i	J_i^o	n_i^o	i	J_i^o	n_i^o
1[a]	0	$-0.969\,276\,865\,002\,17 \times 10^{1}$	6	−2	$0.142\,408\,191\,714\,44 \times 10^{1}$
2[a]	1	$0.100\,866\,559\,680\,18 \times 10^{2}$	7	−1	$-0.438\,395\,113\,194\,50 \times 10^{1}$
3	−5	$-0.560\,879\,112\,830\,20 \times 10^{-2}$	8	2	$-0.284\,086\,324\,607\,72$
4	−4	$0.714\,527\,380\,814\,55 \times 10^{-1}$	9	3	$0.212\,684\,637\,533\,07 \times 10^{-1}$
5	−3	$-0.407\,104\,982\,239\,28$			

TABLE 3.2 Numerical values of the coefficients and exponents of the ideal-gas part γ^{ρ} of the dimensionless Gibbs free energy for region 2

The form of the residual part γ r of the dimensionless Gibbs free energy is as follows:

$$\gamma^r = \sum_{i=1}^{43} n_i \cdot \tau^{I_i} (\tau - 0.5)^{J_i} \tag{3.21}$$

where $\pi = p/p^*$ and $\tau = T^*/T$ with $p^* = 1$ MPa and $T^* = 540$ K. Table 3.2 contains the coefficients and exponents of equation 3.2.

All thermodynamic properties can be derived from Eq. (15) by using the appropriate combinations of the ideal-gas part γ o and the residual part γ r of the dimensionless Gibbs free energy and their derivatives. Equation 3.19 covers region 2 of IAPWS-IF97 defined by the following range of temperature and pressure:

$$273.15\ \text{K} \le T \le 623.15\ \text{K}\ 0 < p \le p_s(T)$$
$$623.15\ \text{K} < T \le 863.15\ \text{K}\ 0 < p \le p(T)$$
$$863.15\ \text{K} < T \le 1073.15\ \text{K}\ 0 < p \le 100\ \text{MPa}$$

In particular K_T coefficient can be expressed as:

$$K_T = -\frac{1}{v}\left(\frac{\partial V}{\partial p}\right)_T = \frac{1}{v}\left(\frac{\partial^2 g}{\partial p^2}\right)_T \tag{3.16}$$

Where:

$$v = \left(\frac{\partial g}{\partial p}\right)_T = \frac{RT}{p}\pi\frac{\partial \gamma^0}{\partial \pi} + \frac{RT}{p}\pi\frac{\partial \gamma^r}{\partial \pi} \tag{3.17}$$

$$\left(\frac{\partial^2 g}{\partial p^2}\right)_T = \frac{R}{p^2}\pi^2\frac{\partial^2 \gamma^0}{\partial \pi^2}T + \frac{R}{p^2}\pi^2\frac{\partial^2 \gamma^r}{\partial \pi^2}T \tag{3.18}$$

For β is:

$$\beta = \frac{1}{v}\left(\frac{\partial V}{\partial T}\right)_p = \frac{1}{v}\left(\frac{\partial}{\partial T}\left(\frac{\partial g}{\partial p}\right)_T\right)_p \tag{3.16}$$

Where:

$$v = \left(\frac{\partial g}{\partial p}\right)_T = \frac{RT}{p}\pi\frac{\partial \gamma^0}{\partial \pi} + \frac{RT}{p}\pi\frac{\partial \gamma^r}{\partial \pi} \tag{3.17}$$

$$\left(\frac{\partial}{\partial T}\left(\frac{\partial g}{\partial p}\right)_T\right)_p = \frac{RT}{p}\left(\frac{\partial \gamma^0}{\partial \pi}\right) - \tau\left(\frac{\partial^2 \gamma^0}{\partial \pi \partial \tau}\right) + \frac{RT}{p}\left(\frac{\partial \gamma^r}{\partial \pi}\right) - \tau\left(\frac{\partial^2 \gamma^r}{\partial \pi \partial \tau}\right) \tag{3.18}$$

i	I_i	J_i	n_i
1	1	0	$-0.177\,317\,424\,732\,13 \times 10^{-2}$
2	1	1	$-0.178\,348\,622\,923\,58 \times 10^{-1}$
3	1	2	$-0.459\,960\,136\,963\,65 \times 10^{-1}$
4	1	3	$-0.575\,812\,590\,834\,32 \times 10^{-1}$
5	1	6	$-0.503\,252\,787\,279\,30 \times 10^{-1}$
6	2	1	$-0.330\,326\,416\,702\,03 \times 10^{-4}$
7	2	2	$-0.189\,489\,875\,163\,15 \times 10^{-3}$
8	2	4	$-0.393\,927\,772\,433\,55 \times 10^{-2}$
9	2	7	$-0.437\,972\,956\,505\,73 \times 10^{-1}$
10	2	36	$-0.266\,745\,479\,140\,87 \times 10^{-4}$
11	3	0	$0.204\,817\,376\,923\,09 \times 10^{-7}$
12	3	1	$0.438\,706\,672\,844\,35 \times 10^{-6}$
13	3	3	$-0.322\,776\,772\,385\,70 \times 10^{-4}$
14	3	6	$-0.150\,339\,245\,421\,48 \times 10^{-2}$
15	3	35	$-0.406\,682\,535\,626\,49 \times 10^{-1}$
16	4	1	$-0.788\,473\,095\,593\,67 \times 10^{-9}$
17	4	2	$0.127\,907\,178\,522\,85 \times 10^{-7}$
18	4	3	$0.482\,253\,727\,185\,07 \times 10^{-6}$
19	5	7	$0.229\,220\,763\,376\,61 \times 10^{-5}$
20	6	3	$-0.167\,147\,664\,510\,61 \times 10^{-10}$
21	6	16	$-0.211\,714\,723\,213\,55 \times 10^{-2}$
22	6	35	$-0.238\,957\,419\,341\,04 \times 10^{2}$
23	7	0	$-0.590\,595\,643\,242\,70 \times 10^{-17}$
24	7	11	$-0.126\,218\,088\,991\,01 \times 10^{-5}$
25	7	25	$-0.389\,468\,424\,357\,39 \times 10^{-1}$
26	8	8	$0.112\,562\,113\,604\,59 \times 10^{-10}$
27	8	36	$-0.823\,113\,408\,979\,98 \times 10^{1}$
28	9	13	$0.198\,097\,128\,020\,88 \times 10^{-7}$
29	10	4	$0.104\,069\,652\,101\,74 \times 10^{-18}$
30	10	10	$-0.102\,347\,470\,959\,29 \times 10^{-12}$
31	10	14	$-0.100\,181\,793\,795\,11 \times 10^{-8}$
32	16	29	$-0.808\,829\,086\,469\,85 \times 10^{-10}$
33	16	50	$0.106\,930\,318\,794\,09$
34	18	57	$-0.336\,622\,505\,741\,71$
35	20	20	$0.891\,858\,453\,554\,21 \times 10^{-24}$
36	20	35	$0.306\,293\,168\,762\,32 \times 10^{-12}$
37	20	48	$-0.420\,024\,676\,982\,08 \times 10^{-5}$
38	21	21	$-0.590\,560\,296\,856\,39 \times 10^{-25}$
39	22	53	$0.378\,269\,476\,134\,57 \times 10^{-5}$
40	23	39	$-0.127\,686\,089\,346\,81 \times 10^{-14}$
41	24	26	$0.730\,876\,105\,950\,61 \times 10^{-28}$
42	24	40	$0.554\,147\,153\,507\,78 \times 10^{-16}$
43	24	58	$-0.943\,697\,072\,412\,10 \times 10^{-6}$

TABLE 3.3 Numerical values of the coefficients and exponents of the ideal-gas part γ^o of the dimensionless Gibbs free energy for region 2

Formulas for regions 3 and 4 hasn't been implemented yet because the range of the simulation that will be done are completely contained inside region 1 and 2. However an extension for regions 3 and 4 could be may quite easily in future.

Finally, it must be said, that for equilibrium model, which is characterized by an accuracy far lower than the non-equilibrium ones, the thermodynamic partial derivatives appearing in $\Psi_{\text{EQUILIBRIUM-MODEL}}$:

$$\left(\frac{\partial \rho}{\partial X}\right)_p \qquad \left(\frac{\partial \rho}{\partial p}\right)_X \qquad \left(\frac{\partial \rho}{\partial X}\right)_p \qquad \left(\frac{\partial \rho}{\partial p}\right)_X$$

are computed using finite difference without affecting the degree of precision of the simulation program, which is poor.

In the case of non-equilibrium model, the second block composing the pressurizer dynamic one, the so-called State, is an integrator and switching block. In fact, although for some state variables only their time derivative is of interest, i.e. flashing and rainout mass flow rates, for all the others the quantities of interest are not their time derivatives, but the integral values.

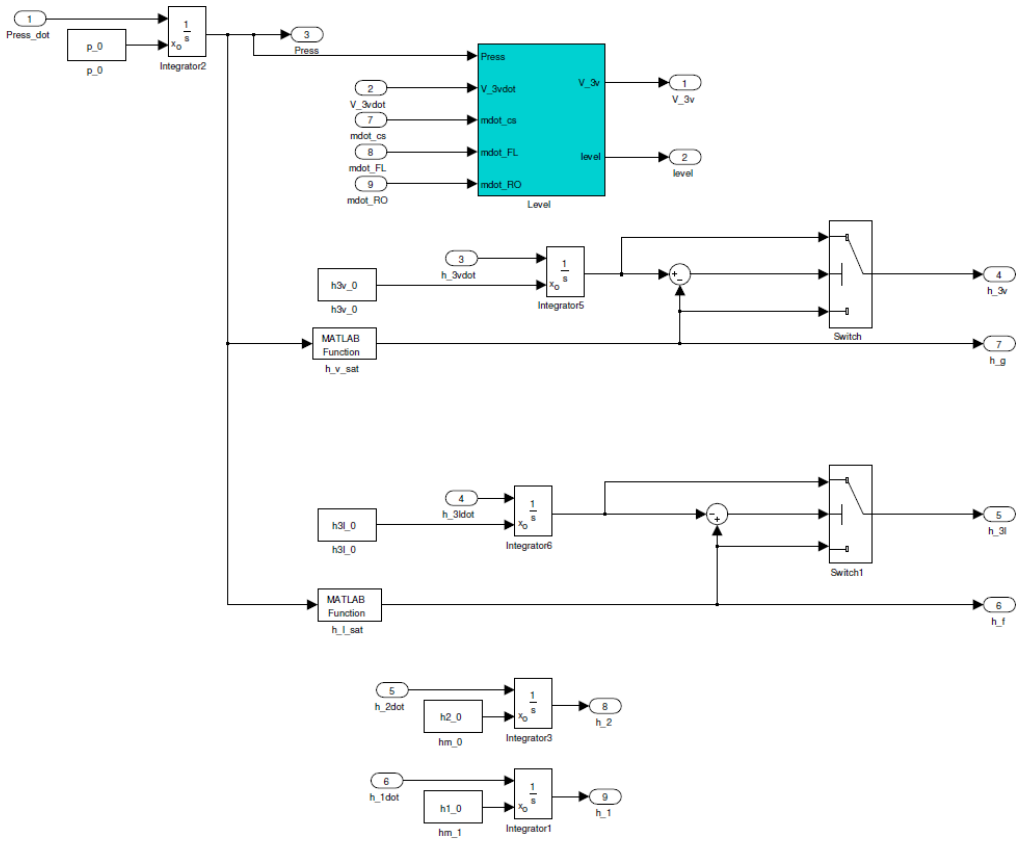

FIG. 3.4 State block non-equilibrium model

So, inside State block, there are integration sub-blocks for pressure and volumes, which are initialized at starting condition of the pressurizer. Then, switching sub-blocks are necessary to automatically select the correct thermodynamic state happening inside the pressurizer. These switches compare the values of steam and water enthalpies computed

by core static function to the respectively saturation values computed directly using XSteam utility, which uses as input the pressure computed by the core static MATLAB® function.
As steam cannot be subcooled and water cannot be superheated in this model, if the calculated enthalpy of steam is less then saturation one, the switch commutes the output value of enthalpy from the one computed by the core function to the one computed by XSteam. Similarly, if the calculated enthalpy of water is greater then saturation one, the switch commutes the output value of enthalpy from the one computed by the core function to the one computed by XSteam.
Finally, inside the core function there are if statements comparing enthalpies values coming from Simulink® to those coming from XSteam. Depending on the relative values the matrix representing the thermodynamic state happening inside the pressurizer is selected.

`if (h_3l < h_f && h_3v > h_g)`	Then is selected STATE 1
`elseif (h_3l >= h_f && h_3v > h_g)`	Then is selected STATE 2
`elseif (h_3l < h_f && h_3v <= h_g)`	Then is selected STATE 3
`else (h_3l >= h_f && h_3v <= h_g)`	Then is selected STATE 4

TABLE 3.4 State selection logic

In the equilibrium model case, the State block is composed by only two integrators which are needed to compute pressure and quality integral values.

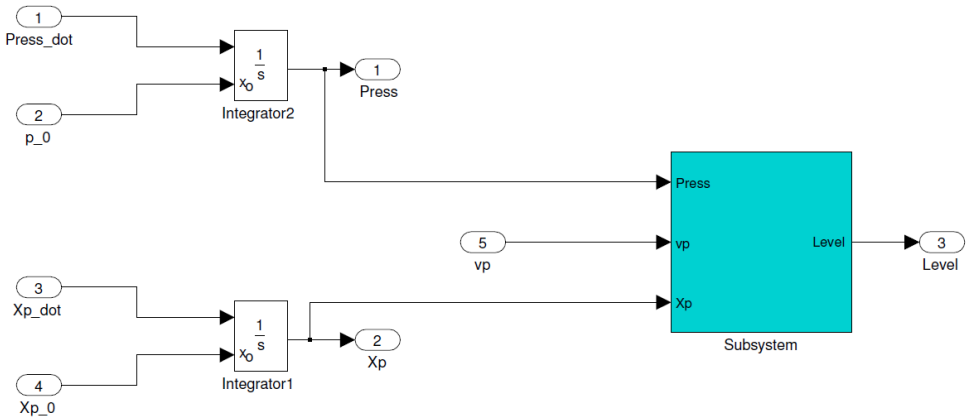

FIG. 3.5 State block equilibrium model

Moreover, inside the State block, both for equilibrium and non-equilibrium models, there are one sub-block needed to compute the water level.
In the non-equilibrium case the water-level block computes the steam volume variation too: the level of liquid region is obtained integrating the time derivative of vapour volume, subtracting this one to the total volume of pressurizer and finally dividing the result by the cross sectional area of the pressurizer.
More precisely, inside the level sub-block there is another subsystem, in which, to take into account the effect of flashing and rainout, the integration of their mass flow rates is done. The integrated values are then multiplied for the respectively specific volumes computed by XSteam to obtain the volume of water which has flashed and of steam which has condensed.

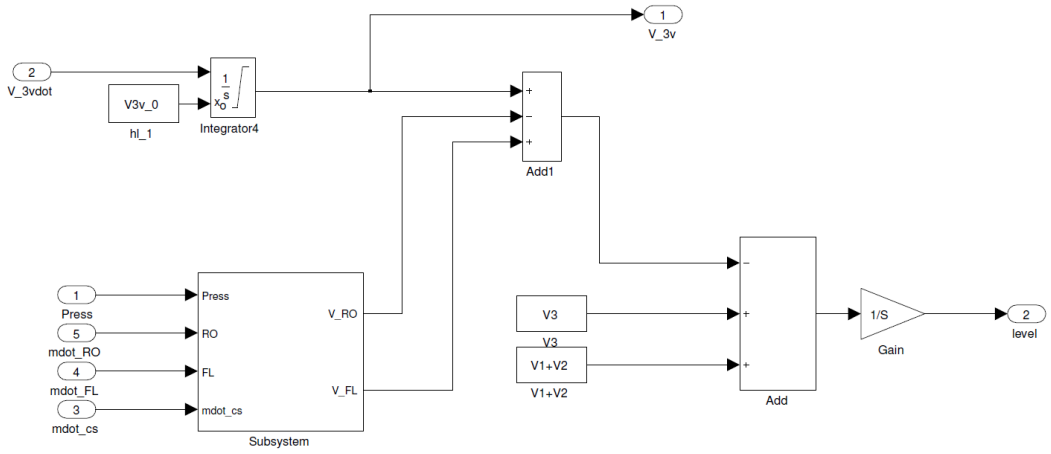

FIG. 3.6 Level block non-equilibrium models

In equilibrium case, instead, the water level block using the vapour quality:

$$L = A \cdot (1 - X) \frac{V_P}{v_P} v_P \tag{3.19}$$

Where A is the cross sectional area of the pressurizer tank.

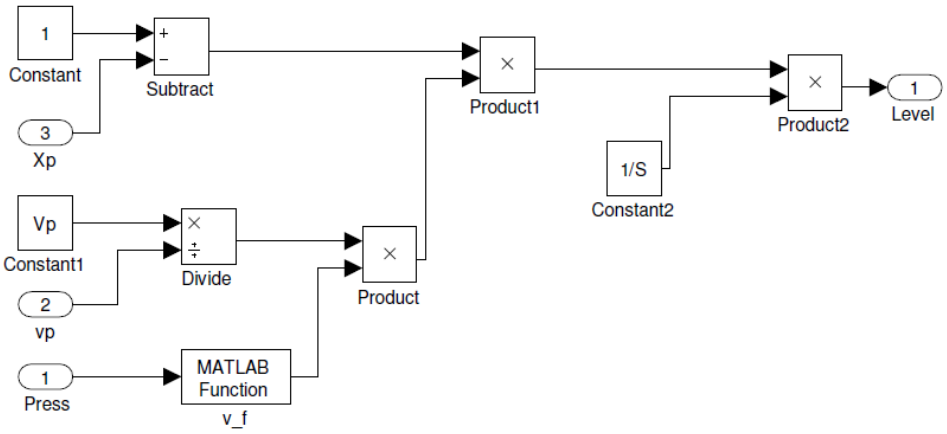

FIG. 3.7 Level block equilibrium model

The last block, the Wall block (contained in the pressurizer non-equilibrium dynamics one) is needed to compute the wall temperature which is used to define the heat transfer coefficient according to the Nusselt's theory. In this block the balance of heat fluxes crossing the pressurizer wall is integrated in order to obtain the desired temperature.

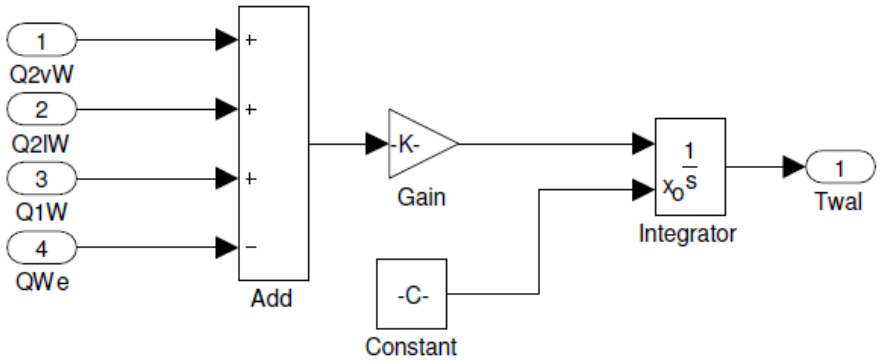

FIG. 3.8 Wall block non-equilibrium model

The other main block which is present in figure 3.1 is the Controller one, where different control scheme for the pressurizer can be implemented. In this regard, the causal approach on which Similink® is based, allows to develop all kinds of control logic in a natural way. For Shippingport transients simulations, the control of the pressurizer is ON-OFF type. The controlled variables are pressure and water temperature, but other control scheme, based on PID and more sophisticated system can be implemented easily.

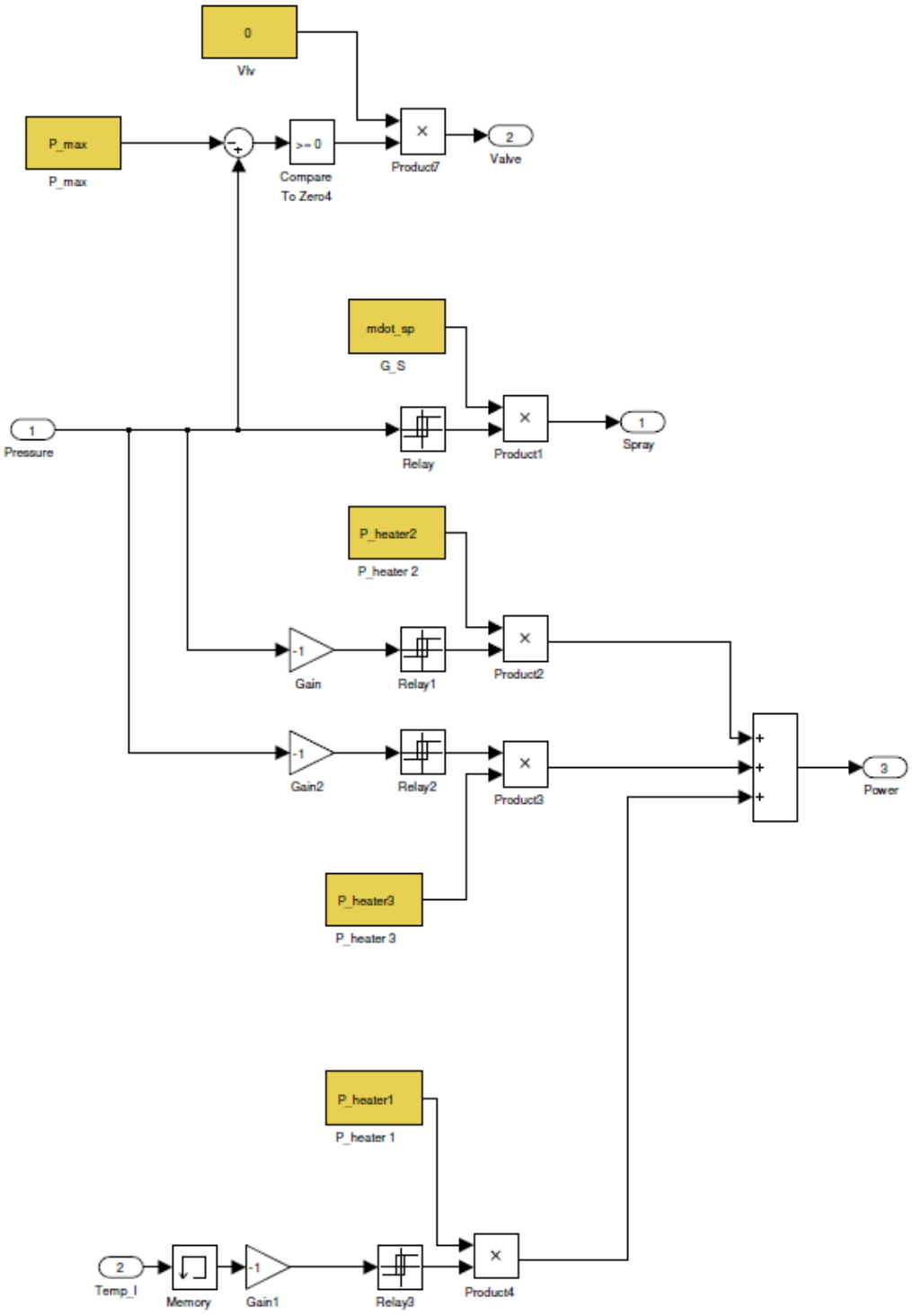

FIG. 3.9 Shippingport control block

The last block of figure 3.1 is the monitor one: here there are all the scopes to view the computed outputs.

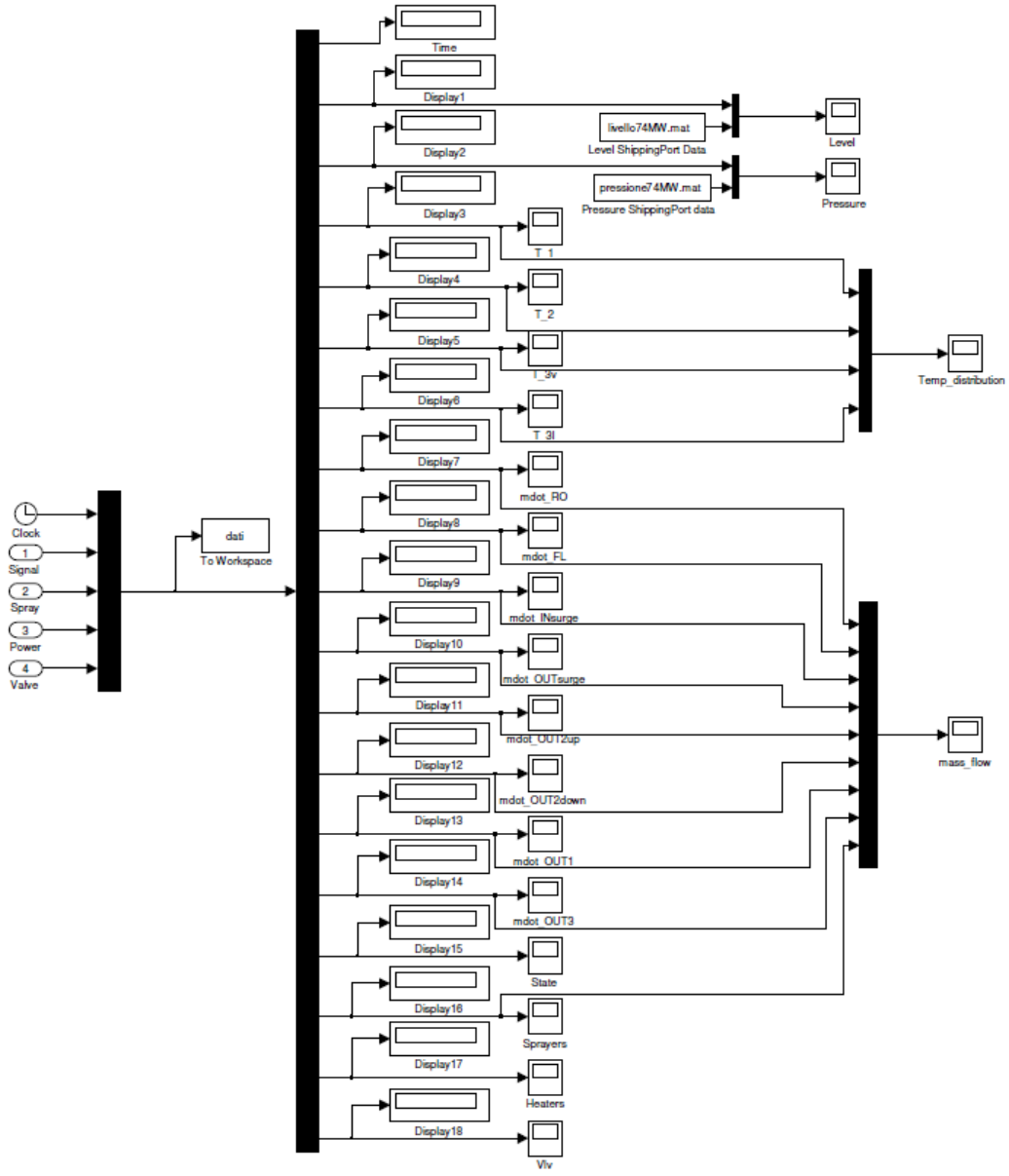

FIG. 3.10 Monitor block

3.4 ACAUSAL APPROACH

Block diagrams allow to create models which can be easily simulated by a computer. In fact the formulation of the problem in a series of mathematical operation is done by the user. One of the most penalizing aspect consists in the inability to change the realized model: if you wanted to monitor another quantity of the system, originally not expected, you would re-define the outputs vector and reformulate completely the problem.
So it would be advantageous, during the simulation, having all the variables and quantities of the system, also ones not observable and not accessible in the real physical system. In the last years, thanks to the increased computer capabilities, another type of modelling approach has been widespread: the acausal one.
Using this new design philosophy, the model of each system is given by the constituent equations and the model formulation is independent of the actual boundary conditions.
Therefore it is re-usable in different contexts and a truly modular approach can be developed. Links between components are represented by connection equations, which keep sense and structure of real physical connection, so none quantity must be defined a priori as input or output. Causality relationships remain unspecified and they are fixed only when equations are solved. For this reason you speak about acausal modelling. Often you can hear the term physical modelling, which is used to underline that the acausal approach is proper to represent the physical structure of the system.
Using equations and not assignments, as causal one, acausal modelling does not prescribe a given data flow direction or execution order, it can automatically change from time to time depending on application contest. The main advantage with acausal modeling is that the solution direction of equations will adapt to the data flow context in which the solution is computed.
However the simulation of an aggregate system becomes a difficult task, the physical systems is generally described by DAEs, which cannot be resolved directly using general purpose ODE solvers [25].
Problems which can be written in this general form:

$$F\left(t, y, \frac{dy}{dt}\right) = 0 \tag{3.20}$$

include standard ODE systems as well as problems which are substantially different from standard ODE's. Some of the differential/algebraic systems can be solved using numerical methods which are commonly used for solving stiff systems of ordinary differential equations. Other problems can be solved using codes based on the stiff methods, but only after extensive modifications to the error estimates and other strategies in the code. A further class of problems cannot be solved at all with such codes, because changing the stepsize causes large errors in the solution.
So, a number of difficulties can arise when numerical methods are used to solve systems of differential/algebraic equations (DAE) of the form 3.20.

Then the solution of the mathematical problem requires some form of symbolic manipulation of the system of equations, prior to the use of some numerical integration algorithm.
One of the most promising programming languages using acausal approach is Modelica. Specifically Modelica is an object-oriented programming language [26].
An object is a collection of instance variables and equations that share a set of data.
Modelica respects the so-called Object-oriented paradigm:

- Encapsulation
- Abstraction
- Hierarchical modularity
- Inheritance

The encapsulation principle states that models can interact only through interface (connector) variables. Models must have well-defined connectors for communicating and coupling between an object and the outside world. Connectors and connector design, so, are crucial for the modular modelling of complex physical systems. Connectors define interface variables, based on the balance of power principle, of two kinds: effort variables and flux variables. The abstraction principle, instead, states that interfaces must be independent from model implementation. According to hierarchical modularity, model can be hierarchically structured. Finally, the inheritance principle allows to define some subclass by specializing a superclass.
It must be said that Modelica is important for the interpretation that it gives to the object-oriented paradigm and not for being the first object-oriented programming language. Many other object-oriented programming languages were born before Modelica. Traditional object-oriented programming languages support programming with operations on stored data. The stored data of the program include variable values and object data. The number of objects often changes dynamically.
In particular classical languages view of object-orientation emphasizes sending messages between (dynamically) created objects.
Instead, the Modelica view on object-orientation is different, since the Modelica language emphasizes structured mathematical modelling.
Object-orientation is thus viewed as a structuring concept that is used to handle the complexity of large system descriptions.
A Modelica model is primarily a declarative mathematical description, which simplifies further analysis. Dynamic system properties are expressed in a declarative way through equations. The concept of declarative programming is inspired by mathematics, where it is common to state or declare what holds, rather than giving a detailed stepwise algorithm on how to achieve the desired goal as is required when using procedural languages. This relieves the programmer from the burden of keeping track of such details. Furthermore, the code becomes more concise and easier to change without introducing errors.

Thus, the declarative Modelica view of object-orientation, from the point of view of object-oriented mathematical modeling, can be summarized as follows:

- Object-orientation is primarily used as a structuring concept, emphasizing the declarative structure and reuse of mathematical models. Our three ways of structuring are hierarchies, component-connections, and inheritance.
- Dynamic model properties are expressed in a declarative way through equations.
- An object is a collection of instance variables and equations that share a set of data.

However:

- Object-orientation in mathematical modelling is not viewed as dynamic message passing.

The declarative object-oriented way of describing systems and their behaviour offered by Modelica is at a higher level of abstraction than the usual object-oriented programming since some implementation details can be omitted. For example, you do not need to write code to explicitly transport data between objects through assignment statements or message passing code. Such code is generated automatically by the Modelica compiler based on the given equations. Just as in ordinary object-oriented languages, classes are blueprints for creating objects. Both variables and equations can be inherited between classes. Function definitions can also be inherited. However, specifying behaviour is primarily done through equations instead of via methods. There are also facilities for stating algorithmic code including functions in Modelica, but this is an exception rather than the rule.
To illustrate the idea of acausal physical modeling it is given an example of a simple electrical circuit. The connection diagram of the electrical circuit shows how the components are connected. It may be drawn with component placements to roughly correspond to the physical layout of the electrical circuit on a printed circuit board. The physical connections in the real circuit correspond to the logical connections in the diagram. Therefore the term physical modelling is quite appropriate.

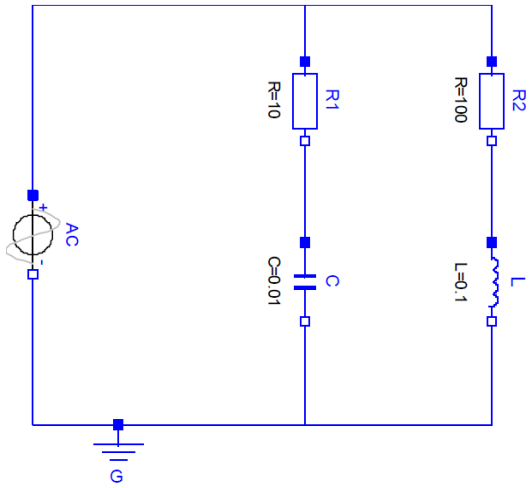

FIG. 3.11 Connection diagram of the acausal simple circuit model.

The Modelica *SimpleCircuit* model below directly corresponds to the circuit depicted in the connection diagram of Figure 3.11. Each graphic object in the diagram corresponds to a declared instance in the simple circuit model. The model is acausal since no signal flow, i.e., cause-and-effect flow, is specified. Connections between objects are specified using the *connect* equation construct, which is a special syntactic form. The circuit is realized using default components of Modelica libraries: *Resistor, Capacitor, Inductor, VsourceAC*, and *Ground.*

```
model SimpleCircuit
Resistor R1(R=10);
Capacitor C(C=0.01);
Resistor R2(R=100);
Inductor L(L=0.1);
VsourceAC AC;
Ground G;
equation
connect(AC.p, R1.p); // Capacitor circuit
connect(R1.n, C.p);
connect(C.n, AC.n);
connect(R1.p, R2.p); // Inductor circuit
connect(R2.n, L.p);
connect(L.n, C.n);
connect(AC.n, G.p); // Ground
end SimpleCircuit;
```

As a comparison it is showed the same circuit modelled using causal block-oriented modelling depicted as a diagram in Figure 3.12. Here the physical topology is lost: the structure of the diagram has no simple correspondence to the structure of the physical circuit board. This model is causal since the signal flow has been deduced and is clearly shown in the diagram. Even for this simple example the analysis to convert the intuitive

physical model to a causal block-oriented model is nontrivial. Another disadvantage is that the resistor representations are context dependent. For example, the resistors R1 and R2 have different definitions, which makes reuse of model library components hard. Furthermore, such system models are usually hard to maintain since even small changes in the physical structure may result in large changes to the corresponding block-oriented system model.

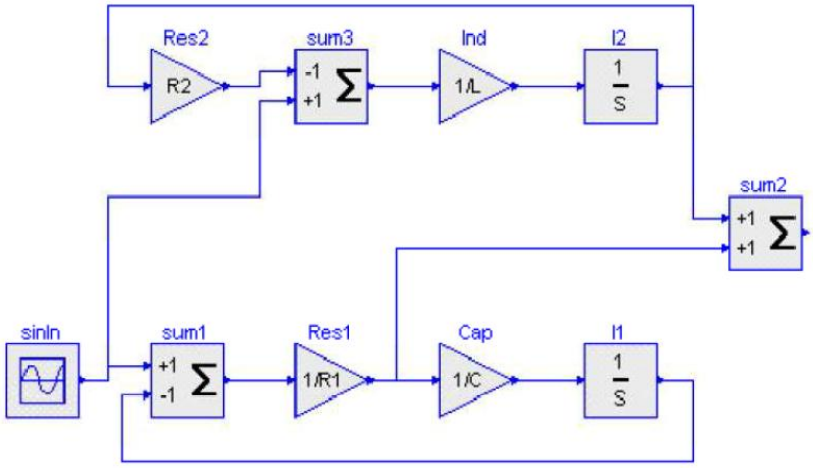

FIG. 3.12 The simple circuit model using causal block-oriented modeling with explicit signal flow.

It must be underlined that Modelica language is not finalized to any specified branches of engineering, but it allows modelling of various nature systems.
To actually simulate a Modelica model you must use proper software instruments. Currently, a lot of software packages supporting Modelica exist. Some of them are commercial, as Dymola®, other are open-source as OpenModelica. In this study Dymola® (Dynamic Modelling Laboratory) has been used. Dymola® is a design ambient realized for the development of heterogeneous physical models. It supports a lot of libraries and default reusable components and carries out symbolic analysis and numerical manipulation of equations in order to generate high effective simulation code. Dymola® code translation includes different steps:

- Translation: in this phase code parsing, type checking, classes expansion and generation of connection equations are executed
- Analysis: in this phase DAE system obtained in the previous step is checked in order to verify if it is structurally non-singular. If a DAE is structurally non-singular to each equation can be assigned a single variable and vice-versa. Then using Pantelides algorithm [27], it is possible to transform the DAE system into an ODE one. Moreover, if the DAE system is structurally non-singular equations can be sorted in data-dependency order. This allows to solving several smaller DAE system in cascade, rather than a single large DAE system, thus gaining efficiency. The sorting procedure is known as BLT-transformation

- Optimization: this step includes algebraic simplification, elimination of trivial equations, conversion of some equations into assignments in order to obtain a minimal set of equation
- C code generation: in this phase the C code needed for the simulation is generated and the system of equations is connected to a numerical solver (DASSL, backward Euler, BDF etc... [27]).
- C compilation: the generated code is compiled to produce the executable file.

It must be said that block diagrams are almost always very useful and for this reason they are supported by the Modelica language too.
Generally speaking a problem can be solved using both the causal approach (block diagrams) and the a-causal formulation obtaining the same final result. Therefore the key point is the subsequent: which method can be faster and more effective to solve the problem ?
In this regard Dymola® allows to automatically extract the same information contained in a block diagram from the a-causal formulation, which is usually faster to obtain as the next paragraph is going to show.

3.5 DYMOLA® MODEL

Dymola® pressurizer is a very simple model.
As of the original set of equation coming from mass and energy conservation principle and from the volume constrain is naturally a DAE system, no manual manipulations of equations are needed. Therefore no matrix is necessary, just conservation equations must be written down in code. Moreover, no partial derivative must be manually computed, all calculations are done by the Dymola® interpreter.

```
DerDensityByPressure drvdp "vapor density derivative wrt pressure";
DerDensityByPressure drldp "liquid density derivative wrt pressure";
DerDensityByEnthalpy drvdh "vapor density derivative wrt enthalpy";
DerDensityByEnthalpy drldh "liquid density derivative wrt enthalpy";

Vl*(drldh*der(hl)) + rhol*dVldy*der(y) = derMl;
derMl = - wev -wse + wc + wcs + wd+ wsp+wcsp;
Ml=rhol*Vl;

Vv*(drvdp*der(p) + drvdh*der(hv)) + rhov*dVvdy*der(y) = derMv;
derMv = wev +wse - wc - wcs -wcsp;
Mv=rhov*Vv;
Mtot=Ml+Mv;

(drldh*der(hl))*Vl*hl+dVldy*der(y)*rhol*hl+der(hl)*rhol*Vl-p*dVldy*der(y)- Vl*der(p)=derHl;
derHl = Qml + Qhl - wev*hvs -wse*hse + wc*hls + wcs*hls +wcsp*hvs+wd*hd+wsp*hsp;

(drvdp*der(p)+drvdh*der(hv))*Vv*hv+dVvdy*der(y)*rhov*hv+der(hv)*rhov*Vvp*dVvdy*
der(y)- Vv*der(p) = derHv;
derHv = wev*hvs + wse*hse - wc*hls - wcs*hv-wcsp*hvs;
```

As said before, thanks to acausal approach, the virtual model results much more physical: now the pipe connection between pressurizer and hot leg is just one connector which allows the flux inversion. Of course, the control logic remains a causal block, because control is itself causal, and so it is very similar to Simulink® counterpart. The model has been developed using components of ThermoPower library, which was built for conventional power plant modelling.

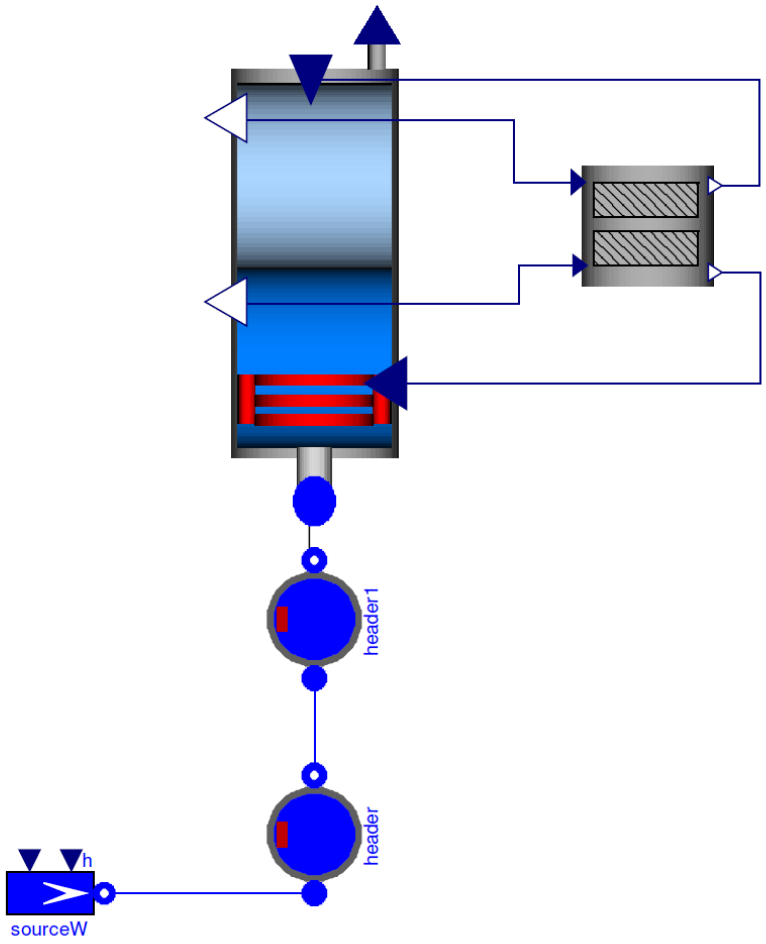

FIG. 3.13 Dymola® pressurizer components

The main subsystem of the model is the two phase control volume, which, in the simple two-regions-one-volume model, represents the only component. (As of the equilibrium model has been developed only to demonstrated the poor performances of this kind of approach, it has not been implemented in Dymola®).
The surge line of this subsystem has been modelled using flange_b connector type made available by the already quoted ThermoPower library.
Flange_b, in fact, assigns to the mass flow rate the enthalpy value coming from the reactor in case of insurge and the enthalpy coming from the pressurizer in case of outsurge:

```
bottomFlange.p = p;
bottomFlange.w = wd;
hd = if noEvent(wd > 0) then bottomFlange.hBA else hl;
bottomFlange.hAB = hl;
```

Sprayers mass flow rate and enthalpy have been introduced using causal connector of type real_input and real_output because of the unidirectional flux of these quantities. In a similar way heaters and valve have been implemented.
The equations characterizing this subsystem are those described in the previous chapter, that is: mass continuity equation and energy conservation both for liquid and vapour regions.

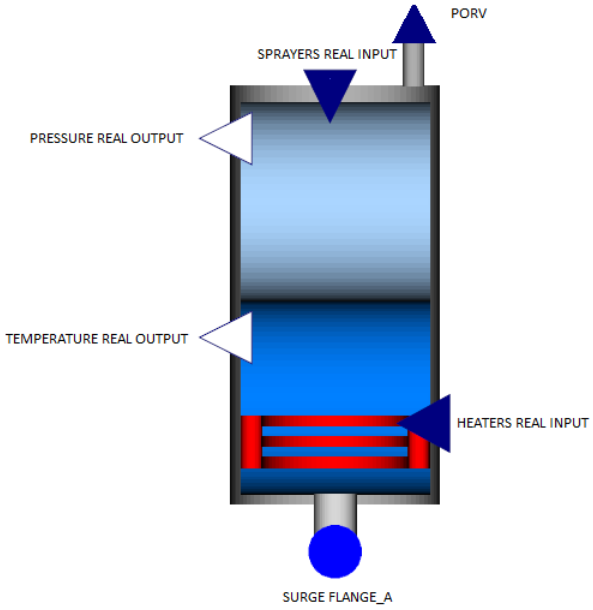

FIG. 3.14 Dymola® pressurizer main component

For two-regions-two-volumes and two-regions-three volumes models, the added control volumes are modelled using a particular component of ThermoPower library called Header. This subsystem is composed by two connectors type: flange_a and flange_b, which act as input and out of the water allowing the flux inversions.

```
hi = if inlet.w >= 0 then inlet.hBA else h;
ho = if outlet.w >= 0 then outlet.hAB else h;
inlet.hAB = h;
outlet.hBA = h;
inlet.p = p+fluid.d*Modelica.Constants.g_n*H;
outlet.p = p;
thermalPort.T = T;
```

The equations describing the component are energy and mass conservation for single phase system.

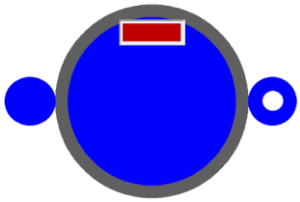

FIG. 3.15 Dymola® header model

Finally there is the control component, which is a causal block very similar to Simulink® one. It is characterized by two RealInput and two RealOutput connectors type in order to receive from the pressurizer pressure and water temperature value and to send to heaters and sprayers the ON/OFF command.

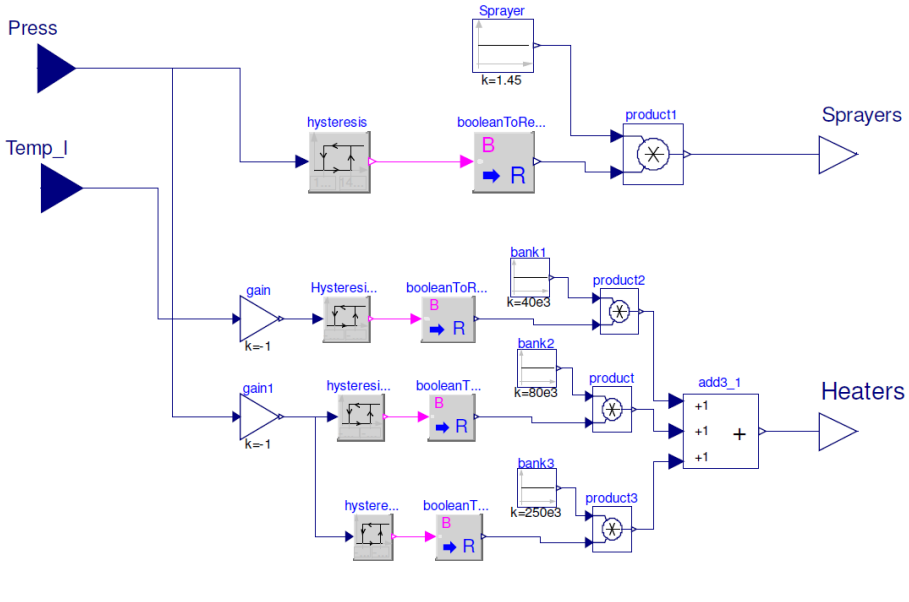

FIG. 3.16 Dymola® pressurizer control

3.6 RELAP5®

The RELAP5® [28]code has been developed for best-estimate transient simulation of light water reactor coolant systems during postulated accidents. The code models the coupled behaviour of the reactor coolant system and the core for loss-of-coolant accidents and operational transients such as anticipated transient without scram, loss of offsite power, loss of feedwater, and loss of flow. A generic modelling approach is used that permits simulating a variety of thermal hydraulic systems.

The light water reactor (LWR) transient analysis code, RELAP5®, was developed at the Idaho National Engineering Laboratory (INEL) for the U.S. Nuclear Regulatory Commission (NRC). Code uses include analyses required to support rulemaking, licensing audit calculations, evaluation of accident mitigation strategies, evaluation of operator guidelines, and experiment planning analysis.

RELAP5® is a highly generic code that, in addition to calculating the behaviour of a reactor coolant system during a transient, can be used for simulation of a wide variety of hydraulic and thermal transients in both nuclear and nonnuclear systems involving mixtures of steam, water, non-condensable, and solute.

The RELAP5® code is based on a non-homogeneous and non-equilibrium model for the two-phase system that is solved by a fast, partially implicit numerical scheme to permit economical calculation of system transients. The objective of the RELAP5® development effort from the outset was to produce a code that included important first-order effects necessary for accurate prediction of system transients but that was sufficiently simple and cost effective so that parametric or sensitivity studies were possible. The code includes many generic component models from which general systems can be simulated. The component models include pumps, valves, pipes, heat releasing or absorbing structures, reactor point kinetics, electric heaters, jet pumps, turbines, separators, accumulators, and control system components.

The system mathematical models are coupled into an efficient code structure. The code includes extensive input checking capability to help the user discover input errors and inconsistencies.

The development of the models and code versions that constitute RELAP5® has spanned more than 20 years from the early stages of RELAP5® numerical scheme development to RELAP5/MOD3.3 is written in FORTRAN 77 for a variety of 64-bit and 32-bit computers.

The RELAP5® hydrodynamic model is a one-dimensional, transient, two-fluid model for flow of a two-phase steam-water mixture that can contain non-condensable components in the steam phase and/or a soluble component in the water phase.

The two-fluid equations of motion that are used as the basis for the RELAP5® hydrodynamic model are formulated in terms of volume and time-averaged parameters of the flow. Phenomena that depend upon transverse gradients, such as friction and heat transfer, are formulated in terms of the bulk properties using empirical transfer coefficient formulations. In situations where transverse gradients cannot be represented within the

framework of empirical transfer coefficients, such as subcooled boiling, additional models specially developed for the particular situation are employed. The system model is solved numerically using a semi-implicit finite-difference technique. The user can select an option for solving the system model using a nearly-implicit finite-difference technique, which allows violation of the material Courant[1] limit.

The basic two-fluid differential equations possess complex characteristic roots that give the system a partially elliptic character and thus constitute an ill-posed initial boundary value problem. In RELAP5®, the numerical problem is rendered well-posed by the introduction of artificial viscosity terms in the difference equation formulation that damp the high frequency spatial components of the solution.

The semi-implicit numerical solution scheme uses a direct sparse matrix solution technique for time step advancement. The method has a material Courant time step stability limit. The nearly-implicit numerical solution scheme also uses a direct sparse matrix solution technique for time step advancement.

The RELAP5® thermal-hydraulic model solves eight field equations for eight primary dependent variables. The primary dependent variables are pressure (p), phasic specific internal energies (U_g, U_f), vapour volume fraction (void fraction) (α_g), phasic velocities (v_g, v_f), non-condensable quality (X_n), and boron density (ρ_b). The independent variables are time (t) and distance (x). Non-condensable quality is defined as the ratio of the noncondensable gas mass to the total gaseous phase mass. The basic two-fluid differential equations that form the basis for the hydrodynamic model are next presented.

The basic field equations for the two-fluid non-equilibrium model consist of two phasic continuity equations, two phasic momentum equations, and two phasic energy equations. The equations are recorded in differential stream tube form with time and one space dimension as independent variables and in terms of time and volume-average dependent variables.

The phasic continuity equations are:

$$\frac{\partial}{\partial t}(\alpha_g \rho_g) + \frac{1}{A}\frac{\partial}{\partial x}(\alpha_g \rho_g v_g A) = \dot{m}_g \tag{3.21}$$

$$\frac{\partial}{\partial t}(\alpha_f \rho_f) + \frac{1}{A}\frac{\partial}{\partial x}(\alpha_f \rho_f v_f A) = \dot{m}_f \tag{3.22}$$

Where A is the cross sectional area.

These equations come from the one-dimensional phasic mass equations. The phasic conservation of momentum equations are used in terms of momenta per unit volume using the phasic primitive velocity variables v_g and v_f. The spatial variation of momentum term is expressed in terms of $(v_g)^2$ and$(v_f)^2$. This form has the desirable feature that the

[1] In mathematics, the Courant–Friedrichs–Lewy condition (CFL condition) is a necessary condition for convergence while solving certain partial differential equations (usually hyperbolic PDEs) numerically by the method of finite differences. It arises in the numerical analysis of explicit time-marching schemes, when these are used for the numerical solution. As a consequence, the time step must be less than a certain time in many explicit time-marching computer simulations, otherwise the simulation will produce incorrect results. The condition is named after Richard Courant, Kurt Friedrichs, and Hans Lewy who described it for the frist time in 1928.

momentum equation reduces to Bernoulli's equations for steady, incompressible, and frictionless flow. A guiding principle used in the development of the RELAP5® momentum formulation is that momentum effects are secondary to mass and energy conservation in reactor safety analysis and a less exact formulation (compared to mass and energy conservation) is acceptable, especially since nuclear reactor flows are dominated by large sources and sinks of momentum (i.e., pumps, abrupt area change).
The momentum equation for the vapour phase is and for the liquid phase is

$$\begin{aligned}\alpha_g\rho_g A\frac{\partial v_g}{\partial t}+\frac{1}{2}\alpha_g\rho_g\frac{\partial v_g^2}{\partial x}&\\ =-\alpha_g A\frac{\partial P}{\partial x}+\alpha_g\rho_g B_x A-\left(\alpha_g\rho_g A\right)FWG\left(v_g\right)&\\ +\dot{m}_g A\left(v_{gI}-v_g\right)-\left(\alpha_g\rho_g A\right)FIG\left(v_g-v_f\right)&\\ -C\alpha_g\rho_m A\left[\frac{\partial\left(v_g-v_f\right)}{\partial t}+v_f\frac{\partial v_g}{\partial x}-v_g\frac{\partial v_f}{\partial x}\right]&\end{aligned} \tag{3.23}$$

$$\begin{aligned}\alpha_f\rho_f A\frac{\partial v_f}{\partial t}+\frac{1}{2}\alpha_f\rho_f\frac{\partial v_f^2}{\partial x}&\\ =-\alpha_f A\frac{\partial P}{\partial x}+\alpha_f\rho_f B_x A-\left(\alpha_f\rho_f A\right)FWF\left(v_f\right)&\\ +\dot{m}_g A\left(v_{fI}-v_f\right)-\left(\alpha_f\rho_f A\right)FIF\left(v_g-v_f\right)&\\ -C\alpha_f\rho_m A\left[\frac{\partial\left(v_g-v_f\right)}{\partial t}+v_g\frac{\partial v_f}{\partial x}-v_f\frac{\partial v_g}{\partial x}\right]&\end{aligned} \tag{3.24}$$

Where B_X is the body force in x coordinate direction, C is the coefficient of virtual mass and the subscript I is for interface.
These equations come from the one-dimensional phasic momentum equations with the following simplifications: the Reynolds stresses are neglected, the phasic pressures are assumed equal, the interfacial pressure is assumed equal to the phasic pressures (except for stratified flow), the covariance terms are universally neglected (unity assumed for covariance multipliers), interfacial momentum storage is neglected, phasic viscous stresses are neglected, the interface force terms consist of both pressure and viscous stresses, and the normal wall forces are assumed adequately modelled by the variable area momentum flux formulation.
The phasic continuity equations are multiplied by the corresponding phasic velocity, and are subtracted from the momentum equations.
The force terms on the right sides of equation 3.21 and equation 3.22 are, respectively, the pressure gradient, the body force (i.e., gravity and pump head), wall friction, momentum transfer due to interface mass transfer, interface frictional drag, and force due to virtual mass.
The terms FWG and FWF are part of the wall frictional drag, which are linear in velocity, and are products of the friction coefficient, the frictional reference area per unit volume, and the magnitude of the fluid bulk velocity.

The interfacial velocity in the interface momentum transfer term is the unit momentum with which phase appearance or disappearance occurs. The coefficients FIG and FIF are part of the interface frictional drag; two different models (drift flux and drag coefficient) are used for the interface friction drag, depending on the flow regime. Virtual mass represents real physical effects to accomplish the dissipation for numerical stability.
The phasic thermal energy equations are:

$$\frac{\partial}{\partial t}(\alpha_g \rho_g U_g) + \frac{1}{A}\frac{\partial}{\partial x}(\alpha_g \rho_g U_g v_g A) = -P\frac{\partial \alpha_g}{\partial t} - \frac{P}{A}\frac{\partial}{\partial x}(\alpha_g v_g A) + Q_{wg} + Q_{ig} - \dot{m}_{ig} h_g - \dot{m}_w h_g + DISS_g \tag{3.25}$$

$$\frac{\partial}{\partial t}(\alpha_f \rho_f U_f) + \frac{1}{A}\frac{\partial}{\partial x}(\alpha_f \rho_f U_f v_f A) = -P\frac{\partial \alpha_f}{\partial t} - \frac{P}{A}\frac{\partial}{\partial x}(\alpha_f v_f A) + Q_{wf} + Q_{if} - \dot{m}_{if} h_f - \dot{m}_w h_f + DISS_f \tag{3.26}$$

These equations come from the one-dimensional phasic thermal energy equations with the following simplifications: the Reynolds heat flux is neglected, the covariance terms are universally neglected (unity assumed for covariance multipliers), interfacial energy storage is neglected, and internal phasic heat transfer is neglected. In the phasic energy equations, Qwg and Qwf are the phasic wall heat transfer rates per unit volume where Q is the total wall heat transfer rate to the fluid per unit volume. DISS is the energy dissipation function. Q_{ig} and Q_{if} are interfaces heat transfer effects due to evaporation and condensation processes.

3.7 RELAP5® MODEL

The pressurizer body is modelled with 7-cell pipe 341.
Generally, good agreement with experimental and plant data has been attained for slow and fast pressurizer insurges and outsurges with this nodalization. However a more finer nodalization with 16, 32 and 64 volumes has been developed to check the numerical results of the model. The surge line is modeled with 3-cell pipe 343.
The functions of the power-operated relief valve (PORV) is lumped into valve 344. The valves open in response to a significant primary coolant system overpressure.
The pressurizer spray system is modelled with single-volume 339. The spray turns on in response to a mild primary coolant system over-pressurization. The flow area of all valves is that necessary for delivering the rated flow capacity at the rated upstream pressure. Heat structures are used to represent the cylindrical pressurizer shell and its spherical lower and upper heads, and the pressurizer surge line pipe wall. Heat structures are also used to simulate operation of the pressurizer heaters. Heater power is increased in response to an under-pressurization of the primary coolant system pressure.
So the heat structures simulate both energy storage in the material mass and energy transfer to or from the material mass to the fluid in the simulated stream-tubes. Energy storage and transfer in the heat structures is calculated by the code using the geometry defined by the user; each heat structure is sized to interact with particular stream-tubes and each heat structure can be finely nodalized to provide a rather detailed temperature distribution in one dimension.
Because RELAP5® uses a first-order upwind differencing scheme that has considerable numerical diffusion, there is significant mixing of hot and cold fluid on some applications of the code. This has an unfavourable effect on the accuracy of the solution. To counteract this, the thermal stratification model was developed with the following features: have a sharp temperature profile that will separate the hot fluid from the cold fluid whenever thermal stratification occurs, correct donoring of liquid internal energy at the junctions for the cell where the thermal stratification occurs. Only the hot fluid in a cell that contains the thermal front is allowed to flash. The trip logic is used to modelling the pressurizer control, which is taken from Shippingport reactor control scheme.
The trip logic is used to turn on or turn off heaters, sprayers and valves components. In general, the trip's condition is either true or false.

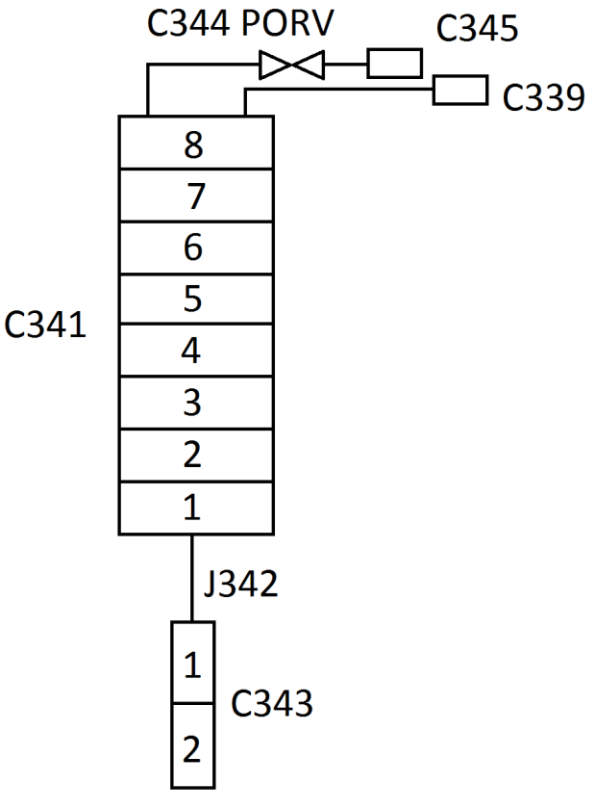

FIG. 3.17 RELAP5® pressurizer model

The trip's condition is determined at each time step by checking the status of the trip-defined test. The test consists of comparing the specified variable to either another variable or a parameter using specified conditions such as equal to, greater than, less than, greater than or equal, less than or equal, or not equal.

In essence, the control variables can be used for three primary functions: to simulate equipment control systems, to create "lumped node" parameters, and to add further dimensions to the boundary conditions imposed on the thermal-hydraulic group and heat structure group components.

3.8 CONCLUDING REMARKS

In this chapter three different simulation approaches have been showed: control-oriented, object-oriented and thermal-hydraulics-oriented. The first one, i.e. Simulink® model, is a block-diagrams program based on the causal approach specifically developed for the control analysis of the pressurizer: that is stability properties and studies of control logic. The second one, i.e. Dymola® model, is an example of the potentialities and the ease of use of the acausal approach which can give the same results of the causal one without completely transform the physical system into a form which is close to the solution algorithm. The third one, i.e. RELAP5® model, is realized using a best-estimate code, which represents the standard reference for nuclear power plant simulations. RELAP5® allows, on one hand, a detailed study of the thermo-hydraulics phenomena occurring inside simulated component, but, on the other, just a poor coupling of the dynamic model with an advanced control logic. Finally, it is important to point out that RELAP5® model has been developed in order to verify . Simulink® and Dymola® ones.

3.9 REFERENCES

[24] CONTINUOUS SYSTEM SIMULATION
Francois E. Cellier
Ernesto Kofman
Universidad Nacional de Rosario
Laboratory for System Dynamics and Signal Processing
School of Electronic Engineering – FCEIA
Printed on acid-free paper. 2006 Springer Science+Business Media, Inc.

[25] PRINCIPLES OF OBJECT-ORIENTED MODELING AND SIMULATION WITH MODELICA 2.1
Peter Fritzson Wiley-IEEE -2003

[26] COSTANTINOS C. PANTELIDES
The consistent initialization of Differential-Algebraic Systems
SIAM J. SCI. STAT. COMPUT.1988

[27] COMPUTER METHODS FOR ORDINARY DIFFERENTIAL EQUATIONS AND DIFFERENTIAL-ALGEBRAIC EQUATIONS
Uri M. Ascher and Linda R. Petzold
December 2 1997

[28] RELAP5/MOD3.3 CODE MANUALVOLUME I: CODE STRUCTURE, SYSTEM MODELS, AND SOLUTION METHODS
Nuclear Safety Analysis Division
December 2001 Information Systems Laboratories, Inc.

Chapter 4 – PRESSURIZER MODEL VALIDATION

4.1 INTRODUCTION

The purpose of this chapter is a code to code comparison: results of various models are presented and compared to each other.
First of all, Simulink®, Dymola® and RELAP5® "free-dynamics" transients are matched with the experimental data coming from Shippingport pressurizer tests: in this first case, heaters and sprayers are not controlled variables, but inputs whose operating times refer to Redfiled, Prescop and Margolis' report [4].
This paper is the most detailed among all publications about Shippingport pressurizer experiments and the reported operating times of pressure control system should be the true ones, although it is not explicitly said.
In fact, as it will be shown in the first part of this chapter, the good degree of agreement between "free-dynamics" results of multiple-volumes simulations and the real transients can be considered a proof that Redfiled, Prescop and Margolis' heaters and sprayers data are effectively the experimental ones.
However, as other papers ([13] [14]), which are not as detailed as Redfiled, Prescop and Margolis' one, use data which are slightly different, some doubt about the reliability of sprayers and heaters operating times remains. For this reason, the second part of the chapter is focalized on the "controlled dynamics" of the pressurizer.
In this second case, sprayers and heaters operations are treated as controlled variables which are governed by a control-block (showed in the previous chapter) which reproduces exactly the Shippingport control logic, which is available to the author.
Then, controlled-transients simulated using Simulink® and Dymola® are matched with the experimental data coming from Shippingport pressurizer tests (where Redfiled, Prescop and Margolis' data are used as reference for heaters and sprayers operation): therefore it is be possible to see again the increasing accuracy of various models starting from the rough equilibrium formulation, to the highly accurate two-regions and three-regions ones.
Then RELAP5® results are more deeply presented: first of all, they are compared with experimental data, then they are used as reference for Simulink® and Dymola® results for

which experimental data are not available, i.e. temperature distribution inside liquid region, and mass flow rates between different control volumes (RELAP5® is essentially used to verify Simulink® and Dymola® models).
For every model a sensitivity analysis has been performed: in Simulink® and Dymola® case all the simulations have been carried on using different fixed and variables step integration algorithms [27].
For RELAP5® programs different nodalizations have been tested and both a semi-explicit and fully implicit integration methods have been used [28].

4.2 VERIFICATION AND VALIDATION OF MODELS

A mathematical model can be on the paper perfect: elegant, simple, formally correct. Its creator can fall in love whit it. However, if a model is not tested, it will remain just a mental exercise without any real usefulness. A model must agree with the real physics world, otherwise it is not correct or not sufficiently accurate. You must not think that is the reality to be wrong as a lovestruck programmer thinks!

Really what constitutes a good model is subjective, but from a performance modelling point of view the criteria for judging the goodness of models will be based on how accurately measures extracted from the model correspond to the measures which would be obtained from the represented system. By its nature a model is more abstract than the system it represents. Viewed in one way, abstraction and assumptions made to achieve it, eliminate unnecessary detail and allow to focus on the elements within the system which are important from a performance point of view; in another way, this abstraction process introduces inaccuracy. Some degree of inaccuracy may be necessary, desirable even, to make the model solution tractable and/or efficient. Inevitably some assumptions must be made about the system in order to construct the model. However, having made such assumptions you must expect to put some effort into answering questions about the goodness of our model. There are two steps to judge how good a model is with respect to the system. You must ascertain whether the model implements the assumptions correctly (model verification) and whether the assumptions which have been made are reasonable with respect to the real system (model validation).

Verification and validation of computer simulation models must be conducted during the development of a simulation model with the ultimate goal of producing an accurate and credible model.

In the context of computer simulation, verification of a model is the process of confirming if it is correctly implemented with respect to the conceptual ideal (it matches specifications and assumptions deemed acceptable for the given purpose of application). During verification the model is tested to find and fix errors in the implementation of the model.

Validation is the task of demonstrating that the model is a reasonable representation of the actual system: that it reproduces system behaviour with enough fidelity to satisfy analysis objectives. Whereas model verification techniques are general the approach taken to model validation is likely to be much more specific to the model, and system, in question. Indeed, just as model development will be influenced by the objectives of the performance study, so will model validation be. A model is usually developed to analyse a particular problem and may therefore represent different parts of the system at different levels of abstraction.

As a result, the model may have different levels of validity for different parts of the system across the full spectrum of system behaviour. Comparison with a real system is the most reliable and preferred way to validate a simulation model. In practice, however, this is often infeasible either because the real system does not exist or because the

measurements would be too expensive to carry out. In this case just the comparison between different codes is possible.
Assumptions, input values, output values, workloads, configurations and system behaviour should all be compared with those observed in the real world. In the case of simulation models, when full measurement data is available it may be possible to use trace-driven simulation to observe the model under exactly the same conditions as the real system.
Therefore the purpose of this chapter is to validate the pressurizer models presented in the previous chapters. Verification step was done as code debugging. The simulation results of the different models will be compared together and matched to experimental Shippingport data, in particular 74 MW and 105 MW loss of load transients which are the most interesting.
To make simulations meaningful, the pressurizer geometry, initial conditions and the pressure control parameters used in this study are taken from the Shippingport test data. The reactor coolant system surge needed for this study, is calculated from the pressurizer level by the following procedure: having the water level time history from the Shippingport data, the time rate of change of liquid mass in the pressurizer is first calculated. The time history of spray flow is then used to calculate the steam condensate formed on the spray.
Subtracting the sum of flow rates due to spray and steam condensate on spray from the time rate of change of liquid mass in pressurizer, the surge rate was determined. This surge rate is shown in figure 4.1 and 4.2.
It should be borne in mind that the detailed log sheets for Shippingport experiments were not available to the author and the above computations are based on the curves given m the above reference and the application of a certain amount of judgment for the interpretation of pressurizer parameters and initial conditions. For these reasons the surge flow plots shown in figure 4.1 and 4.2 should be considered approximate.

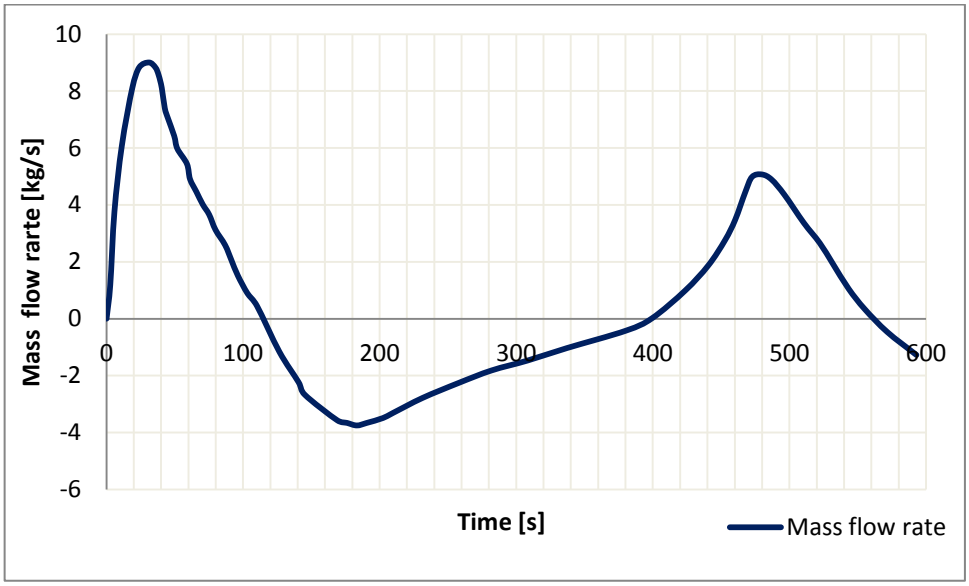

FIG. 4.1 Mass flow rate during 74 MW loss-of-load transient [kg/s vs. S]

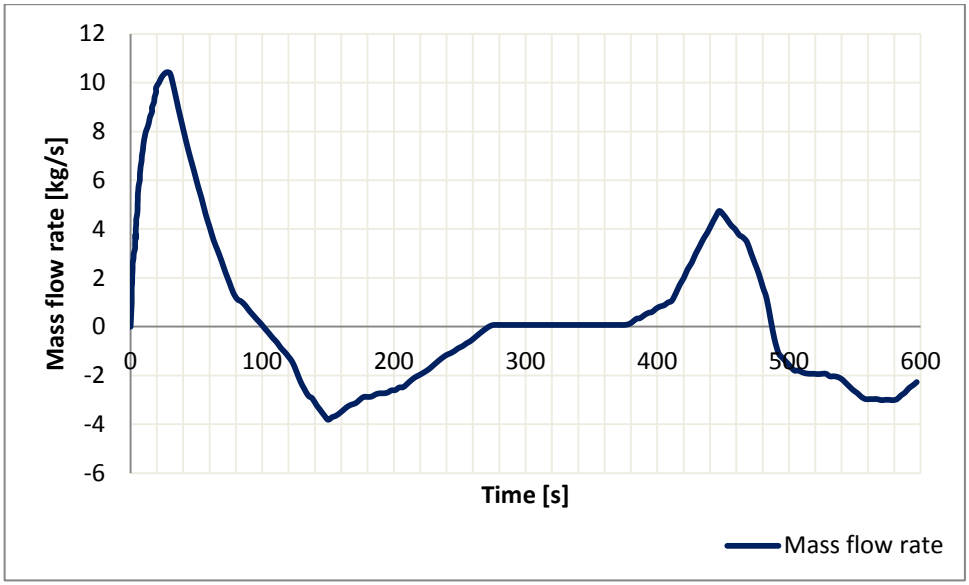

FIG. 4.2 Mass flow rate during 105 MW loss-of-load transient [kg/s vs. s]

4.3 FREE-DYNAMICS SIMULATIONS RESULTS

In the following pages, the "free-dynamics" transients obtained using Simulink® and Dymola® simulations programs are shown. Heaters and sprayers operations are treated as inputs taken from Redfiled, Prescop and Margolis' paper [4].
These data should be the experimental ones, in fact, using them in the case of RELAP5® "free-dynamics" model, the real pressure transients are followed. Moreover, multiple-volume models results agree quite with the experimental ones. Instead, for one-volume simulations, the actual pressure behaviour is not reproduced. This fact shows that single-volume models cannot be used to effectively reproduce the pressurizer.
RELAP5® "free-dynamics" results are assumed, together with the experimental ones, as reference.

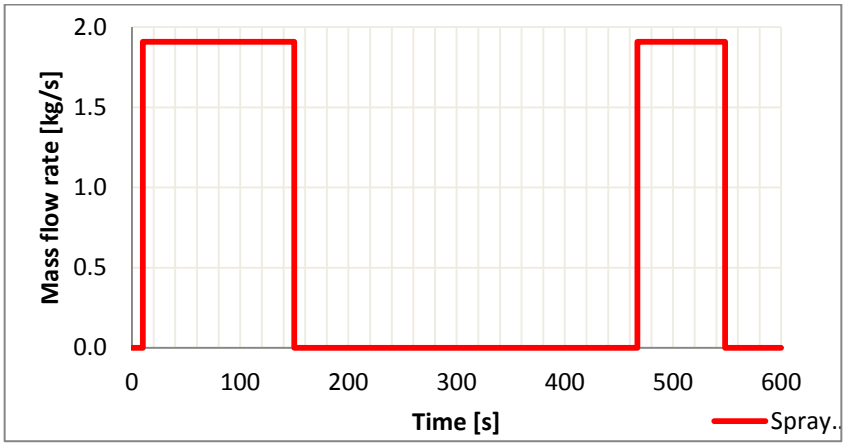

FIG. 4.3 Sprayers operations during 74 MW loss-of-load transient [kg/s vs. s]

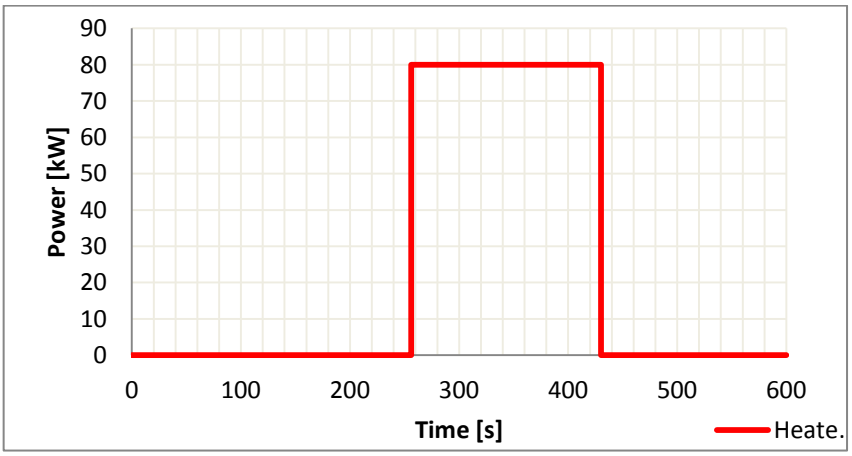

FIG. 4.4 Heaters operations during 74 MW loss-of-load transient [kg/s vs. s]

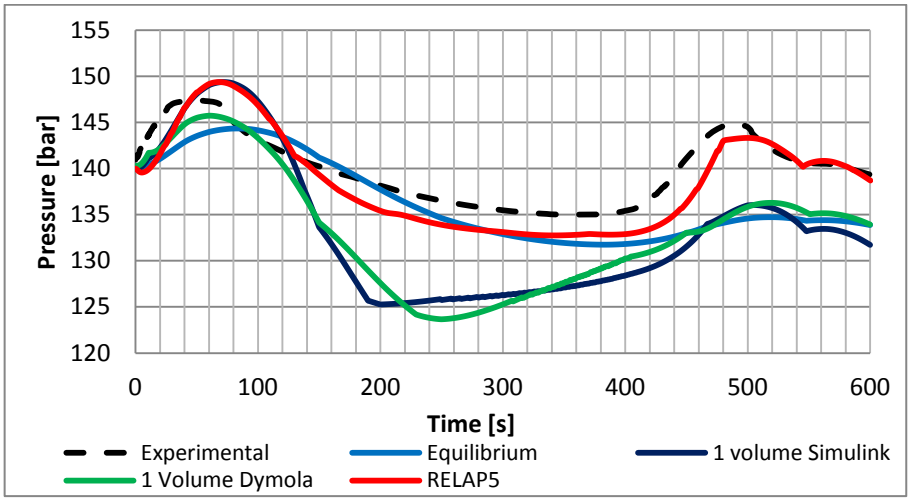

FIG. 4.5 Pressure Free-dynamics 74 MW loss-of-load for one-volume model [kg/s vs. s]

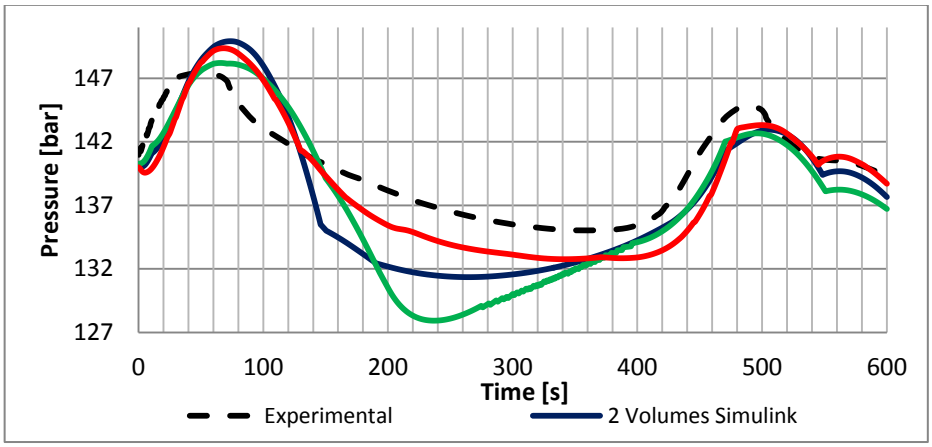

FIG. 4.6 Pressure free-dynamics 74 MW loss-of-load for two-volumes model [kg/s vs. s]

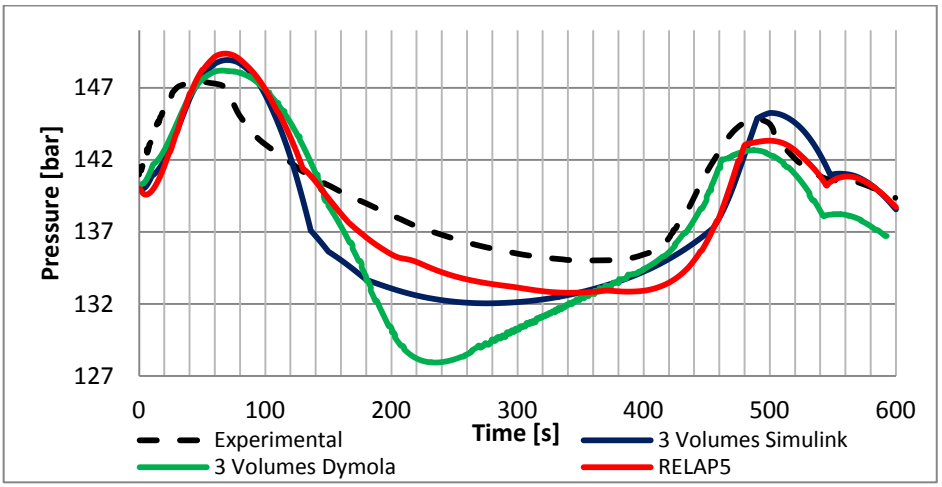

FIG. 4.7 Pressure free-dynamics 74 MW loss-of-load for three-volumes model [kg/s vs. s]

Figure 4.5 shows that one-volume models are not suitable to reproduce the pressurizer behaviour.
Figures 4.6 and 4.7 demonstrate that operating times of heaters and sprayers present in Redfiled, Prescop and Margolis' paper can be the experimental ones really.
However some doubt remains because other reports, which are not as detailed as the Redfiled, Prescop and Margolis' one, refer to data which are slightly different.
For this reason, now the controlled pressurizer dynamics follows. Here all the results are compared with the experimental ones, which are reliable for pressure, temperature and level; for heaters and sprayers the experimental data are assumed to be the Redfiled, Prescop and Margolis' ones with a certain amount of judgment.

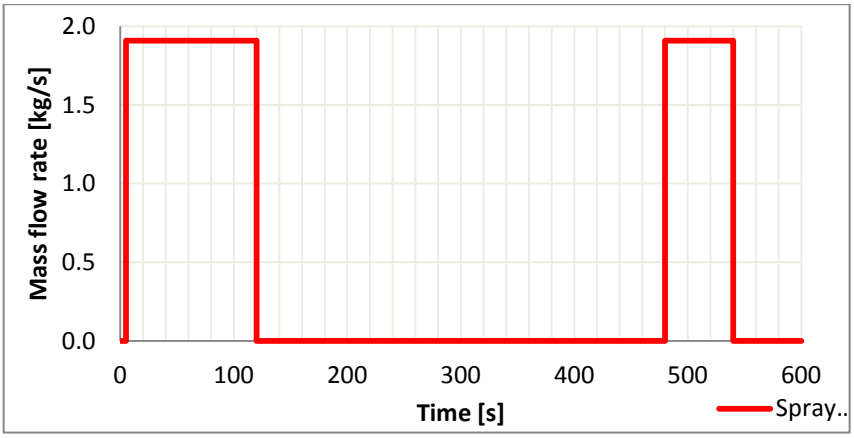

FIG. 4.8 Sprayers operations during 105 MW loss-of-load [kg/s vs. s]

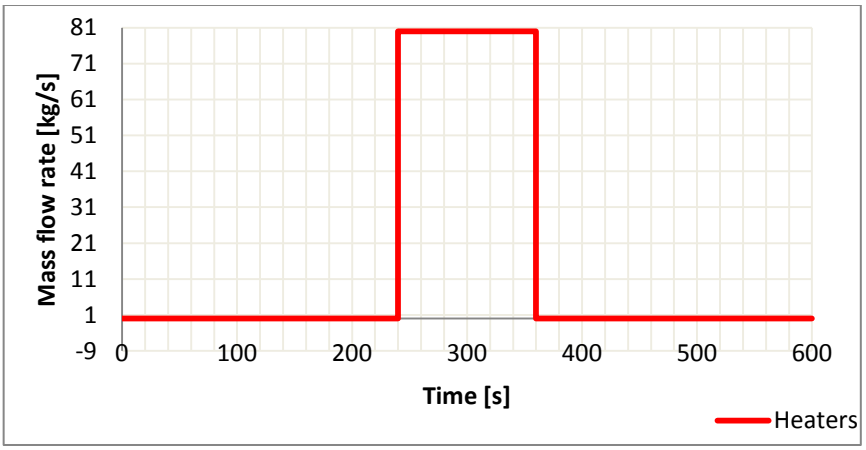

FIG. 4.9 Heaters operations during 105 MW loss-of-load [kg/s vs. s]

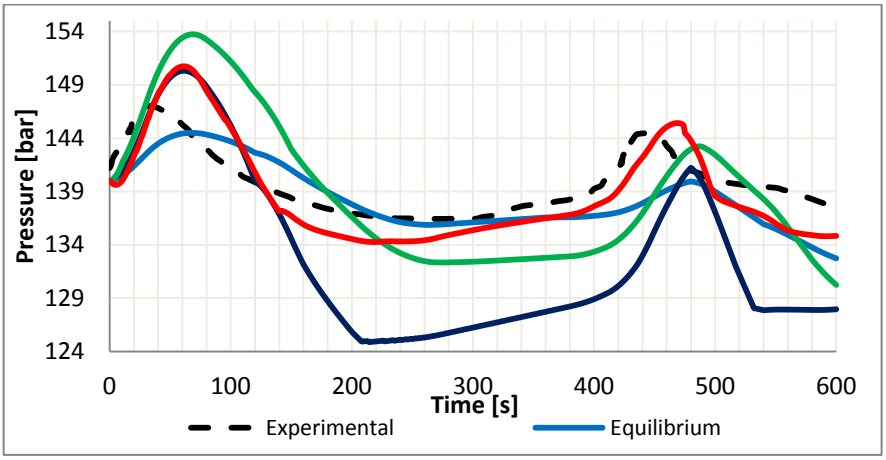

FIG. 4.10 Pressure free-dynamics 105 MW loss-of-load for one-volume model [kg/s vs. s]

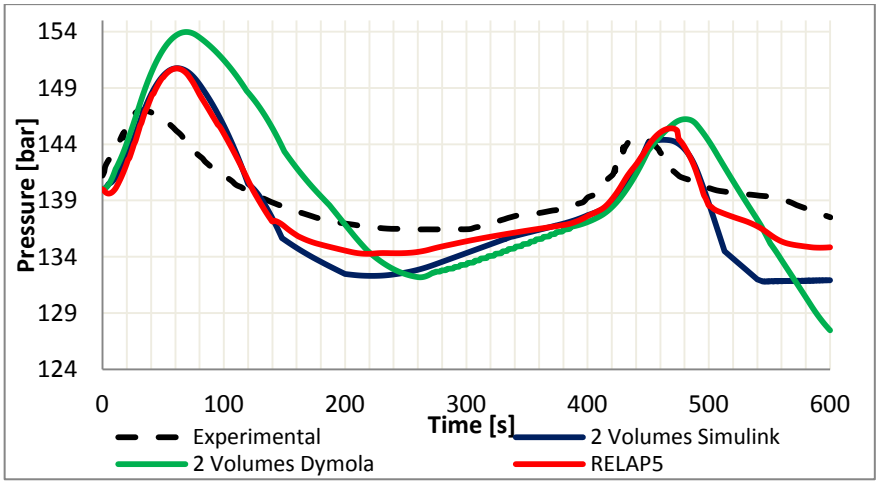

FIG. 4.11 Pressure free-dynamics 74 MW loss-of-load for two-volumes model [kg/s vs. s]

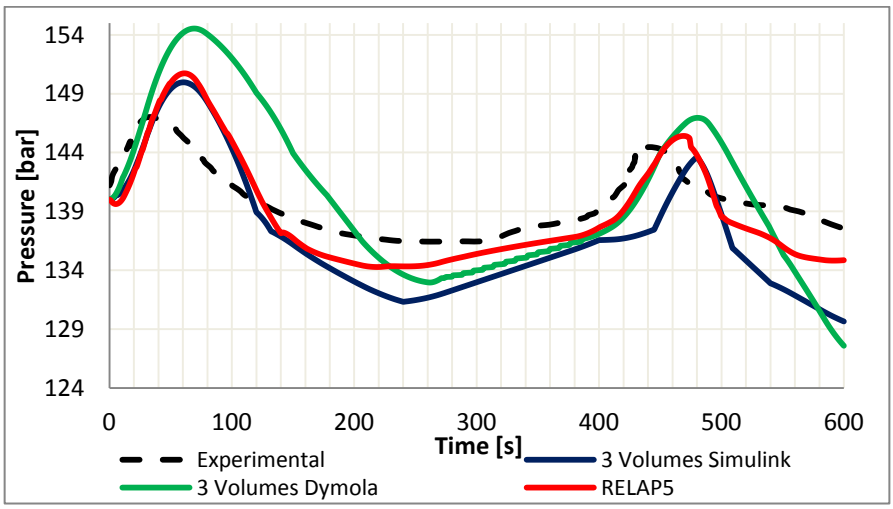

FIG. 4.12 Pressure free-dynamics 105 MW loss-of-load for three-volumes model [kg/s vs. s]

4.4 SIMULINK® CONOTROLLED-MODELS RESULTS

In this section results coming from controlled-dynamics Simulink® models are presented. Now, sprayers and heaters operation are controlled variables governed by the action of the control-block described in the previous chapter.
Firstly, equilibrium models results are presented. Equilibrium approaches are traditionally the most used for the development of control-oriented models. However these models introduce a lot of simplifications which make them too rough to follow real physics transients. From this assumption, the necessity of a new control-oriented model able to be in good agreement with real transients and to achieve better control performances arises.

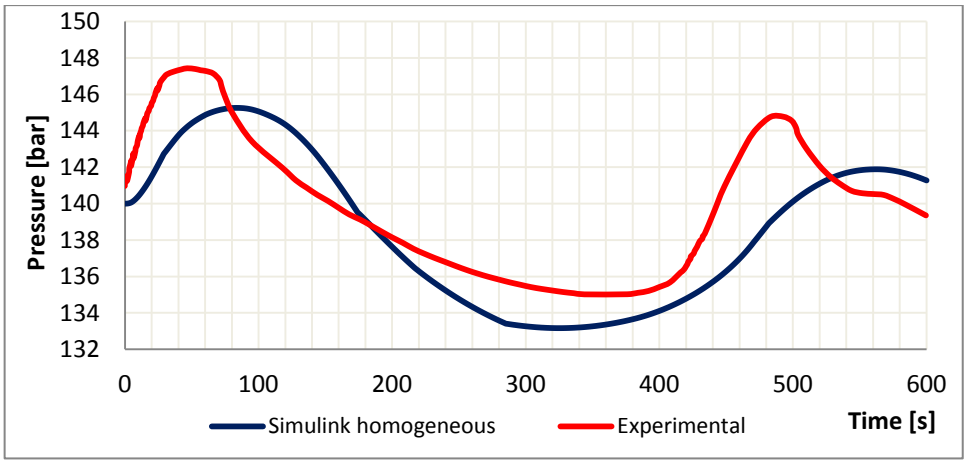

FIG. 4.13 Pressure variation during 74 MW loss-of-load transient [bar vs. s]

Pressure graph confirms the poor agreement between experimental data and simulation results of homogeneous model. Moreover it must be remembered that, among the hypothesis on which equilibrium model is based, there is the entry of insurge water at saturation conditions which is very far from reality. If this assumption is removed results do not follow in any way the experimental data as it is possible to see in figure 4.4.
Under the assumption $T^{SURGE} = T^{SATURATION}$, in figure 4.5 the level dynamics is depicted showing the rough behaviour of equilibrium model again. The temperature graph of figure 4.6 shows, instead, a good behaviour when the pressurizer is really at saturation condition, i.e. between 200 and 400 seconds. It must be kept in mind that the temperature computed by the equilibrium model is, of course, the saturation one.

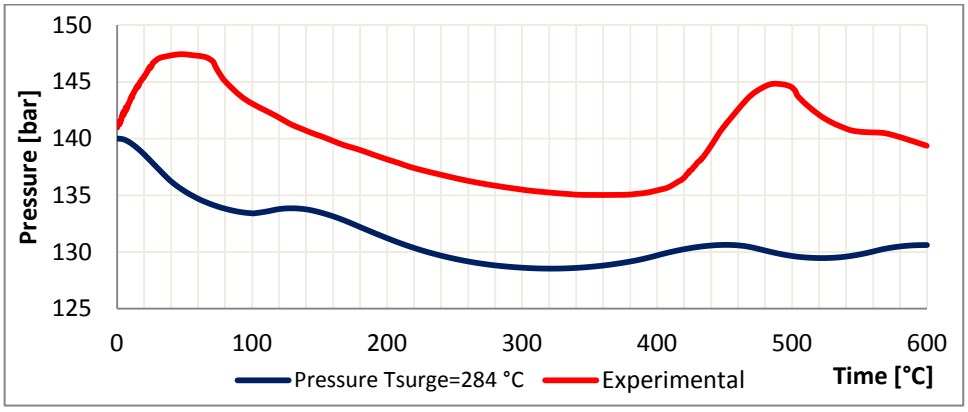

FIG. 4.14 Pressure variation if Tsurge is the real one (284°C)[bar vs. s]

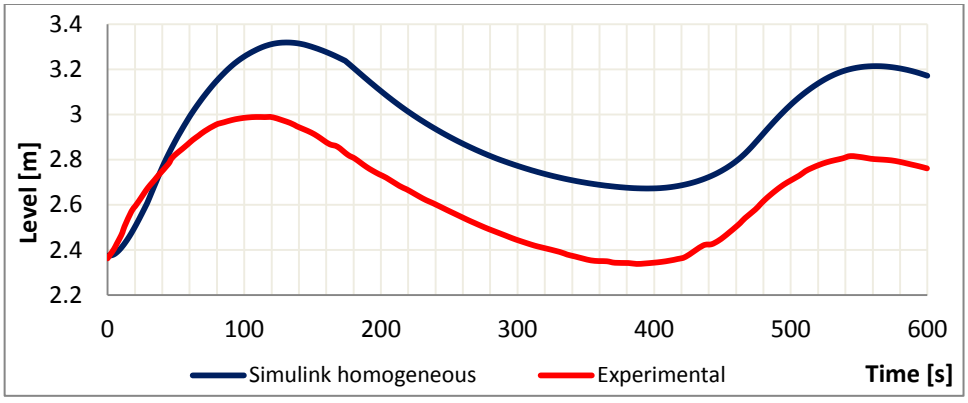

FIG. 4.15 Level variation during 74 MW loss-of-load transient [m vs. s]

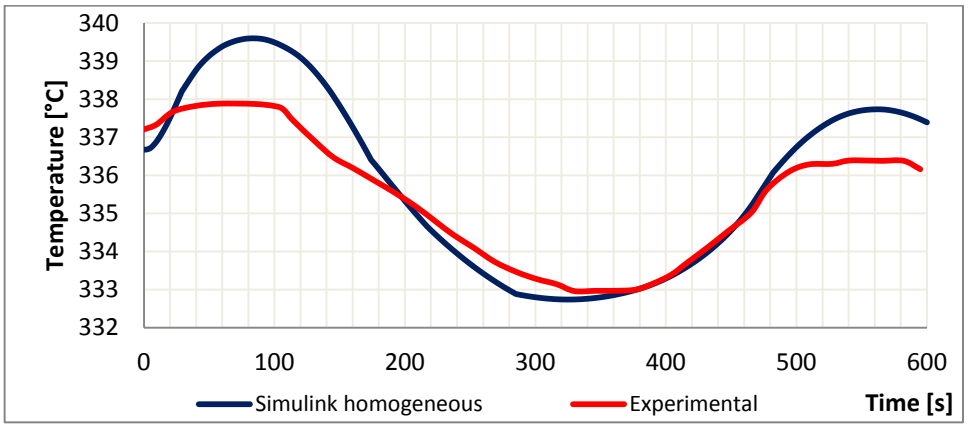

FIG. 4.16 Temperature variation during 74 MW loss-of-load transient [°C vs. s]

Regarding sprayers and heaters simulated behaviour, it is very different from the real one, sprayers activate themselves just one time, showing that the equilibrium model cannot account for the second pressure peak. On the other hand, all three heaters bank are used in the simulation, while in the experiments just the 80 kW one was turned on and off by the

system control. This fact indicates an excessive decrease of pressure, which will be a problem of one-volume and two-volumes non-equilibrium models too. However for the equilibrium model there is also a time delay in heaters operations.

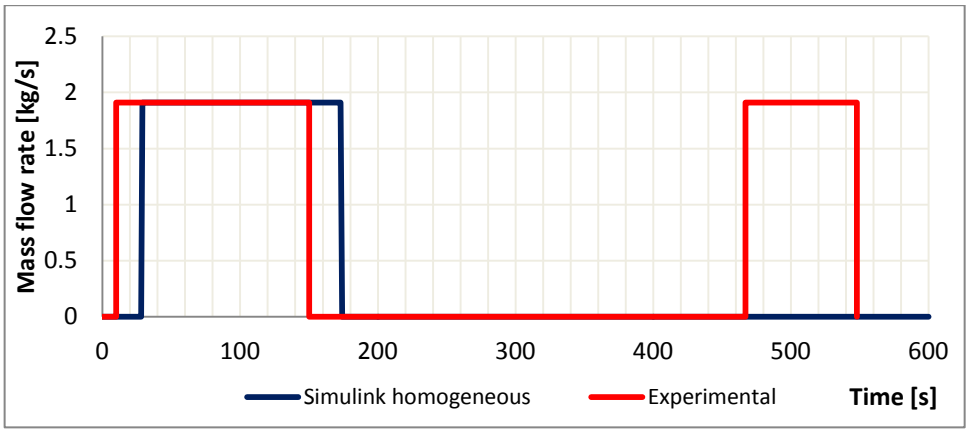

FIG. 4.17 Sprayers operations during 74 MW loss-of-load transient [kg/s vs. s]

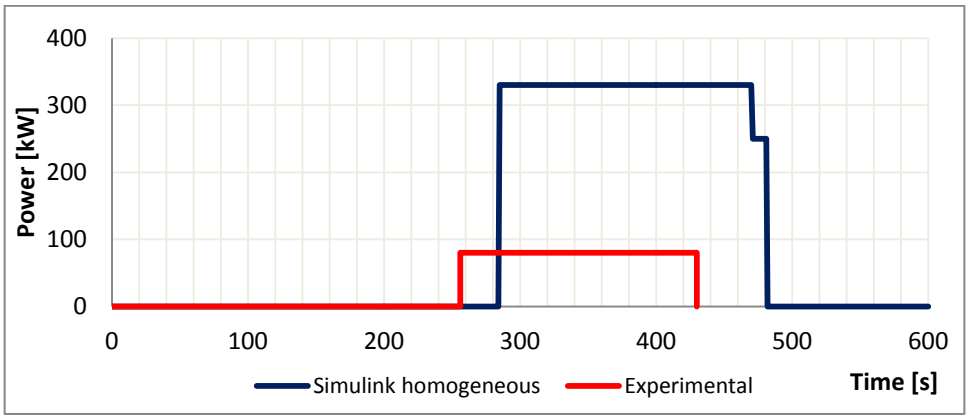

FIG. 4.18 Heaters operations during 105 MW loss-of-load transient [kW vs. s]

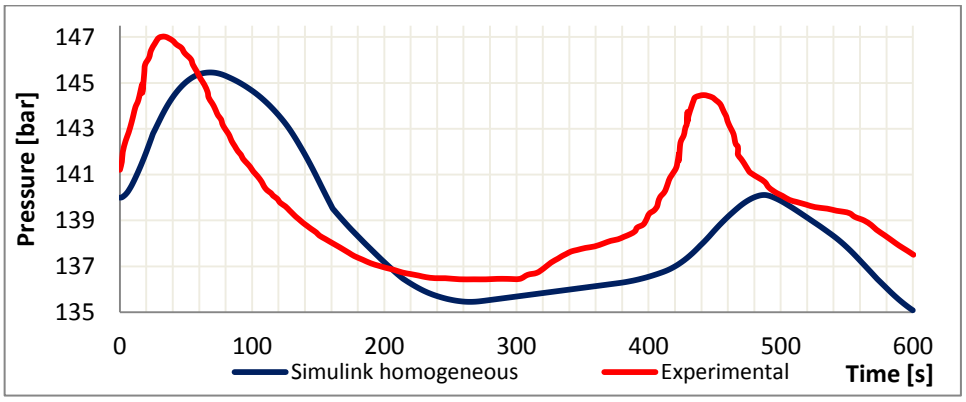

FIG. 4.19 Pressure variation during 105 MW loss-of-load transient [bar vs. s]

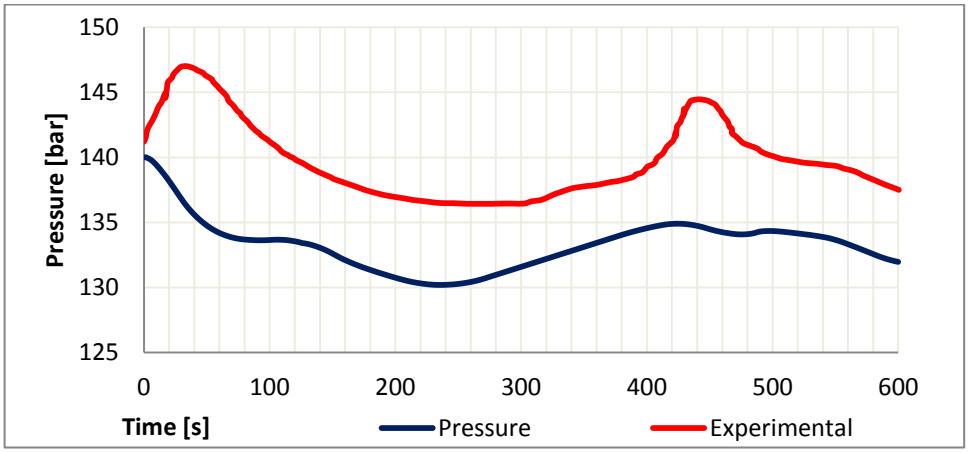

FIG. 4.20 Pressure variation if Tsurge is the real one (284°C)[bar vs. s]

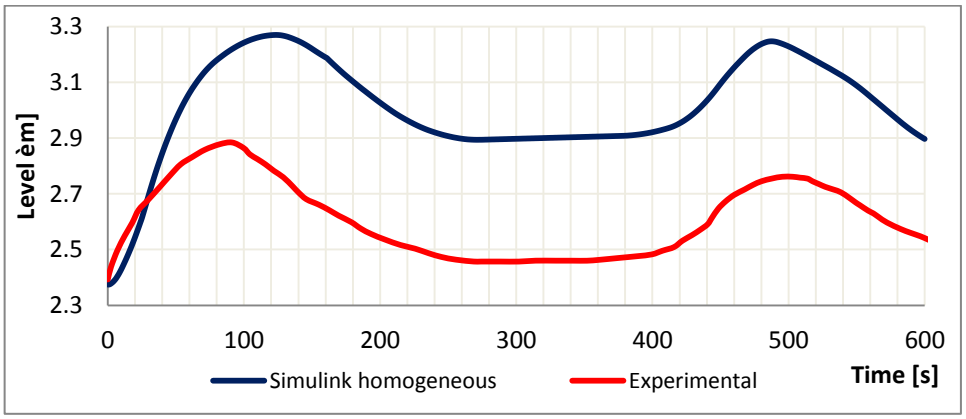

FIG. 4.21 Level variation during 105 MW loss-of-load transient [m vs. s]

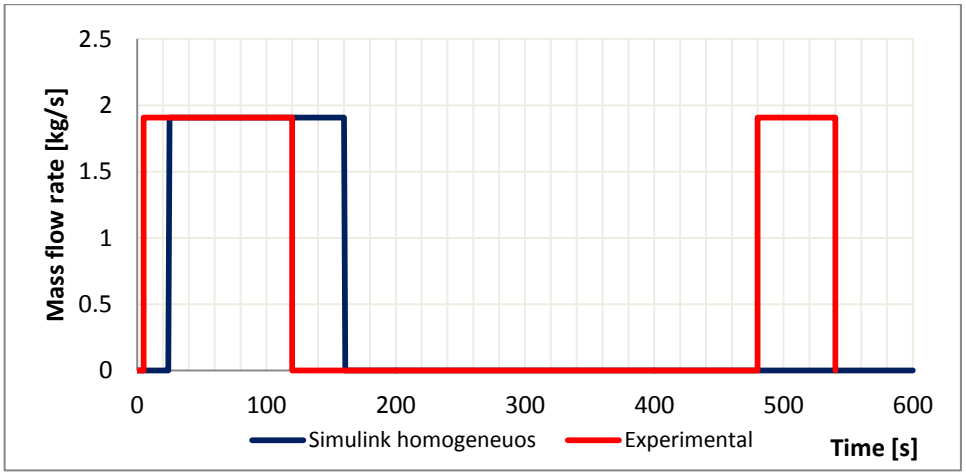

FIG. 4.22 Sprayers operations during 105 MW loss-of-load transient [kg/s vs. s]

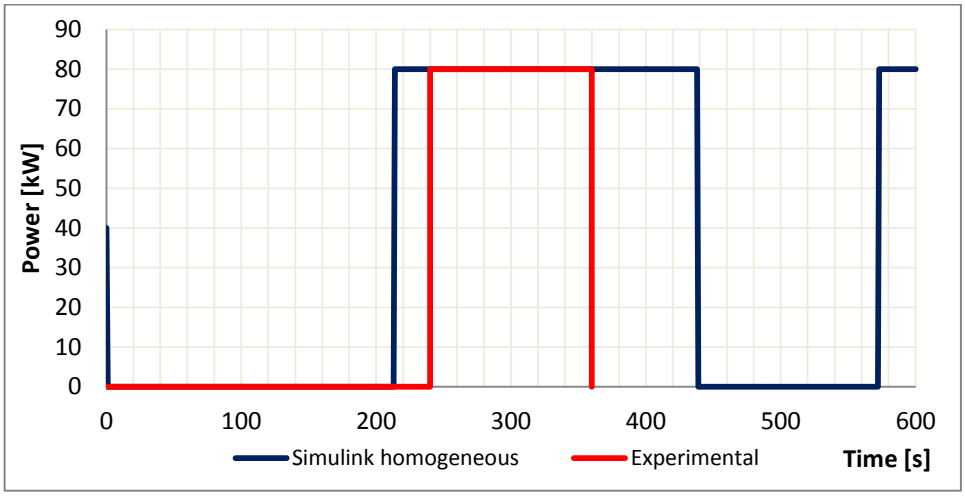

FIG. 4.23 Heaters operations during 105 MW loss-of-load transient [kW vs. s]

In the following pages, the comparison between two-region-one-volume-model (with the control block activated) and Shippingport data is shown.

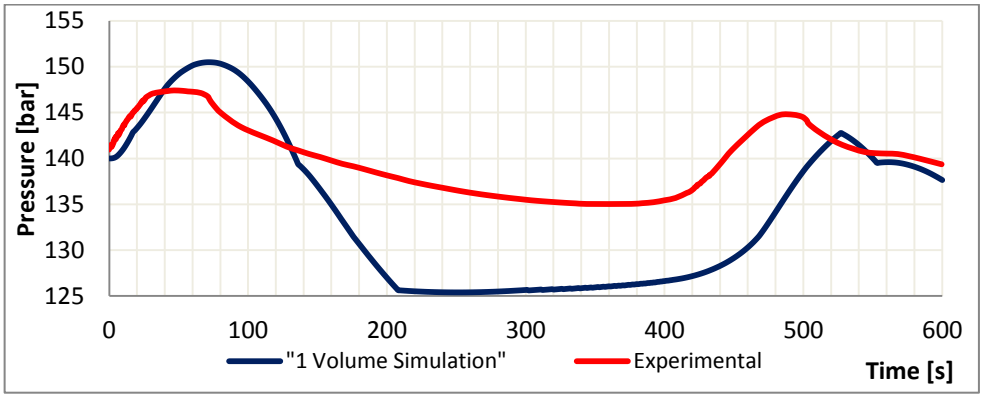

FIG. 4.24 Pressure variation during 74 MW loss-of-load transient [bar vs. s]

From the graph it is possible to see the low matching between simulation results and experimental data. The reason of this difference is, as already mentioned, the temperature distribution across liquid region, which cannot be seen by this very simple model: two-region-one-volume pressurizer is substantially based on a zero dimensional approach of liquid and vapour region, which cannot take into account spatial distributions of physical quantities.

Experimental evidence supports the hypothesis of a non-uniform temperature distribution in liquid region, in fact water temperature data, which are registered by a detector mounted on the pressurizer wall at a height of 1.422 m from the bottom of the pressurizer, are much higher than the simulated one. This can be explained in the following way: the insurge mass flow rate cools mostly the lower layer of pressurizer water, instead in the upper shell, insurge water does not arrive instantaneously and directly, but only warmer water, pushed from the bottom layer of pressurizer, comes. Temperature non-uniformity

phenomenon does not occur in a significant way into vapour phase, because there isn't any mass flow inside this region. Comparing two-region-one-volume model with the equilibrium one, you can see that: on one hand, pressure decrease is much bigger for the non-equilibrium approach than for the homogeneous mixture one, but on the other, at the end of simulation, pressure succeeds to climb up again to experimental values. For this reason, sprayers and heaters operations, although quite far from the experimental one, are now more precise: sprayers are twice activated as in the real experiment and heaters turn-on time is centred around the real one and not shifted.

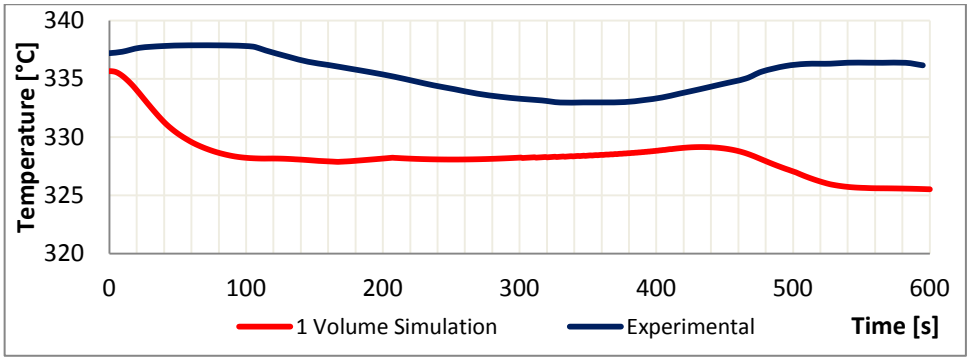

FIG. 4.25 Temperature variation during 74 MW loss-of-load transient [°C vs. s]

Unfortunately only water temperature data of 74 MW loss of load transient were available to the author, to verify reliability of water temperature data the RELAP5® codes will be very useful. Therefore two-regions-one-volume model cannot follow in a quantitative way transients inside the pressurizer. Only the dynamic is respected: all simulated quantities, including sprayers and heaters operations, are affected by the instantaneous mixing inside the liquid region. Finally, it is important to underline that all these observations have been possible thanks to the comparison between experimental data and simulated ones. If no experimental results were not available, the single volume model could be wrongly considered valid.

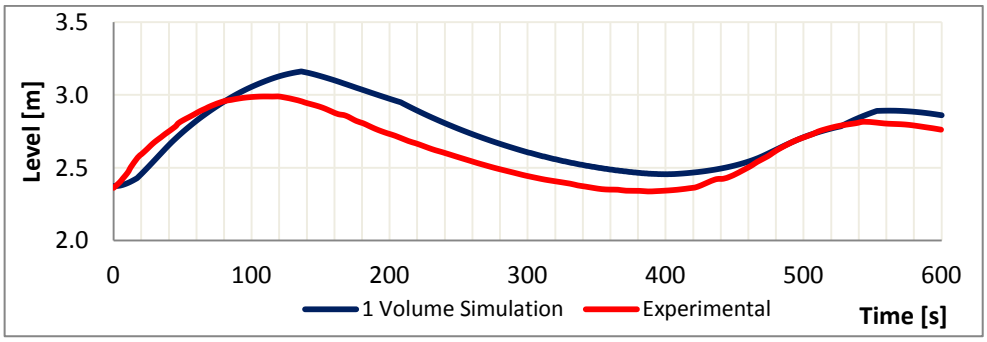

FIG. 4.26 Level variation during 74 MW loss-of-load transient [m vs. s]

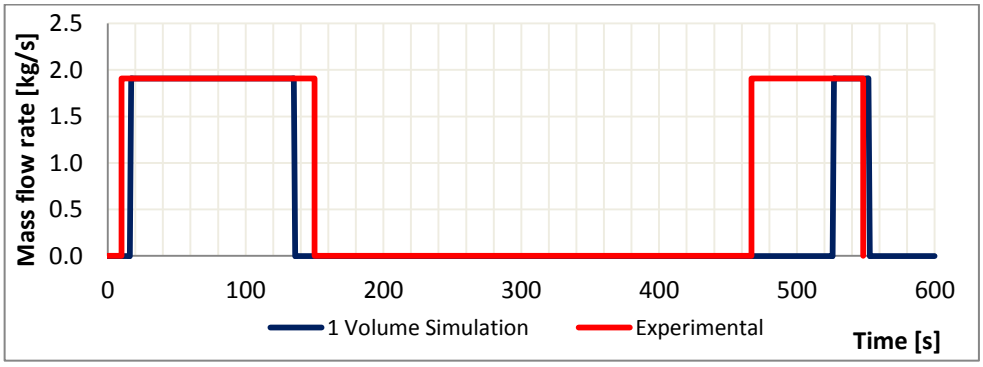

FIG. 4.27 Sprayers operations during 74 MW loss-of-load transient [kg/s vs. s]

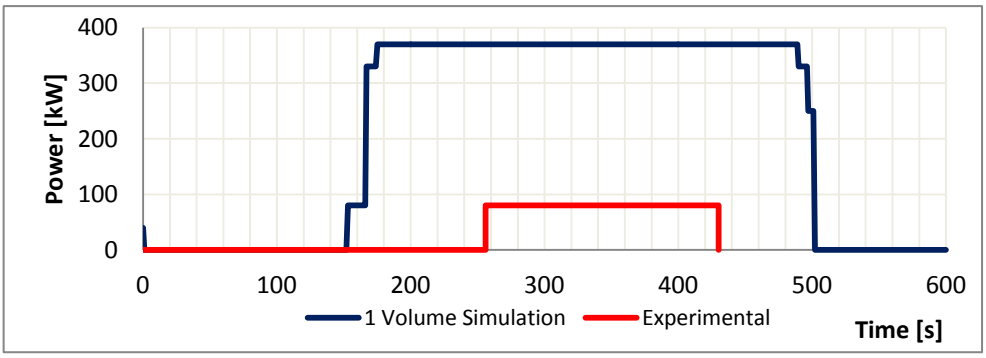

FIG. 4.28 Heaters operations during 74 MW loss-of-load transient [kW vs. s]

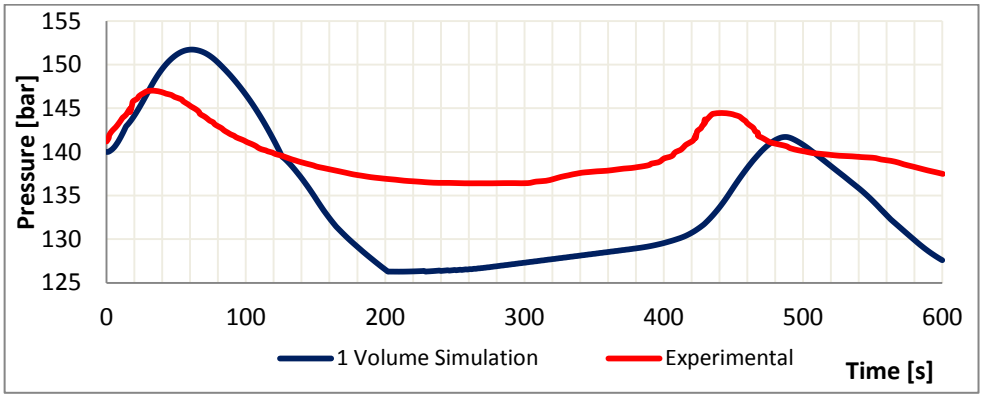

FIG. 4.29 Pressure variation during 105 MW loss-of-load transient [bar vs. s]

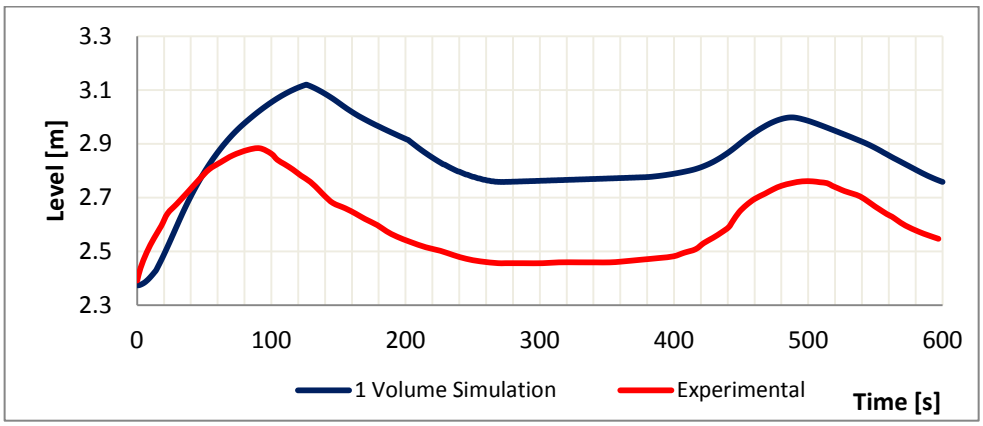

FIG. 4.30 Level variation during 105 MW loss-of-load transient [m vs. s]

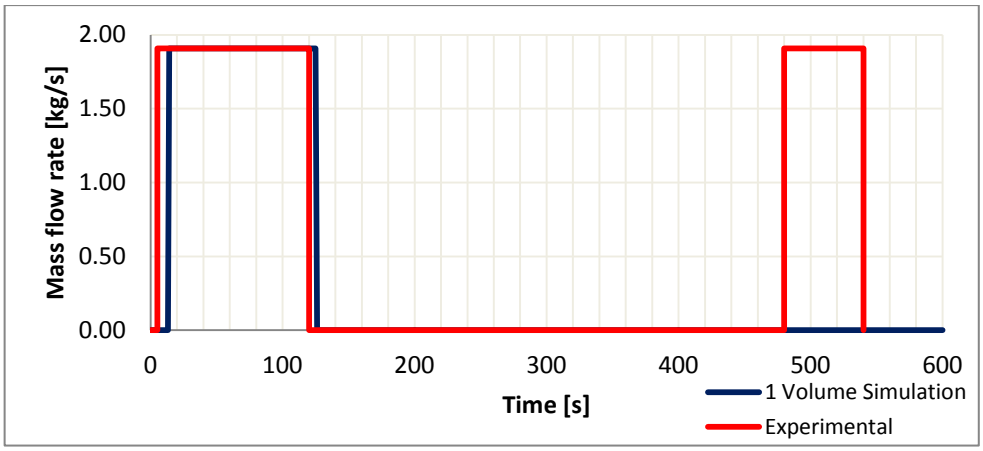

FIG. 4.31 Sprayers operations during 105 MW loss-of-load transient [kg/s vs. s]

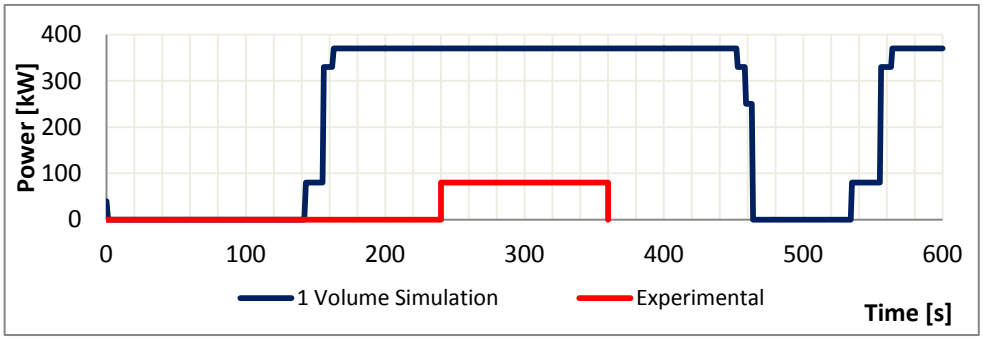

FIG. 4.32 Heaters operations during 105 MW loss-of-load transient [kW vs. s]

To take into account the temperature distribution across the liquid region, the two-regions-two-volumes model has been developed. As said in the second chapter, this model is characterized by a further only liquid volume. In this way the model can register a temperature distribution along the water region, which matches quite well with the experimental temperature results. Adding the second volume, the improvements of the

result are substantial. Of course this model is more complex than the previous one, but computational time requested by the simulation is essentially the same.

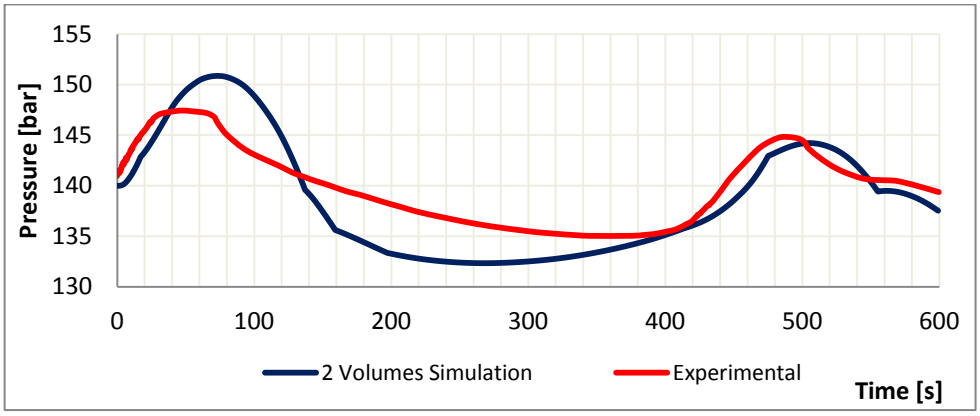

FIG. 4.33 Pressure variation during 74 MW loss-of-load transient [bar vs. s]

Results of two-regions-two-volumes controlled-model are quite similar to the experimental ones and a further improvement will be seen with the two-regions-three-volume controlled-model.

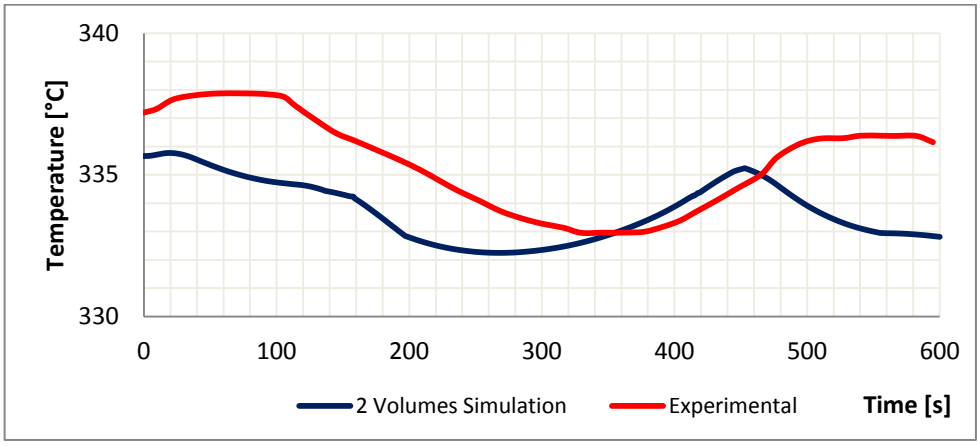

FIG. 4.34 Temperature variation during 74 MW loss-of-load transient [°C vs. s]

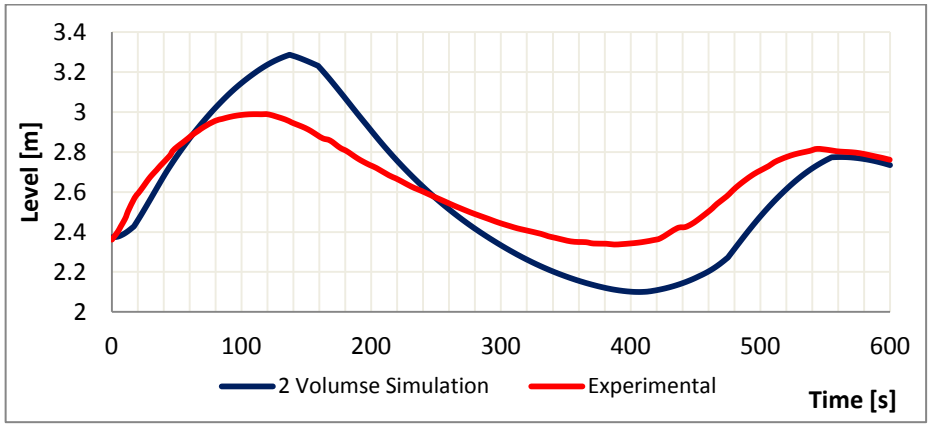

FIG. 4.35 Level variation during 74 MW loss-of-load transient [m vs. s]

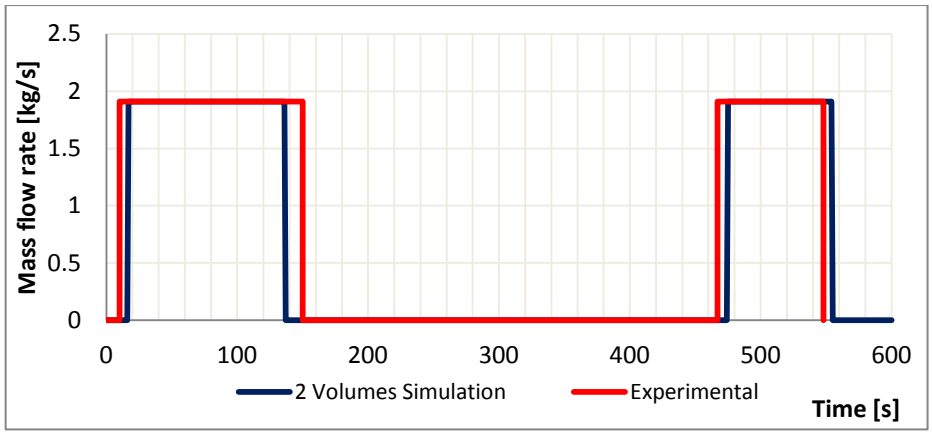

FIG. 4.36 Sprayers operations during 74 MW loss-of-load transient [kg/s vs. s]

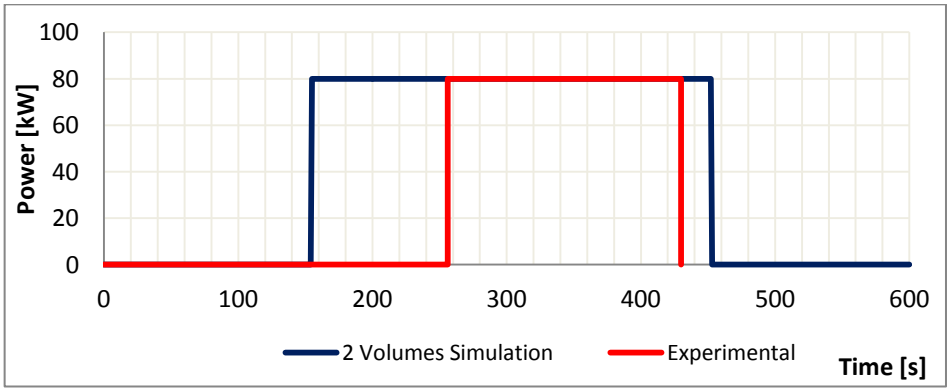

FIG. 4.37 Heaters operations during 105 MW loss-of-load transient [kW vs. s]

Taking into account temperature distribution across liquid region, two-regions-two-volumes model can be more accurate than the previous one. In this sense figure 4.28 and 4.29 are very meaningful. The first one depicts temperature distribution through the liquid volume: as you can see the temperature of upper water volume does not change very

much, instead, the lower layer temperature experiments big temperature variation due to insurges and outsurges transients. In particular, the temperature of lower liquid volume decreases during insurge because of the cold water incoming and increases during outsurges because the hot water of upper layer goes down to the bottom volume. It is very important that simulated temperature data, which, in the previous model, do not matches with the experimental ones, now are very similar to them.

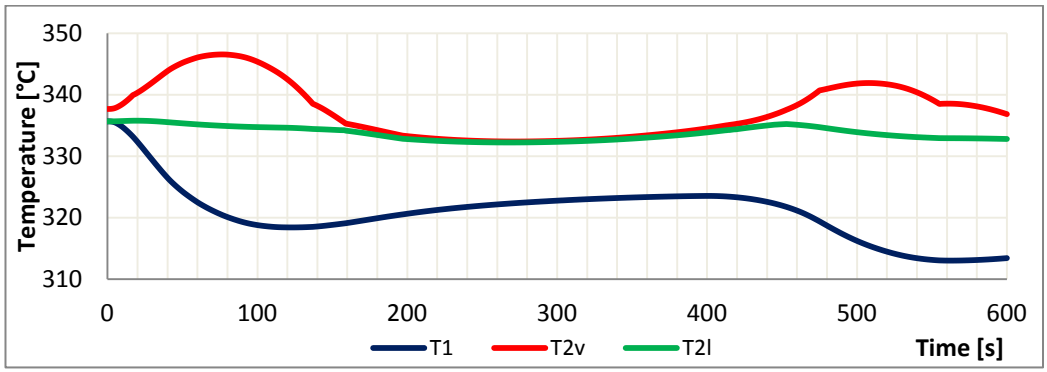

FIG. 4.38 Temperature distribution during 74 MW loss-of-load transient [°C vs. s]

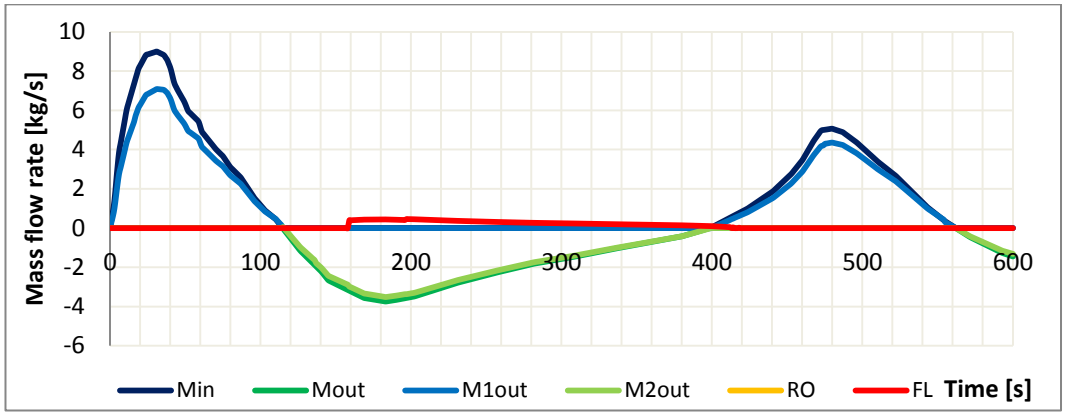

FIG. 4.39 Mass flow rates during 74 MW loss-of-load transient [kg/s vs. s]

The second figure, instead, shows the different mass flow rates inside the pressurizer; due to temperature difference along the pressurizer liquid volume, mass flow rates between volumes are not equal to the insurge or outsurge ones. This is an effect of changing density of water. In two-regions-one-volume model, flashing occurs slightly, and this is another cause of the sudden drop of the pressure, now this physical phenomenon takes place in agreement with experimental data, which show flashing happening respectively between 160:250 seconds for 74 MW transient and 120:200-570:600 seconds for 105 MW one. A big improvement can be seen also for control action, now only 80 kW heaters bank turns ON, moreover time intervals of control operations are now much more similar to the experimental ones.

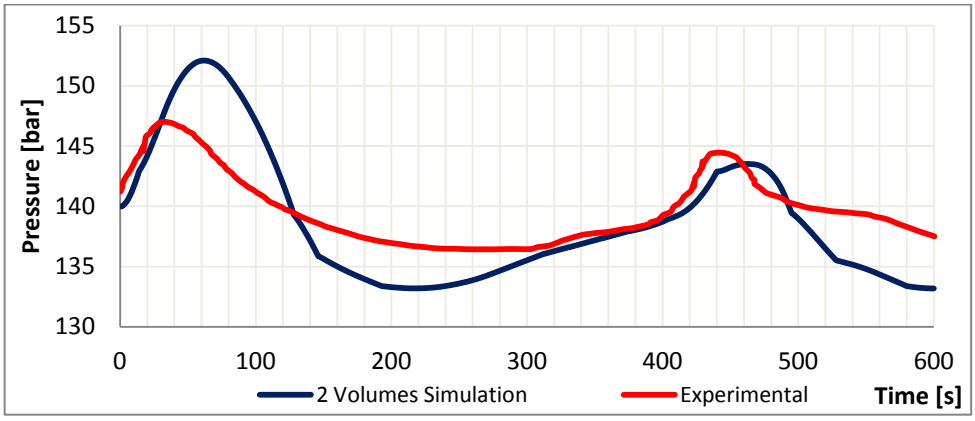

FIG. 4.40 Pressure variation during 105 MW loss-of-load transient [bar vs. s]

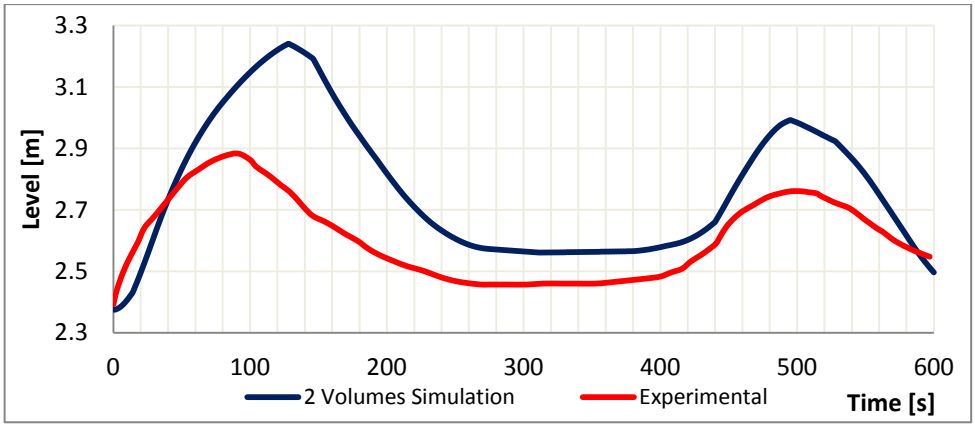

FIG. 4.41 Level variation during 105 MW loss-of-load transient [m vs. s]

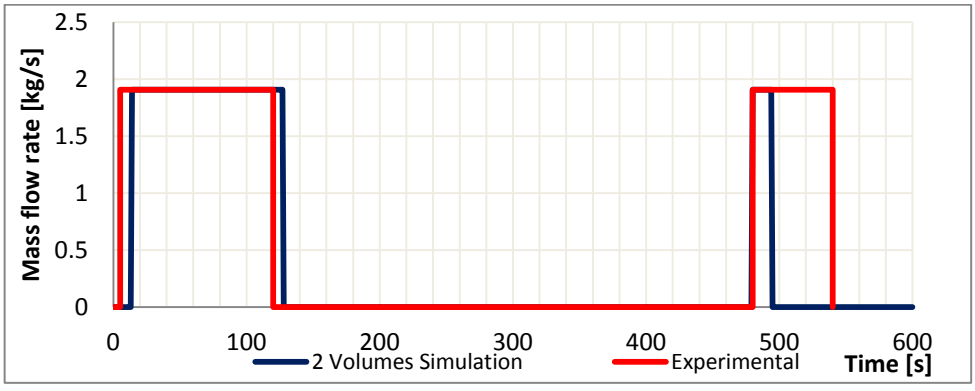

FIG. 4.42 Sprayers operations during 105 MW loss-of-load transient [kg/s vs. s]

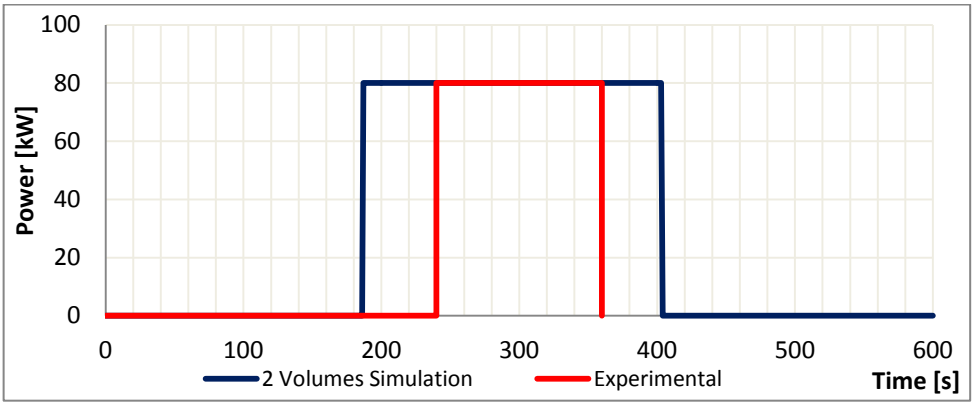

FIG. 4.43 Heaters operations during 105 MW loss-of-load transient [kW vs. s]

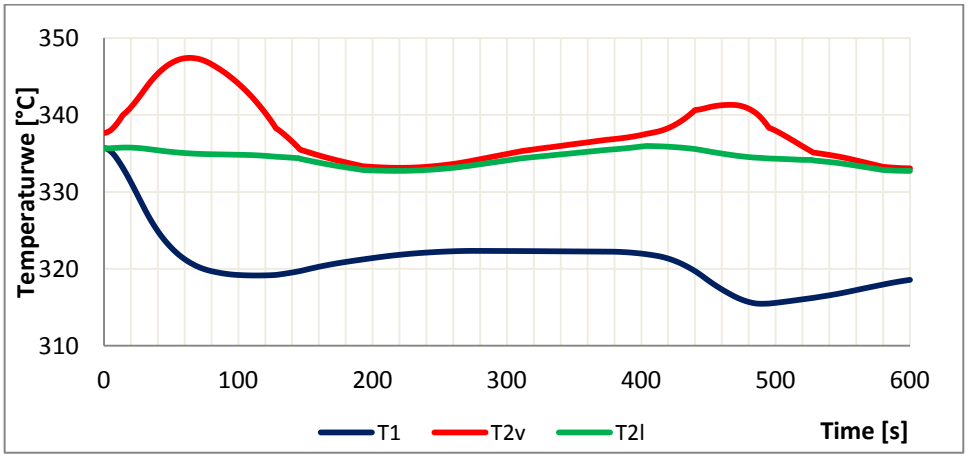

FIG. 4.44 Temperature distribution during 105 MW loss-of-load transient [kg/s vs. s]

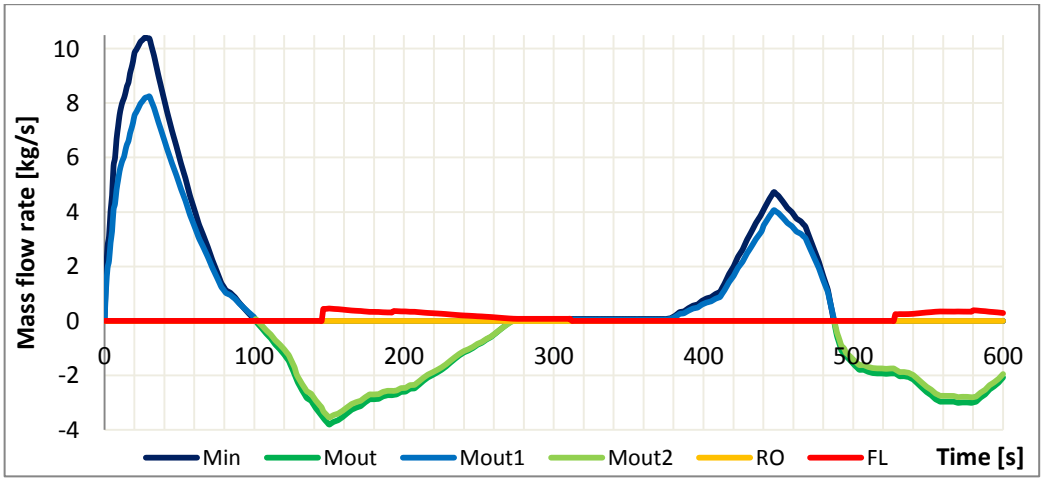

FIG. 4.45 Mass flow rates during 105 MW loss-of-load transient [kg/s vs. s]

Finally, the results of two-regions-three-volumes (with dynamic control) are presented. This model is an improvement of the previous one and can compute in a better way the temperature distribution across the liquid region. Now the pressure does not abruptly decrease during outsurge, this is a consequence of the small temperature variation of the top water layer. In this model, also the rainout mass flow rate comes into play. This physical process takes place also in RELAP5® simulations as you will see later on.

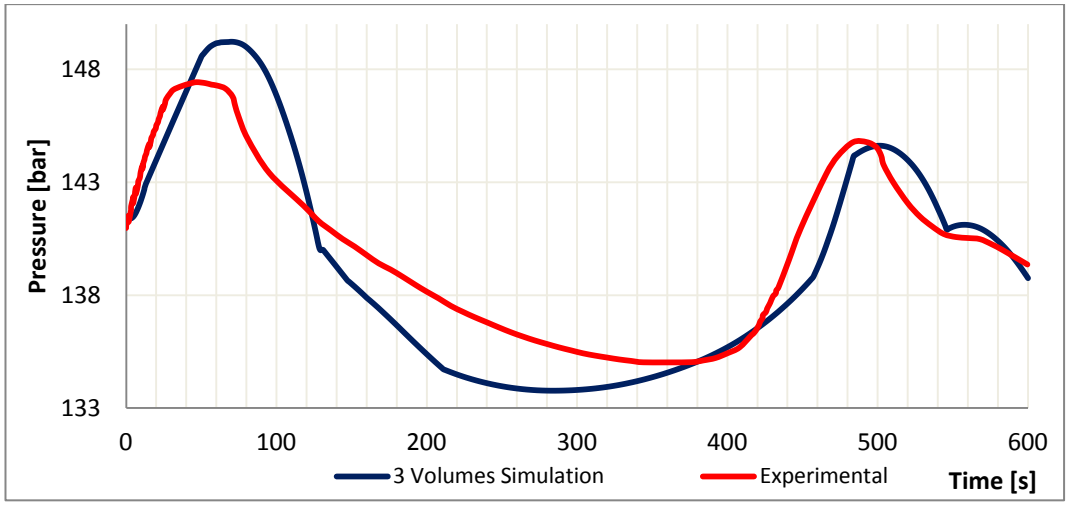

FIG. 4.46 Pressure variation during 74 MW loss-of-load transient [bar vs. s]

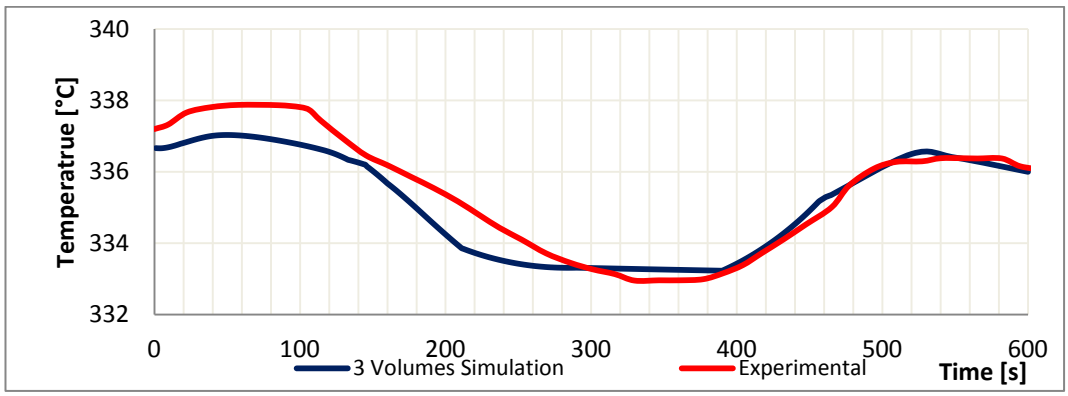

FIG. 4.47 Temperature variation during 74 MW loss-of-load transient [°C vs. s]

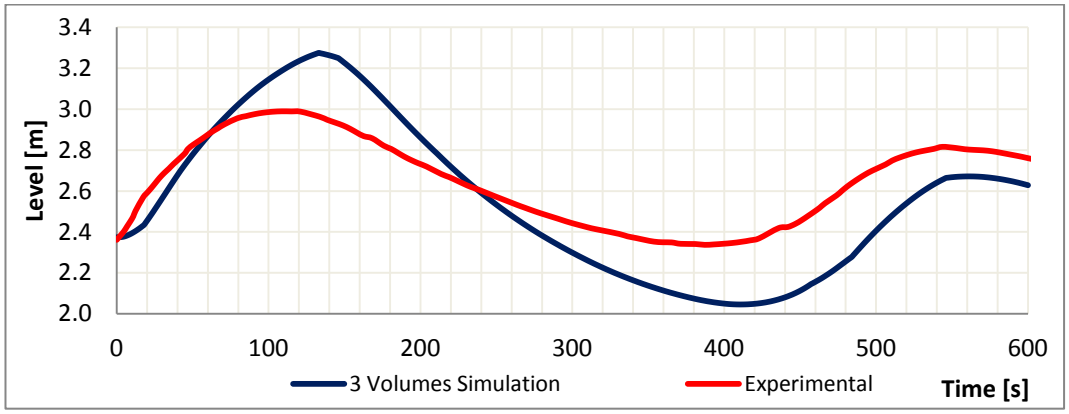

FIG. 4.48 Level variation during 74 MW loss-of-load transient [m vs. s]

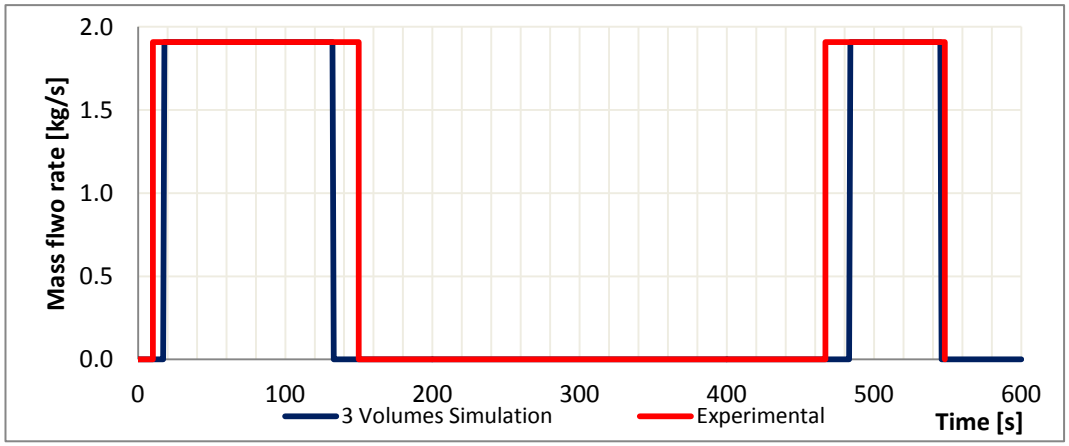

FIG. 4.49 Sprayers operations during 74 MW loss-of-load transient [kg/s vs. s]

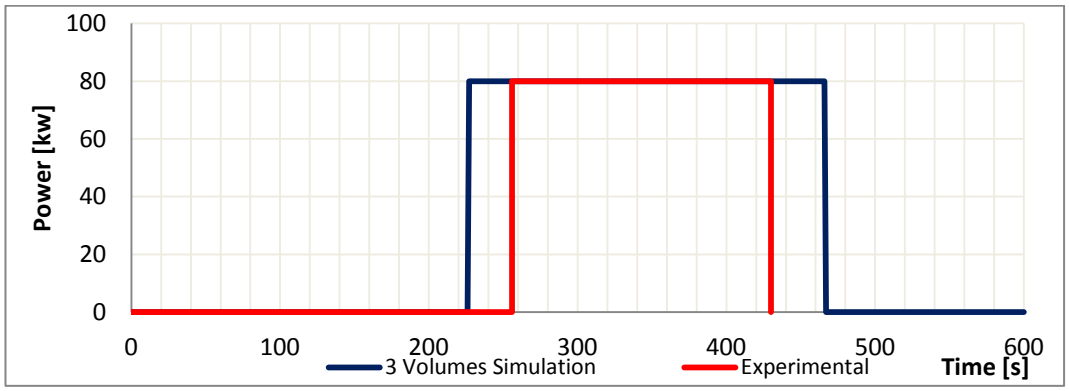

FIG. 4.50 Heaters operations during 74 MW loss-of-load transient [kW vs. s]

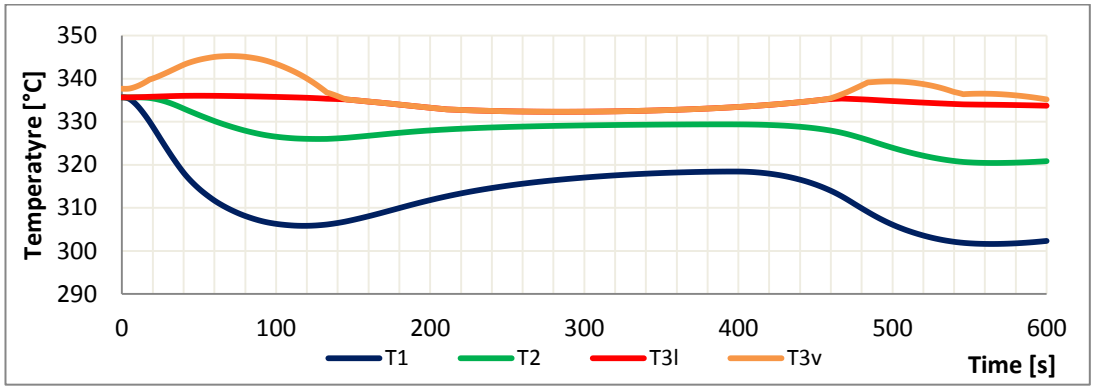

FIG. 4.51Temperature distribution during 105 MW loss-of-load transient [kg/s vs. s]

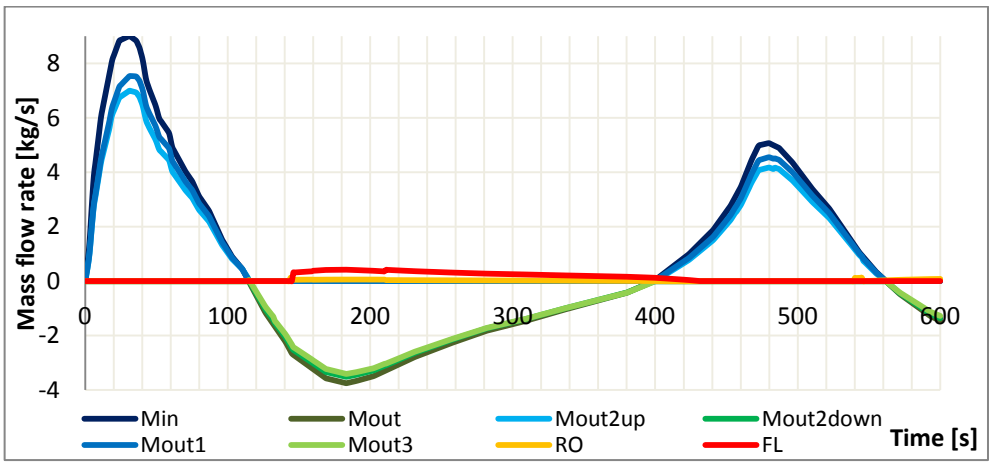

FIG. 4.52 Mass flow rates during 74 MW loss-of-load transient [kg/s vs. s]

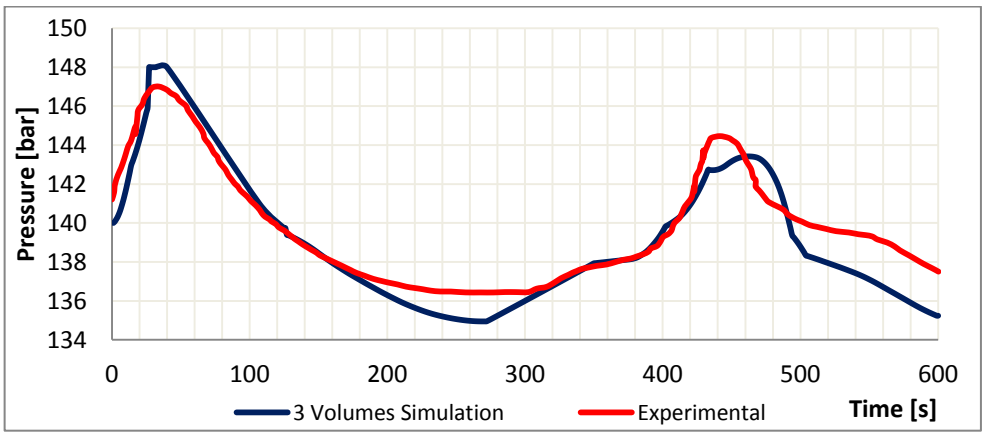

FIG. 4.53 Pressure variation during 105 MW loss-of-load transient [bar vs. s]

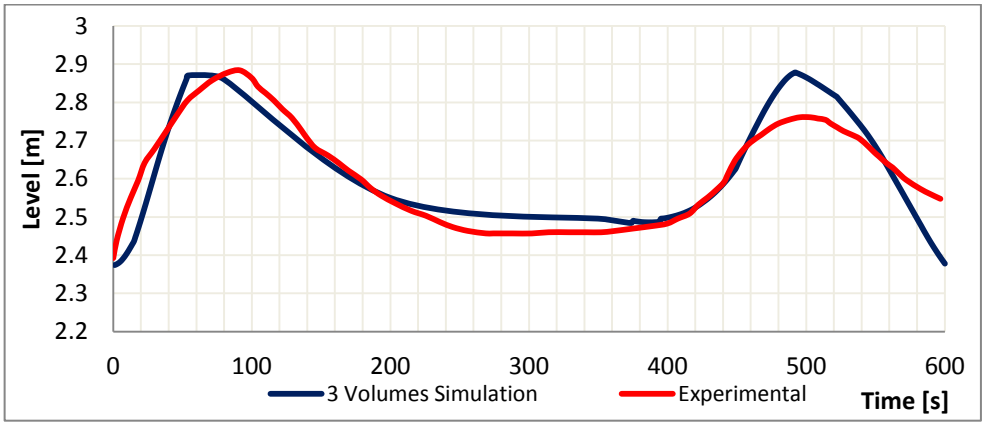

FIG. 4.54 Level variation during 105 MW loss-of-load transient [m vs. s]

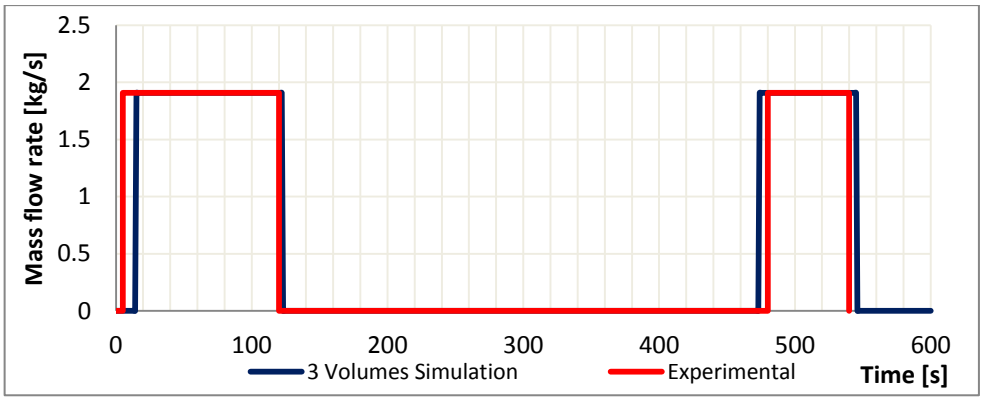

FIG. 4.55 Sprayers operations during 105 MW loss-of-load transient [kg/s vs. s]

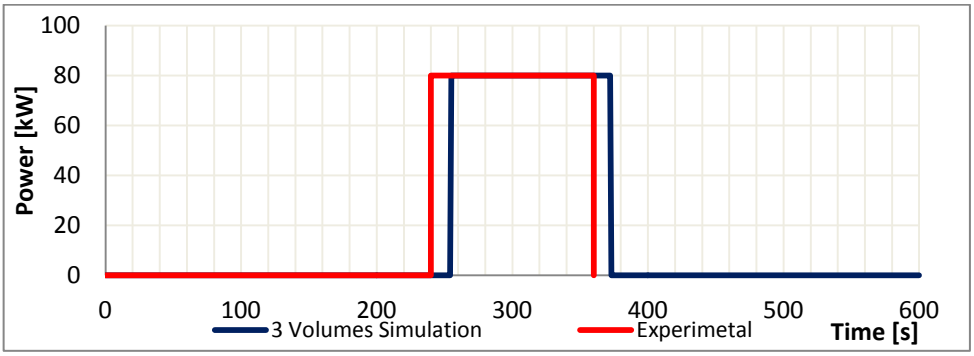

FIG. 4.56 Heaters operations during 105 MW loss-of-load transient [kW vs. s]

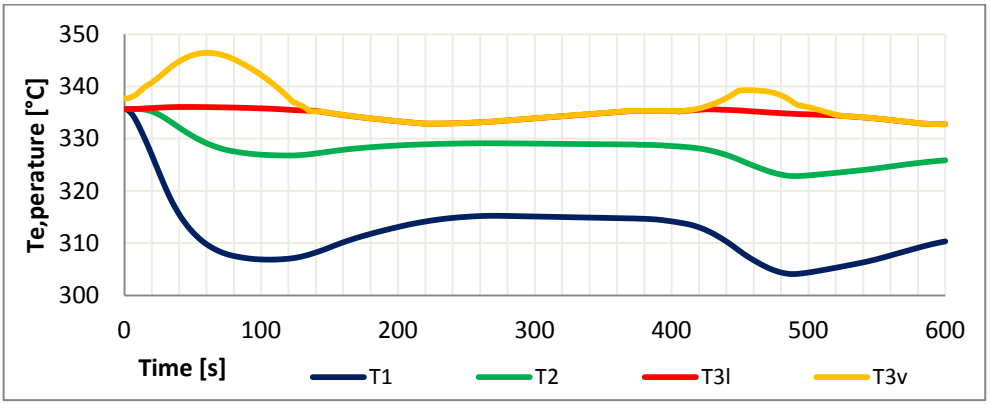

FIG. 4.57 Temperature distribution during 105 MW loss-of-load transient [°C vs. s]

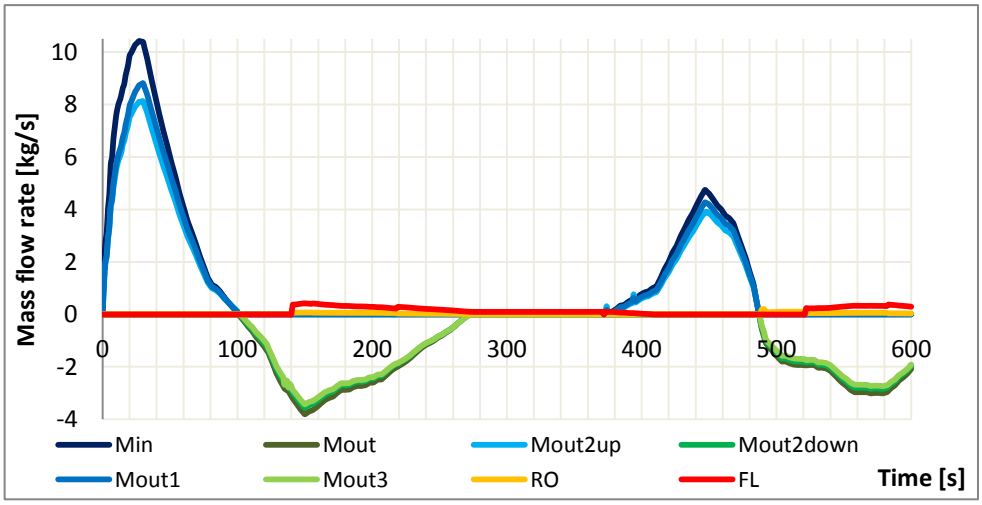

FIG. 4.58 Mass flow rates during 74 MW loss-of-load transient [kg/s vs. s]

All simulations have been run using different numerical solvers: fixed step methods as ODE- 1 (Euler) [27] and ODE-3 (Bogacki-Shampine) [29] and variable step ones as ODE-45 (Domand-Prince) [27] and ODE-15s [30]. To verify numerical stability of the simulation programs, during code verification, also time step for fixed step methods and absolute/relative tolerance for variable step ones have been changed.

For two-regions-one-volume model, fixed step integration gives results which are very similar to each other; instead, variable step integration fails.

In fact, as the mixing of pressurizer water with the insurge one is instantaneous in one volume model, the resulting temperature drop of liquid region is too pronounced and this causes a slightly flashing which occurs in series of discontinuous evaporation processes. Therefore a lot of oscillations between state 3[1] and state 4[2] occur.

In case of fixed step methods, the frequency of these oscillations is itself fixed. Instead, in case of variable step methods, at every jump the algorithm reduces the integration

[1] Satured vapour - subcooled water
[2] Satured vapour – subcooled water

interval, so time steps become smaller and smaller and the simulation does not proceed any more.
For two-regions-two-volumes and two-regions-three-volumes models fixed and variable step methods give almost the same results. Just little differences have been found, mostly in the computation time: ODE 1-5s is the fastest, due to the fact that the simulated transients are very stiff.
In the previous pages the results shown were obtained using ODE 1, i.e. the backward Euler integration method which is a very stable algorithm [27].
Sensitivity analysis results are shown in figures 4.44, 4.45, 4.46, 4.47, 4.48, 4.49, 4.50 for different models and different transients.

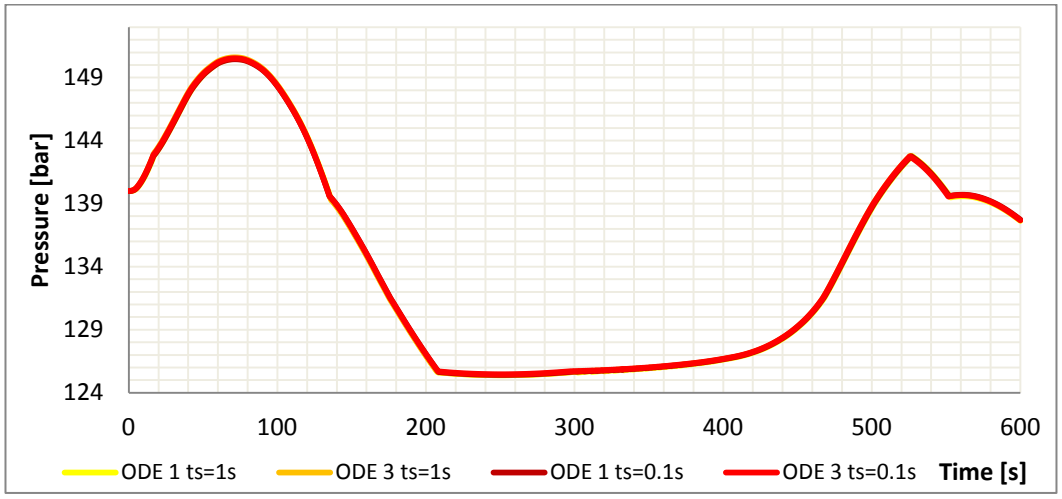

FIG. 4.59 Sensitivity analysis for single volume model during74 MW loss-of-load transient

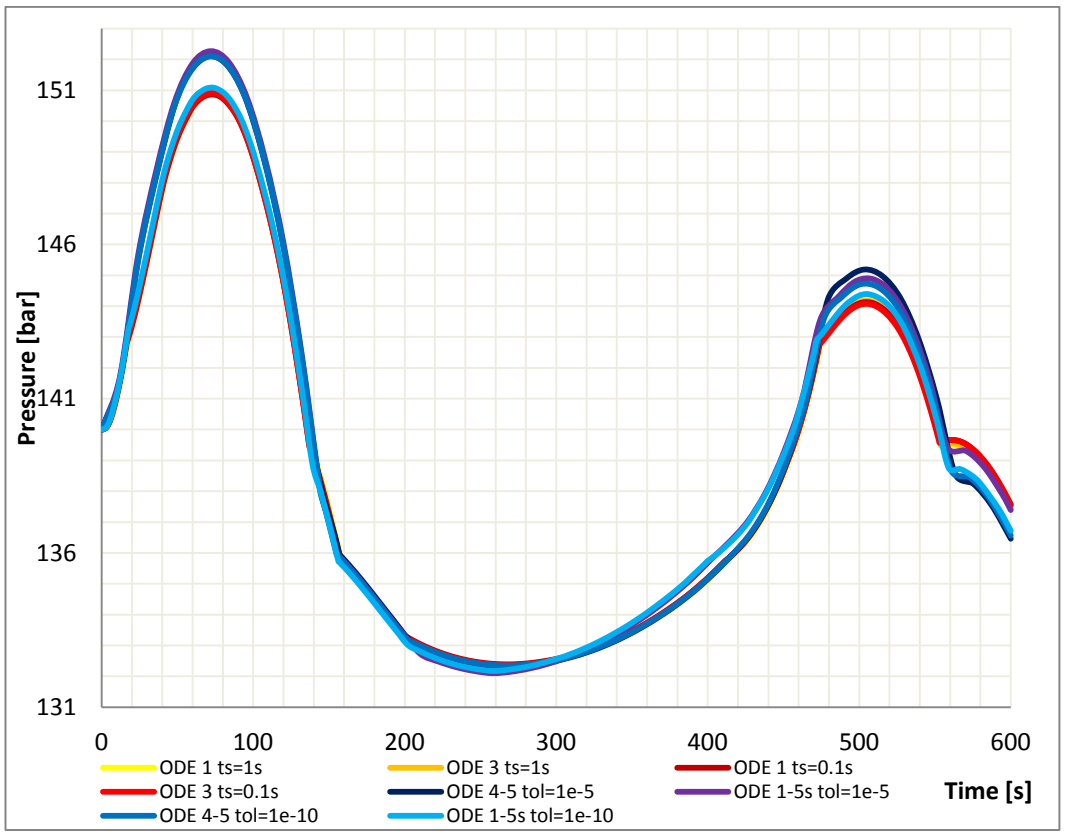

FIG. 4.60 Sensitivity analysis for 2 volumes model during 74 MW loss-of-load transient

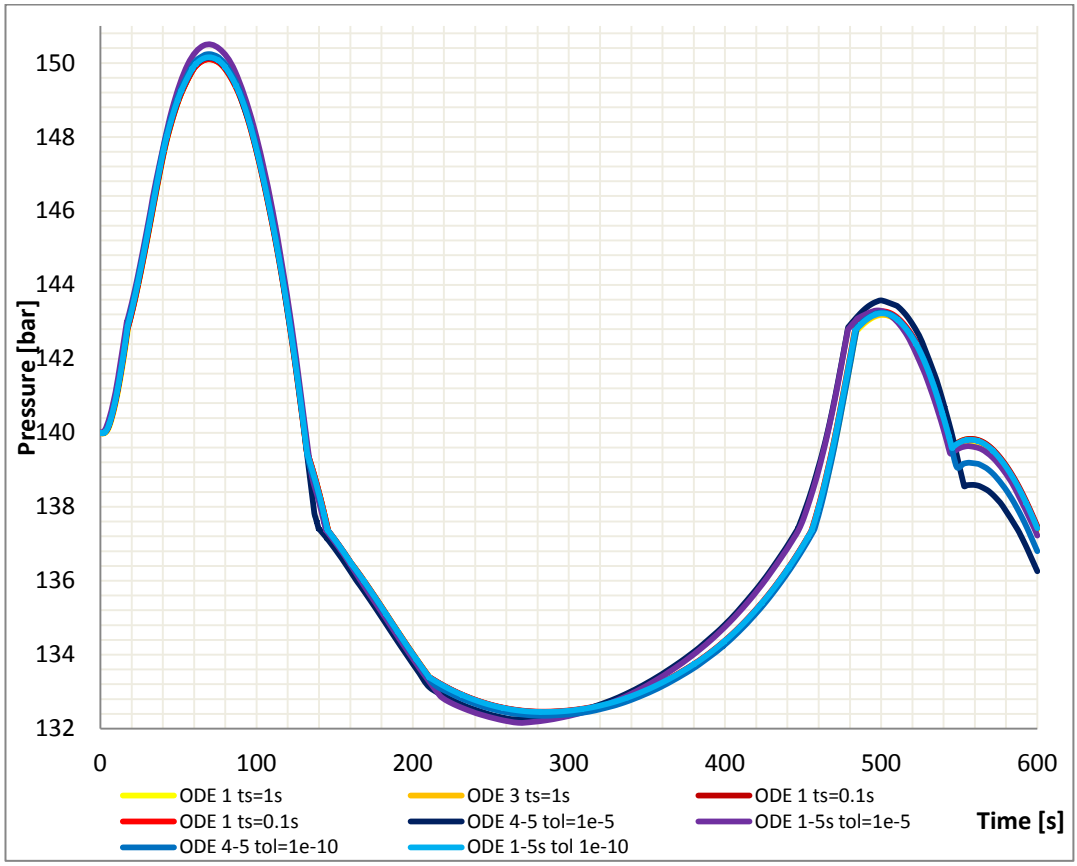

FIG. 4.61 Sensitivity analysis for 3 volumes model during 74 MW loss-of-load transient

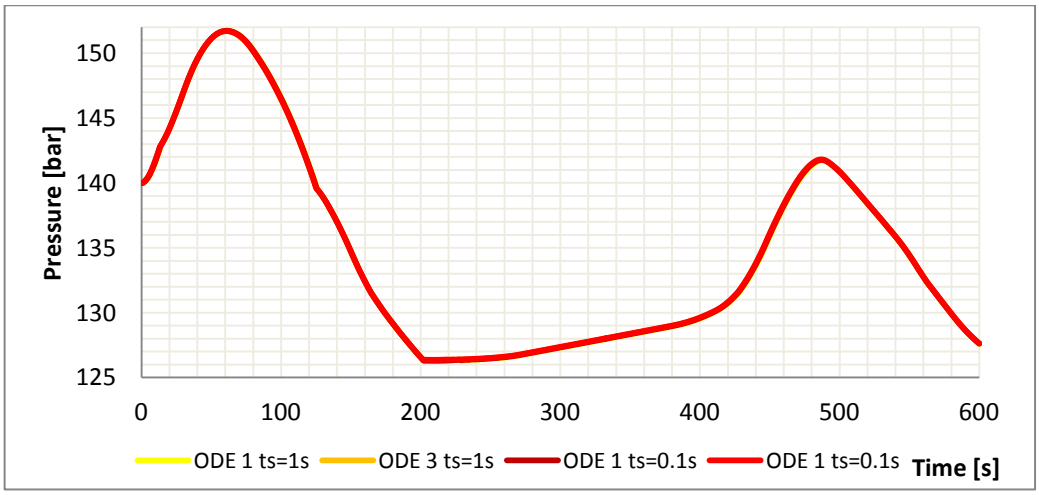

FIG. 4.62 Sensitivity analysis for 1 volume model during 105 MW loss-of-load transient

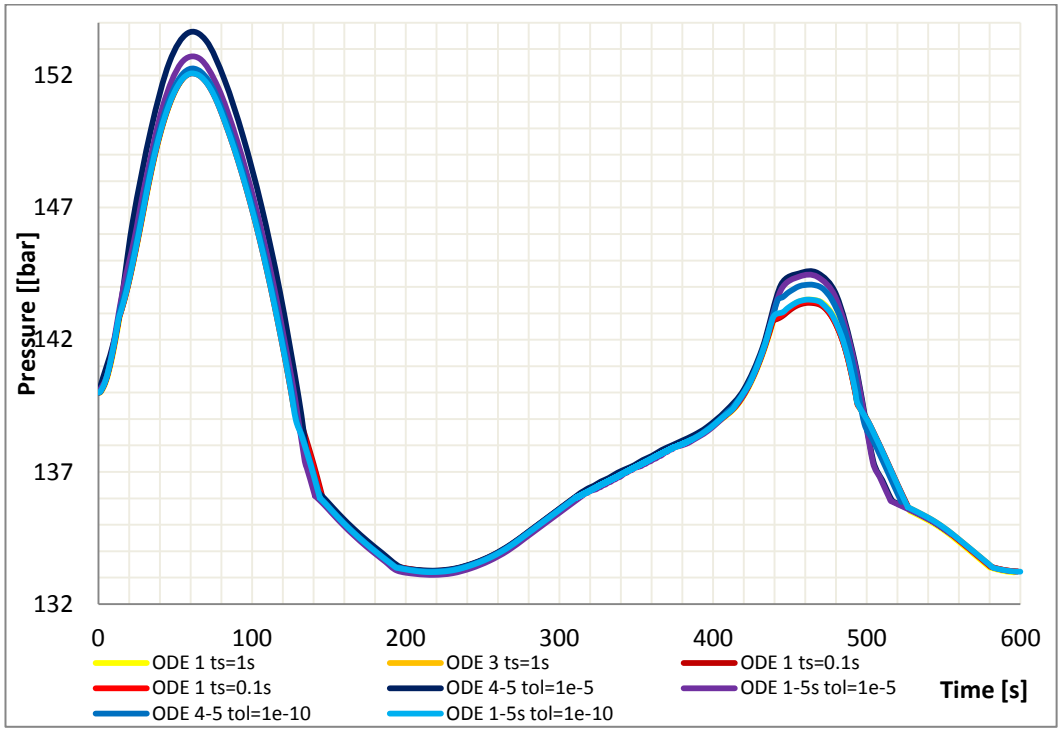

FIG. 4.63 Sensitivity analysis for 2 volumes model during 105 MW loss-of-load transient

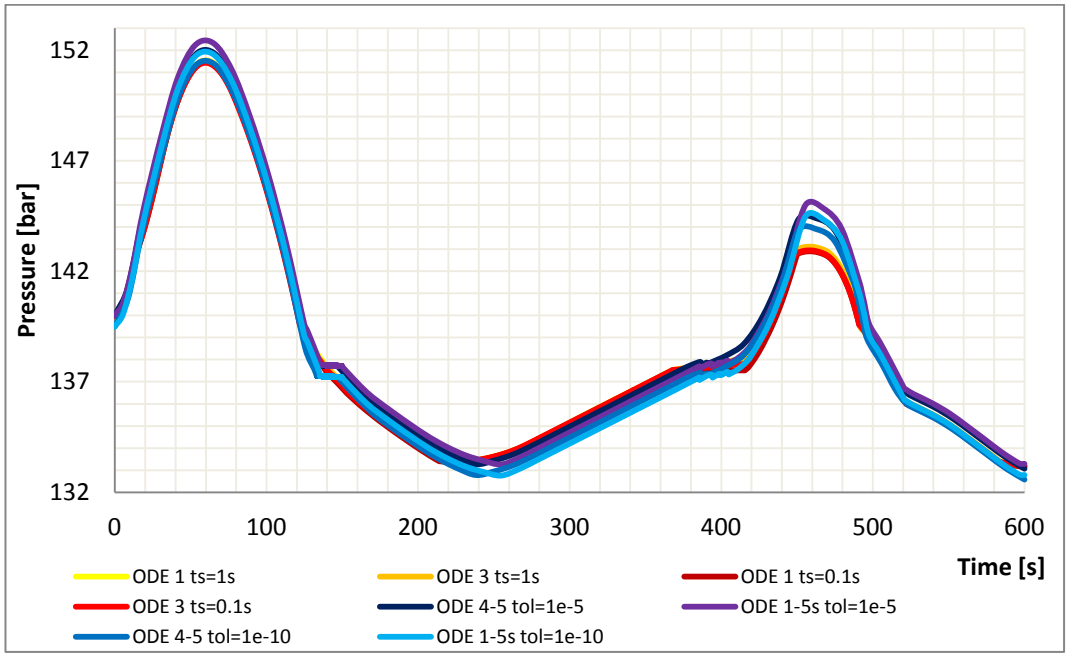

FIG. 4.64 Sensitivity analysis for 3 volumes model during 105 MW loss-of-load transient

4.5 DYMOLA® CONTROLLED-MODELS RESULTS

The pressurizer Dymola® model has been developed to evaluate acausal approach potentialities. The results of these models substantially agree with Simulink® ones. Two-regions-one-volume model with dynamic control presents the usual problems due to the excessive cooling of water temperature. Two-regions-two-volume and two-regions-three-volume controlled-models give better results. The used integration method was Euler.

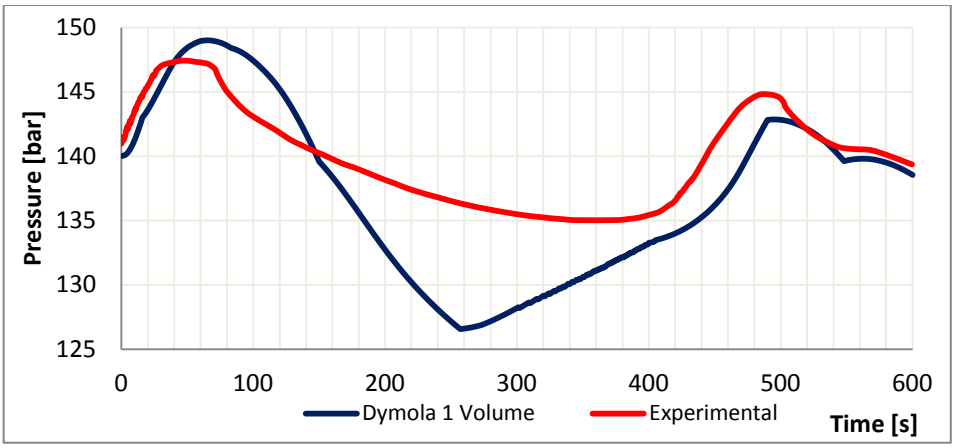

FIG. 4.65 Pressure variation during 74 MW loss-of-load transient [bar vs. s]

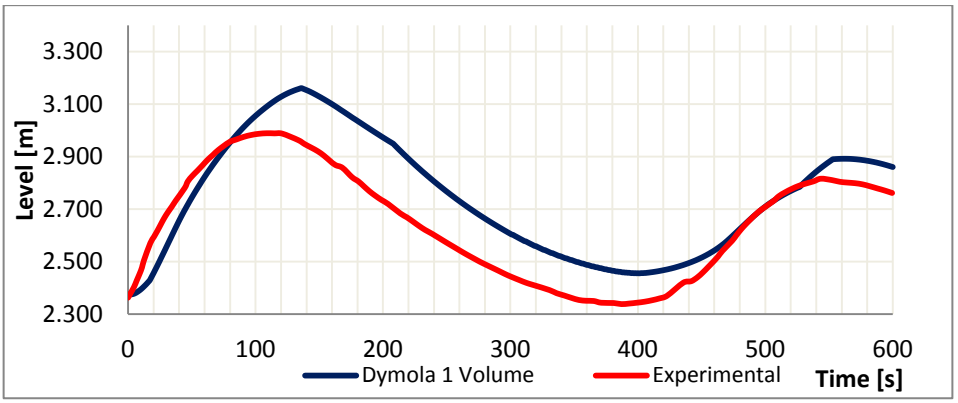

FIG. 4.66 Level variation during 74 MW loss-of-load transient [m vs. s]

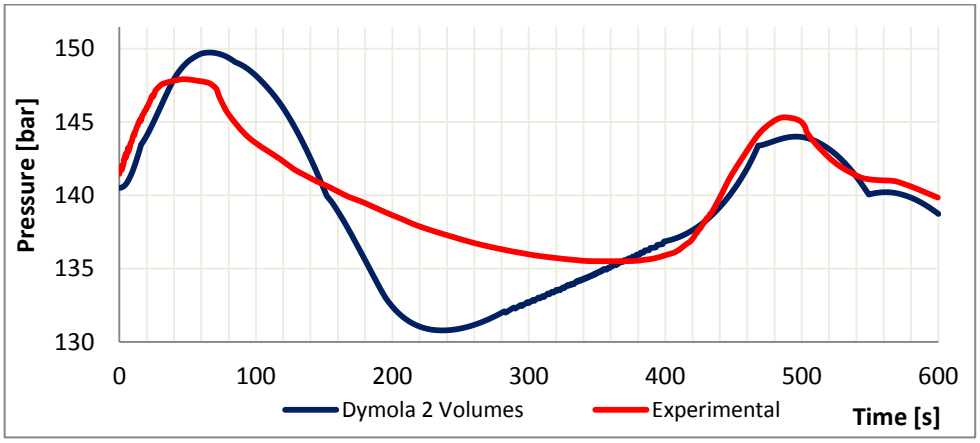

FIG. 4.67 Pressure variation during 74 MW loss-of-load transient [bar vs. s]

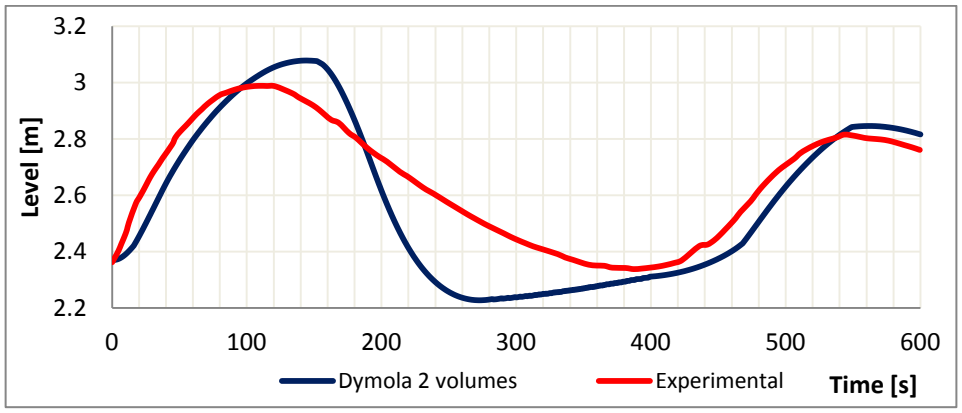

FIG. 4.68 Level variation during 74 MW loss-of-load transient [m vs. s]

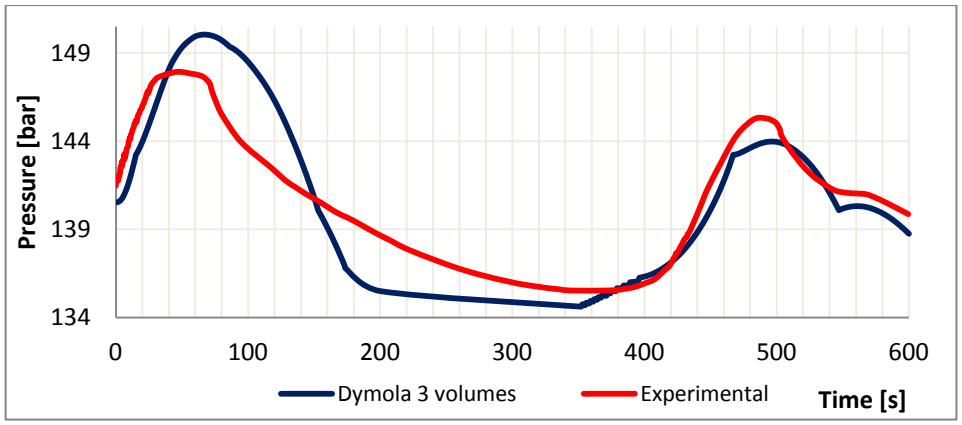

FIG. 4.69 Pressure variation during 74 MW loss-of-load transient [bar vs. s]

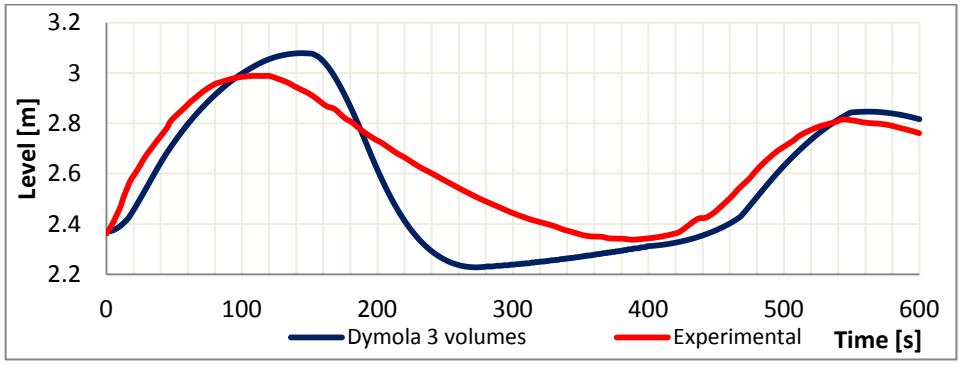

FIG. 4.70 Level variation during 74 MW loss-of-load transient [m vs. s]

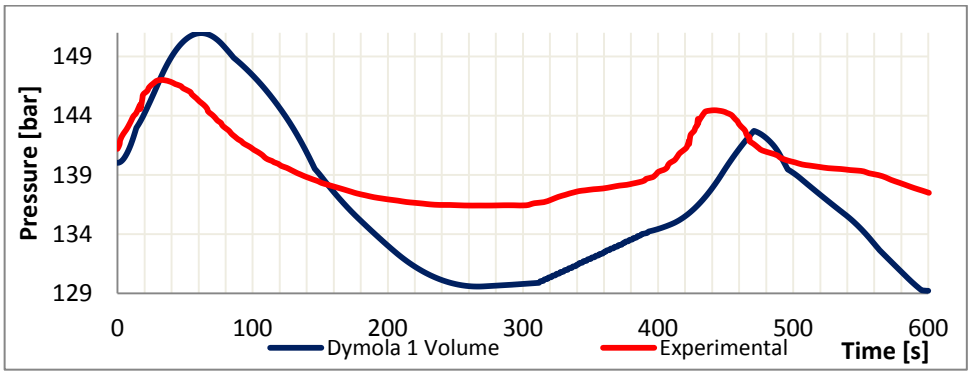

FIG. 4.71 Pressure variation during 105 MW loss-of-load transient [bar vs. s]

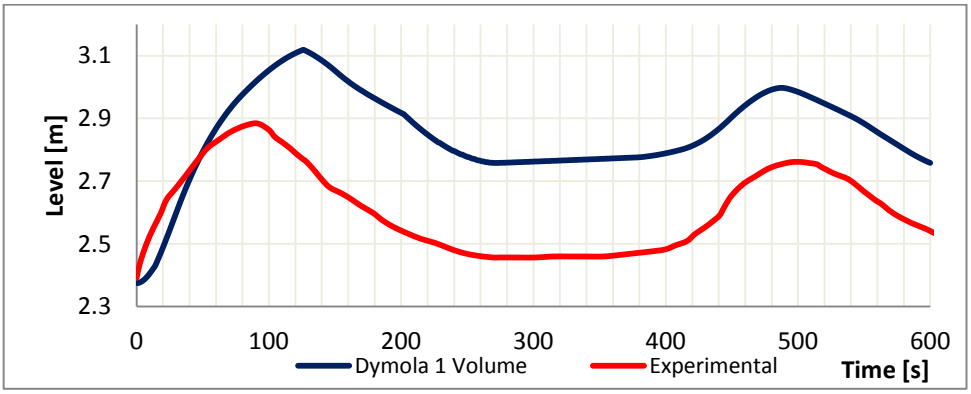

FIG. 4.72 Level variation during 105 MW loss-of-load transient [m vs. s]

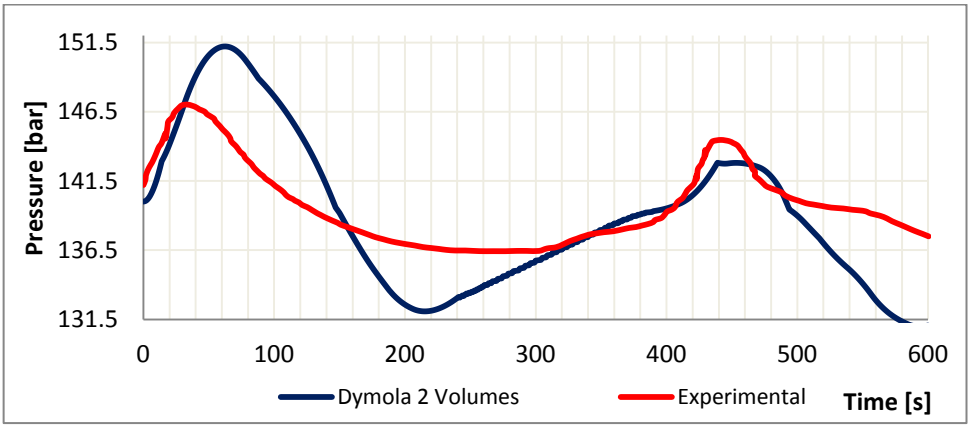

FIG. 4.73 Pressure variation during 105 MW loss-of-load transient [bar vs. s]

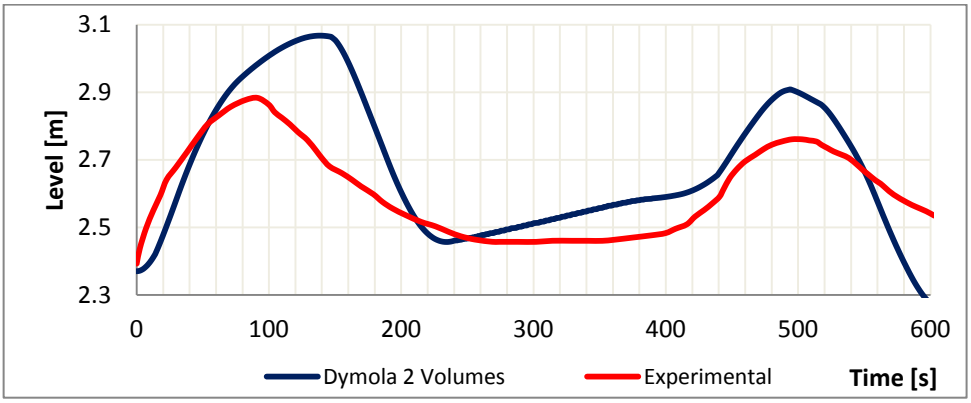

FIG. 4.74 Level variation during 105 MW loss-of-load transient [m vs. s]

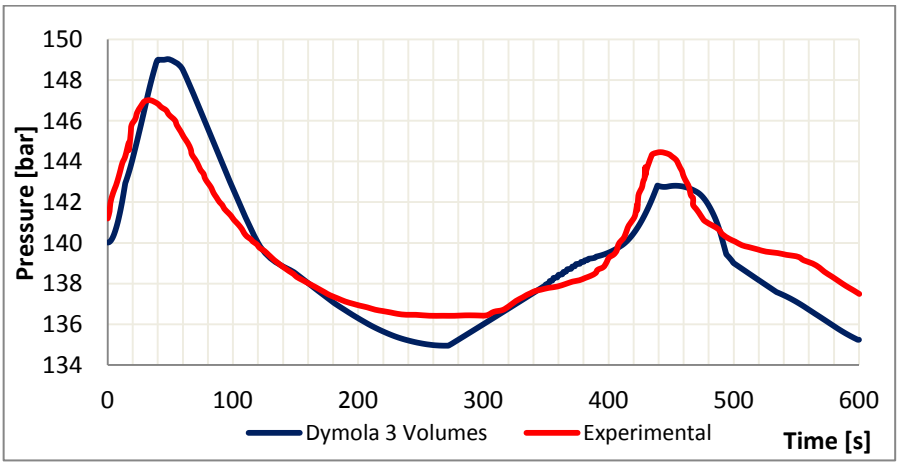

FIG. 4.75 Pressure variation during 105 MW loss-of-load transient [bar vs. s]

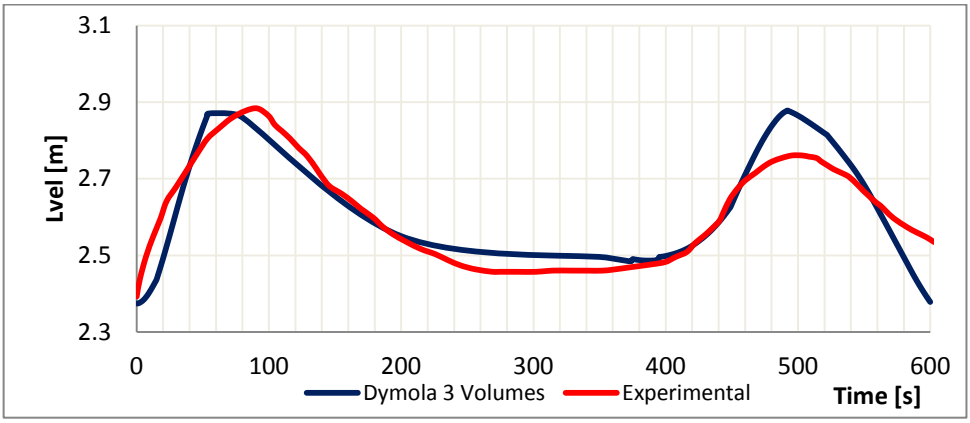

FIG. 4.76 Level variation during 105 MW loss-of-load transient [m vs. s]

Sensitivity analysis has been executed, as for the Simulink®, using different integration algorithm: in particular ODE 1 and ODE 3 (fixed step method) and DASSL [31] and RADAU [32] (variable step method). Small differences have been encountered between different numerical solvers. For one-volume models the same oscillation problem remains as already seen in Simulink®.

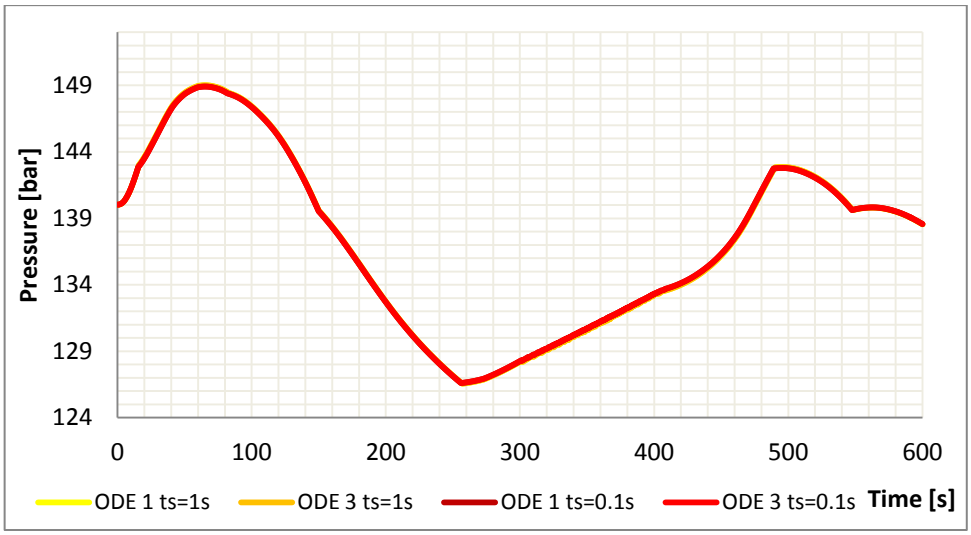

FIG. 4.77 Sensitivity analysis for 1 volume model during 74 MW loss-of-load transient

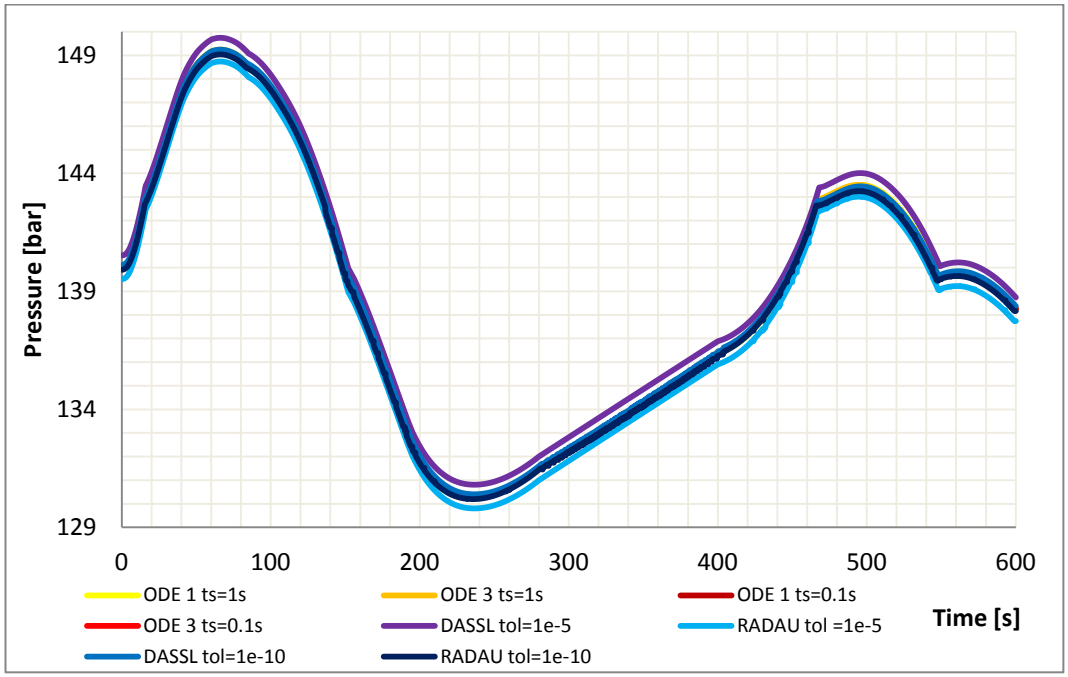

FIG. 4.78 Sensitivity analysis for 2 volumes model during 74 MW loss-of-load transient

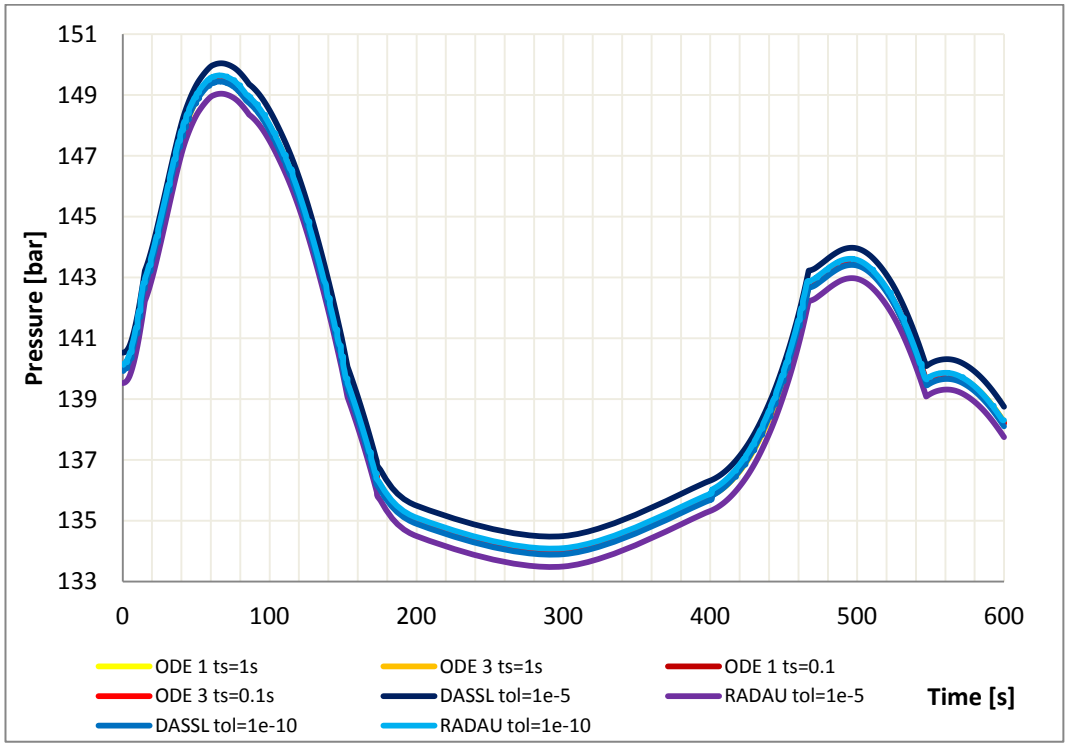

FIG. 4.79 Sensitivity analysis for 3 volumes model during 74 MW loss-of-load transient

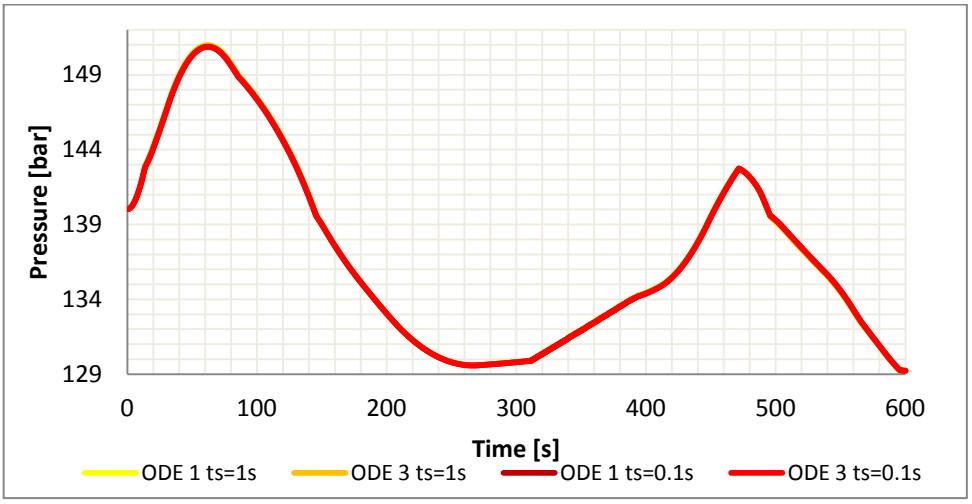

FIG. 4.80 Sensitivity analysis for 1 volume model during 105 MW loss-of-load transient

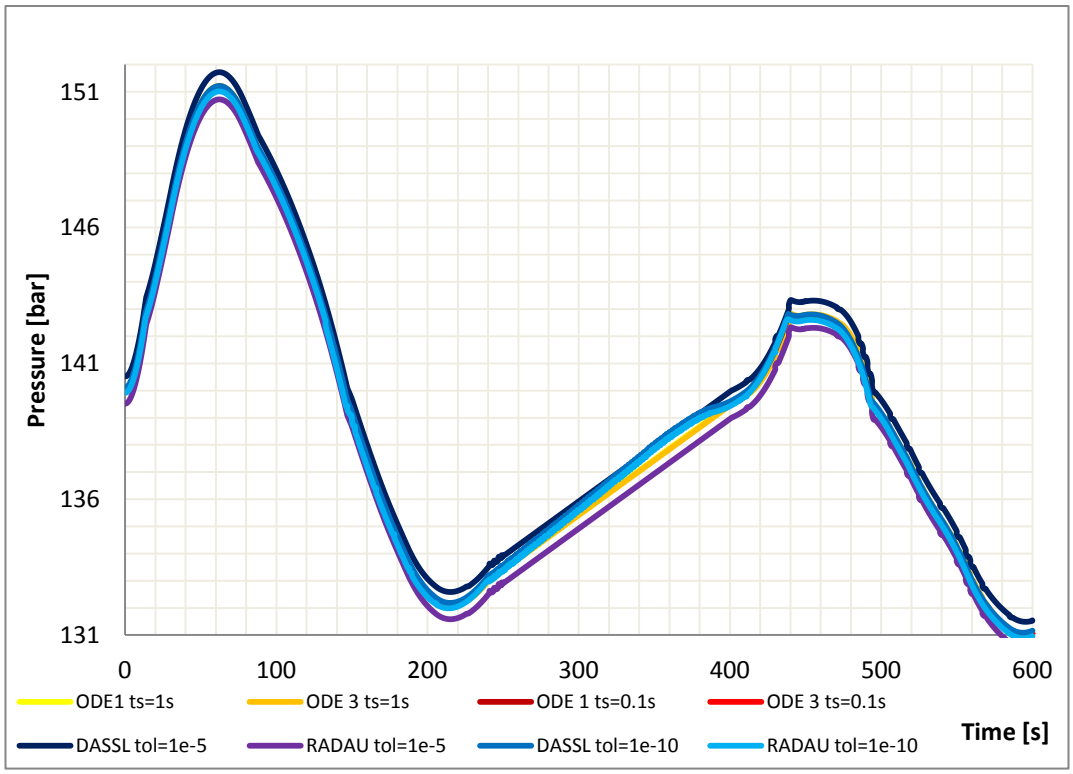

FIG. 4.81 Sensitivity analysis for 2 volumes model during 105 MW loss-of-load transient

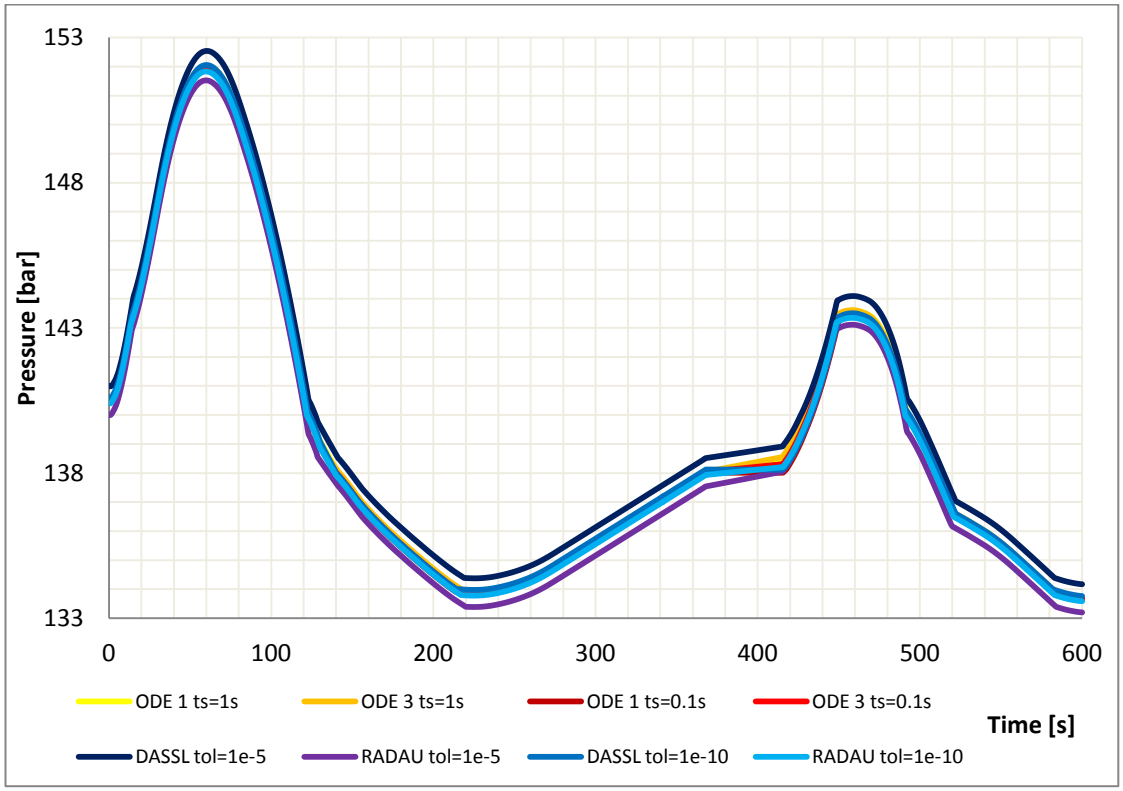

FIG. 4.82 Sensitivity analysis for 3 volumes model during 105 MW loss-of-load transient

4.6 RELAP5® CONTROLLED-MODELS RESULTS

RELAP5® model has been developed for the subsequent reasons:

- To demonstrate that a more simple approach, i.e. Simulink® and Dymola® programs, can reach results very similar to those of more complex "system codes"
- To confirm, in absence of experimental data, the temperature distribution hypothesis on which Simulink® and Dymola® two and three volumes models are based.

Basic RELAP5® model contemplates the subdivision of the pressurizer volume into 8 control volumes: however, to evaluate numerical stability of the code, also 16, 32 and 64 volumes meshes have been tested. In this section, firstly, the results of RELAP5® 8 volumes controlled-model will be compared to the experimental ones, then code to code comparison will follow. Free-dynamics and controlled-dynamics RELAP5® substantially give the same results. This fact points out that the Redfiled, Prescop and Margolis' data are quite reliable.

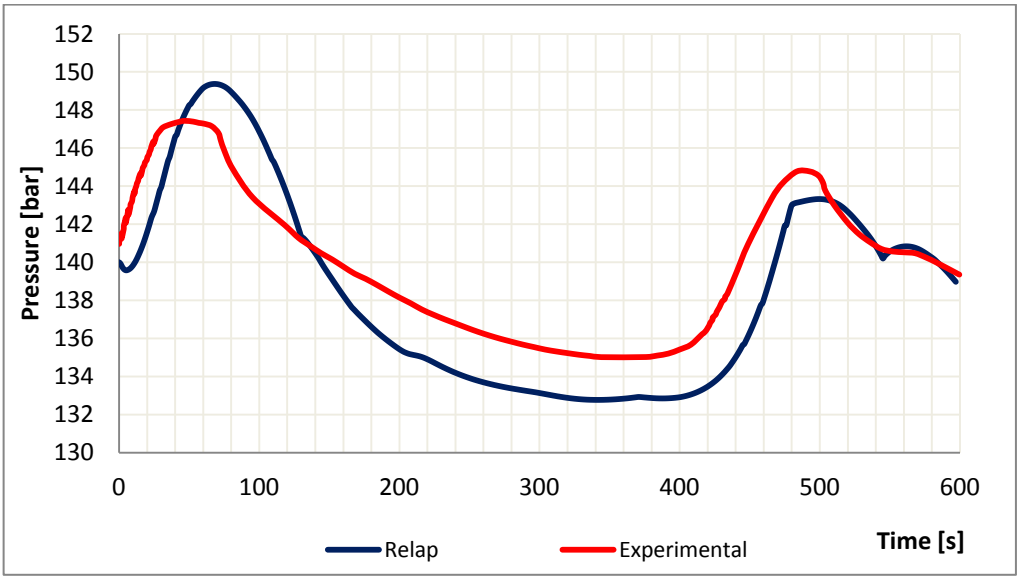

FIG. 4.83 Pressure variation during 74 MW loss-of-load transient [bar vs. s]

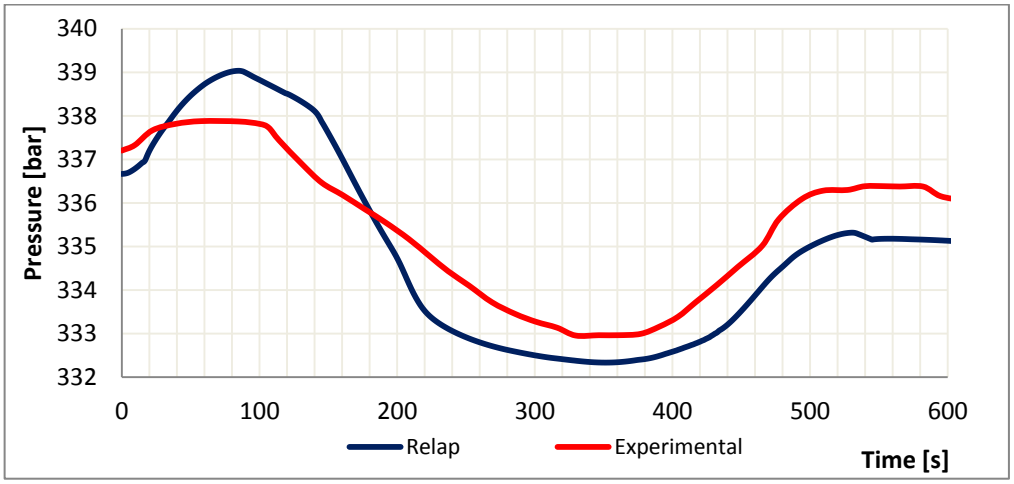

FIG. 4.84 Temperature variation during 74 MW loss-of-load transient [°C vs. s]

Pressure graph confirms the high capacities of RELAP5® code, but the temperature one is even more interesting: in it experimental temperature data (at 1.422 m with respect the pressurizer bottom) and the RELAP5® ones (taken from the corresponding volume) are put together. Simulated temperature are very similar to the real ones. Therefore the subsequent graph is highly meaningful representing temperature distribution through the pressurizer liquid region:

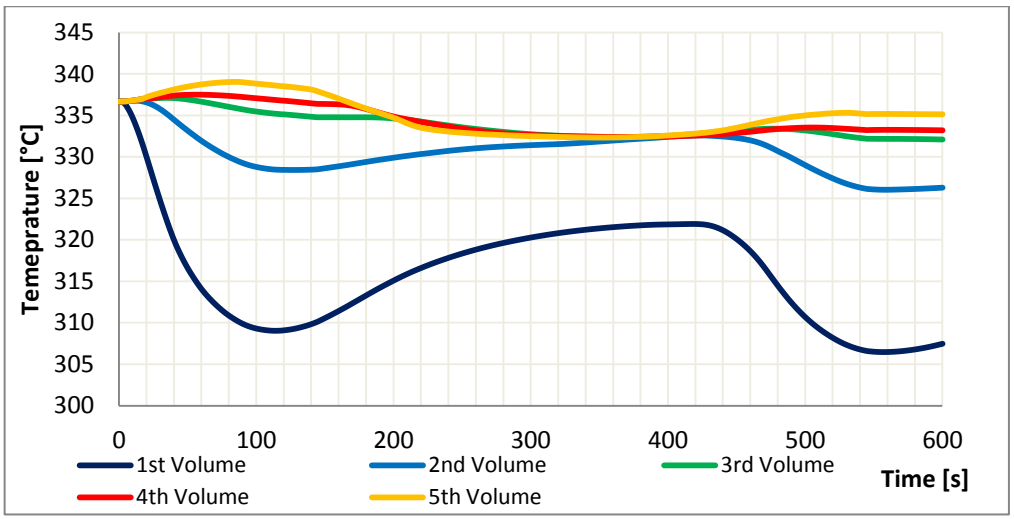

FIG. 4.85 Temperature distribution during 74 MW loss-of-load transient [°C vs. s]

These data confirm Simulink® and Dymola® 3 volumes models results showing the temperature distribution inside the pressurizer especially for the first two volumes. The comparison between Simulink® and Dymola® and RELAP5® results confirms the goodness of the first ones:

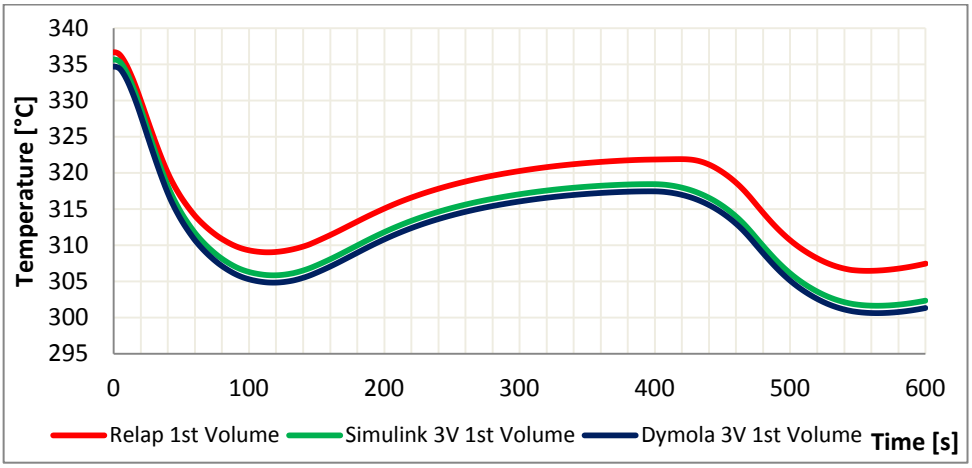

FIG. 4.86 Temperature distribution inside 1st volume during 74MWloss-of-load transient[°C vs. s]

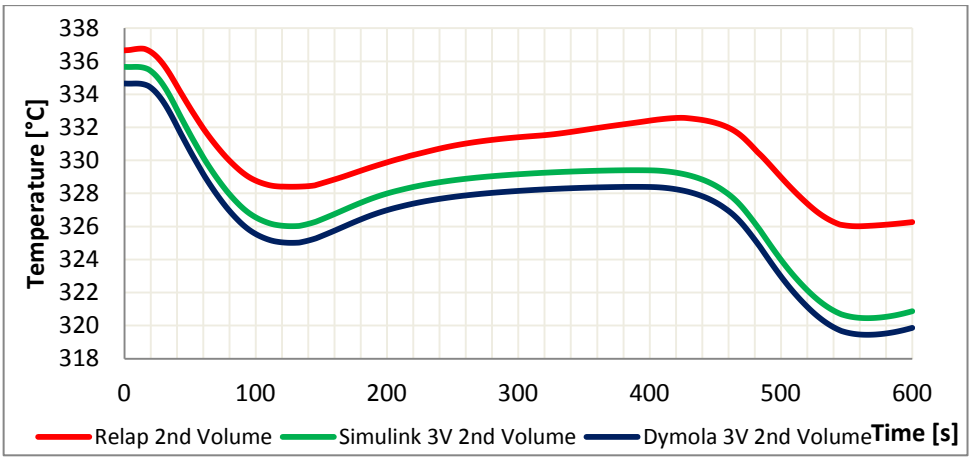

FIG. 4.87 Temperature distribution inside 2nd volume during 74MW loss-of-load transient[°C vs.s]

As you can see, both first and second volume temperatures of Simulink® and Dymola® model are very similar to the RELAP5® one. In fact first and second volumes of Simulink®and Dymola® models are essentially based on the RELAP5® control volume philosophy. For the third volume temperature distributions of Simulink® and Dymola® there are some differences with respect to the RELAP5® ones, due to the fact that third Simulink® and Dymola® volume compresses almost four RELAP5® ones.

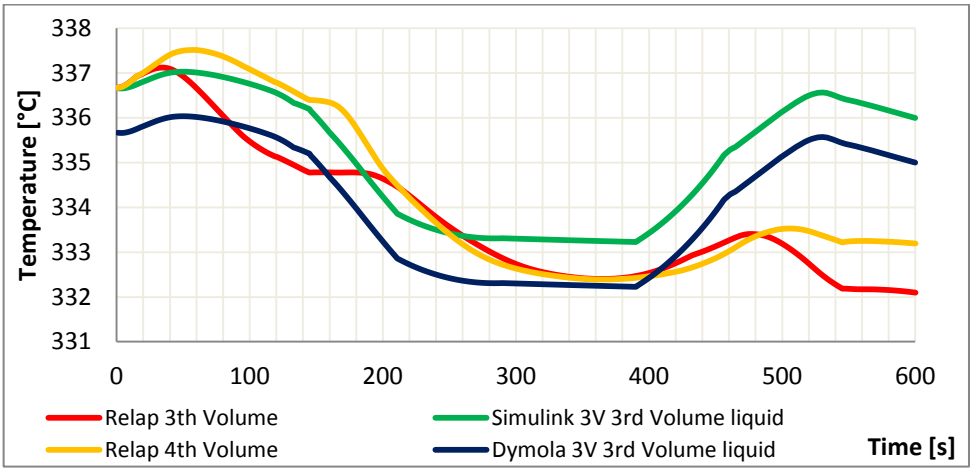

FIG. 4.88 Temperature distribution inside 3rd volume during 74MWloss-of-load transient[°C vs. s]

The degree of agreement between the three model is attested also by the pressure result comparison: Simulink®, Dymola® and RELAP5® are very similar to each other and trace enough the experimental data.

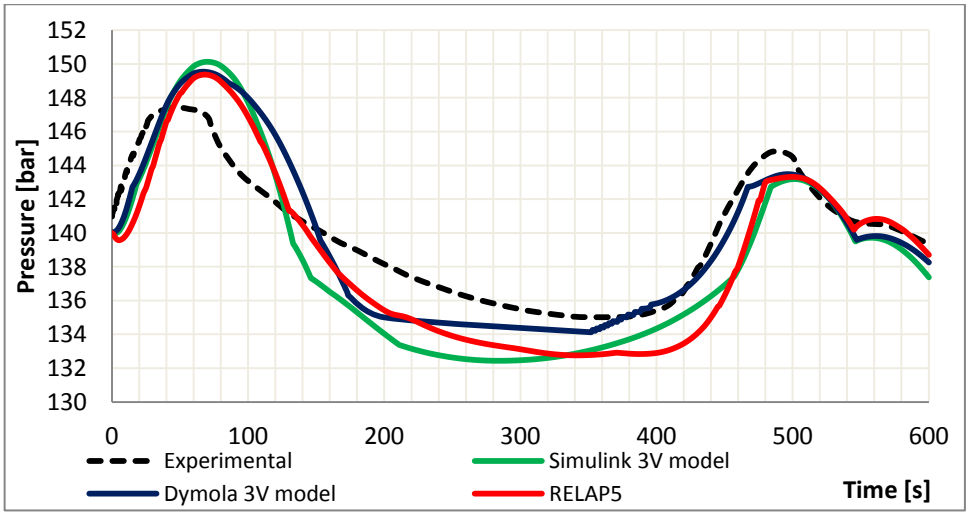

FIG. 4.89 Pressure results comparison for 74 MW loss-of-load transient [bar vs. s]

Also mass flux rates of Simulink® and Dymola® models are confirmed by the RELAP5® ones. Finally the verification of RELAP5® results is given by a comparison between different meshes:

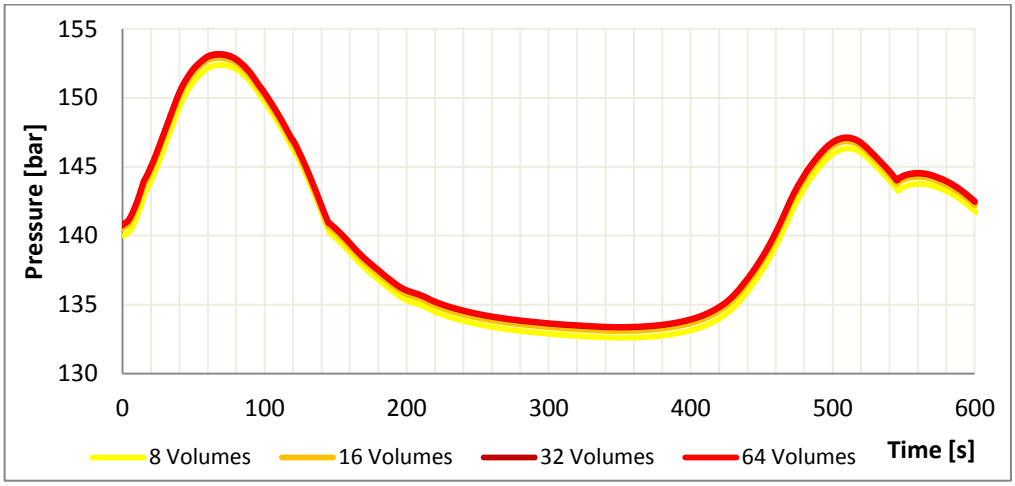

FIG. 4.90 Different mashes for Pressure 74 MW loss-of-load transient [°C vs. s]

Different meshes results are quite similar to each other, of course increasing the number of volumes the simulation becomes more precise, but the computational cost increases rapidly. No differences between semi-explicit (the RELAP5® default routine) and the completely implicit integration method [28], which is the least numerically diffusive, have been pointed out.

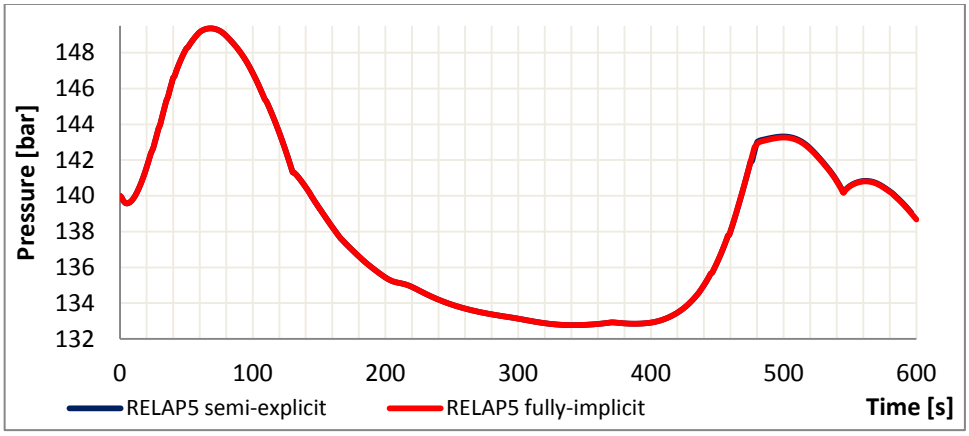

FIG. 4.91 Different numerical methods for Pressure 74 MW loss-of-load transient [°C vs. s]

RELAP5® simulation results of 105 MW loss-of-load transient confirms all the 74 MW one carried out observations.

FIG. 4.92 Pressure variation during 105 MW loss-of-load transient [bar vs. s]

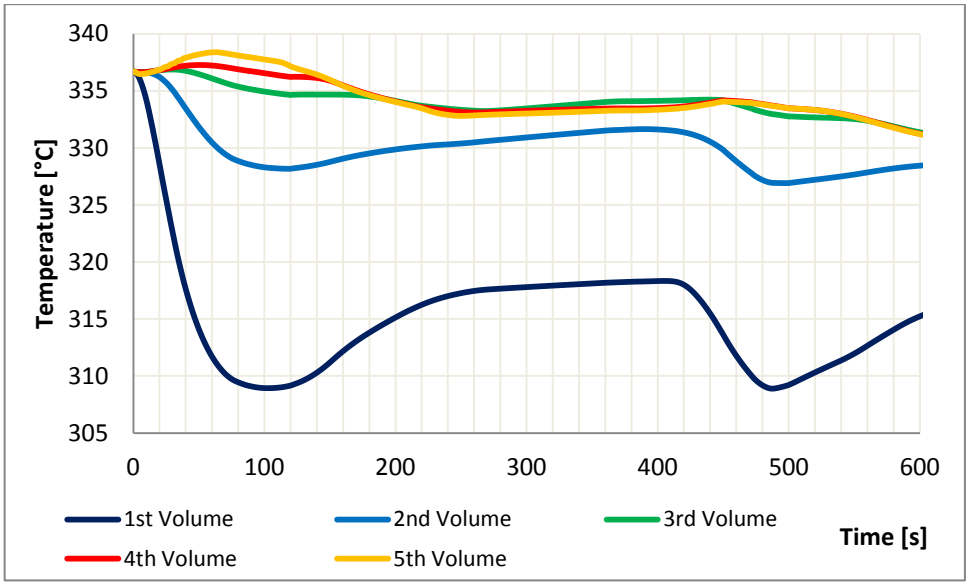

FIG. 4.93 Temperature distribution during 105 MW loss-of-load transient [°C vs. s]

It must be remembered that experimental temperature data for 105 MW loss-of-load transient were not available to the author. So the comparison takes place only between Relap®, Simulink® and Dymola® results.

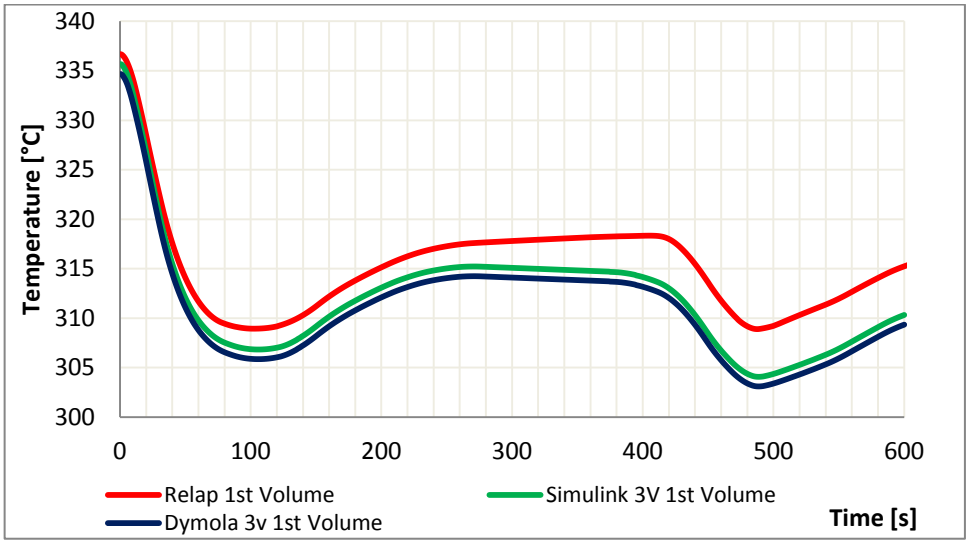

FIG. 4.94 Temperature distribution inside 1st volume during 105 MW loss-of-load transient[°C vs. s]

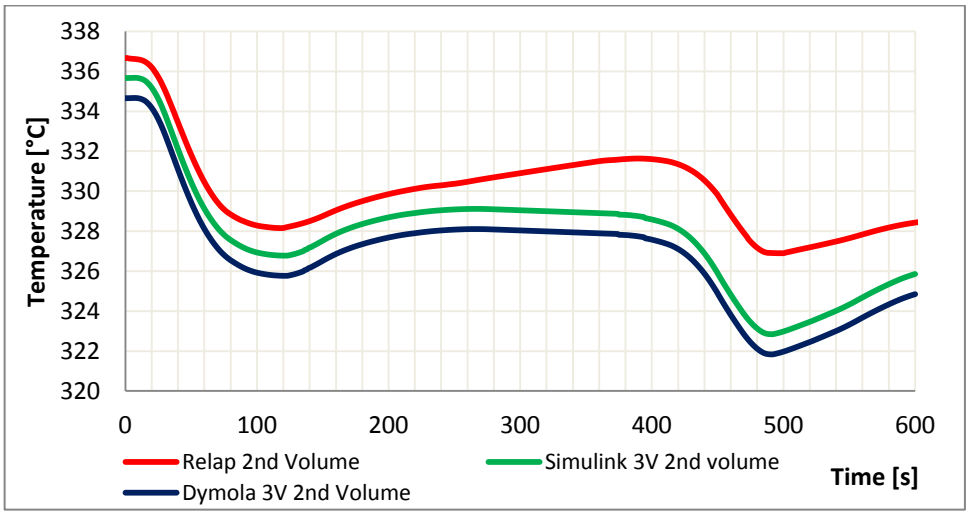

FIG. 4.95 Temperature distribution inside 2nd volume during 105 MW loss-of-load transient [°C vs. s]

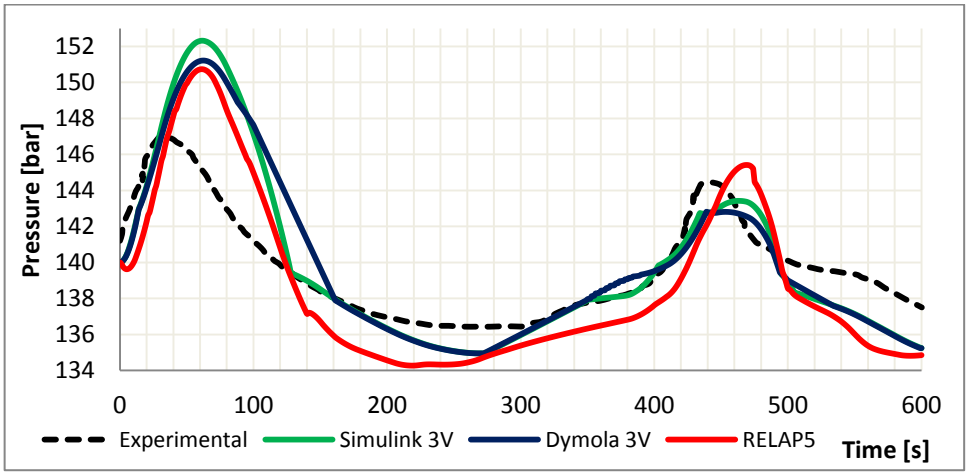

FIG. 4.96 Pressure results comparison for 105 MW loss-of-load transient [bar vs. s]

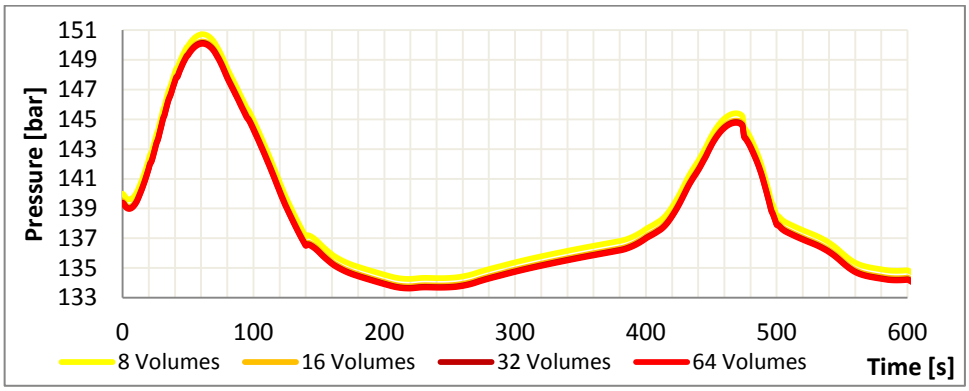

FIG. 4.97 Different mashes for Pressure 105 MW loss-of-load transient [°C vs. s]

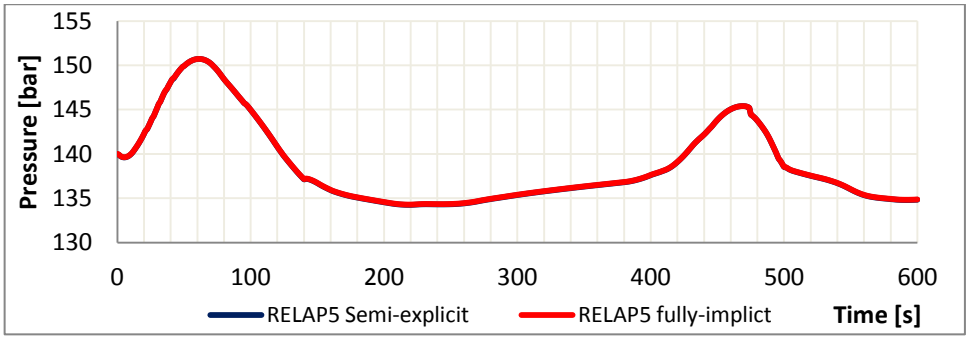

FIG. 4.98 Different numerical methods for Pressure 105 MW loss-of-load transient [°C vs. s]

4.7 CONCLUNDING REMARKS

This chapter has been dedicated to the analysis and comparison of different models and programs results. To summarize:

- Complete lumped parameter model as the equilibrium and one-volume non-equilibrium one give the worst results. However, among them, the non-equilibrium approach succeeds to follow the experimental data in a better way. This is the proof that equilibrium approach has been exceeded.
- A temperature distribution occurs inside the pressurizer liquid region, therefore partially 1D models must be developed
- RELAP5® is confirmed to be the best estimate simulation transient program.
- Two and three volumes models supply quite good results (in both of the cases of free and controlled dynamics) which can be compared to the RELAP5® ones (RELAP5® free and controlled dynamics results are very similar to each other). The results are stable with respect different tolerances and integration algorithms.
- Therefore they can be an inviting alternative to simulate complex pressure transient in order to closely couple the dynamic model of the system to the control one.

4.8 REFERENCES

[4] REDFIELD, J.A.; PRESCOP, V.; MARGOLIS, S.G.
Pressurizer performance during-load drop. Tests at Shippingport: analysis and test.
Trans. Am. Nucl. Soc: 323, June1967.

[13] NAHAVANDI, A.N.; MAKKENCHERY, S, An improved pressurizer model with bubble rise and condensate drop dynamics. Nuc. Eng. & Design, 12: 135-47, 1970.

[14] BARON, R.C. Digital simulation of a nuclear pressurizer.
Nuc. Sei. Eng., 52: 283-91, 1973.

[27] COMPUTER METHODS FOR ORDINARY DIFFERENTIAL EQUATIONS AND DIFFERENTIAL-ALGEBRAIC EQUATIONS
Uri M. Ascher and Linda R. Petzold
December 2 1997

[28] RELAP5/MOD3.3 CODE MANUALVOLUME I: CODE STRUCTURE, SYSTEM MODELS, AND SOLUTION METHODS
Nuclear Safety Analysis Division
December 2001
Information Systems Laboratories, Inc.
Rockville, Maryland
Idaho Falls, Idaho
Prepared for the
Division of Systems Research
Office of Nuclear Regulatory Research
U. S. Nuclear Regulatory Commission
Washington, DC 20555

[29] P. BOGACKI and L. F. SHAMPINE
An Efficient Runge-Kutta Method
Department of Mathematics and Statistics, Old Dominion University
Norfolk, VA 23529, U.S.A.
Mathematics Department, Southern Methodist University
Dallas, TX 75275, U.S.A.

[30] KEVIN BURRAGE and LINDA PETZOLD
On order reduction for runge-kutta methods Applied to differential/algebraic systems and to Stiff systems of odes
SIAM J. NUMER. ANAL.
Vol, 27, No. 2, pp. 447-456, April 1990
1990 Society for Industrial and Applied Mathematics

[31] L. EYBERGER
DASSL Tape Description and Implementation Information
NESC Note 92-24 (November 13, 1991).
[32] ERNST HAIRER
GERHARD WANNER
Stiff differential equations solved by Radau methods
Dept. de mathématiques, Université de Genève, CH-1211 Genève 24.

Chapter 5 – THE LINEARIZED PRESSURIZER MODEL

5.1 INTRODUCTION

This final chapter would be a short introduction to the analysis of the stabilities properties of the pressurizer system.
To do that, the pressurizer model, for simplicity the two-regions-single-volume one, is linearized around the saturation equilibrium point.
First of all, this new model will be compared with the corresponding non-linear one: results will be similar only in case of small perturbations around the equilibrium point chosen for the linearization process.
Then, using the tools given by control theory, it will be possible to study the stability properties of the pressurizer.
So the characteristic of open-loop system will be studied using the eigenvalues of dynamic matrix criterion.

5.2 THE LINEARIZATION PROCESS

For the mathematician or theoretical physicist, the natural definition of a dynamical system is the axiomatic one. In the physical world, however, a dynamical system must be described in terms of observable relationships between inputs (stimuli), outputs (responses) and state variables; using mathematical formalism [21]:

$$\dot{x} = f(x(t), y(t), t) \tag{5.1}$$
$$y(t) = g(x(t), y(t), t) \tag{5.2}$$

Where $u \in R^m, x \in R^n \; and \; y \in R^p$ are respectively the vector of inputs, of state variables and of outputs; f and g are two vector functions

Dynamical systems can be linear or nonlinear. Linear dynamical systems are dynamical systems whose evaluation functions f and g are linear with respect to inputs and state variables, therefore the superposition principle is valid. f and g are linear if and only if $\dot{x}(t)$ and $y(t)$ are linear combination of vector $x(t)$ and $y(t)$ components. Then the system 5.1 and 5.2 can be written in the sequent form:

$$\dot{x} = A(t)x(t) + B(t)u(t) \tag{5.3}$$
$$y(t) = C(t)x(t) + D(t)u(t) \tag{5.4}$$

Where matrices $A(t) \in \mathbb{R}^{n\times n}, B(t) \in \mathbb{R}^{n\times m}, C(t) \in \mathbb{R}^{p\times n} \; and \; D(t) \in \mathbb{R}^{p\times m}$ are in general function of time. A very important case of this kind of systems are time-invariant systems for which A, B, C, D are constant matrices.

In this situation the system is based on linear functions with constant coefficients and it is defined only by the elements appearing in the above matrices.

For linear dynamical system a lot of analysis and synthesis methods exist, for example stability properties can be investigated evaluating eigen-values of matrix A, which is the so-called matrix of dynamics.

Linear systems are significantly easier to work with, and are the basis of stability analysis.

Few physical systems are linear, but all can be locally approximated as linear. In fact, although almost every physical system contains nonlinearities, oftentimes its behaviour within a certain operating range of an equilibrium point $\bar{x}$ can be reasonably approximated by that of a linear model.

A point $\bar{x}$ for the differential equation:

$$\dot{x} = f(x, t) \tag{5.5}$$

It is an equilibrium one if:

$$f(\bar{x}, t) = 0 \tag{5.6}$$

For all t.
One reason for approximating the nonlinear by a linear model of the form is that, by so doing, one can apply rather simple and systematic linear control design techniques.
In fact stability analysis of the linearized system allows to compute stabilities properties of the equilibrium state $\bar{x}$ of the original nonlinear system. Although the linearized model is an approximate version of the nonlinear one, stability results are exact because of stability properties are, for definition, local. We must keep in mind, however, that a linearized model is valid only when the system operates in a sufficiently small range around the equilibrium point $\bar{x}$. Given the nonlinear system 5.1 and 5.2 and an equilibrium point $\bar{x} = [\bar{x}_1 \dots \bar{x}_n]^T$ obtained when $u = \bar{u}$, you can define a coordinate transformations as follows. Denote $\Delta x = x - \bar{x}$, i.e.,

$$\Delta x = \begin{bmatrix} \Delta x_1 \\ \vdots \\ \Delta x_n \end{bmatrix} = \begin{bmatrix} x_1 - \bar{x}_1 \\ \vdots \\ x_n - \bar{x}_n \end{bmatrix} \tag{5.7}$$

Further, denote $\Delta u = u - \bar{u}$ and $\Delta y = y - h(\bar{x}.\bar{u})$. Then the coordinates $\Delta x, \Delta u$ and Δy represent the variation of x, u and y from equilibrium values. We have to think of these as a new state, new input and new output respectively.
The linearization of 5.1 and 5.2 is given by:

$$\dot{\Delta x} = A\Delta x + B\Delta u \tag{5.8}$$
$$\Delta y = C\Delta x + D\Delta u \tag{5.9}$$

Where

$$A = \left[\frac{\partial f}{\partial x}\right]_{\bar{x},\bar{u}} = \begin{bmatrix} \frac{\partial f_1}{\partial x_1}(\bar{x}_1, \dots, \bar{x}_n, \bar{u}_1, \dots \bar{u}_n) & \cdots & \frac{\partial f_n}{\partial x_n}(\bar{x}_1, \dots, \bar{x}_n, \bar{u}_1, \dots \bar{u}_n) \\ \cdots & \ddots & \cdots \\ \frac{\partial f_n}{\partial x_1}(\bar{x}_1, \dots, \bar{x}_n, \bar{u}_1, \dots \bar{u}_n) & \cdots & \frac{\partial f_n(\bar{x}_1, \dots, \bar{x}_n, \bar{u}_1, \dots \bar{u}_n)}{\partial x_n} \end{bmatrix} \tag{5.10}$$

$$B = \left[\frac{\partial f}{\partial u}\right]_{\bar{x},\bar{u}} = \begin{bmatrix} \frac{\partial f_1}{\partial u_1}(\bar{x}_1, \dots, \bar{x}_n, \bar{u}_1, \dots \bar{u}_n) & \cdots & \frac{\partial f_n}{\partial u_n}(\bar{x}_1, \dots, \bar{x}_n, \bar{u}_1, \dots \bar{u}_n) \\ \cdots & \ddots & \cdots \\ \frac{\partial f_n}{\partial u_1}(\bar{x}_1, \dots, \bar{x}_n, \bar{u}_1, \dots \bar{u}_n) & \cdots & \frac{\partial f_n}{\partial u_n}(\bar{x}_1, \dots, \bar{x}_n, \bar{u}_1, \dots \bar{u}_n) \end{bmatrix} \tag{5.11}$$

$$C = \left[\frac{\partial h}{\partial x}\right]_{\bar{x},\bar{u}} = \begin{bmatrix} \frac{\partial h_1}{\partial x_1}(\bar{x}_1, \dots, \bar{x}_n, \bar{u}_1, \dots \bar{u}_n) & \cdots & \frac{\partial h_n}{\partial x_n}(\bar{x}_1, \dots, \bar{x}_n, \bar{u}_1, \dots \bar{u}_n) \\ \cdots & \ddots & \cdots \\ \frac{\partial h_n}{\partial x_1}(\bar{x}_1, \dots, \bar{x}_n, \bar{u}_1, \dots \bar{u}_n) & \cdots & \frac{\partial h}{\partial x_n}(\bar{x}_1, \dots, \bar{x}_n, \bar{u}_1, \dots \bar{u}_n) \end{bmatrix} \tag{5.12}$$

$$D = \left[\frac{\partial h}{\partial x}\right]_{\bar{x},\bar{u}} = \begin{bmatrix} \frac{\partial h_1}{\partial u_1}(\bar{x}_1, \dots, \bar{x}_n, \bar{u}_1, \dots \bar{u}_n) & \cdots & \frac{\partial h_n}{\partial u_n}(\bar{x}_1, \dots, \bar{x}_n, \bar{u}_1, \dots \bar{u}_n) \\ \cdots & \ddots & \cdots \\ \frac{\partial h_n}{\partial u_1}(\bar{x}_1, \dots, \bar{x}_n, \bar{u}_1, \dots \bar{u}_n) & \cdots & \frac{\partial h}{\partial u_n}(\bar{x}_1, \dots, \bar{x}_n, \bar{u}_1, \dots \bar{u}_n) \end{bmatrix} \quad (5.13)$$

The linearization 5.8 and 5.9 , also referred to as a small-signal model, is valid only in a sufficiently small neighbourhood of the equilibrium point $\bar{x}$. Notice that, as expected, it has the linear structure.

5.3 TRANSFER FUNCTION, OPEN AND CLOSED LOOP

In this section a new representation of dynamics system will be introduced: the so called transfer function (TF). The transfer function connects together the Laplace transforms[1] of input and output variables [21]. Considering the subsequent system:

$$\dot{x} = Ax(t) + Bu(t) \tag{5.14}$$
$$y(t) = Cx(t) + Du(t) \tag{5.15}$$

using U(s), X(s) and Y(s), function of the complex variables s, to indicate the Laplace transforms of u(t), x(t) and y(t) and applying to such equations the Laplace transformation, the flowing expressions can be obtained:

$$sX(s) - x(0) = AX(s) + BU(s) \tag{5.14}$$
$$Y(s) = CX(s) + DU(s) \tag{5.15}$$

Then:

$$X(s) = (sI - A)^{-1}BU(s) + (sI - A)^{-1}x(0) \tag{5.16}$$
$$Y(s) = [C(sI - A)^{-1}B + D]U(s) + C(sI - A)^{-1}x(0) \tag{5.17}$$

Equations 5.16 and 5.17 give the Laplace transform of output and states movements. The $p \times m$ matrix

$$G(s) = C(sI - A)^{-1}B + D \tag{5.18}$$

appearing in equation 5.17 is called transfer function. The product of the transfer function with the input Laplace transform gives the Laplace transform of the output:

$$Y(s) = G(s)U(s) \tag{5.18}$$

The transfer function is an external representation of the system, on the contrary the state variables representation is an internal one. For SISO (single-input and single-output) system the transfer function is scalar. Considering a linear input/output system described by a set of ordinary differential equations of order n, the transfer function is a rational function:

$$G(s) = \frac{N(s)}{D(s)} = \frac{s^n + a_1 s^{n-1} + a_2 s^{n-2} + \cdots + a_n}{b_0 s^m + b_1 s^{m-1} + bs^{m-2} + \cdots + b_m} \tag{5.19}$$

[1] The Laplace transform is an integral transform perhaps second only to the Fourier transform in its utility in solving physical problems. The Laplace transform is particularly useful in solving linear ordinary differential equations such as those arising in the analysis of electronic circuits. The (unilateral) Laplace transform $\mathcal{L}$(not to be confused with the Lie derivative) is defined by :

$$\mathcal{L}[f(t)] = \int_0^\infty f(t)e^{-st}dt$$

The roots of N(s) are called zeros, those of D(s) poles.

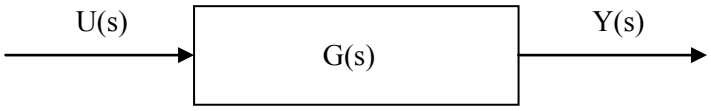

FIG. 5.1 Block diagram describing the system in the s-domain

In order to adjust the behaviour of a dynamic system, a controller is usually needed. In this regard, two different strategies exist: the open loop and the closed loop one.
An Open-loop system, also referred to as non-feedback system, is a type of continuous control system in which the output has no influence or effect on the control action of the input signal. In other words, in an open-loop control system the output is neither measured nor "feedback" for comparison with the input.
Therefore, an open-loop system is expected to faithfully follow its input command or set point regardless of the final result. Also, an open-loop system has no knowledge of the output condition so cannot self-correct any errors it could make when the preset value drifts, even if this results in large deviations from the preset value.
Another disadvantage of open-loop systems is that they are poorly equipped to handle disturbances or changes in the conditions which may reduce its ability to complete the desired task.

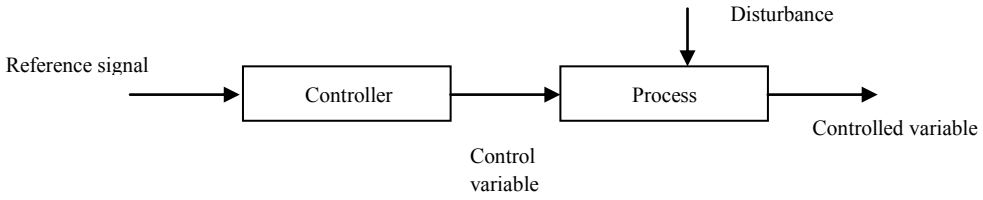

FIG. 5.2 Open-loop controlled system

Instead a closed-loop control system is one in which an input forcing function is determined in part by the system response. The measured response of a physical system is compared with a desired response. The difference between these two responses initiates actions that will result in the actual response of the system to approach the desired response. This in turn drives the difference signal toward zero.
Typically the difference signal is processed by another physical system, which is called a compensator, a controller, or a filter for real-time control system applications.

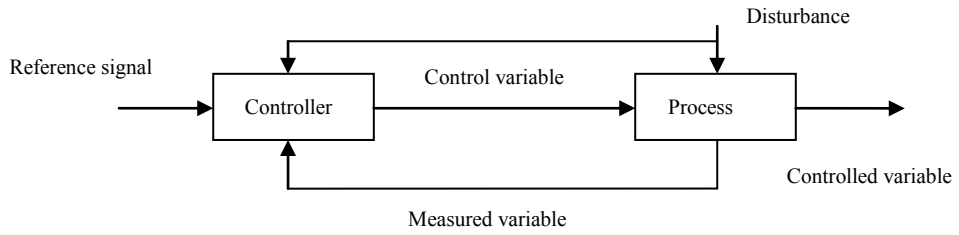

FIG. 5.3 Closed-loop controlled system

The simplest case of close loop system is:

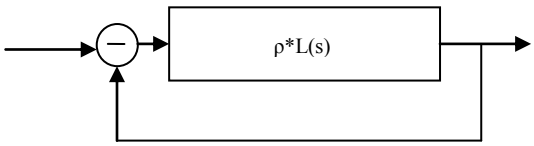

FIG. 5.4 Negative-feedback controlled system

Which is a negative feed-back controlled system.
To study the stability properties of an open loop controlled system is easy: you have to compute the eigenvalues of matrix A and check if their real part is negative or equal to zero. If $Re\{\lambda_i\} \leq 0 \; \forall i$ then the system is stable. Instead, for closed loop system, a very useful tool has been developed by Walter R. Evans in order to analyze the stability of the system for any value of the gain (ρ): the root locus.
The root locus technique is a graphical method for sketching the locus of poles of closed-loop transfer function in the *s*-plane as a parameter is varied and has been utilized extensively in control engineering practice. It provides the engineer with a measure of the sensitivity of roots of the system a variation in parameter being considered. It is important to underline that closed loop systems can be made stable even when the open loop system is unstable and vice versa. In the following pages the open-loop pressurizer analysis will be carried on.

5.4 BEYNON-KURIDAN PRESSURIZER MODEL

T.D. Beynon snd R.M. Kuridan [17] proposed in 1998 a linearized model for the pressurizer of the Safe Integral Reactor (SIR). The mathematical model derives from general conservation equation includes all important thermal-hydraulic processes occurring in the pressurizer, that is to say spray condensation, interfacial condensation, vapour rise, condensate fall, and heat transfer from heaters. However heat exchanges and thermal dissipations are neglected. As in the case of two-regions-two-volumes and two-regions-three-volumes models, insurge and outsurge events are modelled separately. The assumptions on which the model is bases are the usual ones, which were described in Chapter 2.
Basing on fundamental conservation equation, the mathematical form of Beynon-Kuridan model is quite similar to two-regions-one-volume model developed in this study. After the derivation of non linear formulation, the system has been linearized using saturation conditions as equilibrium point and considering all the thermodynamics partial derivatives as constants.

$$p = p_0 + \delta p \tag{5.14}$$
$$\dot{m}_{IN} = \dot{m}_{IN\_0} + \delta\dot{m}_{IN} \tag{5.15}$$
$$\dot{m}_{SP} = \dot{m}_{SP\_0} + \delta\dot{m}_{SP} \tag{5.16}$$
$$\dot{m}_{CS} = \dot{m}_{CS\_0} + \delta\dot{m}_{CS} \tag{5.17}$$
$$h_F = h_{F\_0} + \delta h_F \tag{5.18}$$
$$h_G = h_{G\_0} + \delta h_G \tag{5.19}$$
$$z = Z_0 + \delta Z \tag{5.20}$$

Where $\dot{m}_{IN\_0}, \dot{m}_{SP\_0}, \dot{m}_{CS\_0} = 0$.
Final system assumes the sequent form:

$$\frac{d\delta p}{dt} = A_1\delta\dot{m}_{IN} + A_2\delta\dot{m}_{SP} \tag{5.14}$$
$$\frac{d\delta h_F}{dt} = B_1\delta\dot{m}_{IN} + B_2\delta\dot{m}_{SP} \tag{5.15}$$
$$\frac{d\delta h_G}{dt} = C_1\delta\dot{m}_{IN} + C_2\delta\dot{m}_{SP} \tag{5.16}$$
$$\frac{d\delta Z}{dt} = D_1\delta\dot{m}_{IN} + D_2\delta\dot{m}_{SP} \tag{5.17}$$

Where p, h_F, h_G are respectively pressure, liquid enthalpy and vapour enthalpy at saturation conditions, z in the water level, which in Beynon-Kuridan model is used as reference variables in place of the vapour volume.

As you can see this model, although it seems in state-space formulation, it is written in a non-dynamic way, the variables which are under the derivative sign depend only on inputs.
When this model is applied to the Shippingport Pressurizer, the pressure response is satisfactory.

5.5 LINEARIZATION AND STABILITY ANALYSIS

The only physical equilibrium point in the pressurizer dynamics happens when both steam and water are satured, in other words, when all the system is at thermal equilibrium. So, considering the case of two-regions-one-volume model, the system of equations to linearize is:

$$\Psi * \dot{z} = \eta \tag{5.18}$$

Where:

$$\Psi = \begin{vmatrix} V_V * \frac{d\rho_G}{dp} & \rho_G & 1 & -1 \\ (V - V_V) * \frac{d\rho_F}{dp} & -\rho_F & -1 & 1 \\ V_V * \left(\rho_G * \frac{dh_G}{dp} - 1\right) & 0 & (h_F - h_G) & 0 \\ (V - V_V) * \left(\rho_F * \frac{dh_F}{dp} - 1\right) & 0 & 0 & (h_G - h_F) \end{vmatrix}$$

$$\dot{z} = \left\{\dot{p}, \dot{V}_v, \dot{m}_{RO}, \dot{m}_{FL}\right\}^T$$

$$\eta = \begin{vmatrix} -\dot{m}_{CS} - \dot{m}_{WC} - \dot{m}_{VLV} \\ \dot{m}_{CS} + \dot{m}_{WC} + \dot{m}_{SP} + \dot{m}_{INSURGE} - \dot{m}_{OUTSURGE} \\ -\dot{Q}_{Wv} \\ \dot{m}_{CS} \cdot (h_G - h_F) + \dot{m}_{WC} \cdot (h_G - h_F) + \dot{m}_{SP} \cdot (h_{SP} - h_F) + \dot{m}_{INSURGE} \cdot (h_{INSURGE} - h_F) + \dot{Q}_H - \dot{Q}_{Wl} \end{vmatrix}$$

With

$$\dot{m}_{cs} = \dot{m}_{SP} \frac{(h_F - h_{SP})}{(h_G - h_F)} \tag{5.19}$$

$$\dot{Q}_{Wv} = h_v S_v (T_{SAT} - T_{WALL}) \tag{5.20}$$

$$\dot{Q}_{Wl} = h_l S_l (T_{SAT} - T_{WALL}) \tag{5.20}$$

This system can be written in the subsequent form:

$$\Psi * \dot{z} - \eta = 0 \tag{5.21}$$

Now, by expanding equations 5.19 in Taylor series to the first order, the linearized form of the pressurizer can be obtained. Particularly the system of equations is linearized using the following relations:

$$p = p_0 + \delta p \tag{5.22}$$

$$V_V = V_{V_0} + \delta V_V \tag{5.22}$$

$$\dot{m}_{FL} = \dot{m}_{FL\_0} + \delta\dot{m}_{FL} \tag{5.23}$$

$$\dot{m}_{RO} = \dot{m}_{RO\_0} + \delta\dot{m}_{RO} \tag{5.24}$$

$$\dot{m}_{IN} = \dot{m}_{IN\_0} + \delta\dot{m}_{IN} \tag{5.25}$$

$$\dot{m}_{SP} = \dot{m}_{SP\_0} + \delta\dot{m}_{SP} \tag{5.26}$$

$$\dot{Q}_H = \dot{Q}_{H\_0} + \delta Q_H \tag{5.27}$$

$$\dot{m}_{CS} = \dot{m}_{CS\_0} + \delta\dot{m}_{CS} = \left(\dot{m}_{SP\_0} + \delta\dot{m}_{SP}\right)\left(\frac{h_{F\_0} + \frac{dh_F}{dp}\delta p - h_{SP}}{h_{G\_0} + \frac{dh_g}{dp}\delta p - h_{F\_0} + \frac{dh_F}{dp}\delta p}\right) \tag{5.28}$$

$$h_F = h_{F\_0} + \frac{dh_F}{dp}\delta p \tag{5.29}$$

$$h_G = h_{G\_0} + \frac{dh_g}{dp}\delta p \tag{5.30}$$

Regarding heat flux terms, you can consider h_l, h_v and T_{WALL} constant, while the heat transfer surface and the saturation temperature can be written as:

$$S_V = \frac{2V_V}{R_{in}} \tag{5.31}$$

$$S_L = \frac{2(V - V_V)}{R_{in}} \tag{5.32}$$

$$T_{SAT} = T_{SAT_0} + \frac{dT_{SAT}}{dp}\delta p \tag{5.33}$$

Where Rin is the internal radius of the pressurizer tank. The derivative of T_{SAT} with respect to the pressure can be computed using Clausius-Clapeyron.
Therefore:

$$\dot{Q}_{Wv} = h_v \frac{2}{R_{in}}\left(V_{V_0} + \delta V_V\right)\left(T_{SAT_0} + \frac{dT_{SAT}}{dp}\delta p - T_{WALL}\right) \tag{5.34}$$

$$\dot{Q}_{Wl} = h_l \frac{2}{R_{in}}\left(V - V_{V_0} - \delta V_V\right)\left(T_{SAT_0} + \frac{dT_{SAT}}{dp}\delta p - T_{WALL}\right) \tag{5.35}$$

Finally the wall condensate mass flow rate:

$$\dot{m}_{WC} = \dot{m}_{WC_0} + \delta\dot{m}_{WC} = \frac{h_v \frac{2}{R_{in}}\left(V_{V_0} + \delta V_V\right)\left(T_{SAT_0} + \frac{dT_{SAT}}{dp}\delta p - T_{WALL}\right)}{h_{G\_0} + \frac{dh_g}{dp}\delta p - h_{F\_0} + \frac{dh_F}{dp}\delta p} \tag{5.36}$$

Ignoring higher order terms, and noting the flow and heaters initial conditions

$$\delta\dot{m}_{IN} = 0 \quad (5.37) \qquad \delta\dot{m}_{FL} = 0 \quad (5.39)$$
$$\delta\dot{m}_{SP} = 0 \quad (5.38) \qquad \delta\dot{m}_{RO} = 0 \quad (5.40)$$
$$\delta Q_H = 0 \quad (5.41) \qquad \delta\dot{m}_{OUT} = 0 \quad (5.42)$$

after some algebra:

$$\Psi = \begin{vmatrix} V_{V_0} * \left[\frac{d\rho_G}{dp}\right]_{p_0} & \rho_{G_0} & 1 & \textit{-1} \\ \left(V - V_{V_0}\right) * \left[\frac{d\rho_F}{dp}\right]_{p_0} & -\rho_{F_0} & \textit{-1} & 1 \\ V_{V_0} * \left(\rho_{G_0} * \left[\frac{dh_G}{dp}\right]_{p_0} - 1\right) & \textit{0} & \left(h_{F_0} - h_{G_0}\right) & \textit{0} \\ \left(V - V_{V_0}\right) * \left(\rho_{F_0} * \left[\frac{dh_F}{dp}\right]_{p_0} - 1\right) & \textit{0} & \textit{0} & \left(h_{G_0} - h_{F_0}\right) \end{vmatrix}$$

$$\dot{z} = \left\{\delta\dot{p}, \delta\dot{V}_v, \delta\dot{m}_{RO}, \delta\dot{m}_{FL}\right\}^T$$

$$\eta = \begin{vmatrix} -\delta\dot{m}_{SP}\frac{\left(h_{F_0} - h_{SP}\right)}{\left(h_{G_0} - h_{F_0}\right)} - \frac{2h_V}{R_{in}}\frac{\left(T_{SAT_0} - T_{WALL}\right)}{\left(h_{G_0} - h_{F_0}\right)} - \delta\dot{m}_{VLV} \\ \delta\dot{m}_{SP}\frac{\left(h_{F_0} - h_{SP}\right)}{\left(h_{G_0} - h_{F_0}\right)} + \frac{2h_V}{R_{in}}\frac{\left(T_{SAT_0} - T_{WALL}\right)}{\left(h_{G_0} - h_{F_0}\right)} + \delta\dot{m}_{SP} + \delta\dot{m}_{INSURGE} - \delta\dot{m}_{OUTSURGE} \\ -\frac{2h_V}{R_{in}}V_{V_0}\left(T_{SAT_0} + \left[\frac{dT_{SAT}}{dp}\right]_{p_0}\delta p - T_{WALL}\right) - \frac{2h_V}{R_{in}}\delta V_V\left(T_{SAT_0} - T_{WALL}\right) \\ \delta\dot{m}_{INSURGE}\cdot\left(h_{INSURGE} - h_{F_0}\right) + \delta\dot{Q}_H - \frac{2h_V}{R_{in}}\left(V - V_{V_0}\right)\left(T_{SAT_0} + \left[\frac{dT_{SAT}}{dp}\right]_{p_0}\delta p - T_{WALL}\right) + \\ + \frac{2h_V}{R_{in}}\delta V_V\left(T_{SAT_0} - T_{WALL}\right) + \frac{2h_V}{R_{in}}V_{V_0}\left(T_{SAT_0} + \left[\frac{dT_{SAT}}{dp}\right]_{p_0}\delta p - T_{WALL}\right) + \frac{2h_V}{R_{in}}\delta V_V\left(T_{SAT_0} - T_{WALL}\right) \end{vmatrix}$$

At thermal equilibrium $T_{WALL} = T_{SAT_0}$, therefore:

$$\eta = \begin{vmatrix} -\delta\dot{m}_{SP}\frac{\left(h_{F_0} - h_{SP}\right)}{\left(h_{G_0} - h_{F_0}\right)} - \delta\dot{m}_{VLV} \\ \delta\dot{m}_{SP}\frac{\left(h_{F_0} - h_{SP}\right)}{\left(h_{G_0} - h_{F_0}\right)} + \delta\dot{m}_{INSURGE} - \delta\dot{m}_{OUTSURGE} \\ -\frac{2h_V}{R_{in}}V_{V_0}\left[\frac{dT_{SAT}}{dp}\right]_{p_0}\delta p \\ \delta\dot{m}_{INSURGE}\cdot\left(h_{INSURGE} - h_{F_0}\right) + \delta\dot{Q}_H - \frac{2h_V}{R_{in}}\left(V - V_{V_0}\right)\left[\frac{dT_{SAT}}{dp}\right]_{p_0}\delta p + \frac{2h_V}{R_{in}}V_{V_0}\left[\frac{dT_{SAT}}{dp}\right]_{p_0}\delta p \end{vmatrix}$$

It is very important to point out that some state variables, i.e. the flashing mass flow rate and the rainout mass flow rate appear only under the derivation sign, therefore they never contribute to define the dynamics matrix A.
Moreover, thermal dissipations due to the interaction of pressurizer with the external ambient become of primary importance both in stability analysis and in the definition of the intrinsic nature of the system.
In fact, if no heat exchange is taken into account, the pressurizer system does not have a proper dynamics. In this case the system does not show an intrinsic evolution when all the inputs are turned off. It could be seen in the pole-zero map, where the only pole is at the origin of Gauss-plane. In this situation, the entire model falls into the Beynon-Kuridan one and the pressurizer acts as pure integrator.
Instead, taking into account thermal exchange and dissipation phenomena, the situation changes: the pressurizer shows a proper free dynamics and not only a forced one due to the inputs action.
You can see that, if the wall temperature is different from the saturation one, the system is characterized by two state variables, the pressure and the vapour volume. Instead, if the system is exactly at thermal equilibrium , $T_{WALL} = T_{SAT_0}$, there is only one state variable, which is pressure.
In this case, the only real equilibrium one, the pole of the system moves to the left side of complex plane.
Therefore, at saturation and thermal equilibrium conditions, the only state variable is the pressure. In fact rainout and flashing masses are not integrated while a constraint acts on the volume variable.
Now, using thermodynamics saturation properties at the nominal pressure of the system (p_0=140 bar) and expliciting all constants the system (5.21) in its linearized form can be put in ODE form inverting the Ψ matrix. Therefore the dynamics matrix can be obtained in numerical form as follows:

$$A = \begin{vmatrix} -4.3506\,e^{-4} & 0 & 0 & 0 \\ 2.0295\,e^{-6} & 0 & 0 & 0 \\ 2.1675\,e^{-3} & 0 & 0 & 0 \\ 7.8033\,e^{-3} & 0 & 0 & 0 \end{vmatrix}$$

Whose eigenvalues are:

$\lambda_1 = -4.3506\ e^{-4}$
$\lambda_2 = 0$
$\lambda_3 = 0$
$\lambda_4 = 0$

So there is a negative eigenvalue, the other ones are zero.
The other linearized system matrices are:

$$B = \begin{vmatrix} -1.4810\,e^{-2} & -1.5719\,e^{-2} & -2.3785\,e^{-2} & -1.1219\,e^{-1} & 9.0397\,e^{-1} \\ -1.8029\,e^{-3} & 1.9453\,e^{-3} & -1.7610\,e^{-3} & 2.3954\,e^{-3} & -4.2168\,e^{-3} \\ 1.2276\,e^{-2} & 1.3030\,e^{-2} & 1.9716\,e^{-2} & 9.2995\,e^{-2} & -7.4929\,e^{-2} \\ -1.9789\,e^{-1} & 1.2585\,e^{-1} & 1.9042\,e^{-1} & 8.9820\,e^{-1} & 2.1331\,e^{-1} \end{vmatrix}$$

Considering the pressure as the only variable for the output equation:

$$C = \begin{vmatrix} 1 & 0 & 0 & 0 \end{vmatrix}$$

$$D = \begin{vmatrix} 0 & 0 & 0 & 0 & 0 \end{vmatrix}$$

Therefore the transfer function of the entire system can be computed using 5.18 equation. From this one the pole-zero map of the system can be obtained.

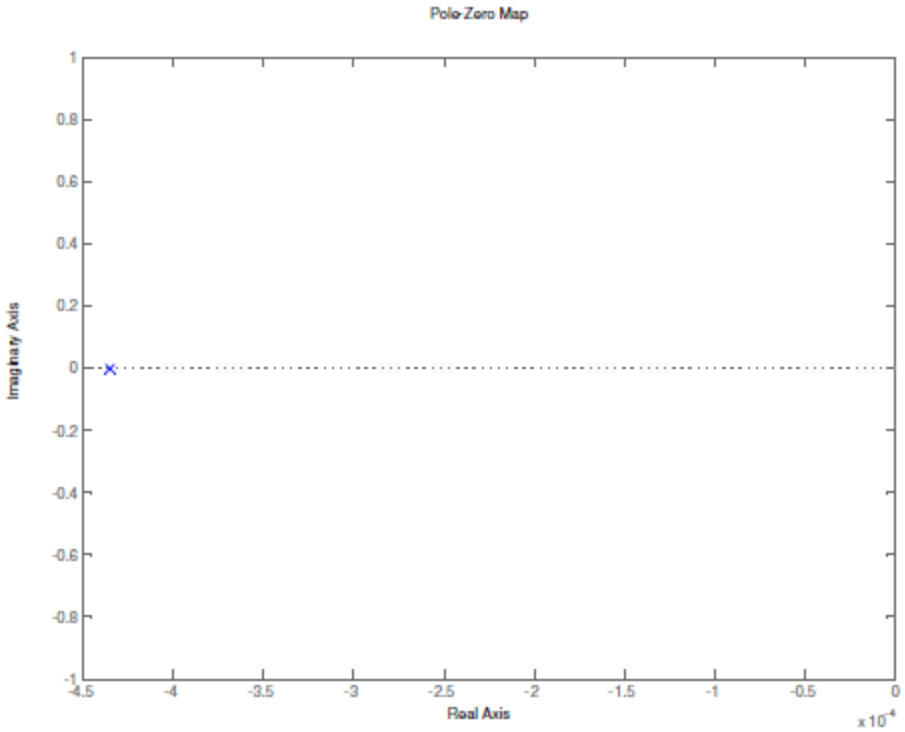

FIG. 5.5 Poles-zeros map with heat exchange

If the heat exchange is neglected:

$$A = \begin{vmatrix} 0 & 0 & 0 & 0 \\ 0 & 0 & 0 & 0 \\ 0 & 0 & 0 & 0 \\ 0 & 0 & 0 & 0 \end{vmatrix}$$

Whose eigenvalues are:

$\lambda_1 = 0$

$\lambda_2 = 0$
$\lambda_3 = 0$
$\lambda_4 = 0$

So there is a negative eingenvalue, the other ones are zero.
The other linearized system matrices are:

$$B = \begin{vmatrix} -1.4810\,e^{-2} & -1.5719\,e^{-2} & -2.3785\,e^{-2} & -1.1219\,e^{-1} & 9.0397\,e^{-1} \\ -1.8029\,e^{-3} & 1.9453\,e^{-3} & -1.7610\,e^{-3} & 2.3954\,e^{-3} & -4.2168\,e^{-3} \\ 1.2276\,e^{-2} & 1.3030\,e^{-2} & 1.9716\,e^{-2} & 9.2995\,e^{-2} & -7.4929\,e^{-2} \\ -1.9789\,e^{-1} & 1.2585\,e^{-1} & 1.9042\,e^{-1} & 8.9820\,e^{-1} & 2.1331\,e^{-1} \end{vmatrix}$$

$$C = \begin{vmatrix} 1 & 0 & 0 & 0 \end{vmatrix}$$

$$D = \begin{vmatrix} 0 & 0 & 0 & 0 & 0 \end{vmatrix}$$

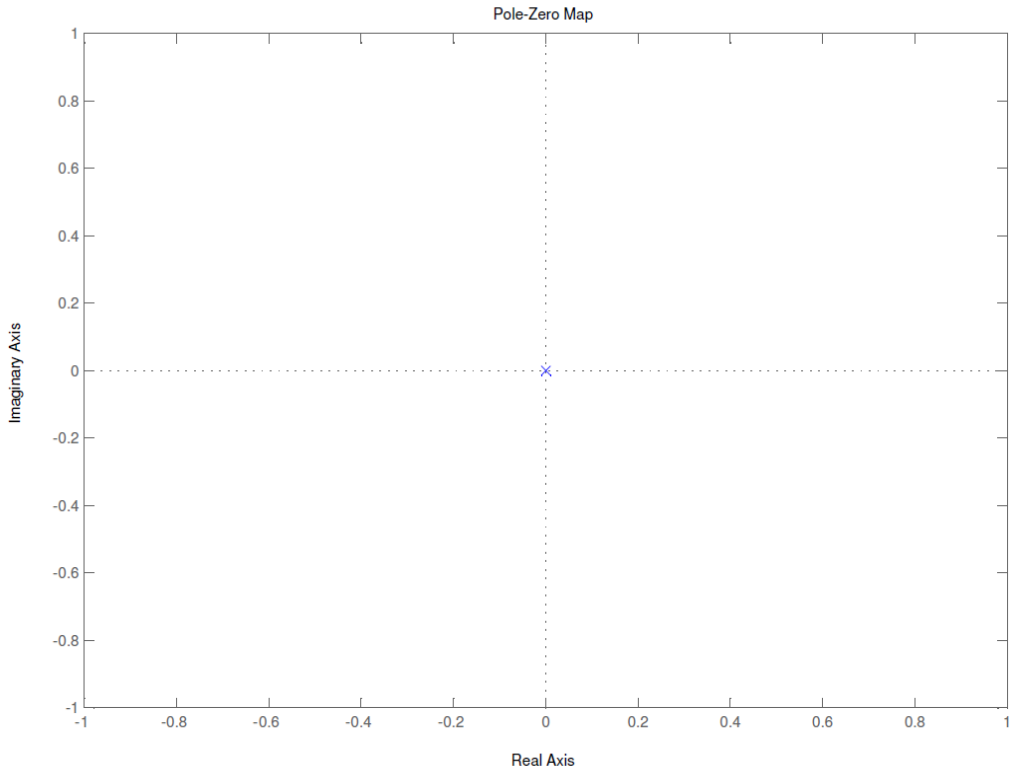

FIG. 5.6 Poles-zeros map without heat exchange

Obtained the A,B,C,D matrices the linearized model can be implemented in a computer program using Simulink® State-Space block:

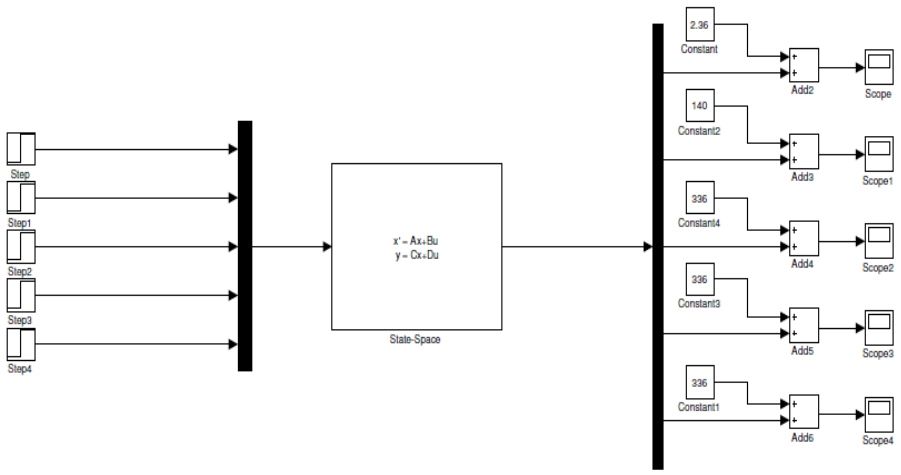

FIG. 5.7 The Linearized Pressurizer System

A comparison between linear and non-linear model follows:

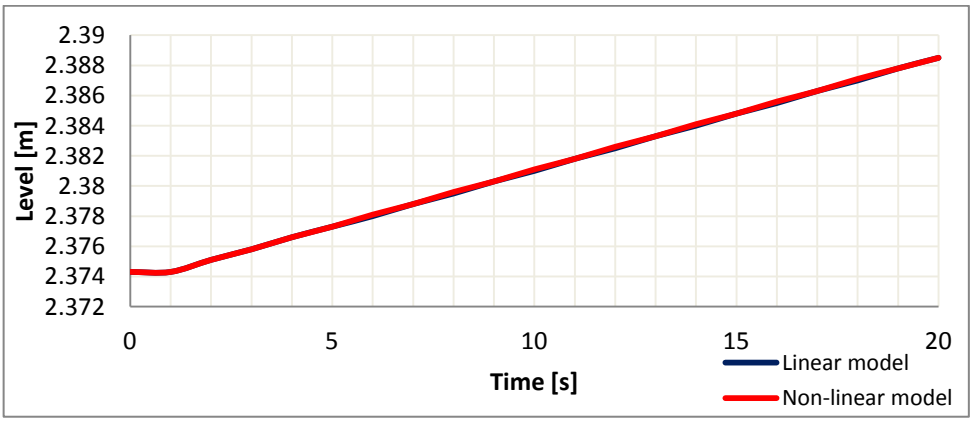

FIG. 5.8 1 kg/s insurge level response [m vs. s]

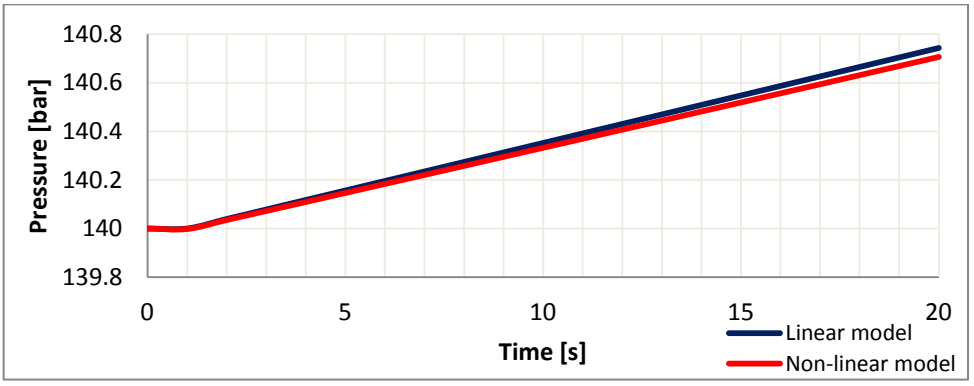

FIG. 5.9 1 kg/s insurge pressure response [bar vs. s]

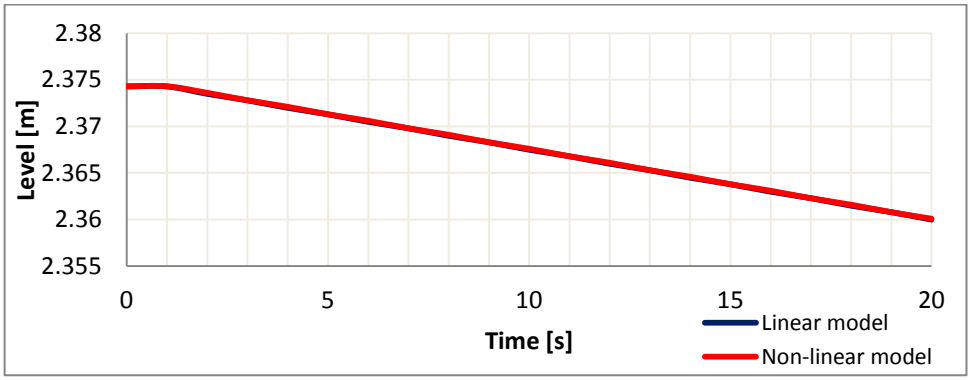

FIG. 5.10 1 kg/s outsurge level response [m vs. s]

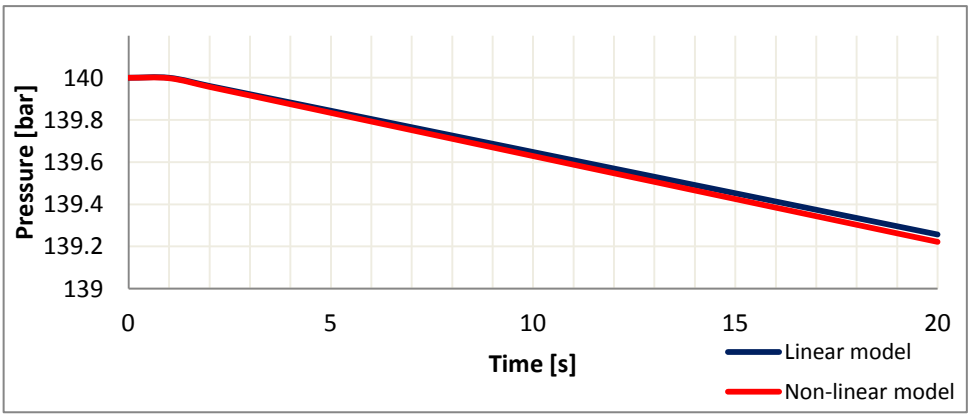

FIG. 5.1 1 kg/s outsurge pressure response [bar vs. s]

Around the equilibrium point, for little perturbation input, linear and non-linear model give quite same results. Instead, if the real inputs are used the linear model fails, because you are not working around its equilibrium point.

5.4 CONCLUDING REMARKS

In this final chapter the linearization of pressurizer model equations has been performed.
The linearized pressure model can follow the non-linear one for little transients, near the equilibrium point, but cannot be used for large transients.
If the Shippingport surge flow inputs were applied to the linearized model, it would fail poorly because of the forced variations would carry the model too far from the equilibrium point.
Moreover the linearization process has allowed to study the stability properties of the pressurizer. In this regard, the obtained results are very interesting and remark the central role of heat exchange for the dynamical behaviour of the system, which was ignored in previous models. In fact pressurizer is a real dynamic system if and only if heat exchange and thermal dissipations are taken into account, otherwise it does not have a proper dynamics but depends on inputs only.

5.5 REFERENCES

[17] R. M. KURIDAN and T. D. BEYNON
A LINEARIZED NON STEADY STATE MODEL FOR THE PRESSURIZER OF THE SAFE INTEGRAL REACTOR CONCEPT
Nuclear Engineering Department, Alfateh University, P.O. Box 13292, Tripoli, Libya
School of Physics and Space Research, University of Birmingham, Edgbaston,
Birmingham, B15 2TT, U.K

[21] FONDAMENTI DI CONTROLLI AUTOMATICI
Paolo Bolzern, Riccardo Scattolini, Nicola Schiavoni
McGraw-Hill Companies
3rd edition 2008

CONCLUDING REMARKS

Three non-linear mathematical models representing a generic pressurizer system for PWR reactor have been developed. The natural equation system form is the DAE one, more precisely ODE with constraints.
The models include the thermal hydraulics processes such as spray condensation, bulk evaporation, bulk condensation, wall condensate, heat transfer between control volume and thermal dissipations.
These mathematical models have been programmed using both Simulink® and Modelica languages, which represent two opposite approaches to the computer modelling.
Simulink® causal code is based on a matrix formulation of the pressurizer fundamental equations, which requires a long algebraic manipulation to transform the original DAE system into an ODE one.
Apart from the case of the simple two-region-one-volume model, insurge and outsurge events must be modelled separately. Simulink® code has been developed for this main reason: to create a base for a deeply future study for innovative control logic of pressurizer, which is intrinsically causal.
Modelica code, instead, is based directly on the primitive constituent equations of pressurizer, this fact allows a reduced manual reorder of the equation system, which can be left in DAE form.
This system is treated directly by the Modelica interpreter Dymola®, which uses particular algorithms, as the Pantelides and Duff ones, to automatically generate an equivalent ODE form of the original DAE system.
Modelica code has been developed for this main reason: to demonstrate the high elasticity of a-causal approach.
Finally, using the linearization process, a preliminary study of the stability properties of pressurizer system has been carried on.

Both Simulink® and Modelica codes have been compared with the Shippingport pressurizer experimental data giving the following very similar results:

- Two-regions-one-volume model response is not satisfactory, this fact indicates that a completely lumped parameter approach for the liquid region is not suitable to simulate pressurizer transient due to the non-uniformity of liquid region temperature
- Two-regions-two-volumes model gives a better response taking into account (in a very simple way) the temperature distribution along the liquid region
- Two-regions-three-volumes model results are very satisfactory thanks to the use of more volumes through which the temperature inside the liquid region can be computed in a more effective way
- Heat exchange and thermal dissipation phenomena, which are usually neglected in previous models, becomes fundamental, not only for a more precise response of the simulation, but also for the pressurizer dynamics study

Furthermore a third computer program, based on RELAP5® language, has been developed in order to demonstrate:

- The validity of hypothesis of temperature distribution along the liquid region, neglected in almost all previous models, in absence of experimental data
- The very good performances of Simulink® and Dymola® pressurizer models. These programs are much simpler than RELAP5® one, but the results are very similar. Moreover they can be used not only to simulate the pressurizer behaviour, but also (thanks to the control-oriented approach on which they are based) to develop new approaches for the pressurizer dynamic control. In this sense it will be very interesting to obtain an Hamiltonian formulation for the problem. This could allow to link the time derivative of Hamiltonian to entropy generation and exergy destruction during pressurizer transients to develop an innovative optimum control.

For this last reason the carried out study has dealt more with Simulink® causal approach, as a matter of fact, although the declarative modelling way is very convenient for modellers, the procedural one intrinsically imposes a much deeper and more reasoned work to the developer, who has to investigate the physical system thoroughly.

REFERENCES

[1] IMPIANTI NUCLEARI
Carlo Lombardi
Polipress
3rd edition 2009

[2] IMPIANTI NUCLEARI
Maurizio Cumo
Università la Sapienza
3rd edition 2009

[3] NUCLEAR SYSTEMS VOLUME 0NE-THERMAL-HYDRAULICS FUNDAMENTALS
Neil E. Todreas and Mujid J. Kazimi
CRC PRESS –Second Ediction 2012

[4] REDFIELD, J.A.; PRESCOP, V.; MARGOLIS, S.G.
Pressurizer performance during-load drop. Tests at Shippingport: analysis and test.
Trans. Am. Nucl. Soc: 323, June1967.

[5] GAJEWSKI, W.M.
Study by simulator techniques of transient pressures in high pressure water systems utilizing a surge tank. Westinghouse Eletric Co.1955.

[6] SORENSON, C.W.
Procedure for sizing pressurizers for pressurized water reactor;
3.10-32, 1960 (KAPL--2000-10),

[7] COUGHREN, K.D.
Pressurizing vessel performance equations.
Pacific Northwest Lab., 1965. {BNWL-116).

[8] DRUCKER, E.E.; TONG, K.N.
Behaviour of a steam - -pressurizer surge tank. Trans. Am. Nucl. Society

[9] DRUCKER, E.E.; GORMAN, D.J.
A method predicting steam-surge tank transients based on one-dimensional heat sink transients based on one-dimensional heat sink.
NUC. Sci. Eng., 21: 473-80, 1965.

[10] G.BROWN
Insurge transient from a surge tank using CSMP. 109-14, Oct. 1974.

[11] DONALD BRITTON BOSLEY , Lieutenant, United States Navy
ROTH SUMNER LEDDICK, Lieutenant, United States Navy-
Simulation of steam pressurizing tank transients by analog computer

[12] NAHAVANDI, A.N. The loss-of-coolant accident analysis in pressurized water reactors.
Nuc. Sci. Eng., 36;159-88, 1969.

[13] NAHAVANDI, A.N.; MAKKENCHERY, S, An improved pressurizer model with bubble rise and condensate drop dynamics. Nuc. Eng. & Design, 12: 135-47, 1970.

[14] BARON, R.C. Digital simulation of a nuclear pressurizer.
Nuc. Sei. Eng., 52: 283-91, 1973.

[15] J.F.WILSON, R.J GRENDA and J.F.PATTERSON,
Steam volume fraction in a bubbling two-phase mixture, Transactions American Nuclear Society, Session 25 (1961).

[16] HACK YEONG CHUNG, TAE WOON KIM,SOON HEUNG CHANG, BYUNG HO LEE
Dept. of Nuclear Engineering
Korea Advanced Institute of Science and Technology,
Adaptive kalman gain approach to on-line instrument failure detection with improved glr method and suboptimal control on loft pressurizer

[17] R. M. KURIDAN and T. D. BEYNON
A LINEARIZED NON STEADY STATE MODEL FOR THE PRESSURIZER OF THE SAFE INTEGRAL REACTOR CONCEPT
Nuclear Engineering Department, Alfateh University, P.O. Box 13292, Tripoli, Libya
School of Physics and Space Research, University of Birmingham, Edgbaston,
Birmingham, B15 2TT, U.K

[18] DAVID A. BOTELHO, PAULO A.B. DE SAMPAIO, CELSO M.F. LAPA, CLAUDIO M.N.A. PEREIRA,MARIA DE LOURDES MOREIRA, ANTONIO CARLOS DE O. BARROSO
The iris pressurizer: simulation of out-surge transients and optimization procedure to design scaled experiments
Progress in Nuclear Energy 50 (2008) 730e739

[19] I.G. SHEKRILADZE,
V.I. GOMELAURI
Theoretical study of laminar film condensation of flowing vapour
Georgian Research Power Institute, Tbilisi, U.S.S.R.

[20] FUNDAMENTALS OF HEAT AND MASS TRANSFER
Theodore l. Bergman
Department of mechanical engineering
University of connecticut
Adrienne s. Lavine
Mechanical and aerospace engineering
Department
University of california, los angeles
Frank p. Incropera
College of engineering
University of notre dame
David p. Dewitt
School of mechanical engineering
Purdue university
JOHN Wiley Seventh Edition 2011

[21] FONDAMENTI DI CONTROLLI AUTOMATICI
Paolo Bolzern, Riccardo Scattolini, Nicola Schiavoni
McGraw-Hill Companies
3rd edition 2008

[22] LINDA PETZOLD
Differential/algebraic equations are not ode's
Siam j. Sci. Stat. Comput.
Vol. 3, no. 3, september 1982
1982 society for industrial and applied mathematics
0196-5204/82/0303-0007 $01.00/0

[23] J. R. COOPER, DR. R. B. DOOLEY
Revised Release on the IAPWS Industrial Formulation 1997
for the Thermodynamic Properties of Water and Steam
School of Engineering and Materials Science
Queen Mary, University of London
Mile End Road London E1 4NS, England
Executive Secretary:
Structural Integrity Associates, Inc.
2616 Chelsea Drive Charlotte, NC 28209, USA

[24] CONTINUOUS SYSTEM SIMULATION
Francois E. Cellier, Ernesto Kofman
Universidad Nacional de Rosario, Laboratory for System Dynamics and
Signal Processing, School of Electronic Engineering – FCEIA
Printed on acid-free paper. 2006 Springer Science+Business Media, Inc.

[25] PRINCIPLES OF OBJECT-ORIENTED MODELING AND SIMULATION WITH MODELICA 2.1
Peter Fritzson
Wiley-IEEE -2003

[26] COSTANTINOS C. PANTELIDES
The consistent initialization of Differential-Algebraic Systems
SIAM J. SCI. STAT. COMPUT.1988

[27] COMPUTER METHODS FOR ORDINARY DIFFERENTIAL EQUATIONS AND DIFFERENTIAL-ALGEBRAIC EQUATIONS
Uri M. Ascher and Linda R. Petzold
December 2 1997

[28] RELAP5/MOD3.3 CODE MANUALVOLUME I: CODE STRUCTURE, SYSTEM MODELS, AND SOLUTION METHODS
Nuclear Safety Analysis Division
December 2001
Information Systems Laboratories, Inc.
Rockville, Maryland
Idaho Falls, Idaho
Prepared for the
Division of Systems Research
Office of Nuclear Regulatory Research
U. S. Nuclear Regulatory Commission
Washington, DC 20555

[29] P. BOGACKI and L. F. SHAMPINE
An Efficient Runge-Kutta Method
Department of Mathematics and Statistics, Old Dominion University
Norfolk, VA 23529, U.S.A.
Mathematics Department, Southern Methodist University
Dallas, TX 75275, U.S.A.

[30] KEVIN BURRAGE and LINDA PETZOLD
On order reduction for runge-kutta methods Applied to differential/algebraic systems and to Stiff systems of odes
SIAM J. NUMER. ANAL.
Vol, 27, No. 2, pp. 447-456, April 1990
1990 Society for Industrial and Applied Mathematics

[31] L. EYBERGER
DASSL Tape Description and Implementation Information
NESC Note 92-24 (November 13, 1991).

[32] ERNST HAIRER
GERHARD WANNER
Stiff differential equations solved by Radau methods
Dept. de mathématiques, Université de Genève, CH-1211 Genève 24.